# Use of electron paramagnetic resonance spectroscopy for characterization of chemical and structural properties of foods and related matrices

by

Bade Tonyali

B.S., Middle East Technical University, 2011

M.S., Middle East Technical University, 2014

AN ABSTRACT OF A DISSERTATION

submitted in partial fulfillment of the requirements for the degree

DOCTOR OF PHILOSOPHY

Food Science

KANSAS STATE UNIVERSITY

Manhattan, Kansas

2021

# Abstract

Electron paramagnetic resonance (EPR) spectroscopy is a widely used tool to unambiguously detect free radicals in food and related matrices. It is a fast, sensitive, and non-destructive technique. The broad analysis range of EPR includes detection and identification of free radicals via direct or indirect methods (e.g., reactive oxygen and reactive nitrogen species), oxidative stability analysis (e.g., lipid oxidation and antioxidant assays), detection and quantification of irradiation-derived radicals (e.g., cellulose derived radicals) in various foods, and structural characterization (e.g., membrane mobility).

The first objective is to use EPR spectroscopy as a non-destructive technique to characterize the changes in a bacterial membrane. Bacterial cell characteristics, such as size, morphology, and membrane integrity, are affected by environmental conditions such as thermal treatment. In this objective, the effect of heating on the cell morphology and membrane mobility of *E. coli* were evaluated by the combined analytical techniques of EPR, dynamic light scattering (DLS), and transmission electron microscopy (TEM). The change in membrane integrity was quantified via the mobility of 16-doxylstearic acid (16-DSA) spin probe, a stable nitroxide that can align with the membrane, using EPR spectroscopy. Two order parameters S1 and S2 defined on x- and y-axes, respectively, decreased with increasing temperature indicating loss of membrane integrity (0.78 and 0.65 at 65 °C for S1 and S2, respectively). The size of *E. coli* cells increased from 2.3 μm to 3.0 μm with heating up to 50 °C followed by a shrinkage with further heating up to 70 °C. Our findings suggested the analysis of cell size, morphology, and membrane mobility can be used in parallel to provide a deeper understanding of structural changes related to bacterial thermal resistance. Therefore, the combined approach proposed in this study is helpful to characterize survival behavior and inactivation kinetics of microorganisms.

The second objective is to use EPR spectroscopy for the detection and quantification of irradiation-derived radicals in cellulose-rich foods. Dried sweet potatoes (SP), which are often irradiated and consumed as human and pet foods, can provide a crystalline cellulose-rich environment to stabilize the irradiation-specific free radicals. SP samples were prepared at two moisture contents (48.3 and 9.7 % by drying at 150 °F for 24 or 48 h) and irradiated at 0, 5, 10, 20, 30, and 50 kGy. The irradiation-derived radicals were analyzed using EPR spectroscopy at

X-band. The signal characteristics (intensity and peak shape) were evaluated at different sample locations (skin and flesh), as a function of the sample preparation method (grinding, sieving, and pelletizing). The flesh of irradiated SP showed complex EPR spectra with multiple satellite peaks of cellulose radicals (333.5 and 338.8 mT) and a split peak of dextrose radicals (337.4 mT); while skin spectra were distinctive of cellulose radicals. In this study, the effects of sample composition and preparation method on the formation and analysis of irradiation-specific radicals were detected using EPR spectroscopy. However, the quantification of free radicals in multiline spectra due to complex food matrices is challenging.

The third objective of this dissertation is to improve the quantification of free radicals and the performance of EPR analysis by implementing a peak enhancement method. Peak enhancement is an artificial intelligence tool applied for the analysis of complex spectra to improve resolution in various spectroscopy data. The complex EPR spectra were analyzed as a function of irradiation dose by calculating total areas under all peaks (TPA) and areas of irradiation-specific satellite peaks (SPA) using GRAMS software. TPA increased with irradiation dose at a rate of 573.4 AU/dose ($R^2 = 0.98$) and 14.7 AU/dose ($R^2 = 0.65$) for low- and high-moisture samples, respectively. High-field SPA was shown to be more sensitive to irradiation dose as compared to low-field SPA, however with high variability for both. The resolution of satellite peaks was further improved by peak enhancement procedure: higher linearity ($R^2$ of SPA increased from 0.98 to 0.99 for low moisture and 0.77 to 0.94 for high-field of high moisture SP) and lower variability (coefficient of variation of low field SPA of high-moisture SP samples were less than 25% at all doses). The technique proposed in this study can be used to detect and quantify irradiation-specific cellulose satellite peaks and glucose split peak in EPR spectra in both low- and high-moisture plant-based foods rich in sugar and cellulose, such as dried sweet potatoes.

The fourth objective of this dissertation is to use EPR spectroscopy for the detection and quantification of irradiation-derived radicals in other matrices such as chicken jerky treats and pig ears. Chicken jerky treats (CJT) and pig ears (PE) are irradiated foods that were commercially analyzed with gas chromatography (GC-MS). These lipid-rich products produce irradiation-specific 2-dodecylcyclobutanone (2-DCB), a radiolysis product of palmitic acid during irradiation. EPR spectroscopy and solid-phase microextraction (SPME)-coupled gas chromatography were used to estimate the irradiation history of these products. In addition, the

factors such as IS concentration, matrix properties, and analyte concentrations that are important for the sensitivity of GC-MS analysis were investigated. Two irradiation levels (10 and 50 kGy) and different internal standard (IS) concentrations (8 and 80 ng/g sample for CJT; 8, 80, and 800 ng/g sample for PE) were studied to evaluate the interaction of IS and 2-DCB as a function of their concentrations and matrix properties to improve the precision and accuracy of SPME-coupled GC-MS analysis. IS and 2-DCB were quantified by calculating the area under IS peak (ISA) and the area under 2-DCB peak (DCA), respectively. EPR spectra of non-irradiated PE and CJT exhibited a singlet line. After irradiation, irradiated PE had a signal centered at g = 1.996 ± 0.003 due to isotropic $CO_2^-$ radical, while the signal intensity of singlet line in CJT increased. Although the irradiation-specific peak in PE and the increased signal intensity of the central peak in CJT can be used for irradiation detection, they could not be resolved to quantify irradiation doses. For GC-MS analysis, ISA of CJT irradiated at 50 kGy was significantly higher ($p<0.01$) than that of 10 kGy at IS concentration of 8 ng/g CJT. ISA remained unchanged at high IS concentration. Similar results were obtained for PE samples. The significant increase in IS areas with increasing 2-DCB concentration suggests an interaction and competition phenomena between IS and 2-DCB at low IS concentrations. The results of this study showed that EPR analysis can indicate the irradiation process, it was limited for dose identification in CJT and PE. Choosing the correct IS concentration can solve the problems and improve the accuracy and precision of the GC-MS analysis.

This study showed that when used for membrane characterization, EPR analysis can provide information on the structural characterization of biological membranes under external stresses. In addition, it can be used as a non-destructive technique to detect and quantify irradiation-derived radicals in cellulose-rich foods. The peak enhancement method proposed in this study can improve the quantification of irradiation-specific cellulose satellite peaks and glucose split peak in EPR spectra of plant-based foods. In contrast, EPR spectroscopy can serve for the detection of irradiation process in lipid-rich products, however, it needs more studies for dose identification analysis. The EPR methods used in the present work can be used and further be developed to understand thermal inactivation kinetics on microorganisms and establish guidelines for the irradiation detection and the irradiation dose quantification in cellulose-rich plant-based products.

# Use of electron paramagnetic resonance spectroscopy for characterization of chemical and structural properties of foods and related matrices

by

Bade Tonyali

B.S., Middle East Technical University, 2011
M.S., Middle East Technical University, 2014

A DISSERTATION

submitted in partial fulfillment of the requirements for the degree

DOCTOR OF PHILOSOPHY

Food Science

KANSAS STATE UNIVERSITY
Manhattan, Kansas

2021

Approved by:

Major Professor
Dr. Umut Yucel

# Abstract

Electron paramagnetic resonance (EPR) spectroscopy is a widely used tool to unambiguously detect free radicals in food and related matrices. It is a fast, sensitive, and non-destructive technique. The broad analysis range of EPR includes detection and identification of free radicals via direct or indirect methods (e.g., reactive oxygen and reactive nitrogen species), oxidative stability analysis (e.g., lipid oxidation and antioxidant assays), detection and quantification of irradiation-derived radicals (e.g., cellulose derived radicals) in various foods, and structural characterization (e.g., membrane mobility).

The first objective is to use EPR spectroscopy as a non-destructive technique to characterize the changes in a bacterial membrane. Bacterial cell characteristics, such as size, morphology, and membrane integrity, are affected by environmental conditions such as thermal treatment. In this objective, the effect of heating on the cell morphology and membrane mobility of *E. coli* were evaluated by the combined analytical techniques of EPR, dynamic light scattering (DLS), and transmission electron microscopy (TEM). The change in membrane integrity was quantified via the mobility of 16-doxylstearic acid (16-DSA) spin probe, a stable nitroxide that can align with the membrane, using EPR spectroscopy. Two order parameters S1 and S2 defined on x- and y-axes, respectively, decreased with increasing temperature indicating loss of membrane integrity (0.78 and 0.65 at 65 °C for S1 and S2, respectively). The size of *E. coli* cells increased from 2.3 μm to 3.0 μm with heating up to 50 °C followed by a shrinkage with further heating up to 70 °C. Our findings suggested the analysis of cell size, morphology, and membrane mobility can be used in parallel to provide a deeper understanding of structural changes related to bacterial thermal resistance. Therefore, the combined approach proposed in this study is helpful to characterize survival behavior and inactivation kinetics of microorganisms.

The second objective is to use EPR spectroscopy for the detection and quantification of irradiation-derived radicals in cellulose-rich foods. Dried sweet potatoes (SP), which are often irradiated and consumed as human and pet foods, can provide a crystalline cellulose-rich environment to stabilize the irradiation-specific free radicals. SP samples were prepared at two moisture contents (48.3 and 9.7 % by drying at 150 °F for 24 or 48 h) and irradiated at 0, 5, 10, 20, 30, and 50 kGy. The irradiation-derived radicals were analyzed using EPR spectroscopy at

X-band. The signal characteristics (intensity and peak shape) were evaluated at different sample locations (skin and flesh), as a function of the sample preparation method (grinding, sieving, and pelletizing). The flesh of irradiated SP showed complex EPR spectra with multiple satellite peaks of cellulose radicals (333.5 and 338.8 mT) and a split peak of dextrose radicals (337.4 mT); while skin spectra were distinctive of cellulose radicals. In this study, the effects of sample composition and preparation method on the formation and analysis of irradiation-specific radicals were detected using EPR spectroscopy. However, the quantification of free radicals in multiline spectra due to complex food matrices is challenging.

The third objective of this dissertation is to improve the quantification of free radicals and the performance of EPR analysis by implementing a peak enhancement method. Peak enhancement is an artificial intelligence tool applied for the analysis of complex spectra to improve resolution in various spectroscopy data. The complex EPR spectra were analyzed as a function of irradiation dose by calculating total areas under all peaks (TPA) and areas of irradiation-specific satellite peaks (SPA) using GRAMS software. TPA increased with irradiation dose at a rate of 573.4 AU/dose ($R^2 = 0.98$) and 14.7 AU/dose ($R^2 = 0.65$) for low- and high-moisture samples, respectively. High-field SPA was shown to be more sensitive to irradiation dose as compared to low-field SPA, however with high variability for both. The resolution of satellite peaks was further improved by peak enhancement procedure: higher linearity ($R^2$ of SPA increased from 0.98 to 0.99 for low moisture and 0.77 to 0.94 for high-field of high moisture SP) and lower variability (coefficient of variation of low field SPA of high-moisture SP samples were less than 25% at all doses). The technique proposed in this study can be used to detect and quantify irradiation-specific cellulose satellite peaks and glucose split peak in EPR spectra in both low- and high-moisture plant-based foods rich in sugar and cellulose, such as dried sweet potatoes.

The fourth objective of this dissertation is to use EPR spectroscopy for the detection and quantification of irradiation-derived radicals in other matrices such as chicken jerky treats and pig ears. Chicken jerky treats (CJT) and pig ears (PE) are irradiated foods that were commercially analyzed with gas chromatography (GC-MS). These lipid-rich products produce irradiation-specific 2-dodecylcyclobutanone (2-DCB), a radiolysis product of palmitic acid during irradiation. EPR spectroscopy and solid-phase microextraction (SPME)-coupled gas chromatography were used to estimate the irradiation history of these products. In addition, the

factors such as IS concentration, matrix properties, and analyte concentrations that are important for the sensitivity of GC-MS analysis were investigated. Two irradiation levels (10 and 50 kGy) and different internal standard (IS) concentrations (8 and 80 ng/g sample for CJT; 8, 80, and 800 ng/g sample for PE) were studied to evaluate the interaction of IS and 2-DCB as a function of their concentrations and matrix properties to improve the precision and accuracy of SPME-coupled GC-MS analysis. IS and 2-DCB were quantified by calculating the area under IS peak (ISA) and the area under 2-DCB peak (DCA), respectively. EPR spectra of non-irradiated PE and CJT exhibited a singlet line. After irradiation, irradiated PE had a signal centered at g = 1.996 ± 0.003 due to isotropic $CO_2^-$ radical, while the signal intensity of singlet line in CJT increased. Although the irradiation-specific peak in PE and the increased signal intensity of the central peak in CJT can be used for irradiation detection, they could not be resolved to quantify irradiation doses. For GC-MS analysis, ISA of CJT irradiated at 50 kGy was significantly higher ($p<0.01$) than that of 10 kGy at IS concentration of 8 ng/g CJT. ISA remained unchanged at high IS concentration. Similar results were obtained for PE samples. The significant increase in IS areas with increasing 2-DCB concentration suggests an interaction and competition phenomena between IS and 2-DCB at low IS concentrations. The results of this study showed that EPR analysis can indicate the irradiation process, it was limited for dose identification in CJT and PE. Choosing the correct IS concentration can solve the problems and improve the accuracy and precision of the GC-MS analysis.

This study showed that when used for membrane characterization, EPR analysis can provide information on the structural characterization of biological membranes under external stresses. In addition, it can be used as a non-destructive technique to detect and quantify irradiation-derived radicals in cellulose-rich foods. The peak enhancement method proposed in this study can improve the quantification of irradiation-specific cellulose satellite peaks and glucose split peak in EPR spectra of plant-based foods. In contrast, EPR spectroscopy can serve for the detection of irradiation process in lipid-rich products, however, it needs more studies for dose identification analysis. The EPR methods used in the present work can be used and further be developed to understand thermal inactivation kinetics on microorganisms and establish guidelines for the irradiation detection and the irradiation dose quantification in cellulose-rich plant-based products.

# Table of Contents

# List of Figures

# List of Tables

# Acknowledgements

I would like to thank my advisor Dr. Umut Yucel for his support and guidance during my PhD studies. I also would like to express my gratitude to my committee members, Dr. Scott Smith, Dr. Valentina Trinetta, Dr. Yonghui Li, and Dr. Placidus Amama for serving on my committee. I would like to extend my gratitude to FDA Vet-LIRN group, especially Andriy Tkachenko, for their help during my studies.

I am very grateful for my lab mates and fellow graduate students. It was a great experience to work with them who always helped me through my studies. I would especially like to thank Bennett Uhl and Daniel Vega for their support and friendship.

I would like to thank Ayca Aydogdu, Sevil Cikrikci, and Emrah Kirtil for their friendship and support. We were there for any milestones in each other's lives (well, sometimes through video calls) and I hope we won't miss in the future. I feel lucky to call them friends.

I would like to thank Hazal Turasan and Oguz Kaan Ozturk. Our friendship runs deep, and I know they always have my back. Their support during my PhD, either for sending me the articles that I did not have the access to or for emotionally supporting me when I was down, is invaluable. I would especially like to thank Duru for making me smile and happy with her daily photos and videos.

I would like to thank my best friends, Hilal Isik and Selen Caner, for their support, love, and encouragement not only during my PhD studies but also for every step of my life. It might not be always easy to keep up with our friendship due to time differences, but there are always on the other side of the phone whenever I need them. Our friendship makes me feel supported, safe, and loved. I am grateful to the day that you two came into my life in a small dormitory room.

Finally, I would like to express deepest gratitude to my family, my father Cemil Tonyali, my mother Seliha Tonyali, my sister Gokcem Tonyali, and my brother-in-law Hakan Karsli. My parents unconditionally loved me and endlessly supported and encouraged me for my decisions. I would not be who I am today without them, and I hope I can make them proud of me now and future. My sister is the person that I fight most, but my love for her does not have limits. She is the one that I share my childhood and my happiest memories. I cannot imagine finishing this work without the love of my family. Hence, this one is for you.

# Dedication

I dedicate this dissertation to my family.

# Chapter 1 - Introduction - Use of EPR spectroscopy for biochemical and physical studies for food functionality and stability


## Abstract

Electron paramagnetic resonance (EPR) spectroscopy is a highly used tool for the detection of free radicals in food systems. It is a fast, sensitive, and non-destructive technique. The broad analysis range of EPR includes detection and identification of free radicals via direct or indirect methods (e.g., reactive oxygen and reactive nitrogen species), oxidative stability analysis (e.g., lipid oxidation and antioxidant assays), detection and quantification of irradiation-derived radicals (e.g., cellulose derived radicals) in various foods, and structural characterization (e.g., membrane mobility).

In this review, we provide fundamental information about EPR spectroscopy and an overview of its applications in biochemical and physical studies for food functionality, toxicology, and stability. Moreover, we discuss the limitations and challenges of EPR spectroscopy using some example studies from literature and underline EPR spectroscopy`s advantages over traditional methods.


## Introduction

### Working principle of EPR

Electron paramagnetic resonance (EPR) spectroscopy, also referred to as electron spin resonance (ESR) spectroscopy, is based on the interaction of unpaired electrons with the magnetic component of microwave radiation. The EPR spectroscopy detection is based on the spin of an unpaired electron and its magnetic moment. Every electron has a spin number, i.e., s= 1/2. The spin has two magnetic moments that are -1/2 and +1/2. These magnetic moments align themselves either parallel ($m_s$= -1/2) or anti-parallel ($m_s$= +1/2) to the direction of the field in the presence of an external magnetic field ($B_0$) (Chauhan et al., 2009). Electrons in these states have different energies: lower or higher energy states than their natural state, where they have non-

zero spin angular momenta and their magnetic moment randomly orient (Hagen, 2013). The difference between these two energy states (ΔE) is defined as the Zeeman effect and can be explained with Planck`s law as follows:

$$\Delta E = E_+ - E_- = hv \quad \text{(Eqn 1)}$$

where $E_+$ and $E_-$ are energies of two Zeeman states, h is Planck`s constant, and v is the frequency of microwave radiation. The difference between these two energy states (ΔE) increases with increasing magnetic field strength (Figure 1-1).

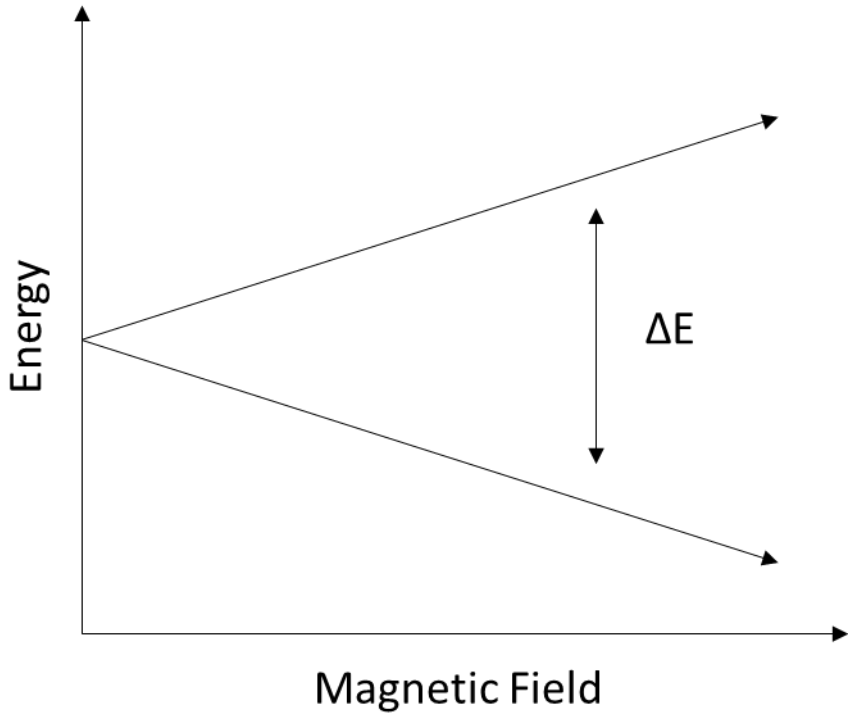


**Figure 1-1** The energy states of the electrons under an external magnetic field

When the magnetic field strength matches the energy difference between the energy states, the microwave radiation is absorbed (Rana et al., 2010). Therefore, energy level difference (ΔE) can also be defined with magnetic field strength as follows (Rana et al., 2010):

$$\Delta E = g\beta_e B_0 \quad \text{(Eqn 2)}$$

where g is the g factor, $B_0$ is the magnetic field strength, and $\beta_e$ is the electron Bohr magneton. g-factor is a proportionality constant that defines the magnetic moment of an atom. For example,

the g factor of a free electron is 2.0023; however, it changes due to interactions with other paramagnetic species in the sample (Hagen, 2013).

The absorption signal is collected with constant radiation frequency and varying magnetic fields (Eqn 2). Similar to other spectroscopic methods, the absorption spectrum (upper spectrum in Figure 1-2) is obtained. The first derivative of the absorption spectrum (lower spectrum in Figure 2) is usually used to present EPR data. This first derivative is obtained using a phase-sensitive detector in EPR spectroscopy. The maxima of the absorption spectrum correspond to the point where the signal crosses the zero on the x-axis in the first derivative spectrum. This point is usually referred to as the center of the signal (Weil & Bolton, 2007).

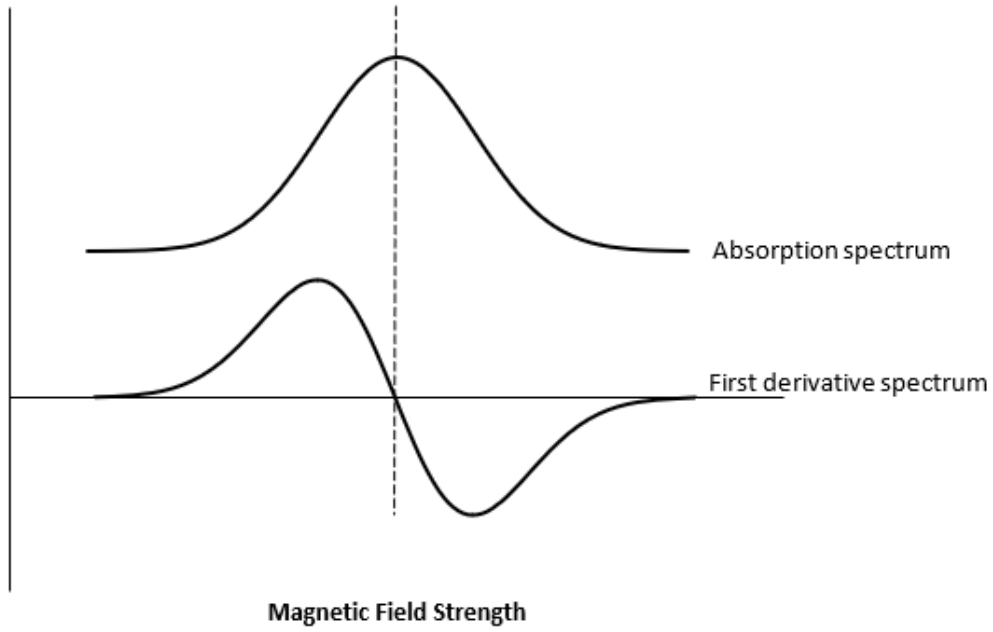


**Figure 1-2** Absorption spectrum (upper spectrum) and the first derivative of absorption spectrum (lower spectrum)

## EPR parameters

The position and shape of a peak in an EPR spectrum are linked to the nature of free radicals. In fact, the g-factor is characteristic of free radicals and is frequently used for compound identification in EPR experiments (Desrosiers, 1996).

The correlation time ($\tau_R$) is the time scale that a molecule stays in the same orientation (Nordio, 1976). In a fast-tumbling analysis, the EPR spectrum has sharp Lorentzian lines due to short

correlation time (e.g., $\tau_R < 10^{-9}$ s). In fast-tumbling spectra, hyperfine splitting constant, line shape, and peak-to-peak height are other parameters frequently studied in EPR studies (Figure 1-3). Hyperfine splitting constant is the separation between two consecutive peaks and can be used to provide information about mobility of a spin probe, polarity, and fluidity of the environment (Desrosiers, 1996). Peak-to-peak height is the intensity difference between the minima and maxima of a peak and is correlated to the free radical concentration of a sample (Desrosiers, 1996). Line shape or line width gives information about the molecular motion of unpaired electrons in the sample. For example, the sharp line shape and small line width in fast-tumbling spectra are due to fast tumbling (short correlation time).

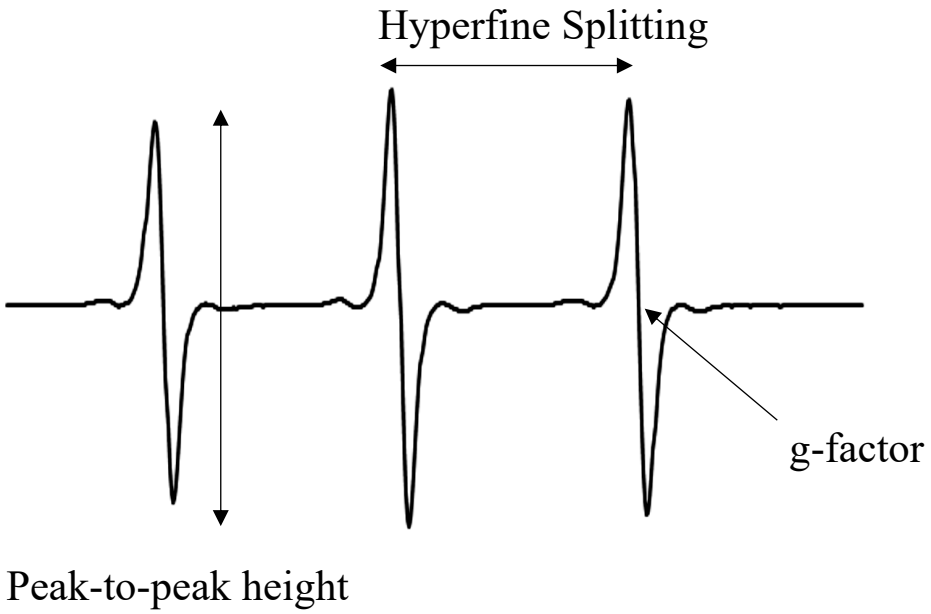


**Figure 1-3** Commonly used EPR parameters for fast-tumbling analysis

In a slow-tumbling analysis, the EPR spectrum cannot be explained with simple superposition of Lorentzian lines because of broadening of peaks due to longer correlation time (e.g., $\tau_R > 10^{-9}$ s) (Freed, 1976). Although the spin motion of electrons in the slow-tumbling region is not as fast as in the fast-tumbling region, it is still faster than the rigid spectra (Freed, 1976). In a slow-tumbling spectra, hyperfine splitting constant and peak-to-peak height are not easily distinguished as in fast-tumbling spectra due to complex spectra (Figure 1-4). In addition, line shape distorts and line width increases. In these spectra, the hyperfine splitting constant

correlates with the motion and orientation of the paramagnetic species. In some mediums, an external molecule is required to study slow and fast-tumbling spectra. The details will be discussed in the next section.

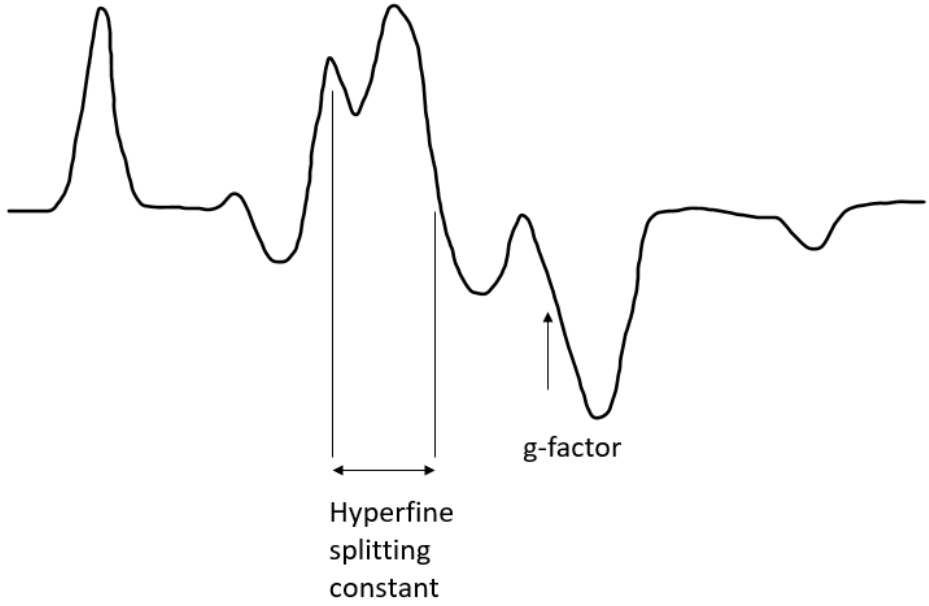


**Figure 1-4** Commonly used EPR parameters for slow-tumbling analysis

## Spin trapping

Free radicals such as hydroxyl and superoxide radicals are very reactive and usually have short lifetimes to detect. The spin trapping technique is widely used to overcome this problem (Jackson, 2019). The spin trapping agents are diamagnetic compounds (EPR-silent) that interact with free radicals and transform them into more stable radicals (i.e., spin adducts) with longer lifespans (Bagryanskaya et al., 2015). The most commonly used spin trap agents are nitrone compounds such as N-*tert*-butyl- α-phenylnitrone (PBN), α-(4-Pyridyl 1-oxide)-N-*tert*-butylnitrone (POBN), and 5,5-Dimethyl-1-pyrroline *N*-oxide (DMPO) for detection of many radicals such as oxidation radicals (Rana et al., 2010). Some of the examples for PBN use in literature are detection of lipid-oxidation radicals in pork patties (Bolumar et al., 2016), detection of lipid-oxidation radicals in sunflower and extra virgin olive oil (Fadda et al., 2021), detection of lipid-oxidation radicals in semi-solid palm oil (Raitio et al., 2011), and oxidative stability of beer (Lund et al., 2012). Meanwhile, DMPO are used for antioxidant molecules of coffee (Brezová et al., 2009), antioxidant molecules of Tokay wine (Staško et al., 2006); detection of

hydroxyl radicals in white wines (Márquez, Pérez-Navarro, et al., 2019), and detection of hydroxyl radicals in red wine induced by ultrasound (Zhang et al., 2015).

## Spin labeling

Spin labels are widely used to gather structural and dynamic information (e.g., polarity, mobility, and distance measurements) based on the interaction of the spin label with its surrounding molecules (Klare, 2012). However, not all systems (e.g., proteins) have unpaired electrons. Therefore, an external molecule, which has an unpaired electron and a functional group, is introduced to the sample. The introduced molecule, called a spin label, covalently attaches to a functional group of the target molecule and makes them EPR-visible (Klare, 2012). The commonly used spin labels are nitroxide spin labels such as 2,2,6,6-Tetramethyl-1-piperidinyloxy (TEMPO), di-tert-butylnitrocide (DTBN), and phosphatidylcholine [PC(10,3), 1-palmitoyl- 2-palmitoyl(50-doxyl)-sn-glycero-3-phosphocholine]. They are sensitive to environmental conditions (e.g., polarity and viscosity) and are not harmful to biological systems (Krzyminiewski et al., 2014; Sahu & Lorigan, 2015). Among all spin labels, TEMPO was widely used in the studies of model molecule distributions in solid lipid nanoparticle dispersions (Pegi et al., 2003), dose-dependent changes in irradiated wheat, rice, and sunflower seeds (Paktaş & Sünnetçioğlu, 2007), radical quantification in medium-chain triacylglycerol oil (Velasco et al., 2005), and curcumin (Morales et al., 2015).

The terms “spin probes” and “spin labels” are used interchangeably in the literature. Though the principle of spin probes is similar to the spin labels, they do not bond with the target molecules; they make a non-covalent interaction. The spin probes are often used to characterize microenvironments (e.g., mobility and fluidity) such as liposomes, micelles, and cells (Abdel-Rahman et al., 2016; Kong et al., 2018; Serio et al., 2010). Nitroxides, stable free radicals that contain a nitroxyl group with an unpaired electron, such as 5-, 12-, and 16-doxyl-stearic acids (5-DSA, 12-DSA, and 16-DSA) are extensively used to study the membrane fluidity of liposomes (Melnyk et al., 2016; Subongkot & Ngawhirunpat, 2015), physical properties of the plasma membrane (Sgherri et al., 2014), microstructure and microenvironment of amylose-spin probe inclusion complex (Kong et al., 2018), physicochemical properties of aqueous dispersions of nonionic amphiphilic castor oil (Nakagawa, 2009), mobility, and membrane integrity of bacteria (Serio et al., 2010; Tonyali et al., 2019). 5-DSA,12-DSA, and 16-DSA are stearic acid

derivatives that contain a 4,4-dimethyl-3-oxazolinyloxy (DOXYL) group with a nitroxide radical at the $5^{th}$, $12^{th}$, and $16^{th}$ carbon of the acyl chain (Kong et al., 2018; Subongkot & Ngawhirunpat, 2015). Meanwhile, researchers previously utilized another nitroxide compound 4-phenyl-2,2,5,5-tetramethyl-3-imidazoline-1-oxyl nitroxide (PTMIO) study distribution and stability in emulsion-based delivery systems (Yucel et al., 2012) and partitioning and reactivity in nano-structured lipid particles (Uhl et al., 2020).

## Different EPR types

The recording of EPR spectra can be performed at different frequencies such as X-band (8-10 GHz) and Q-band (35 GHz). Q-band EPR spectrometers have higher resolution since the magnetic field magnitude of a Q-band is almost four times the magnetic field magnitude of the X-band. Therefore, peaks with close g-factors, especially in multicomponent food matrices, can be resolved easier in Q-band EPR spectrometers. Moreover, the sensitivity of the Q-band is higher than X-band due to higher frequency. However, Q-band EPR spectrometers have sample size limitation (i.e., less than 5 mg) due to the small sample cavity. The small sample amount can cause problems with replications due to possible sample homogeneity issues. Furthermore, the signal intensity is correlated with sample amount; therefore, EPR spectra of samples analyzed with Q-band have lower signal intensity than the spectra of samples analyzed with X-band. In addition, more X-band spectrometers are available in laboratories than Q-band spectrometers. Therefore, many researchers use X-band EPR spectrometers (Guilarte et al., 2016).

The EPR system that analyzes the interaction of a sample with unpaired electrons to the external magnetic field at a constant frequency by changing magnetic fields is called continuous-wave (CW) EPR spectroscopy. Meanwhile, in the pulse EPR system, the sample is analyzed by exciting a range of frequencies simultaneously with a constant power microwave pulse of a given frequency and magnetic field. Pulse EPR has lower sensitivity than CW EPR due to the large bandwidth of the pulse. In addition, pulse EPR performs better at low temperatures due to short relaxation, while CW EPR can be used at room temperature to collect data. CW EPR is limited with time resolution, while pulse EPR spectroscopy can improve time resolution by studying the interactions individually with pulse sequences (Schweiger & Jeschke, 2001).

# Structural characterization

## Membrane mobility analysis

The cell membrane has a complex and dynamic structure and plays an important role in cell functionality such as permeability and transportation. Therefore, the condition of mobility and fluidity of a cell membrane are generally analyzed to study cell viability. Recently, membrane mobility analysis has been conducted using flow cytometry. However, this method is challenging and time-consuming due to permeabilization and washing steps. Furthermore, the sensitivity might be compromised with cell aggregations (Rieseberg et al., 2001). On the other hand, EPR spectroscopy can provide a non-destructive and disturbing alternative to study membrane mobility using a reporter molecule (i.e., spin probe). After its introduction to the system, the spin probe can align itself with phospholipid molecules in a lipid layer of the membrane and interacts with the membrane (Subongkot & Ngawhirunpat, 2015). The mobility of the spin probe is studied using the parameters of the EPR spectra. The line width and hyperfine splitting constant increase when the mobility of a spin probe is restricted; whereas, the line width is narrow and the hyperfine splitting constant is small when the spin probe moves freely or is partly restricted (Klare, 2012). These changes can be evaluated by using a parameter called order parameter (Rottem et al., 1970). The order parameter is the ratio of hyperfine splitting in the sample to the hyperfine splitting if the spin label was immobilized in a rigid environment (Equation 3). The components of the equation are read from the EPR spectra (Figure 1-5). The order parameter indicates orientational order and is 0 in the fast tumbling spectra and 1 in the rigid spectra (Glover et al., 1999). Values between 0 and 1 represent the intermediate motion of the spin probe. Researchers have widely used lipid-soluble fatty acid spin probes, such as 5-DSA and 16-DSA, to study the different layers of membranes (Nakagawa, 2003; Sgherri et al., 2014), the change in the membrane structure under the external stress such as essential oils (Serio et al., 2010), azole treatment (Sgherri et al., 2014), and heating (Tonyali et al., 2019), change in the physical state of human cell membranes under an external oxidative stimulus (Kveder et al., 2004), effects of oxidation on the membrane properties of retina photoreceptors in the presence of an antioxidant (Duda et al., 2017), characterization of amylose inclusion complexes (Kong et al., 2018), the effect of liquid oil on the distribution and reactivity of a hydrophobic solute in

solid lipid nanoparticles (Yucel et al., 2013), and solute distribution and stability in emulsion-based delivery systems (Yucel et al., 2012).

$$Order\ parameter = \frac{A_{zz} - A_{xx}}{A_{zz,max} - A_{xx,min}} \quad \text{Eqn 3}$$

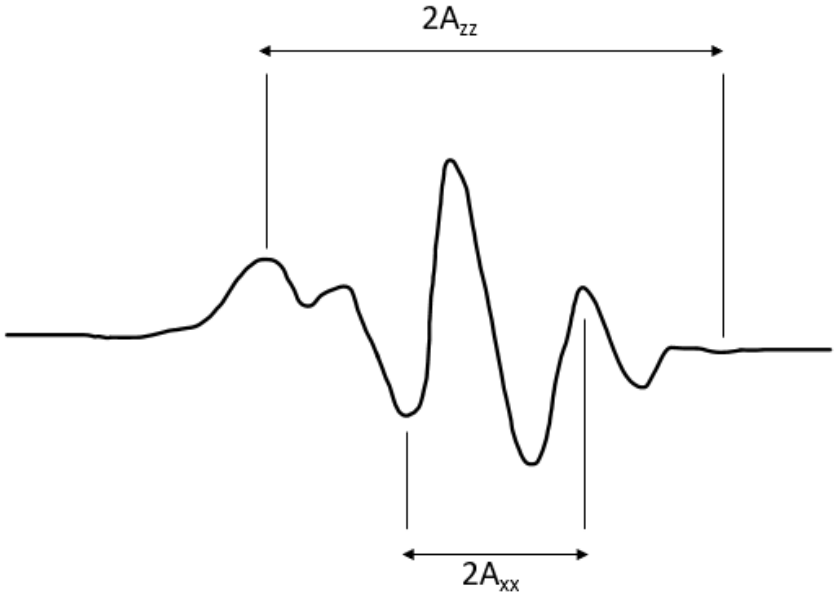


**Figure 1-5** EPR parameters to calculate order parameter

## Protein analysis

Proteins are important biomolecules in food and related matrices since they have various functions such as emulsification in the food industry, transportation in cells, and acting as a messenger (Li et al., 2021). Therefore, gathering information about the physical properties of proteins such as structure and conformational dynamics, is vital to understand their functions (Sahu & Lorigan, 2018). Nuclear magnetic resonance (NMR) spectroscopy is used for structural characterization of proteins, it is often limited by the size and complexity of proteins or micelle systems (Sahu & Lorigan, 2018). EPR spectroscopy can serve as a suitable technique to collect structure information (e.g., side-chain dynamics and inter-molecular distances) of proteins. Moreover, it is not limited to molecular size, and does not disrupt the structure of the target molecule (Li et al., 2021).

Site-directed spin labeling (SDSL) is a site-specific version of spin labeling and is frequently used for proteins and other biomolecules (Klare, 2013). The most common technique of SDSL is

to substitute native non-disulfide-bonded cysteines with other amino acids such as alanine or serine (Sahu & Lorigan, 2018). Then the target protein is mutagenized with a unique cysteine residue and reacted with a sulfhydryl-specific nitroxide reagent to obtain a stable spin label sidechain (Sahu & Lorigan, 2015). An advantage of this method is that size of the target molecule is not a limitation since spin labels are site-specific (Klare, 2013). Therefore, researchers applied the SDSL technique to conduct protein studies such as structural characterization of the transmembrane protein KCNE1 (Coey et al., 2011), characterization of the secondary structure of an inner membrane from *M. smegmatis* (Yu et al., 2021), effects of iron on frataxin protein and its variant (Doni et al., 2020), side-chain dynamics of the lysozyme enzyme of Bacteriophage T4 (Nesmelov & Thomas, 2010), characterization of a receptor in *Escherichia coli* (Klug et al., 1997), the structural characterization of membrane proteins such as sodium/hydrogen antiporter in bacteria membrane (Hilger et al., 2007) and fibril-forming residue protein (Aziz et al., 2010; Drescher et al., 2008). In protein studies, many researchers analyzed secondary, tertiary, and quaternary structures of proteins using the SDSL method. This analysis is based on the reorientation motion of the spin label (e.g., methanethiosulfonate spin label (MTSL)), which is similar to membrane mobility analysis. The line width is typically monitored after the spin label attaches to a protein. For example, the restricted mobility of MTSL causes an increase in line width and hyperfine splitting constant.

Some researchers expanded the use of the SDSL technique to measure molecular size or the distance between different molecules. These measurements are based on magnetic dipolar interactions of two spin labels, which are labeled to the same protein for intramolecular distance or labeled to two proteins for intermolecular distance (Klare, 2012; Sahu & Lorigan, 2018). For example, intramolecular distance in T4 lysozyme (Altenbach et al., 2001; Kazmier et al., 2011), a maltose-binding protein (Nickolaus et al., 2020), an RNA-binding protein (Emmanouilidis et al., 2021), and membrane proteins (Zou & Mchaourab, 2010) while the intermolecular distance between β-lactoglobulin molecules (Kieserling et al., 2021) were studied. Continuous-wave EPR spectroscopy can provide distance and structure information of proteins when the distance between two spin labels is below 2 nm (Klare, 2012; Sahu & Lorigan, 2018). However, researchers faced some challenges such as difficulty in preparing proteins in their natural environment and decreased sensitivity due to high protein concentration using these methods (Zou & Mchaourab, 2010). Jeschke & Polyhach, (2007) suggested optimization of solvent to

extend relaxation times and/or use of optimum excitation bandwidths, which are at higher frequencies than X band (9–10 GHz) to increase sensitivity. Other researchers followed different approaches such as reconstitution of membrane protein in the presence of unlabeled proteins, use of large lipid/protein molar ratios, use of restricted spin label probes, and use of Q-band pulse EPR measurements to overcome these issues (Cunningham et al., 2015; Endeward et al., 2009; Georgieva et al., 2008; Polyhach et al., 2012; Zou & Mchaourab, 2010).

# Irradiation Detection

## Introduction to food irradiation

Irradiation (mostly gamma rays) has been used as a preservation technique in a variety of food products since 1957 (Farkas & Mohácsi-Farkas, 2011). Commercially available irradiated food products include spices, herbs, fresh fruits and vegetables, meat and poultry products for human consumption, as well as chicken jerky treats, pig ears, dog chews, bones, and sweet potato treats for pet consumption (Miller, 2005). The Food and Drug Administration (FDA) approved the use of irradiation in both human and animal food products below a predetermined threshold value (irradiation dose) specific to product type as shown in Table 1-1 (FDA (The Food and Drug Administration), 2001, 2015). The irradiation dose is the amount of applied irradiation energy per unit weight of food product and is given in Gray (Gy) units.

**Table 1-1** Allowed irradiation dose for different types of human food and pet food products (Code of Federal Regulations, 2018).

| Food Product | Maximum Dose Limit (kGy) |
|---|---|
| Control of microbial pathogen on seeds for sprouting | 8 |
| Microbial disinfection of herbs and spices | 30 |
| Control of foodborne pathogens in frozen/ uncooked poultry | Frozen: 7<br>Uncooked: 4.5 |
| Control of foodborne pathogens and extension of shelf life in frozen/ refrigerated meat products | Frozen: 7<br>Refrigerated: 4.5 |
| Control of *Salmonella* in eggs | 3.5 |
| Feed ingredients, animal treats and chews | 50 |
| Control of foodborne pathogens in fresh or frozen molluscan shellfish | 5.5 |
| Control of foodborne pathogens in chilled or frozen raw, cooked, or partially cooked crustaceans or dried crustaceans | 6 |

The maximum irradiation dose is determined based on the type of food as well as the required outcome. For example, irradiation doses used for inhibition of sprouting (e.g., in potatoes and onions) are typically below 1 kGy, while irradiation doses used for pest control (e.g., in papayas) and commercial sterilization of spoilage microorganisms (e.g., *E.coli* in ground beef) are between 1-10 kGy and 10-50 kGy, respectively. Much higher doses (i.e., up to 100 kGy) can be used for special foods, such as astronaut food for complete sterilization (Miller, 2005). Although the irradiation process is accepted as safe within limits, some health concerns persist about this process. The worries such as the formation of radiolytic compounds (e.g., 2-alkylcyclobutanones (2-ACB)) with irradiation causes labeling requirements for irradiated products (Crews et al., 2012). In the last decade, the problems with irradiated pet food products, such as pig ears for dogs in the U.S., jerky pet treats for dogs and cats in the U.S., and cat foods

in Australia raised health concerns again (FDA, 2014). Although the actual reason for these problems is still largely unknown, it shows a need to develop reliable methods to differentiate the irradiated products, quantify the irradiation doses, and monitor whether the food commodity complies with the regulations or not (Ahn, Sanyal, Park, Lim, & Kwon, 2014).

The techniques suitable for characterization of the irradiation history of products commonly target the formation of certain chemical markers specific to the irradiation process. For example, hydrocarbon and 2-ACB analysis by gas chromatography, damaged DNA analysis by DNA comet assay, and silicate minerals analysis by thermoluminescence are some techniques used for irradiation detection (Ahn et al., 2014; Chauhan et al., 2009). However, these methods have challenges such as tedious sample preparation steps or detection limits (D'Oca & Bartolotta, 2018).

## Analysis of irradiation-specific lipid radiolysis products using gas-chromatography mass spectrometry (GC-MS)

2-ACB formation is unique to the irradiation process; therefore, 2-ACB can be used as irradiation markers in lipid-rich foods. Among 2-ACBs, 2- dodecylcyclobutanone (2-DCB), radiolysis product of palmitic acid, and 2-tetradecylcyclobutanone (2-TCB), radiolysis product of stearic acid, have been extensively studied (Blanch et al., 2009; Campaniello et al., 2019; Gadgil et al., 2005). These radiolysis products are cyclic compounds with the same number of carbon atoms as their precursor fatty acids with an alkyl group (Campaniello et al., 2019). Since the formations of these products are only triggered by irradiation, their concentrations can be correlated to irradiation dose in foods (Taghvaei et al., 2020). Many researchers supported the hypothesis that 2-DCB is a radiation-specific compound based on the absence of 2-DCB in non-irradiated foods such as prawns (Chen et al., 2011), turkey, duck, beef, pork, and chicken meat (Campaniello et al., 2019), dried filefish (Kwon et al., 2007), pork (Li et al., 2017), and dairy products (Zianni et al., 2021). An increase in 2-DCB concentration with increasing irradiation dose was observed in the range of 0.5-5 kGy for dairy products (Zianni et al., 2021), 0.5-7 kGy for ground beef (Gadgil et al., 2002; Zhao et al., 2012), 3-10 kGy for filefish (Kwon et al., 2007), 1-5 kGy for chicken and 1-2 kGy for eggs (Tewfik, 2008).

The irradiation detection using 2-DCB in lipid-rich foods is proposed in the European Standard of EN 1785 (European Committee for Standardization (CEN), 2003). This reference procedure contains fat extraction using Soxhlet, clean-up step, and detection of 2-ACBs by gas chromatography-mass spectrometry (GC-MS). Therefore, this method requires a large solvent volume and time-consuming extraction and clean-up steps (Gadgil et al., 2005). Recently, researchers proposed a headspace solid-phase microextraction (SPME) method since SPME is a fast and solvent-free alternative to Soxhlet extraction (Campaniello et al., 2019). In addition, analytes even at low concentrations can be extracted from headspace and concentrated on the fiber (Blanch et al., 2009). Previously, 2-DCB detection using SPME is conducted in chicken jerky treats with glycerol (Taghvaei et al., 2020), chicken, turkey, duck, beef, and pork (Campaniello et al., 2019), ground beef patties (Caja et al., 2008; Soncin et al., 2012), dairy products (Zianni et al., 2021), chicken fat (Taghvaei et al., 2021), and dry-cured ham (Blanch et al., 2009). Some researchers pointed out that 2-DCB was detected in the irradiated samples even at doses as low as 0.5 kGy in meat samples, beef patties, and cured ham (Blanch et al., 2009; Campaniello et al., 2019; Soncin et al., 2012). These researchers identified 2-DCB in irradiated samples; however, a few of them conducted quantification analysis in ground beef patties (Soncin et al., 2012) and chicken fat (Taghvaei et al., 2021).

The efficiency of the SPME method depends on many external parameters such as fiber type, extraction time, incubation temperature, and internal parameters such as food composition and food additives (Caja et al., 2008; Taghvaei et al., 2020). Previously researchers attempted to optimize the external parameters for their samples in the studies such as the fiber type, incubation temperature, and extraction time for irradiated ground beef (Caja et al., 2008); incubation temperature and extraction time for irradiated ground beef patties (Soncin et al., 2012); fiber type and extraction time for dry-cured ham (Blanch et al., 2009); fiber type for chicken jerky treated with glycerol (Taghvaei et al., 2020). Meanwhile, a few studies investigated the effect of internal parameters such as the effect of glycerol addition to chicken jerky treats (Taghvaei et al., 2020), the effect of matrix composition (e.g., fat, salt, and moisture content) of dairy products (Zianni et al., 2021) and meats (Campaniello et al., 2019) on 2-DCB extraction. Some researchers introduced an internal standard (IS) into the SPME method to address the matrix effect. IS, also, accounts for analyte loss during sample preparation, which improves the precision of 2-DCB quantification.

Although there is an increasing number of 2-DCB studies using the SPME method in the literature, these studies are limited to lipid-rich products. However, the irradiation process is approved for many food commodities, including fruits and vegetables lacking lipids. Hence, there is a need for an irradiation detection method to analyze these samples.

## EPR spectroscopy to characterize irradiation as a suitable technique

EPR spectroscopy is suitable for detecting irradiation and potentially quantify the irradiation process since it can directly analyze irradiation-specific free radicals. Currently, the application of the EPR technique for irradiation history detection is standardized by the European Committee of Normalization (CEN). However, the food systems are often complex multicomponent systems; therefore, each food matrix (i.e., plant or animal-based) leads to different types of irradiation-induced radicals (Tomaiuolo et al., 2018). Therefore, the standard methods are based on the origin of irradiation markers: cellulose (EN 1787,2000), crystalline sugar (EN 13708,2001), and bones (EN 1786,1996). For example, cellulose-derived radicals give a triplet peak signal with one center peak (g = 2.0050) and two satellite peaks (located left and right of the center peak with a hyperfine splitting constant of 3 mT) (Raffi et al., 2000). Meanwhile, the European Standard of EN 13708 (2001) proposes that the peak located at g around 2.0035 is due to crystalline sugar. In addition, this method mentions that EPR spectra of crystalline-sugar derived radicals contains multiple peaks since fruits and vegetables have various sugars (e.g., fructose and glucose).

The EPR spectra can also be analyzed for quantification of free radicals. The peak-to-peak height is correlated to the amount of free radical in a sample. Furthermore, the amount of free radicals is proportional to irradiation dose (D'Oca & Bartolotta, 2018). Indeed, EPR spectroscopy is the standard method of analysis for quantifying the irradiation dose with alanine dosimeters, which are typically used as a reference for the calibration of dosimetry systems (Morsy, 2012).

## Cellulose-derived Radicals

The samples with plant origin exhibit a specific EPR spectrum after irradiation. Currently, the European Standard of EN 1787 (2000) proposes an EPR spectroscopy method to analyze irradiated food commodities that contain cellulose. The method is validated using pistachio

nutshells, paprika powder, and fresh strawberries by interlaboratory studies (European Committee for Standardization (CEN), 2000). Many researchers investigated irradiated samples using this method. The EPR spectra of irradiated plant origin foods consist of a triplet peak with a signal intensity ratio of 1:2:1 (Aleksieva & Yordanov, 2018; Raffi et al., 2000). The triplet is structured with a center peak ($g=2.0050 \pm 0.0020$) and two satellite peaks. The satellite peaks are the outermost peaks with a hyperfine coupling of 3 mT and are located on the left and right of the center peak. This specific EPR spectra is a signature of irradiation-specific cellulose-derived radicals and hence, used for irradiation process identification in cellulose-containing foods. Similar EPR spectra were reported for oranges (Jo et al., 2018), apples, pears, peaches, and apricots (Yordanov & Aleksieva, 2009), sea algae (Ahn et al., 2014), sweet potatoes (Tonyali et al., 2020), gingers (Yamaoki et al., 2010), peanuts (Momchilova et al., 2019), and spices (Ahn, Sanyal, Akram, & Kwon, 2014).

The singlet and the center peak of the sextet signal overlap with the center peak of an irradiated sample signal. For this reason, the European Standard of EN 1787 (2000) accepts the presence of cellulose satellite lines as evidence for irradiation treatment. However, researchers who studied the decay constants and saturation characteristics of signals concluded that the central line in irradiated samples is composed of both native (weak singlet or sextet) and irradiated (part of triplet) signals (Korkmaz & Polat, 2001; Raffi et al., 2000).

The European Standard of EN 1787 (2000) mentions that cellulose-derived radicals are detected in solid and dry parts of foods (European Committee for Standardization (CEN), 2000). Free radicals are not stable in an aqueous environment such as the flesh of fruits; therefore, early studies focus on lower-moisture content environments such as seeds of dates (Ghelawi et al., 2001), stones, seeds, and shells of pistachio, apricot, walnut, and hazelnut (Raffi et al., 2000), and seeds of melon, pumpkin, and sunflower (Sin et al., 2006). The European Standard of EN 1787 (2000) states that identification of cellulose-derived radicals is evident of irradiation; however, lack of signal does not prove that the sample is unirradiated (European Committee for Standardization (CEN), 2000).

Since not all fruits and vegetables have stones, seeds, or shells, some researchers attempted to extract the free radicals from the food matrix or decrease the moisture content of the samples to study cellulose-derived radicals. De Jesus, Rossi, & Lopes, (1999) observed cellulose-derived radical signals in kiwi, tomato, and papaya after applying an alcoholic extraction method to

remove water, soluble fraction, and solid residue from fruit pulp. Later, Delincée & Soika, (2002) had a similar observation for strawberries and papayas. Other studies attempted to stabilize and concentrate the radicals by drying them. Some researchers air-dried leafy greens (Prasuna et al., 2009) and senna (Sezer et al., 2019). Others oven-dried carrots, cluster beans, and beetroots (Prasuna et al., 2008), pears, apples, peaches, apricots, avocado, kiwi, and mango (Yordanov & Aleksieva, 2009), while others freeze-dried orange flesh and peels (Jo et al., 2018), and sweet potato flesh and skin (Tonyali et al., 2020) to improve the signal intensity and stability of radicals. Yordanov & Aleksieva, (2009) compared air-dried and oven-dried irradiated fruit samples and observed that the shape of the spectra was not affected by the temperature. However, they mentioned that the oven-dried samples had lower signal intensities compared to air-dried samples. Another research team compared alcoholic extraction of irradiated spices to conventional drying methods and noticed an increase in the intensity of the cellulose-derived radicals peaks in alcohol-extracted samples (Ahn et al., 2014). Jo et al., (2016) applied a combination of alcoholic extraction and oven drying to orange flesh and peels. They mentioned that the extracted and oven-dried samples had higher signal sensitivity than freeze-dried samples since relative total fiber content increased with the removal of alcohol-soluble fruit components during extraction.

The stability of free radicals can also be affected by external conditions such as temperature and humidity of storage conditions (D'Oca & Bartolotta, 2018). Therefore, researchers studied signal intensity and peak shape over a storage period of 10 days to 2 years. As a result, the differentiation of unirradiated from irradiated walnuts for over 2 years for doses above 0.9 kGy (Tomaiuolo et al., 2018), oranges for over 6 weeks for doses above 2 kGy (Jo et al., 2018), and blue plums and peaches for over a year for doses above 10 kGy (Yordanov & Pachova, 2006) was possible.

## Crystalline Sugar-Derived Radicals

Non-irradiated fruits have a singlet, which can become complex spectra after irradiation. This can be due to the different kinds of sugars (e.g., fructose, glucose, and disaccharides) present in the fruits. The European Standard of EN 13708 (2001) describes an EPR spectroscopy method for detecting irradiation in food samples that contain crystalline sugars. The method is validated

using dried figs, dried mangoes, dried papayas, and raisins by interlaboratory studies (European Committee for Standardization (CEN), 2001). The European Standard of EN 13708 (2001) states that the presence of multicomponent EPR spectra is evident of irradiation; however, the absence of the specific spectrum does not prove that the sample is unirradiated (European Committee for Standardization (CEN), 2001).

Guzik & Stachowicz, (2016) mentioned that the distinction of irradiation treatment is very simple due to the multipeak spectrum of irradiated samples compared to weak single EPR lines of non-irradiated samples. Various complex and multipeak EPR spectra can be obtained depending on the type and composition of sugars in irradiated foods. Therefore, the radicals generated from these sugars under irradiation are combined under the name "crystalline sugar derived radicals" and the EPR spectrum is identified as "sugar-like" spectrum (Aleksieva & Yordanov, 2018). This "sugar-like" spectrum is different from the spectrum of starch derived radicals. The starch-derived radicals have a single broadened peak with a split-peak at g factor of 2.0056 ± 0.0003 (Bertolini et al., 2001; Dyrek et al., 2007). Studies on dried figs and raisins (Bayram & Delincée, 2004), rhizome and gardenia fruit (Song et al., 2009), and skins of raisins and figs (Yordanov & Pachova, 2006) showed that the signal centered around g = 2.0035-2.0040 is attributed to crystalline sugar-derived radicals, which is in agreement with EN 13708 (2001). One of the major limitations of sugar radicals is the crystallinity of the environment of the sugar radicals. Researchers did not observe sugar radical signals in irradiated dried apricots (Bayram & Delincée, 2004) and irradiated evodia fruit (Song et al., 2009), although these fruits are rich in sugar. They explained that the sugar should be in crystalline form to stabilize free radicals in order to produce an EPR signal. This agrees with The European Standard of EN 13708 (2001). Similar results were reported by Yordanov et al., (2006) for freeze-dried blue plum, apricot, peach, and melon. The result was attributed to the restricted movement of sugar molecules in reduced water amount and low-temperature conditions. The sugar molecules could not transport to the surface of the fruits where the crystallization might take place during lyophilization. Guzik et al., (2015) observed that the signal intensity from irradiated pineapple was higher than that of irradiated fig in a comparison study of irradiated fruits where the fig is richer in sugar content than pineapple (Guzik et al., 2015). The researchers concluded that the signal intensity is correlated with crystalline sugar rather than the total sugar content of the fruit (Guzik et al., 2015).

Since the sugar-derived radicals needed to be in crystalline form to exhibit an EPR signal, their stability is usually long. In one of the early studies, Stachowicz et al., (1995) showed that the seeds of figs and dates carried sugar-like EPR spectra for over a year. Later, Yordanov & Pachova, (2006) observed that the EPR spectra of figs are the superposition of signal of sugar-like radicals coming from pulp and signal of radicals coming from seed. While different decay constants support this hypothesis, the identification of irradiation treatment is possible up to 100 days. The EPR spectra for radicals derived from irradiated white sugar, glucose, and fructose were recorded for 11 months, although the signal shape of irradiated fructose changed noticeably during this period. It was attributed to the transformation of fructose radicals (Yordanov & Georgieva, 2004). "Sugar-like" EPR spectra were observed for peony roots for 30 days after irradiation (Yamaoki et al., 2015). Yordanov & Aleksieva, (2007) recorded "sugar-like" EPR spectra from papaya, melon, cherry, and fig dehydrated by osmosis stored at low humidity and dark for over 7 months and suggested that The European Standard of EN 13708 can be successfully used to differentiate irradiation in these samples for prolonged times. Recently, Karakirova & Yordanov, (2020) collected an EPR signal from irradiated sugar stored over 6 years; although the signal intensity differed with storage conditions (i.e., in a quartz tube or a plastic bag).

The multiline spectra of irradiated fruits are the results of overlapping signals of different sugar-derived radicals. Recently, researchers studied various monosaccharides such as mannose (Guzik et al., 2019; Guzik & Stachowicz, 2012), glucose and fructose (Yordanov & Georgieva, 2004), disaccharides such as lactose and trehalose (Karakirova et al., 2010), L-sorbose (Guzik & Stachowicz, 2016), and polysaccharides such as amylose and amylopectin (Yamaoki et al., 2010) to identify signals individually. Guzik & Stachowicz, (2012) mentioned that EPR spectra of irradiated mannose contains three major broad peaks overlapping a doublet signal and a quartet signal. Yordanov & Georgieva, (2004) obtained multiline spectra with the center peak located at g factor of 2.0035 ± 0.0002 from irradiated sucrose. Meanwhile, irradiated lactose has a four peak EPR spectrum. These peaks have a signal intensity ratio of 1:7:7:1 with a hyperfine splitting constant of 1.3 mT (Karakirova et al., 2010; Truby & Storey, 1959). Researchers described that the spectra of fructose-derived radicals have a main peak located at a g factor of 2.005 and minor peaks with a hyperfine splitting constant of 1.6 mT from the main peak (Yamaoki et al., 2010; Yordanov & Georgieva, 2004). Similarly, glucose-derived radicals have a

main peak located at a g factor of 2.005 with a hyperfine peak separated by 1.7 mT (Yamaoki et al., 2010; Yordanov & Georgieva, 2004). Another monosaccharide that researchers studied under irradiation is L-sorbose. The EPR spectra of L-sorbose radicals exhibit four broad lines with a signal intensity ratio of 1:3:3:1 (Guzik & Stachowicz, 2016). These hyperfine peaks are separated from each other with 1.8 ± 0.2 mT.

## Carbonate-derived Radicals

The European Standard of EN 1786 (1997) states an EPR spectroscopy method for detection of irradiation in meat and fish samples that contain bone. The method is validated using beef bones, trout bones, and chicken (European Committee for Standardization (CEN), 1997). In addition, they expanded the EPR method to all meat and fish species that contain bones since irradiation-derived radicals are based on hydroxyapatite, which is the principal component of bones. Bone constitutes a large amount of hydroxyapatite [$Ca_{10}$ $(PO)_4$ $(OH)_2$ ], while the remaining fraction is collagen (D'Oca & Bartolotta, 2018). Before irradiation, bone-containing samples have a singlet EPR signal with a g factor around 2.005. This signal is attributed to organic radicals derived from the bone marrow of calcified tissue (D'Oca & Bartolotta, 2018). In addition, some researchers reported a sextet signal in non-irradiated samples, a signature signal of $Mn^{2+}$ ions (Bercu et al., 2012, 2017), meanwhile, others studied EPR-silent samples before irradiation (Chawla et al., 1999; Duliu, 2000; Engin & Demirtas, 2004).
After irradiation, samples with bone tissue consist of two kinds of paramagnetic species, one from bone collagen and another one from carbonate-derived radicals (Chauhan et al., 2009). The latter is more stable as they are trapped in the hydroxyapatite matrix. The carbonate-derived radicals ($CO_2^-$, $CO_3^-$, $CO_3^{3-}$) have an asymmetric signal with a g factor around 2. Among them, $CO_2^-$ is the widely used indicator for irradiation with the signal located around g=1.9970, while $CO_3^{3-}$ (g=2.0034) is generally attributed to be important in the cases of food products that are heat-processed before irradiation (Callens et al., 1998; Stachowicz et al., 1995; Strzelczak et al., 2001). Thus, these radicals were used to identify irradiation in a wide range of foods such as cuttlefish (Duliu, 2000), crayfish (Bercu et al., 2017), lamb leg and rib (Chawla et al., 2002), chicken legs (Chawla & Thomas, 2004), sea mollusk and pearl oyster (Strzelczak et al., 2001), egg shells (Engin & Demirtas, 2004), shellfish (Bhatti et al., 2012), crab carapace (Abdou et al.,

2019), and cow bones (Rudko et al., 2009). In addition, researchers mentioned that the irradiation-specific carbonate radicals are derived in crustaceans (e.g., crayfish and crab) and invertebrates (e.g., oyster, mussel, cuttlefish etc.) from their calcium carbonate-rich cuticles and shells. Similarly, carbonate-derived radicals from bones such as lamb bones, cow bones, and chicken legs are due to hydroxyapatite region and trapped in crystalline bone structure.

The European Standard of EN 1786 (1997) states that the detection limits and stability of carbonate-derived radicals highly depend on the degrees of mineralization and crystallinity of the hydroxyapatite region of the bone-containing sample (European Committee for Standardization (CEN), 1997). Indeed, the early studies showed that the signal intensity of carbonate-derived radicals was affected by various factors, such as bone density and the crystal and mineral structure of bone (Chawla & Thomas, 2004; Stachowicz et al., 1993, 1995). These studies showed that the EPR spectra shape was similar for bones obtained from different parts of animal carcasses, however, with different signal intensity. This observation was attributed to differences in chemical composition (i.e., smaller hydroxyapatite region leads to lower signal intensity) and degree of crystallinity of the bones (i.e., higher the crystallinity, higher the signal intensity) (Chawla et al., 1999; Gray & Stevenson, 1989).

The carbonate-derived radicals in bone samples such as cow bones were not affected by heat treatment (i.e., boiling) (European Committee for Standardization (CEN), 1997). For example, radicals in freshwater crayfish remained unchanged after isothermal annealing at 200 °C for six hours (Bercu et al., 2017) and in cow bones tissue after annealing up to 210 °C for 30 minutes (Rudko et al., 2009). In addition, Tomaiuolo et al., (2019) applied oven-drying, freeze-drying, and sample ashing to irradiated mechanical separated meat in order to obtain EPR spectra without the interference of other radicals such as lipid-radicals. The researchers identified six characteristic peaks from bone fragments in irradiated mechanical separated meat after removal of signals from protein and lipid radicals without disturbing the signal from bone fragments. In comparison, Chawla et al., (1999) noticed a decrease in signal intensity upon boiling or microwave cooking in the irradiated lamb hind leg bone. The same research group later noticed that pressure cooking of irradiated lamb bones significantly decreased the signal intensity of the EPR signal without changing the signal or peak shape (Chawla et al., 2002). The signal intensity changing with heating treatments was mainly attributed to the thermal decay of organic components.

Later studies focused on the dose-response relationship (Engin & Demirtas, 2004; Yarkov et al., 2000). Engin & Demirtas, (2004) suggested egg shells for a dosimeter in irradiation-related incidents since the dose-response relationship of egg shells is linear within the range of 3 Gy-10 kGy. The signal intensity of $CO_2^-$ radicals derived from the mineral part of the cuttlefish bone increased with irradiation dose up to 10 kGy (Duliu, 2000). Similarly, the signal intensity of $CO_2^-$ radicals derived from porcine, bovine, and chicken linearly increased with irradiation dose (0-10 kGy) (Yarkov et al., 2000). Chawla et al., (2002) showed that the irradiation dose significantly increased the signal intensity of carbonate-derived radicals in lamb leg and lamb rib bones in the range of 0-10 kGy. The concentration of carbonate-derived radicals from irradiated calcite minerals of crab exoskeleton and their EPR signal intensity increased with irradiation dose up to 30 kGy (Abdou et al., 2019).

The signal intensity of carbonate-derived radicals was analyzed for shelf-life studies. A reduction in signal intensity was observed for irradiated cuttlefish stored at room temperature for three months (Duliu, 2000), irradiated lamb leg at ambient temperature in a screw cap tube for 7 months (Chawla et al., 1999), and irradiated crayfish stored at room temperature for 16 months (Bercu et al., 2017). However, these researchers were able to distinguish samples for irradiation treatment since the EPR signal, even after storage, carried the characteristics of carbonate-derived radicals.

## Lipid Oxidation

### Lipid Auto-oxidation

Lipid auto-oxidation is a free-radical chain reaction that causes the deterioration of fats and lipids. Thus, it can cause undesired changes in the functional, nutritional, and sensorial attributes of foods (Aydın et al., 2021). The reaction has three critical steps: initiation, propagation, and termination.

In the initiation, a hydrogen atom is abstracted from a lipid molecule to generate a lipid radical. The propagation step starts with lipid radicals reacting with oxygen to generate peroxyl radicals- the peroxyl radicals, then, abstract hydrogen from other lipid molecules. Therefore, reactive free radicals are continuously generated. Finally, the radicals come together to form non-radical

species in the termination step (Belitz & Grosch, 2009). A simplified representation of the reactions is given below in Figure 1-6.

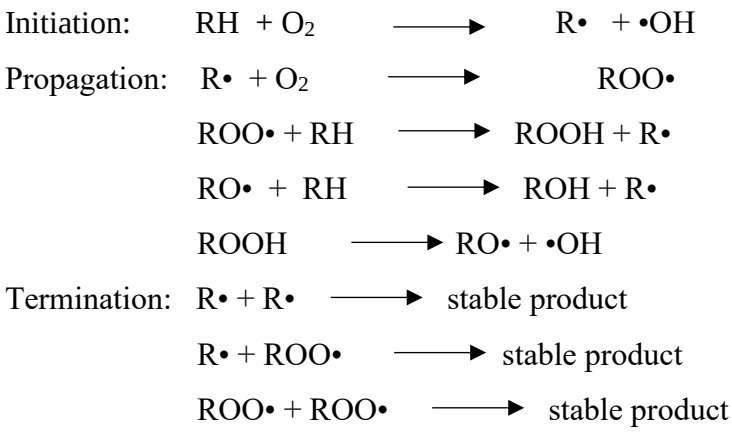


Where RH is a lipid, R• is an alkyl radical, ROO• is a peroxyl radical, •OH is a hydroxyl radical, RO• is an alkoxy radical, ROOH is a lipid peroxide, ROH is a lipid alkoxide. The end products formed in the termination are non-radical stable products (Belitz & Grosch, 2009).

**Figure 1-6** A representation of a lipid oxidation reaction**.**

## Irradiation-triggered lipid oxidation

Prooxidants are factors or compounds that initiate or accelerate lipid oxidation reactions. Prooxidants accelerate the reaction rate either by interacting with unsaturated fatty acids to form lipid peroxides (e.g., interference of lipoxygenase enzyme) or by promoting the formation of free radicals (e.g., irradiation treatment). Irradiation causes the formation of hydroxyl radicals (•OH) from water molecules. Hydroxyl radicals are very reactive free radicals; therefore, they abstract hydrogen (H) from lipid molecules (RH) and generate lipid radicals (R•) (McClements & Decker, 2017).

## Measurement of lipid oxidation

The lipid oxidation products vary with time, oxidation status, mechanism, and lipid source. For example, a single lipid can have different unsaturated fatty acids and can participate in various reactions depending on the presence/absence of prooxidants and antioxidants. As a result, many

decomposition products are formed. Therefore, the analysis of lipid oxidation is a complicated and challenging task.

Primary lipid oxidation products are compounds that are formed during initiation and propagation. Some of the analytical assays used for the analysis of primary lipid oxidations are conjugated double bonds and peroxide value determinations (Velasco et al., 2005). Removal of hydrogen from polyunsaturated acid forms conjugated double bonds compounds. The amount of conjugated double bonds compounds is measured using spectrophotometric methods. However, this method is not accurate for complex food systems since other compounds can also absorb the same wavelength with conjugated double bonds compounds causing interference. Another method to study the primary products is the peroxide value determination. This peroxide value determination is based on the oxidation of an indicator compound (e.g., iodine) by peroxides. This titration method is not very sensitive due to the high detection limit (McClements & Decker, 2017). One of the disadvantages of studying primary products is that they are not volatile and do not directly affect the flavor or aroma of the food. Therefore, they cannot be detected with sensory analysis. Moreover, they undergo the termination reactions after initiation and propagation, and their formation rates are slower than their decomposition rates at the latter stages of lipid oxidation.

Secondary lipid oxidation products are decomposition products of hydroperoxides. These products can be analyzed using the 2-Thiobarbituric Acid Reactive Substances (TBARS) assay, GC-MS, and anisidine value assay (Velasco et al., 2005). In anisidine value assay, the reaction between compounds with carbonyl groups (i.e., a functional group of C=O) and anisidine is measured spectrophotometrically. TBARS assay is based on the reaction between thiobarbituric acid (TBA) and compounds with carbonyl groups. TBARS assay might cause overestimation since TBA reacts not only with secondary reaction products but also other non-lipid carbonyl-containing compounds such as carbohydrates and amino acids (Barriuso et al., 2013). The volatile compounds (e.g., hexanal) can be measured using GC-MS; however, this method requires long analysis time and precise condition adjustments (Eldin, 2010). In addition, the methods for measurements of secondary lipid oxidation products do not provide information on intermediate products and radicals, which are important for understanding reaction mechanisms and kinetics (Merkx et al., 2021).

## EPR measurements for lipid oxidation

Contrary to previous methods, EPR spectroscopy relies on the detection of free radicals produced during lipid oxidation reactions instead of end products and, therefore, can provide information on lipid oxidation reaction steps. Lipid radicals are highly reactive, with half-times of $10^{-2}$ – $10^{-6}$ seconds (Barba et al., 2020). In addition, they become unstable under elevated temperatures and high moisture environments. Roman et al., (2010) used EPR spectroscopy to detect, identify, and determine the lifetime of lipid radicals derived from rapeseed oil. Zhu & Sevilla, (1990) studied autoxidation kinetics of triglycerides at temperatures ranging from 95 to 200 K. However, a more common approach to monitor the formation of unstable free radicals is by forming stable spin adducts with spin traps in liquid environments; the technique also known as spin trapping (Barriuso et al., 2013; Eldin, 2010; Feng et al., 2020; Raitio et al., 2011). Researchers used the spin trapping method to study the inhibiting effect of PBN on lipid oxidation of fish and sunflower oil (Velasco et al., 2005), oxidative stability of salmon viscera oil and cod liver oil (Falch et al., 2005), oxidative stability of extra virgin oil (Papadimitriou et al., 2006), the effect of temperature on palmitic acid (Chen et al., 2017), the early stages of lipid oxidation in dried microencapsulated oils (Velasco et al., 2021), oxidative reactions in semisolid palm oil (Raitio et al., 2011), and effect of antioxidants on oxidative stability of peanut oil (Zhao et al., 2020). Spin trapped lipid radicals are identified with their characteristic hyperfine couplings and g factors (Aydın et al., 2021; Feng et al., 2020; Velasco et al., 2005). However, lipid identification based on hyperfine couplings is sometimes problematic due to line broadening issues. Restriction of rotational mobility of spin adducts might cause line broadening (Raitio et al., 2011; Velasco et al., 2005). Raitio et al., (2011) suggested the line broadening in palm oil samples was due to viscous oil medium environment. While, Velasco et al., (2005) and Falch et al., (2005) mentioned that the reason for line broadening was due to restricted mobility caused by the high molecular volume of PBN-lipid radical adducts.

Other parameters that affect the lipid analysis using EPR spectroscopy are the solubility of spin traps, stability of spin adducts, interaction of spin traps with other molecules, medium properties, etc. For instance, degradation of spin traps in the presence of reducing agents (e.g., ascorbic acid) or interaction of spin traps with antioxidants instead of target radicals would cause inaccurate results (Barba et al., 2020; Roman et al., 2010). Meanwhile, the presence of spin traps in the sample medium can interfere with the oxidation reaction by changing the course of the reaction

pathway and rate. Velasco et al., (2005) had a similar observation in their study with rapeseed oil, sunflower oil, and fish oil. PBN had an inhibiting effect on lipid oxidation in the samples due to the interaction of PBN with peroxyl radicals. Similarly, Cui et al., (2017) mentioned that storage of samples with spin adducts alters the free radical concentration in the system since the spin traps might prevent lipid oxidation of the sample. Therefore, they suggested that spin traps should be introduced to the system right before EPR scans for accurate determination of free radical concentration. However, the lipid oxidation prevention effect of spin traps could cause loss of sensitivity and accuracy of the analysis.

The induction period (IP) is defined as the time at which the concentration of spin adducts had a sharp increase after a slow increase (Fadda et al., 2021). Researchers used EPR spectroscopy to study IP in rapeseed oil, soybean oil, sunflower seed oil, corn oil, peanut oil, palm oil, and fish oil (Jiang et al., 2020); peanut oil (Silvagni et al., 2010); olive oil (Papadimitriou et al., 2006); and sunflower oil and extra virgin olive oil (Fadda et al., 2021). These researchers collected the signal intensity of spin adducts as a function of time and estimated IP from bilinear regression of slow increase period and sharp increase period. Some research groups compared the EPR method to one of the traditional methods for the detection of lipid oxidation such as electrochemical measurements of oxygen depletion in pork meat (Carlsen et al., 2001), rancimat and chemiluminescence in linseed oil and borage oil (Szterk et al., 2011), rancimat in antioxidant added peanut oil (Jiang et al., 2020). These researchers found a correlation between the EPR method and other methods and suggested that EPR spectroscopy is a fast and sensitive method for evaluating IP.

After investigation of lipid radicals and the induction period, researchers shifted their research area to the oxidative stability of oils in the presence of antioxidants. Antioxidants scavenge free radicals formed in the lipid oxidation reactions, as shown in Figure 1-7.

$$ROO\bullet + AH \longrightarrow ROOH + A\bullet$$
$$RO\bullet + AH \longrightarrow ROH + A\bullet$$

Where AH is an antioxidant, ROO• is a peroxyl radical, RO• is an alkoxy radical, ROOH is a lipid peroxide, ROH is a lipid alkoxide.

**Figure 1-7** Interaction of antioxidants with lipid radicals in lipid oxidation

After the donation of a hydrogen atom, A• can further react with lipid radicals or other A• molecules to form non-radical products at the termination stage of lipid oxidation (McClements & Decker, 2017).

Researchers used EPR spectroscopy to study the effects of antioxidants on lipid oxidation in many studies such as citrus peel extracts such as orange, lemon, mandarin, etc. added sunflower oil (Aydın et al., 2021), sunflower and rapeseed oil systems supplemented with herb extracts such as thyme, basil, oregano, and sage (Kozłowska & Zawada, 2015), tocopherol added corn, canola, and soybean oil (Cui et al., 2017). During these studies, some researchers observed that the signal intensity and the spin adduct formation were affected by the addition of antioxidants. For example, Cui et al., (2017) did not obtain an EPR signal from the tocopherol added corn, canola, and soybean oil until after antioxidant concentration decreased to 50-65% of its initial concentration. The antioxidants in their study inhibited the formation of spin adducts by competing with spin traps to react with lipid oxidation radicals, i.e., peroxyl and alkoxyl radicals (Cui et al., 2017). Similarly, Jiang et al., (2020) found out that the addition of synthetic antioxidants such as dibutyl hydroxytoluene and butylated hydroxyanisole decreased the signal intensity of spin adducts in edible oils (i.e., peanut oil, corn oil, palm oil, rapeseed oil, fish oil, sunflower oil, etc.). Merkx et al., (2021) stated that PBN addition disturbed the oxidation reaction mechanism after observing the degradation of the spin adducts (i.e., ROO-PBN) to alkoxy radical (RO•), benzaldehyde, and 2-methyl-2-nitrosopropane (MNP) under the heat treatment (e.g., 180 °C). The authors mentioned that after degradation MNP formed spin adducts with alkyl radicals (R•). They attributed the hyperfine coupling constants of 14.5 G and 3.2 G to PBN spin adducts (PBN-R) and assigned the second hyperfine interaction with hyperfine coupling constants of 2.1 G to MNP adducts (MNP-R). The researchers suggested the use of both NMR and EPR spectroscopy to study peroxyl radicals (ROO•).

## Measurement of reactive oxygen species (ROS) and reactive nitrogen species (RNS) in other biological systems

Reactive oxygen species (ROS) (e.g., superoxide and hydroxyl radical species) are oxygen-based free radicals generated during metabolic functions such as lipid oxidation (Khan & Swartz, 2002). These radicals play a role in intercellular signaling and frequently interact with lipids,

proteins, and DNA. They are constantly formed in the daily routine of cells and are needed at certain levels. Excess amount of ROS is capable of damaging biomolecules (e.g., nucleic acids and lipids) and cell structure and can cause cell dysfunctionality and diseases such as cancer and neurodegenerative diseases (Khan & Swartz, 2002; Mrakic-Sposta et al., 2014; Suzen et al., 2017). The damage that an excessive amount of ROS causes to the cellular structure is called oxidative stress (Mrakic-Sposta et al., 2014).

Reactive nitrogen species (RNS) (e.g., nitrate, nitrite, and nitric oxide) are nitrogen-based free radicals derived from biological functions. These molecules participate in the regulatory redox mechanism, cellular signaling, and immune response (Locatelli et al., 2009). However, overproduction of these molecules might damage key systems (e.g., DNA and proteins) in biological systems and can cause neurodegenerative and chronic inflammatory diseases (Nash et al., 2012). The damage that an excessive amount of RNS causes to the cellular structure is called nitrosative stress (Nash et al., 2012).

### Traditional Spectrophotometric Assays

The commonly used methods to study ROS and RNS are based on the scavenging activity of antioxidants against these radicals. Antioxidants scavenge and inhibit ROS and RNS production following one of the two mechanisms: electron transfer (e(-)) mechanism or hydrogen (H) atom transfer mechanism (Zang et al., 2017). In the e(-) transfer mechanism, an electron in an antioxidant is transferred to a free radical. In the H atom transfer mechanism, antioxidants donate their H atom to radicals to scavenge them. All antioxidant capacity assays used in literature are based on one of these mechanisms. DPPH (2,2-diphenyl-1-picrylhydrazyl), FRAP (ferric reducing antioxidant power), and ABTS (2,2-azinobis-(3-ethylbenzothiazole-6-sulphonate) assays follow electron transfer mechanism. Meanwhile, other assays such as TRAP (total peroxyl radical trapping antioxidant parameter), TEAC (trolox equivalent antioxidant capacity), and ORAC (oxygen radical absorbance capacity) work with hydrogen atom transfer mechanism (Apak et al., 2016).

These antioxidant assays rely on a UV-vis spectrophotometer to measure color change. Thus, the antioxidant concentration in the sample is correlated to the color change and is expressed as an equivalent of a standard external material (e.g., Trolox, ferulic acid, or vitamin C). However, this correlation is not always reliable, as in some cases the change in absorbance is not due to the

concentration change but other effects such as discoloration due to extraction solvent (Polak et al., 2013). Moreover, many of these assays use different reagents, wavelengths, and solvents which cause variation between them (Li, 2017). For example, an antioxidant can show different radical scavenging activities in different solvents following the same assay (Li, 2017).

### Use of EPR spectroscopy for analysis of ROS and RNS

In contrast to the indirect approach of UV-vis spectrophotometric assays, EPR spectroscopy provides a direct approach by correlating the signal intensity to free radical concentration. In addition, it eliminates the transparent sample limitation of the UV-vis spectrophotometer since it can analyze cloudy samples as well (Jawad et al., 2007). Many researchers use commercially available semi-stable free radicals (e.g., galvinoxyl radical and DPPH) to study antioxidants in sage extracts (Nutrizio et al., 2020); curcumin (Barzegar & Moosavi-Movahedi, 2011); red beetroots (Esatbeyoglu et al., 2014); microemulsions loaded with phenolic antioxidants (Chatzidaki et al., 2015); oregano oil (Assiri et al., 2016); snapdragon seed oil (Ramadan & El-Shamy, 2013); astaxanthin, a feed additive, (Dose et al., 2016); fruit liqueur (Polak & Bartoszek, 2015); fruits such as strawberry, mulberry, lemon, and banana (Zang et al., 2017); beer (Polak et al., 2013); honey (Zalibera et al., 2008); coffee (Brezová et al., 2009); pomegranate juice (Kozik et al., 2015); and alcoholic beverages such as martini, red wine, gin, vodka, brandy, and malibu (Bartoszek & Polak, 2012).

These studies focused on the determination of antioxidant activity and radical scavenging activity of samples against DPPH (Bartoszek & Polak, 2012; Brezová et al., 2009; Kozik et al., 2015; Polak et al., 2013; Polak & Bartoszek, 2015; Zalibera et al., 2008; Zang et al., 2017) and against both DPPH and galvinoxyl radical (Assiri et al., 2016; Dose et al., 2016; Esatbeyoglu et al., 2014; Ramadan & El-Shamy, 2013). The latter studied the radical scavenging activity of the antioxidants against oxygen-centered radicals (galvinoxyl radical) and nitrogen-centered radicals (DPPH). Meanwhile, another group investigated these activities using spin traps to capture unstable radicals in antioxidant-rich food samples. Researchers used DMPO or POBN to study radical scavenging activity against hydroxyl radicals in honey (Zalibera et al., 2008), in coffee (Brezová et al., 2009), and in Tokay wines (Staško et al., 2006), radical scavenging activity against ROS in white tea (Azman et al., 2014), and tea extracts (Polovka et al., 2003).

The quantification of antioxidant capacity was performed using external standard curves. Therefore, the antioxidant capacity of the sample was expressed as an equivalence of antioxidant capacity of an external standard such as Trolox. Researchers presented the antioxidant capacities of their samples using Trolox for vegetables such as leek, onion, spinach, and cabbage (Kameya et al., 2014), fruit juices (Bartoszek & Polak, 2016), pomegranate juices (Kozik et al., 2015), and beers (Polak et al., 2013); ferulic acid for white tea (Azman et al., 2014), and vitamin C for fruits such as strawberry, mulberry, and banana (Zang et al., 2017).

Some recent studies focused on the investigation of antioxidant decay kinetics using EPR spectroscopy. For example, Osorio et al., (2011) studied the antioxidant-rich extracts of corozo fruit with ABTS and DPPH radicals separately to differentiate the constituents of its antioxidants (i.e., cyanidin-3-rutinoside, cyanidin 3-glucoside, and peonidin-3-rutinoside) by measuring decay kinetics. Similarly, Pérez-López et al., (2014) investigated the decay kinetics of DPPH in the presence of antioxidants from lettuces with different colors and labeled the kinetic behaviors (e.g., fast- and intermediate-rate) of antioxidants. The authors stated that intermediate-rate antioxidants might be quercetin, while fast-rate antioxidants can be anthocyanins. Thus, there are numerous EPR studies on antioxidant qualification and quantification in the literature, yet there is still a need for further study to expand our knowledge on the kinetic behavior of antioxidants.

## Beer and wine quality

Beer flavor stability is a major quality parameter for the beer industry since it is an indicator for shelf life and freshness (Jenkins et al., 2018; Kocherginsky et al., 2005a; Lund et al., 2012). Therefore, EPR spectroscopy is used to monitor free radical production and breakdown process in beer samples to determine the stability and age of beer (Jenkins et al., 2018; Kocherginsky et al., 2005a, 2005b; Lund et al., 2012). One way to analyze stability is using spin traps to quench free radicals that are formed during the aging of beer (Jenkins et al., 2018). Typically, antioxidants in beer scavenge free radicals until they are depleted (this period is called the lag phase) (Brezová et al., 2002). After the lag phase, the spin traps form spin adducts with free radicals and give an EPR signal (Kocherginsky et al., 2005b). Therefore, the lag phase is used to indicate beer age (Kocherginsky et al., 2005b).

Researchers previously studied the lag phase and the parameters that affect the lag phase such as transition ions (Jenkins et al., 2018), unmalted barley (Kunz et al., 2012), metal ions (Jenkins et

al., 2018), antioxidants and vitamins (Brezová et al., 2002), pasteurization (Lund et al., 2012), and proteins (Kocherginsky et al., 2005b). The authors of these studies suggested the use of EPR spectroscopy for breweries to analyze their beer samples. Moreover, Kocherginsky et al., (2005a) proposed a dimensionless number that includes oxidation reaction kinetics (e.g., rate of hydroxyl radical formation and rate of spin adduct formation) to minimize experimental calibration problems by studying reaction kinetics. In addition, Marques et al., (2017) correlated EPR area data to total staling information from sensory analysis, which shortens the amount of time needed for a sensory evaluation from six months to six days. They also mentioned that they improved the flavor stability of beers in their breweries by using EPR data and sensory analysis as predictive indicators of staling process.

Although reaction steps and radicals are extensively studied in beer, there were not too many studies to detect and identify free radical intermediates in wine until a decade or so. Oxidation of wine takes place when metal-catalyzed reduction of dioxygen triggers a series of reactions that converts ethanol into acetaldehyde (Kreitman et al., 2013). First, oxygen is reduced to hydroperoxyl radicals by transition metals such as iron and copper. Next, hydroperoxyl radicals react with phenolics to form hydrogen peroxide and semiquinone radicals, where hydrogen peroxide further reduces to hydroxyl radicals. The reaction between hydroxyl radicals and ethanol yields ethyl radicals such as 1-hydroxyethyl radical (1-HER) and 2-hydroxyethyl radical. Later, 1-HER is oxidized to acetaldehydes (Kreitman et al., 2013). This series of reactions have a profound effect on wine quality and sensorial attributes since reaction products can alter the flavor, color, and odor (Elias et al., 2009a; Márquez, Contreras, et al., 2019). The traditional methods that are used for wine oxidation analysis (e.g., GC-MS) aim to detect volatile compounds (e.g., 2, 4, 5-trimethyldioxolane) (Escudero et al., 2000). However, these methods are only able to detect later stages of oxidation; therefore, they miss the information about earlier stages, which is important to assess a storage time for wines (Nikolantonaki et al., 2019).

The free radicals (e.g., 1-HER) derived from early and intermediate steps of reactions can be detected by EPR spectroscopy using spin traps. In one of the early studies on this area, Elias et al., (2009a) identified that the major free radical species derived from hydroxyl radical-mediated oxidation of ethanol is 1-HER. Furthermore, the authors mentioned that 1-HER is the most quantitatively abundant free radical in oxidized wine. After this finding, studies focused on the effects of various parameters such as the presence of wine phenolics (Kreitman et al., 2013),

application of ultrasound treatment (Xue et al., 2021; Zhang et al., 2015), application of microwave treatment (Yuan et al., 2021), presence of $SO_2$ (Nikolantonaki et al., 2019), and presence of trace metals (Elias et al., 2009b) on the formation of 1-HER.

Some studies focus on $SO_2$-free wines since the wine industry is in search of alternatives to replace $SO_2$ in wines. $SO_2$ yields sulfurous acid ($H_2SO_3$) and subsequently transforms to bisulfite ($HSO_3^-$) and sulfite ($SO_3^{2-}$) in wines. $HSO_3^-$ acts as an antioxidant since it reacts with hydrogen peroxide. Therefore, researchers substituted $SO_2$ with other antioxidants and studied the antioxidant effects of $SO_2$ alternatives such as chitosan (Castro Marín et al., 2019); inactive dry yeast, natural antioxidants, and freeze-dried extracts of wine industry by-products (e.g., stems) (Marchante et al., 2020a); and chitosan, glutathione, oak and grape seed extracts, and ascorbic acid (Marchante et al., 2020b) on the formation of 1-HER. The investigators concluded that the chitosan in white wine (Castro Marín et al., 2019), grape seed and chitosan in red wine (Marchante et al., 2020b), and inactive dry yeast in red wine could serve as alternative compounds that have antioxidant properties against 1-HER radicals.

# Maillard reaction

## Introduction to Maillard reaction

Maillard reaction is a combination of complex sub-reactions that contributes to color and flavor development in thermally processed foods such as baked (e.g., bread), roasted (e.g., coffee), and dried products (e.g., dried milk). In the initial step, a condensation reaction between a reducing sugar and an amine (i.e., compounds that have a nitrogen atom with a lone pair of electrons) takes place during heating. The products of this reaction subsequently go under Amadori rearrangement to form Amadori products (e.g., 1-amino-1-deoxy-D-fructose). These products are intermediate reaction products of the Maillard reaction. Amadori products can react in several ways (e.g., dehydration and decomposition) to produce different products such as reductones and furfurals (e.g., hydroxymethylfurfural (HMF)). During the final stages of the Maillard reaction, reactive furfural compounds and compounds with amino groups react to form flavor compounds and dark-colored, insoluble, high-molecular-weight pigments called melanoidins (Huber & Bemiller, 2008).

## Traditional techniques to analyze Maillard reaction

Among Maillard reaction products, HMF and Amadori products are mostly used to monitor the reaction. Amadori products, like the other initial stage products, do not absorb UV light; therefore, most of the time, they are studied with high-performance liquid chromatography (HPLC) or liquid chromatography coupled with differential refractometry detection or mass spectroscopy. Yet, colorimetric or fluorimetric assays based on their reaction with a dye are also conducted from time to time. Unlike the Amadori products, HMF has a strong UV absorption; hence, spectrophotometric assays are widely used for the determination of these compounds. Similarly, melanoidins show absorption in UV spectra around 420-450 nm. Some recent attempts to characterize melanoidins include the use of HPLC, GC-MS, and infrared spectroscopy (Silván et al., 2006).

## Analysis of Maillard reaction using EPR spectroscopy

The use of EPR spectroscopy for Maillard reaction-derived free radicals dates back to 1956, where O`Meara et al., (1956) conducted one of the earliest studies on free radicals in roasted coffee. Later, in 1965, Mitsuda et al., (1965) studied melanoidins in a controlled experiment (glycine and glucose mixture) using EPR spectroscopy. Based on these pioneer works, Namiki et al., (1973) heated arabinose and alanine mixture at 100 °C to study radicals directly using EPR spectroscopy. For the first time, they observed two hyperfine couplings in EPR spectra which came from two kinds of radicals. In the early stage of reaction, intermediate radicals gave a complex multiplet EPR signal, whereas later stage radicals gave a single broad line similar to melanoidin signal. The researchers could not identify the radicals back then, however, they presumed that the early stage radicals were derived from amino-carbonyl reactions while the later stage radicals were due to existing radicals in melanoidin structure.

Recent EPR studies investigated the effect of high or low flow of air or nitrogen during roasting of coffee beans (Goodman et al., 2011); roasting time, roasting atmosphere (air or nitrogen), storage period (up to a month), the physical structure of roasted bean (whole, half, and ground) (Yeretzian et al., 2012); storage at high temperature, presence of oxygen and light during storage of milk powder (Thomsen et al., 2005); treatment temperature applied to D-glucose and L-alanine mixture (Mohsin et al., 2018), the storage time for black garlic incubated at 70 °C

(Nakagawa et al., 2020) on free radical formation. Later, Troup et al., (2015) studied the antioxidant properties of molecules (e.g., melanoidins) with respect to roasting time and storage after grinding. In their study, the authors obtained three distinct EPR signals from three different radicals. The first signal was due to endogenous radicals from beans; the second signal was attributed to a stable radical formed during roasting; the third one was associated with roasting-triggered radicals formed during later stages of Maillard reaction. In a recent study, another research group analyzed the signal at 336 mT (g=2.00) from heated black garlic (Nakagawa et al., 2020) and attributed this signal to intermediate Maillard radicals. They stated that unpaired electron of organic radicals reacts similarly to free electrons in EPR analysis. Therefore, organic radicals give a signal at a g factor around 2.00 which is the g-factor of a free electron.

Some researchers mentioned that one of the issues with Maillard-derived free radicals is the identification of radicals that are involved in the formation of melanoidins (Thomsen et al., 2005; Yordanov & Mladenova, 2004). Thomsen et al., (2005) studied the effect of Maillard reaction in milk powder stored at 60 °C on radical types and observed a single peak in EPR spectra due to the late stage of Maillard reaction. Researchers compared g-values of peaks to previous studies, but they could not characterize the origin of free radicals. Therefore, they proposed using other complementary techniques (e.g., NMR) to obtain more information about radicals and therefore, characterize them individually. The same problem surfaced in a free radical study of bread samples with heat-induced paramagnetic species (Yordanov & Mladenova, 2004). The authors mentioned that the EPR spectra had one single peak due to overlapping of different signals; therefore, it was impossible to identify radicals. They stated that the EPR signal is due to thermally generated radicals and it might be attributed to Maillard reaction radicals. They also added that the signal is not attributed to the carbonization process. Carbonization is the conversion of organic substances into carbon at high temperature in the absence of oxygen. The researchers studied at temperatures below 250 °C, which is too low for carbonization reaction. They mentioned that it is necessary to use other analyses such as NMR with EPR spectroscopy to find the origins of the radicals.

There is, indeed, a need for further study to expand the knowledge in Maillard reaction-derived free radicals in different products and processes. The results of future studies can be used to control the type and amount of Maillard reaction products (e.g., melanoidins and free radicals) formed during food processes.

## Conclusion

The main advantages of EPR spectroscopy are its sensitivity and specificity to free radicals. Moreover, it does not require a long analysis time as well as a large amount of sample. Therefore, the EPR spectroscopy can be applied to identify and quantify free radical species in various food reactions important for quality attributes. For example, EPR spectroscopy was used to investigate structures of macromolecules (e.g., proteins) and membranes, to characterize and quantify irradiation-derived radicals, and to study oxidative stability in different types of foods, including but not limited to fruits and vegetables, meat and fishes, oils, and emulsions. To investigate some of these reactions, EPR-silent diamagnetic compounds (i.e., spin traps) can be used to study fast-lived free radicals by transforming them to more stable free radicals with longer lifetimes. In other studies, an external molecule with an unpaired electron and a functional group (i.e., spin label) can be introduced to the sample to gain insight into structural and dynamic properties. In addition, EPR parameters (e.g., hyperfine splitting constant) of fast-tumbling spectra provide information about mobility and polarity of sample environments, while slow-tumbling spectra offer information on the motion and orientation of paramagnetic species.
The studies mentioned in this review support that EPR is a promising technique and powerful tool for many applications. The current methods applied with EPR have many advantages over traditional techniques, yet there is still a need for more research and investigation for wider applications.

# Reference


Abdel-Rahman, E. A., Mahmoud, A. M., Khalifa, A. M., & Ali, S. S. (2016). Physiological and pathophysiological reactive oxygen species as probed by EPR spectroscopy: the underutilized research window on muscle ageing. *The Journal of Physiology*, *594*(16), 4591–4613. https://doi.org/10.1113/JP271471

Abdou, S. M., Ebraheem, S., & Mohamed, R. I. (2019). Spectroscopic studies on irradiated Crab carapace. *Journal of Physics: Conf. Series*, *1253*(012035). https://doi.org/10.1088/1742-6596/1253/1/

Ahn, J.-J., Sanyal, B., Park, E.-J., Lim, H.-K., & Kwon, J.-H. (2014). Effects of sample pretreatments on EPR spectral characteristics of irradiated sea algae – an advanced approach to identify irradiation status. *RSC Advances*, *4*(61), 32312. https://doi.org/10.1039/C4RA03010A

Ahn, J. J., Sanyal, B., Akram, K., & Kwon, J. H. (2014). Alcoholic extraction enables EPR analysis to characterize radiation-induced cellulosic signals in spices. *Journal of Agricultural and Food Chemistry*, *62*(46), 11089–11098. https://doi.org/10.1021/jf502258r

Aleksieva, K. I., & Yordanov, N. D. (2018). Various approaches in EPR identification of gamma-irradiated plant foodstuffs: A review. *Food Research International*, *105*(August 2017), 1019–1028. https://doi.org/10.1016/j.foodres.2017.11.072

Altenbach, C., Oh, K. J., Trabanino, R. J., Hideg, K., & Hubbell, W. L. (2001). Estimation of inter-residue distances in spin labeled proteins at physiological temperatures: Experimental strategies and practical limitations. *Biochemistry*, *40*(51), 15471–15482. https://doi.org/10.1021/bi011544w

Apak, R., Özyürek, M., Güçlü, K., & Çapanoğlu, E. (2016). Antioxidant activity/capacity measurement. 2. Hydrogen atom transfer (HAT)-based, mixed-mode (electron transfer (ET)/HAT), and lipid peroxidation assays. *Journal of Agricultural and Food Chemistry*, *64*(5), 1028–1045. https://doi.org/10.1021/acs.jafc.5b04743

Assiri, A. M. A., Elbanna, K., Al-Thubiani, A., & Ramadan, M. F. (2016). Cold-pressed oregano (Origanum vulgare) oil: a rich source of bioactive lipids with novel antioxidant and

antimicrobial properties. *European Food Research and Technology*, *242*(7), 1013–1023. https://doi.org/10.1007/s00217-015-2607-7

Aydın, S., Sayin, U., Sezer, M. Ö., & Sayar, S. (2021). Antioxidant efficiency of citrus peels on oxidative stability during repetitive deep-fat frying: Evaluation with EPR and conventional methods. *Journal of Food Processing and Preservation*, *March*, 1–10. https://doi.org/10.1111/jfpp.15584

Aziz, A., Hess, J. F., Budamagunta, M. S., Voss, J. C., & FitzGerald, P. G. (2010). Site-directed spin labeling and electron paramagnetic resonance determination of vimentin head domain structure. *Journal of Biological Chemistry*, *285*(20), 15278–15285. https://doi.org/10.1074/jbc.M109.075598

Azman, N. A. M., Peiró, S., Fajarí, L., Julià, L., & Almajano, M. P. (2014). Radical scavenging of white tea and its flavonoid constituents by electron paramagnetic resonance (EPR) spectroscopy. *Journal of Agricultural and Food Chemistry*, *62*(25), 5743–5748. https://doi.org/10.1021/jf501707p

Bagryanskaya, E. G., Krumkacheva, O. A., Fedin, M. V., & Marque, S. R. A. (2015). Development and application of spin traps, spin probes, and spin labels. In *Methods in Enzymology* (1st ed., Vol. 563). Elsevier Inc. https://doi.org/10.1016/bs.mie.2015.06.004

Barba, F. J., Roohinejad, S., Ishikawa, K., Leong, S. Y., El-Din A Bekhit, A., Saraiva, J. A., & Lebovka, N. (2020). Electron spin resonance as a tool to monitor the influence of novel processing technologies on food properties. *Trends in Food Science & Technology*, 421–437. https://doi.org/10.1016/j.tifs.2020.03.032

Barriuso, B., Astiasarán, I., & Ansorena, D. (2013). A review of analytical methods measuring lipid oxidation status in foods: A challenging task. *European Food Research and Technology*, *236*(1), 1–15. https://doi.org/10.1007/s00217-012-1866-9

Bartoszek, M., & Polak, J. (2012). An electron paramagnetic resonance study of antioxidant properties of alcoholic beverages. *Food Chemistry*, *132*(4), 2089–2093. https://doi.org/10.1016/j.foodchem.2011.12.060

Bartoszek, M., & Polak, J. (2016). A comparison of antioxidative capacities of fruit juices,

drinks and nectars, as determined by EPR and UV-vis spectroscopies. *Spectrochimica Acta - Part A: Molecular and Biomolecular Spectroscopy*, *153*, 546–549. https://doi.org/10.1016/j.saa.2015.09.022

Barzegar, A., & Moosavi-Movahedi, A. A. (2011). Intracellular ROS protection efficiency and free radical-scavenging activity of curcumin. *PLoS ONE*, *6*(10), 1–7. https://doi.org/10.1371/journal.pone.0026012

Bayram, G., & Delincée, H. (2004). Identification of irradiated Turkish foodstuffs combining various physical detection methods. *Food Control*, *15*(2), 81–91. https://doi.org/10.1016/S0956-7135(03)00018-5

Belitz, H.-D., & Grosch, W. (2009). *Food Chemistry*. Forth Edition, Springer-Verlag Berlin Heidelberg New York.

Bercu, V., Negut, C. D., & Duliu, O. G. (2012). Detection of irradiated frog (Limnonectes macrodon) leg bones by multifrequency EPR spectroscopy. *Food Chemistry*, *135*(4), 2313–2319. https://doi.org/10.1016/j.foodchem.2012.07.015

Bercu, V., Negut, C. D., & Duliu, O. G. (2017). Irradiation free radicals in freshwater crayfish Astacus leptodactylus Esch investigated by EPR spectroscopy. *Radiation Physics and Chemistry*, *133*(December 2016), 45–51. https://doi.org/10.1016/j.radphyschem.2016.12.008

Bertolini, A. C., Mestres, C., Colonna, P., & Raffi, J. (2001). Free radical formation in UV- and gamma-irradiated cassava starch. *Carbohydrate Polymers*, *44*(3), 269–271. https://doi.org/10.1016/S0144-8617(00)00268-X

Bhatti, I. A., Akram, K., & Kwon, J. (2012). An investigation into gamma-ray treatment of shellfish using electron paramagnetic resonance spectroscopy. *Journal of the Science of Food and Agriculture*, *92*(4), 759–763. https://doi.org/10.1002/jsfa.4639

Blanch, G. P., Caja, M. del M., Flores, G., & Castillo, M. L. R. del. (2009). Identification of 2-dodecylcyclobutanone and linear-alkanes as irradiation markers in sliced dry-cured ham. *Food Chemistry*, *113*(2), 616–620. https://doi.org/10.1016/j.foodchem.2008.07.046

Bolumar, T., LaPeña, D., Skibsted, L. H., & Orlien, V. (2016). Rosemary and oxygen scavenger

in active packaging for prevention of high-pressure induced lipid oxidation in pork patties. *Food Packaging and Shelf Life*, *7*, 26–33. https://doi.org/10.1016/j.fpsl.2016.01.002

Brezová, V., Polovka, M., & Staško, A. (2002). The influence of additives on beer stability investigated by EPR spectroscopy. *Spectrochimica Acta - Part A Molecular and Biomolecular Spectroscopy*, *58*(6), 1279–1291. https://doi.org/10.1016/S1386-1425(01)00717-X

Brezová, V., Šlebodová, A., & Staško, A. (2009). Coffee as a source of antioxidants: An EPR study. *Food Chemistry*, *114*(3), 859–868. https://doi.org/10.1016/j.foodchem.2008.10.025

Caja, M. M., Ruiz del Castillo, M. L., & Blanch, G. P. (2008). Solid phase microextraction as a methodology in the detection of irradiation markers in ground beef. *Food Chemistry*, *110*(2), 531–537. https://doi.org/10.1016/j.foodchem.2008.02.024

Callens, F., Vanhaelewyn, G., Matthys, P., & Boesman, E. (1998). EPR of carbonate derived radicals: Applications in dosimetry, dating and detection of irradiated food. *Applied Magnetic Resonance*, *14*(2–3), 235–254. https://doi.org/10.1007/BF03161892

Campaniello, M., Marchesani, G., Zianni, R., Tarallo, M., Mangiacotti, M., & Chiaravalle, A. E. (2019). Validation of an alternative method for the identification of 2-dodecylcyclebutanone (2-DCB) of irradiated meats by solid-phase microextraction (SPME) gas chromatography–mass spectrometry (GC-MS). *International Journal of Food Science and Technology*, 1–9. https://doi.org/10.1111/ijfs.14353

Carlsen, C. U., Andersen, M. L., & Skibsted, L. H. (2001). Oxidative stability of processed pork. Assay based on ESR-detection of radicals. *European Food Research and Technology*, *213*(3), 170–173. https://doi.org/10.1007/s002170100357

Castro Marín, A., Culcasi, M., Cassien, M., Stocker, P., Thétiot-Laurent, S., Robillard, B., Chinnici, F., & Pietri, S. (2019). Chitosan as an antioxidant alternative to sulphites in oenology: EPR investigation of inhibitory mechanisms. *Food Chemistry*, *285*(September 2018), 67–76. https://doi.org/10.1016/j.foodchem.2019.01.155

Chatzidaki, M. D., Mitsou, E., Yaghmur, A., Xenakis, A., & Papadimitriou, V. (2015). Formulation and characterization of food-grade microemulsions as carriers of natural

phenolic antioxidants. *Colloids and Surfaces A: Physicochemical and Engineering Aspects*, *483*, 130–136. https://doi.org/10.1016/j.colsurfa.2015.03.060

Chauhan, S. K., Kumar, R., Nadanasabapathy, S., & Bawa, A. S. (2009). Detection methods for irradiated foods. *Comprehensive Reviews in Food Science and Food Safety*, *8*(1), 4–16. https://doi.org/10.1111/j.1541-4337.2008.00063.x

Chawla, S. P., Thomas, P., & Bongirwar, D. R. (2002). Factors influencing the yield of radiation induced electron spin resonance (ESR) signal in lamb bones. *Food Research International*, *35*(5), 467–473. https://doi.org/10.1016/S0963-9969(01)00145-4

Chawla, S.P., Paul, P., Thomas, P., Babu, Y., & Sastry, M. D. (1999). Detection of irradiated lamb meat with bone: effect of chilled storage and cooking on ESR signal strength. *Int. J. Food Sci. Technol.*, *34*(1), 41–45.

Chawla, Surinder P., & Thomas, P. (2004). Identification of irradiated meat using electron spin resonance spectroscopy: Results of blind trials. *International Journal of Food Science and Technology*, *39*(6), 653–660. https://doi.org/10.1111/j.1365-2621.2004.00824.x

Chen, H., Wang, Y., Cao, P., & Liu, Y. (2017). Effect of temperature on thermal oxidation of palmitic acid studied by combination of EPR spin trapping technique and SPME-GC–MS/MS. *Food Chemistry*, *234*, 439–444. https://doi.org/10.1016/j.foodchem.2017.04.135

Chen, S., Morita, Y., Saito, K., Kameya, H., Nakajima, M., & Todoriki, S. (2011). Identification of irradiated prawn (Penaeus monodon) using thermoluminescence and 2-alkylcyclobutanone analyses. *Journal of Agricultural and Food Chemistry*, *59*(1), 78–84. https://doi.org/10.1021/jf103439c

Code of Federal Regulations title 21, part 179.26. Irradiation in the production, processing and handling of food (2018). https://www.accessdata.fda.gov/scripts/cdrh/cfdocs/cfcfr/CFRSearch.cfm?fr=179.26

Coey, A. T., Sahu, I. D., Gunasekera, T. S., Troxel, K. R., Hawn, J. M., Swartz, M. S., Wickenheiser, M. R., Reid, R. J., Welch, R. C., Vanoye, C. G., Kang, C., Sanders, C. R., & Lorigan, G. A. (2011). Reconstitution of KCNE1 into lipid bilayers: Comparing the structural, dynamic, and activity differences in micelle and vesicle environments.

*Biochemistry*, *50*(50), 10851–10859. https://doi.org/10.1021/bi2009294

Crews, C., Driffield, M., & Thomas, C. (2012). Analysis of 2-alkylcyclobutanones for detection of food irradiation: Current status, needs and prospects. *Journal of Food Composition and Analysis*, *26*(1–2), 1–11. https://doi.org/10.1016/j.jfca.2011.11.006

Cui, L., Lahti, P. M., & Decker, E. A. (2017). Evaluating electron paramagnetic resonance (EPR) to measure lipid oxidation lag phase for shelf-life determination of oils. *Journal of the American Oil Chemists' Society*, *94*(1), 89–97. https://doi.org/10.1007/s11746-016-2927-1

Cunningham, T. F., Putterman, M. R., Desai, A., Horne, W. S., & Saxena, S. (2015). The double-Histidine Cu 2+ -binding motif: A highly rigid, site-specific spin probe for electron spin resonance distance measurements. *Angewandte Chemie International Edition*, *54*(21), 6330–6334. https://doi.org/10.1002/anie.201501968

D'Oca, M. C., & Bartolotta, A. (2018). Detection of irradiated food and evaluation of the given dose by electron spin resonance, thermoluminescence, and gas chromatographic/mass spectrometric analysis. In *Food Control and Biosecurity* (Vol. 863, pp. 343–372). Elsevier. https://doi.org/10.1016/B978-0-12-811445-2.00010-6

De Jesus, E. F. O., Rossi, A. M., & Lopes, R. T. (1999). An ESR study on identification of gamma-irradiated kiwi, papaya and tomato using fruit pulp. *International Journal of Food Science and Technology*, *34*(2), 173–178. https://doi.org/10.1046/j.1365-2621.1999.00250.x

Delincée, H., & Soika, C. (2002). Improvement of the ESR detection of irradiated food containing cellulose employing a simple extraction method. *Radiation Physics and Chemistry*, *63*(3–6), 437–441. https://doi.org/10.1016/S0969-806X(01)00533-3

Desrosiers, M. F. (1996). Current status of the EPR method to detect irradiated food. *Applied Radiation and Isotopes*, *47*(11–12), 1621–1628. https://doi.org/10.1016/S0969-8043(96)00255-2

Doni, D., Passerini, L., Audran, G., Marque, S. R. A., Schulz, M., Santos, J., Costantini, P., Bortolus, M., & Carbonera, D. (2020). Effects of fe2+/fe3+ binding to human frataxin and its d122y variant, as revealed by site-directed spin labeling (Sdsl) epr complemented by fluorescence and circular dichroism spectroscopies. *International Journal of Molecular*

*Sciences*, *21*(24), 1–20. https://doi.org/10.3390/ijms21249619

Dose, J., Matsugo, S., Yokokawa, H., Koshida, Y., Okazaki, S., Seidel, U., Eggersdorfer, M., Rimbach, G., & Esatbeyoglu, T. (2016). Free radical scavenging and cellular antioxidant properties of astaxanthin. *International Journal of Molecular Sciences*, *17*(1), 1–14. https://doi.org/10.3390/ijms17010103

Drescher, M., Veldhuis, G., Van Rooijen, B. D., Milikisyants, S., Subramaniam, V., & Huber, M. (2008). Antiparallel arrangement of the helices of vesicle-bound α-synuclein. *Journal of the American Chemical Society*, *130*(25), 7796–7797. https://doi.org/10.1021/ja801594s

Duda, M., Kawula, K., Pawlak, A., Sarna, T., & Wisniewska-Becker, A. (2017). EPR studies on the properties of model photoreceptor membranes made of natural and synthetic lipids. *Cell Biochemistry and Biophysics*, *75*(3–4), 433–442. https://doi.org/10.1007/s12013-017-0795-4

Duliu, O. G. (2000). Electron paramagnetic resonance identification of irradiated cuttlefish ( Sepia officinalis L .). *Applied Radiation and Isotopes*, *52*, 1385–1390.

Dyrek, K., Bidzinska, E., ŁAbanowska, M., Fortuna, T., Przetaczek, I., & Pietrzyk, S. (2007). EPR study of radicals generated in starch by microwaves or by conventional heating. *Starch/Staerke*, *59*(7), 318–325. https://doi.org/10.1002/star.200600581

Eldin, A. K. (2010). Methods to determine the extent of lipid oxidation in foods. In E. Decker, R. Elias, & D. J. McClements (Eds.), *Oxidation in Foods and Beverages and Antioxidant Applications* (pp. 181–195). Woodhead. https://doi.org/10.1533/9780857090447.1.181

Elias, R. J., Andersen, M. L., Skibsted, L. H., & Waterhouse, A. L. (2009a). Identification of free radical intermediates in oxidized wine using electron paramagnetic resonance spin trapping. *Journal of Agricultural and Food Chemistry*, *57*(10), 4359–4365. https://doi.org/10.1021/jf8035484

Elias, R. J., Andersen, M. L., Skibsted, L. H., & Waterhouse, A. L. (2009b). Key factors affecting radical formation in wine studied by spin trapping and EPR spectroscopy. *American Journal of Enology and Viticulture*, *60*(4), 471–476.

Emmanouilidis, L., Esteban-Hofer, L., Damberger, F. F., de Vries, T., Nguyen, C. K. X., Ibáñez,

L. F., Mergenthal, S., Klotzsch, E., Yulikov, M., Jeschke, G., & Allain, F. H. T. (2021). NMR and EPR reveal a compaction of the RNA-binding protein FUS upon droplet formation. *Nature Chemical Biology*, *17*(5), 608–614. https://doi.org/10.1038/s41589-021-00752-3

Endeward, B., Butterwick, J. A., MacKinnon, R., & Prisner, T. F. (2009). Pulsed electron-electron double-resonance determination of spin-label distances and orientations on the tetrameric potassium ion channel KcsA. *Journal of the American Chemical Society, 131*(42), 15246–15250. https://doi.org/10.1021/ja904808n

Engin, B., & Demirtas, H. (2004). The use of ESR spectroscopy for the investigation of dosimetric properties of egg shells. *Radiation Physics and Chemistry, 71*(6), 1113–1123. https://doi.org/10.1016/j.radphyschem.2003.12.053

Esatbeyoglu, T., Wagner, A. E., Motafakkerazad, R., Nakajima, Y., Matsugo, S., & Rimbach, G. (2014). Free radical scavenging and antioxidant activity of betanin: Electron spin resonance spectroscopy studies and studies in cultured cells. *Food and Chemical Toxicology, 73*, 119–126. https://doi.org/10.1016/j.fct.2014.08.007

Escudero, A., Cacho, J., & Ferreira, V. (2000). Isolation and identification of odorants generated in wine during its oxidation: a gas chromatography-olfactometric study. *European Food Research and Technology, 211*(2), 105–110. https://doi.org/10.1007/s002179900128

European Committee for Standardization (CEN). (1997). *(EN1786) Foodstuffs-detection of irradiated food containing bone: analysis by electron paramagnetic resonance*. http://ec.europa.eu/food/food/biosafety/irradiation/1786-1996_en.pdf.

European Committee for Standardization (CEN). (2000). *(EN1787) Foodstuffs-detection of irradiated food containing cellulose by ESR spectroscopy.* http://ec.europa.eu/food/food/biosafety/irradiation/1787-2000_en.pdf.

European Committee for Standardization (CEN). (2001). *(EN13708) Foodstuffs-detection of irradiated food containing crystalline sugar by ESR spectroscopy*. http://ec.europa.eu/food/food/biosafety/irradiation/13708-2001_en.pdf.

European Committee for Standardization (CEN). (2003). *(EN1785) Detection of irradiated food*

*containing fat: gas chromatographic/mass spectrometric analysis of 2-alkylcyclobutanones.* https://ec.europa.eu/food/system/files/2016-10/biosafety-irradiation-legislation-1785-2003_en.pdf

Fadda, A., Molinu, M. G., Deiana, P., & Sanna, D. (2021). Electron paramagnetic resonance spin trapping of sunflower and olive oils subjected to thermal treatment: Optimization of experimental and fitting parameters. *ACS Food Science & Technology*. https://doi.org/10.1021/acsfoodscitech.1c00166

Falch, E., Velasco, J., Aursand, M., & Andersen, M. L. (2005). Detection of radical development by ESR spectroscopy techniques for assessment of oxidative susceptibility of fish oils. *European Food Research and Technology*, *221*(5), 667–674. https://doi.org/10.1007/s00217-005-0009-y

Farkas, J., & Mohácsi-Farkas, C. (2011). History and future of food irradiation. *Trends in Food Science & Technology*, *22*(2–3), 121–126. https://doi.org/10.1016/j.tifs.2010.04.002

FDA (The Food and Drug Administration). (2014). *FDA Progress Report on Ongoing Investigation into Jerky Pet Treats*. http://www.fda.gov/AnimalVeterinary/SafetyHealth/ProductSafetyInformation/ucm371465.htm

FDA (The Food and Drug Administration). (2015). *Code of Federal Regulations, Title 21*.

Feng, X., Hua, Y., Zhang, C., Kong, X., Li, X., & Chen, Y. (2020). Effect of soaking conditions on the formation of lipid derived free radicals in soymilk. *Food Chemistry*, *315*(July 2019), 126237. https://doi.org/10.1016/j.foodchem.2020.126237

Freed, J. H. (1976). Theory of slow tumbling ESR spectra for nitroxides. In L. J. Berliner (Ed.), *Spin Labeling* (pp. 53–132). Academic Press, Inc. https://doi.org/10.1016/j.neurobiolaging.2011.12.002

Gadgil, P., Hachmeister, K. A., Smith, J. S., & Kropf, D. H. (2002). 2-Alkylcyclobutanones as irradiation dose indicators in irradiated ground beef patties. *Journal of Agricultural and Food Chemistry*, *50*(20), 5746–5750. https://doi.org/10.1021/jf020323+

Gadgil, P., Smith, J. S., Hachmeister, K. A., & Kropf, D. H. (2005). Evaluation of 2-

dodecylcyclobutanone as an irradiation dose indicator in fresh irradiated ground beef. *Journal of Agricultural and Food Chemistry*, *53*(6), 1890–1893. https://doi.org/10.1021/jf048641r

Georgieva, E. R., Ramlall, T. F., Borbat, P. P., Freed, J. H., & Eliezer, D. (2008). Membrane-bound α-synuclein forms an extended helix: Long-distance pulsed ESR measurements using vesicles, bicelles, and rodlike micelles. *Journal of the American Chemical Society*, *130*(39), 12856–12857. https://doi.org/10.1021/ja804517m

Ghelawi, M. A., Moore, J. S., Bisby, R. H., & Dodd, N. J. F. (2001). Estimation of absorbed dose in irradiated dates (Phoenix dactylifera L.). Test of ESR response function by a weighted linear least-squares regression analysis. *Radiation Physics and Chemistry*, *60*(1–2), 143–147. https://doi.org/10.1016/S0969-806X(00)00309-1

Glover, R. E., Smith, R. R., Jones, M. V., Jackson, S. K., & Rowlands, C. C. (1999). An EPR investigation of surfactant action on bacterial membranes. *FEMS Microbiology Letters*, *177*(1), 57–62. https://doi.org/10.1016/S0378-1097(99)00289-X

Goodman, B. A., Pascual, E. C., & Yeretzian, C. (2011). Real time monitoring of free radical processes during the roasting of coffee beans using electron paramagnetic resonance spectroscopy. *Food Chemistry*, *125*(1), 248–254. https://doi.org/10.1016/j.foodchem.2010.07.072

Gray, R., & Stevenson, M. H. (1989). Detection of irradiated deboned turkey meat using electron spin resonance spectroscopy. *International Journal of Radiation Applications and Instrumentation. Part*, *34*(6), 899–902. https://doi.org/10.1016/1359-0197(89)90327-5

Guilarte, V., Trompier, F., & Duval, M. (2016). Evaluating the potential of Q-band ESR spectroscopy for dose reconstruction of fossil tooth enamel. *PLoS ONE*, *11*(3), 1–14. https://doi.org/10.1371/journal.pone.0150346

Guzik, G. P., & Stachowicz, W. (2012). *EPR study on sugar radicals utilized for detection of radiation treatment of food*. *57*(November 2011), 545–549.

Guzik, G. P., & Stachowicz, W. (2016). Study on radiation-induced radicals giving rise to stable EPR signal suitable for the detection of irradiation in L-sorbose-containing fruits.

*Nukleonika*, *61*(4), 461–465. https://doi.org/10.1515/nuka-2016-0075

Guzik, G. P., Stachowicz, W., & Michalik, J. (2015). Identification of irradiated dried fruits using EPR spectroscopy. *NUKLEONIKA*, *60*(November 2014), 627–631. https://doi.org/10.1515/nuka-2015-0093

Guzik, G. P., Stachowicz, W., & Michalik, J. (2019). Study on irradiated D-mannose isolated from cranberry. *Nukleonika*, *64*(4), 139–143. https://doi.org/10.2478/nuka-2019-0018

Hagen, W. R. (2013). EPR Spectroscopy. In R. R. Crichton & R. O. Louro (Eds.), *Practical Approaches to Biological Inorganic Chemistry* (First, pp. 53–75). Elsevier B.V. https://doi.org/10.1016/B978-0-444-56351-4.00003-8

Hilger, D., Polyhach, Y., Padan, E., Jung, H., & Jeschke, G. (2007). High-resolution structure of a Na+/H+ antiporter dimer obtained by pulsed electron paramagnetic resonance distance measurements. *Biophysical Journal*, *93*(10), 3675–3683. https://doi.org/10.1529/biophysj.107.109769

Huber, K. C., & Bemiller, J. N. (2008). Carbohydrates. In Srinivasan Damodaran, K. L. Parkin, & O. R. Fennema (Eds.), *Fennema's Food Chemistry* (4th ed., pp. 83–154). CRC Press.

Jackson, S. K. (2019). Applications of electron paramagnetic resonance (EPR) spectroscopy in the study of oxidative stress in biological systems. In J. T. Hancock & M. E. Conway (Eds.), *Redox-Mediated Signal Transduction* (Second, Vol. 1990). Springer US. https://doi.org/10.1007/978-1-4939-9463-2

Jawad, M., Schoop, R., Suter, A., Klein, P., & Eccles, R. (2007). Comparative study of polyphenolic content and antiradical activity of cloudy and clear apple juices. *Journal of the Science of Food and Agriculture*, *87*, 573–579. https://doi.org/10.1002/jsfa.2707

Jenkins, D., James, S., Dehrmann, F., Smart, K., & Cook, D. (2018). Impacts of copper, iron, and manganese metal ions on the EPR assessment of beer oxidative stability. *Journal of the American Society of Brewing Chemists*, *76*(1), 50–57. https://doi.org/10.1080/03610470.2017.1402585

Jeschke, G., & Polyhach, Y. (2007). Distance measurements on spin-labelled biomacromolecules by pulsed electron paramagnetic resonance. *Physical Chemistry Chemical Physics*, *9*(16),

1895–1910. https://doi.org/10.1039/b614920k

Jiang, S., Xie, Y., Li, M., Guo, Y., Cheng, Y., Qian, H., & Yao, W. (2020). Evaluation on the oxidative stability of edible oil by electron spin resonance spectroscopy. *Food Chemistry*, *309*(October 2016). https://doi.org/10.1016/j.foodchem.2019.125714

Jo, Y., Sanyal, B., Ameer, K., & Kwon, J. H. (2018). Characterization of DNA comet and cellulose radical signal in Valencia oranges treated with different forms of ionizing radiation. *Postharvest Biology and Technology*, *135*(January 2017), 68–76. https://doi.org/10.1016/j.postharvbio.2017.08.004

Jo, Y., Sanyal, B., Park, H. J., & Kwon, J. H. (2016). Ethanol extraction-based drying enhanced ESR radical detection in oranges irradiated to different ionizing radiations during storage. *Postharvest Biology and Technology*, *112*, 170–175. https://doi.org/10.1016/j.postharvbio.2015.10.005

Kameya, H., Watanabe, J., Takano-Ishikawa, Y., & Todoriki, S. (2014). Comparison of scavenging capacities of vegetables by ORAC and EPR. *Food Chemistry*, *145*, 866–873. https://doi.org/10.1016/j.foodchem.2013.09.015

Karakirova, Y., Yordanov, N. D., De Cooman, H., Vrielinck, H., & Callens, F. (2010). Dosimetric characteristics of different types of saccharides: An EPR and UV spectrometric study. *Radiation Physics and Chemistry*, *79*(5), 654–659. https://doi.org/10.1016/j.radphyschem.2009.12.003

Karakirova, Yordanka, & Yordanov, N. D. (2020). Time dependence of the EPR and optical spectra of irradiated crystal sugar. *Radiation Physics and Chemistry*, *168*(March 2019), 108569. https://doi.org/10.1016/j.radphyschem.2019.108569

Kazmier, K., Alexander, N. S., Meiler, J., & Mchaourab, H. S. (2011). Algorithm for selection of optimized EPR distance restraints for de novo protein structure determination. *Journal of Structural Biology*, *173*(3), 549–557. https://doi.org/10.1016/j.jsb.2010.11.003

Khan, N., & Swartz, H. (2002). Measurements in vivo of parameters pertinent to ROS/RNS using EPR spectroscopy. *Molecular and Cellular Biochemistry*, *234/235*, 341–357.

Kieserling, H., Alsmeier, I. M., Steffen-Heins, A., Keppler, J. K., Sevenich, R., Rauh, C.,

Wagemans, A. M., & Drusch, S. (2021). Interfacial film formation and film stability of high hydrostatic pressure-treated β-lactoglobulin. *Food Hydrocolloids*, *119*(February), 106746. https://doi.org/10.1016/j.foodhyd.2021.106746

Klare, J. P. (2012). Biomedical applications of electron paramagnetic resonance (EPR) spectroscopy. *Biomedical Spectroscopy and Imaging*, *1*(March), 101–124. https://doi.org/10.3233/BSI-2012-0010

Klare, J. P. (2013). Site-directed spin labeling EPR spectroscopy in protein research. *Biological Chemistry*, *394*(10), 1281–1300. https://doi.org/10.1515/hsz-2013-0155

Klug, C. S., Su, W., & Feix, J. B. (1997). Mapping of the residues involved in a proposed β-strand located in the ferric enterobactin receptor FepA using site-directed spin-labeling. *Biochemistry*, *36*(42), 13027–13033. https://doi.org/10.1021/bi971232m

Kocherginsky, N. M., Kostetski, Y. Y., & Smirnov, A. I. (2005a). Antioxidant pool in beer and kinetics of EPR spin-trapping. *Journal of Agricultural and Food Chemistry*, *53*(17), 6870–6876. https://doi.org/10.1021/jf051045s

Kocherginsky, N. M., Kostetski, Y. Y., & Smirnov, A. I. (2005b). Use of nitroxide spin probes and electron paramagnetic resonance for assessing reducing power of beer. Role of SH groups. *Journal of Agricultural and Food Chemistry*, *53*(4), 1052–1057. https://doi.org/10.1021/jf034787z

Kong, L., Yucel, U., Yoksan, R., Elias, R. J., & Ziegler, G. R. (2018). Characterization of amylose inclusion complexes using electron paramagnetic resonance spectroscopy. *Food Hydrocolloids*, *82*, 82–88. https://doi.org/10.1016/j.foodhyd.2018.03.050

Korkmaz, M., & Polat, M. (2001). Radical kinetics and characterization of the free radicals in gamma irradiated red pepper. *Radiation Physics and Chemistry*, *62*(5–6), 411–421. https://doi.org/10.1016/S0969-806X(01)00215-8

Kozik, V., Jarzembek, K., Jedrzejowska, A., Bak, A., Polak, J., Bartoszek, M., & Pytlakowska, K. (2015). Investigation of antioxidant activity of pomegranate juices by means of electron paramagnetic resonance and UV-vis spectroscopy. *Journal of AOAC International*, *98*(4), 866–870. https://doi.org/10.5740/jaoacint.SGE4-Kozik

Kozłowska, M., & Zawada, K. (2015). Evaluation of oxidative stability of vegetable oils enriched with herb extracts by EPR spectroscopy. *Chemical Papers*, *69*(7), 950–957. https://doi.org/10.1515/chempap-2015-0102

Kreitman, G. Y., Laurie, V. F., & Elias, R. J. (2013). Investigation of ethyl radical quenching by phenolics and thiols in model wine. *Journal of Agricultural and Food Chemistry*, *61*(3), 685–692. https://doi.org/10.1021/jf303880g

Krzyminiewski, R., Kubiak, T., Dobosz, B., Schroeder, G., & Kurczewska, J. (2014). EPR spectroscopy and imaging of TEMPO-labeled magnetite nanoparticles. *Current Applied Physics*, *14*(5), 798–804. https://doi.org/10.1016/j.cap.2014.03.021

Kunz, T., Müller, C., Mato-Gonzales, D., & Methner, F. J. (2012). The influence of unmalted barley on the: Oxidative stability of wort and beer. *Journal of the Institute of Brewing*, *118*(1), 32–39. https://doi.org/10.1002/jib.6

Kveder, M., Rakoš, R., Gavella, M., Lipovac, V., Pifat, G., Pečar, S., & Schara, M. (2004). EPR investigation of cell membrane fluidity upon external oxidative stimulus. *Applied Magnetic Resonance*, *27*(1–2), 77–86. https://doi.org/10.1007/BF03166303

Kwon, J. H., Kausar, T., Noh, J., Kim, D. H., Byun, M. W., Kim, K. S., & Kim, K. S. (2007). The identification of irradiated seasoned filefish (Thamnaconus modestus) by different analytical methods. *Radiation Physics and Chemistry*, *76*(11–12), 1833–1836. https://doi.org/10.1016/j.radphyschem.2007.03.011

Li, A., Pan, L. G., Zhang, X. T., Jin, X. X., & Ma, H. Z. (2017). Rapid determination method for 2-DCB in irradiated pork by ASE–Al2O3–GC–MS. *Radiation Physics and Chemistry*, *130*, 277–281. https://doi.org/10.1016/j.radphyschem.2016.09.007

Li, H., Pan, Y., Yang, Z., Rao, J., & Chen, B. (2021). Emerging applications of site-directed spin labeling electron paramagnetic resonance (SDSL-EPR) to study food protein structure, dynamics, and interaction. *Trends in Food Science and Technology*, *109*(December 2020), 37–50. https://doi.org/10.1016/j.tifs.2021.01.022

Li, X. (2017). 2-Phenyl-4,4,5,5-tetramethylimidazoline-1-oxyl 3-Oxide (PTIO•) radical scavenging: A new and simple antioxidant assay in vitro. *Journal of Agricultural and Food*

*Chemistry*, *65*(30), 6288–6297. https://doi.org/10.1021/acs.jafc.7b02247

Locatelli, M., Gindro, R., Travaglia, F., Coïsson, J., Rinaldi, M., & Arlorio, M. (2009). Study of the DPPH -scavenging activity : Development of a free software for the correct interpretation of data. *Food Chemistry*, *114*(3), 889–897. https://doi.org/:10.1016/j.foodchem.2008.10.035

Lund, M. N., Hoff, S., Berner, T. S., Lametsch, R., & Andersen, M. L. (2012). Effect of pasteurization on the protein composition and oxidative stability of beer during storage. *Journal of Agricultural and Food Chemistry*, *60*(50), 12362–12370. https://doi.org/10.1021/jf303044a

Marchante, L., Márquez, K., Contreras, D., Izquierdo-Cañas, P. M., García-Romero, E., & Díaz-Maroto, M. C. (2020a). Impact of oenological antioxidant substances on the formation of 1-hydroxyethyl radical and phenolic composition in SO 2 free red wines . *Journal of the Science of Food and Agriculture*, *March*. https://doi.org/10.1002/jsfa.10374

Marchante, L., Márquez, K., Contreras, D., Izquierdo-Cañas, P. M., García-Romero, E., & Díaz-Maroto, M. C. (2020b). Potential of different natural antioxidant substances to inhibit the 1-Hydroxyethyl radical in SO2-free wines. *Journal of Agricultural and Food Chemistry*. https://doi.org/10.1021/acs.jafc.9b07024

Marques, L., Espinosa, M. H., Andrews, W., & Coors, M. (2017). Advancing flavor stability improvements in different beer types using novel electron paramagnetic resonance area and forced beer aging methods. *Journal of the American Society of Brewing Chemists*, *7*, 1–6. https://doi.org/10.1094/asbcj-2017-1472-01

Márquez, K., Contreras, D., Salgado, P., & Mardones, C. (2019). Production of hydroxyl radicals and their relationship with phenolic compounds in white wines. *Food Chemistry*, *271*(January 2018), 80–86. https://doi.org/10.1016/j.foodchem.2018.07.165

Márquez, K., Pérez-Navarro, J., Hermosín-Gutiérrez, I., Gómez-Alonso, S., Mena-Morales, A., García-Romer, E., & Contreras, D. (2019). Systematic study of hydroxyl radical production in white wines as a function of chemical composition. *Food Chemistry*, *288*(September 2018), 377–385. https://doi.org/10.1016/j.foodchem.2019.03.005

McClements, D. J., & Decker, E. A. (2017). Lipids. In S. Damodaran & K. Parkin (Eds.), *Fennema's Food Chemistry* (5th ed., pp. 155–212). CRC Press. https://doi.org/10.1201/9781315372914

Melnyk, A. K., Sukhoveev, O. V., Kononets, L. A., Khilchevsky, O. M., Shulga, S. M., Kukhar, V. P., & Vovk, A. I. (2016). An EPR spin probe study of liposomes from sunflower and soybean phospholipids. *Journal of Liposome Research*, *26*(1), 80–86. https://doi.org/10.3109/08982104.2015.1039031

Merkx, D. W. H., Plankensteiner, L., Yu, Y., Wierenga, P. A., Hennebelle, M., & Van Duynhoven, J. P. M. (2021). Evaluation of PBN spin-trapped radicals as early markers of lipid oxidation in mayonnaise. *Food Chemistry*, *334*(July 2020), 127578. https://doi.org/10.1016/j.foodchem.2020.127578

Miller, R. B. (2005). *Electronic Irradiation of Foods: An introduction to The Technology*. https://doi.org/10.1007/0-387-28386-2

Mitsuda, H., Yasumoto, K., & Yokoyama, K. (1965). Studies on the free radical in amino-carbonyl reaction. *Agricultural and Biological Chemistry*, *29*(8), 751–756. https://doi.org/10.1080/00021369.1965.10858460

Mohsin, G. F., Schmitt, F. J., Kanzler, C., Dirk Epping, J., Flemig, S., & Hornemann, A. (2018). Structural characterization of melanoidin formed from D-glucose and L-alanine at different temperatures applying FTIR, NMR, EPR, and MALDI-ToF-MS. *Food Chemistry*, *245*(December 2017), 761–767. https://doi.org/10.1016/j.foodchem.2017.11.115

Momchilova, S. M., Taneva, S. P., Totseva, I. R., Nikolova, Y. I., Karakirova, Y. G., Aleksieva, K. I., Mladenova, R. B., & Kancheva, V. D. (2019). Gamma-irradiation of nuts – EPR characterization and effects on lipids and oxidative stability: II. Peanuts. *Bulgarian Chemical Communications*, *51*, 263–269.

Morales, N. P., Sirijaroonwong, S., Yamanont, P., & Phisalaphong, C. (2015). Electron paramagnetic resonance study of the free radical scavenging capacity of curcumin and its demethoxy and hydrogenated derivatives. *Biol. Pharm. Bull.*, *38*(10), 1478–1483.

Morsy, M. a. (2012). Simple EPR / Alanine dosimeter for medical application. *Open Journal of*

*Radiology*, *2012*(December), 120–125. https://doi.org/10.4236/ojrad.2012.24022

Mrakic-Sposta, S., Gussoni, M., Montorsi, M., Porcelli, S., & Vezzoli, A. (2014). A quantitative method to monitor reactive oxygen species production by electron paramagnetic resonance in physiological and pathological conditions. *Oxidative Medicine and Cellular Longevity*, *2014*. https://doi.org/10.1155/2014/306179

Nakagawa, K. (2003). Diffusion coefficient and relaxation time of aliphatic spin probes in a unique triglyceride membrane. *Langmuir*, *19*(12), 5078–5082. https://doi.org/10.1021/la026813d

Nakagawa, K. (2009). EPR investigations of spin-probe dynamics in aqueous dispersions of a nonionic amphiphilic compound. *JAOCS, Journal of the American Oil Chemists' Society*, *86*(1), 1–17. https://doi.org/10.1007/s11746-008-1317-8

Nakagawa, K., Maeda, H., Yamaya, Y., & Tonosaki, Y. (2020). Maillard reaction intermediates and related phytochemicals in black garlic determined by EPR and HPLC analyses. *Molecules*, *25*(19). https://doi.org/10.3390/molecules25194578

Namiki, M., Hayashi, T., & Kawakishi, S. (1973). Free radicals developed in the amino-carbonyl reaction of sugars with amino acids. *Agricultural and Biological Chemistry*, *37*(12), 2935–2936. https://doi.org/10.1080/00021369.1973.10861104

Nash, K. M., Rockenbauer, A., & Villamena, F. A. (2012). Reactive nitrogen species reactivities with nitrones: Theoretical and experimental studies. *Chemical Research in Toxicology*, *25*(8), 1581–1597. https://doi.org/10.1021/tx200526y

Nesmelov, Y. E., & Thomas, D. D. (2010). Protein structural dynamics revealed by site-directed spin labelling and multifrequency EPR. *Biophys. Rev*, *2*(2), 91–99. https://doi.org/10.1007/s12551-010-0032-5.Protein

Nickolaus, C., Vargas, C., Reichenwallner, J., Chakour, M., Selmke, B., Chakraborty, R., Varadarajan, R., Keller, S., & Trommer, W. E. (2020). The molten globule state of maltose-binding protein: Structural and thermodynamic characterization by EPR spectroscopy and isothermal titration calorimetry. *Applied Magnetic Resonance*, *51*(9–10), 877–886. https://doi.org/10.1007/s00723-020-01232-y

Nikolantonaki, M., Coelho, C., Noret, L., Zerbib, M., Vileno, B., Champion, D., & Gougeon, R. D. (2019). Measurement of white wines resistance against oxidation by Electron Paramagnetic Resonance spectroscopy. *Food Chemistry*, *270*(February 2018), 156–161. https://doi.org/10.1016/j.foodchem.2018.07.052

Nordio, P. L. (1976). General Magnetic Resonance Theory. In L. J. Berliner (Ed.), *Spin Labeling Theory and Applications* (pp. 5–52). Academic Press.

Nutrizio, M., Gajdoš Kljusurić, J., Badanjak Sabolović, M., Bursać Kovačević, D., Šupljika, F., Putnik, P., Semenčić Čakić, M., Dubrović, I., Vrsaljko, D., Maltar-Strmečki, N., & Režek Jambrak, A. (2020). Valorization of sage extracts (Salvia officinalis L.) obtained by high voltage electrical discharges: Process control and antioxidant properties. *Innovative Food Science and Emerging Technologies*, *60*(September 2019). https://doi.org/10.1016/j.ifset.2019.102284

O`Meara, J. F., Truby, F. K., & Shaw, T. M. (1956). Free radicals in roasted Coffee. *Food Research*, *22*, 96–101.

Osorio, C., Carriazo, J. G., & Almanza, O. (2011). Antioxidant activity of corozo (Bactris guineensis) fruit by electron paramagnetic resonance (EPR) spectroscopy. *European Food Research and Technology*, *233*(1), 103–108. https://doi.org/10.1007/s00217-011-1499-4

Paktaş, D. D., & Sünnetçioğlu, M. M. (2007). EPR spin probe investigation of irradiated wheat, rice and sunflower seeds. *Radiation Physics and Chemistry*, *76*(1), 46–54. https://doi.org/10.1016/j.radphyschem.2005.10.016

Papadimitriou, V., Sotiroudis, T. G., Xenakis, A., Sofikiti, N., Stavyiannoudaki, V., & Chaniotakis, N. A. (2006). Oxidative stability and radical scavenging activity of extra virgin olive oils: An electron paramagnetic resonance spectroscopy study. *Analytica Chimica Acta*, *573–574*, 453–458. https://doi.org/10.1016/j.aca.2006.02.007

Pegi, A., Julijana, K., Slavko, P., Janez, Š., & Marjeta, Š. (2003). The effect of lipophilicity of spin-labeled compounds on their distribution in solid lipid nanoparticle dispersions studied by electron paramagnetic resonance. *Journal of Pharmaceutical Sciences*, *92*(1), 58–66. https://doi.org/10.1002/jps.10277

Pérez-López, U., Pinzino, C., Quartacci, M. F., Ranieri, A., & Sgherri, C. (2014). Phenolic composition and related antioxidant properties in differently colored lettuces: A study by electron paramagnetic resonance (EPR) kinetics. *Journal of Agricultural and Food Chemistry*, *62*(49), 12001–12007. https://doi.org/10.1021/jf503260v

Polak, J., & Bartoszek, M. (2015). The study of antioxidant capacity of varieties of nalewka, a traditional Polish fruit liqueur, using EPR, NMR and UV-vis spectroscopy. *Journal of Food Composition and Analysis*, *40*, 114–119. https://doi.org/10.1016/j.jfca.2015.01.006

Polak, J., Bartoszek, M., & Stanimirova, I. (2013). A study of the antioxidant properties of beers using electron paramagnetic resonance. *Food Chemistry*, *141*(3), 3042–3049. https://doi.org/10.1016/j.foodchem.2013.05.133

Polovka, M., Brezová, V., & Staško, A. (2003). Antioxidant properties of tea investigated by EPR spectroscopy. *Biophysical Chemistry*, *106*(1), 39–56. https://doi.org/10.1016/S0301-4622(03)00159-5

Polyhach, Y., Bordignon, E., Tschaggelar, R., Gandra, S., Godt, A., & Jeschke, G. (2012). High sensitivity and versatility of the DEER experiment on nitroxide radical pairs at Q-band frequencies. *Physical Chemistry Chemical Physics*, *14*(30), 10762–10773. https://doi.org/10.1039/c2cp41520h

Prasuna, C. P L, Chakradhar, R. P. S., Rao, J. L., & Gopal, N. O. (2008). EPR as an analytical tool in assessing the mineral nutrients and irradiated food products-vegetables. *Spectrochimica Acta - Part A: Molecular and Biomolecular Spectroscopy*, *71*(3), 809–813. https://doi.org/10.1016/j.saa.2008.02.003

Prasuna, C. P Lakshmi, Chakradhar, R. P. S., Rao, J. L., & Gopal, N. O. (2009). EPR and IR spectral investigations on some leafy vegetables of Indian origin. *Spectrochimica Acta - Part A: Molecular and Biomolecular Spectroscopy*, *74*(1), 140–147. https://doi.org/10.1016/j.saa.2009.05.020

Raffi, J., Yordanov, N. D., Chabane, S., Douifi, L., Gancheva, V., & Ivanova, S. (2000). Identification of irradiation treatment of aromatic herbs, spices and fruits by electron paramagnetic resonance and thermoluminescence. *Spectrochimica Acta - Part A: Molecular*

*and Biomolecular Spectroscopy*, *56*(2), 409–416. https://doi.org/10.1016/S1386-1425(99)00252-8

Raitio, R., Orlien, V., & Skibsted, L. H. (2011). Electron spin resonance spectroscopy for evaluation of early oxidative events in semisolid palm oil. *European Journal of Lipid Science and Technology*, *113*(2), 208–213. https://doi.org/10.1002/ejlt.201000087

Ramadan, M. F., & El-Shamy, H. (2013). Snapdragon (Antirrhinum majus) seed oil: Characterization of fatty acids, bioactive lipids and radical scavenging potential. *Industrial Crops and Products*, *42*(1), 373–379. https://doi.org/10.1016/j.indcrop.2012.06.022

Rana, S., Chawla, R., Kumar, R., Singh, S., Zheleva, A., Dimitrova, Y., Gadjeva, V., Arora, R., Sultana, S., & Sharma, R. K. (2010). Electron paramagnetic resonance spectroscopy in radiation research: Current status and perspectives. *Journal of Pharmacy & Bioallied Sciences*, *2*(2), 80–87. https://doi.org/10.4103/0975-7406.67006

Rieseberg, M., Kasper, C., Reardon, K. F., & Scheper, T. (2001). Flow cytometry in biotechnology. *Applied Microbiology and Biotechnology*, *56*(3–4), 350–360. https://doi.org/10.1007/s002530100673

Roman, O., Maillard, M.-N., Plessis, C., & Riquet, A.-M. (2010). Electron spin resonance spectroscopy: a promising method for studying lipid oxidation in foods. *Lipid Technology*, *22*(4), 87–90. https://doi.org/10.1002/lite.201000009

Rottem, S., Hubbell, W. L., Hayflick, L., & McConnell, H. M. (1970). Motion of fatty acid spin labels in the plasma membrane of mycoplasma. *Biochimica et Biophysica Acta (BBA) - Biomembranes*, *219*(1), 104–113. https://doi.org/10.1016/0005-2736(70)90065-9

Rudko, V. V., Vorona, I. P., Baran, N. P., & Ishchenko, S. S. (2009). Thermally stimulated transformation of the EPR spectra in γ-irradiated bone tissue. *Radiation Measurements*, *44*(3), 239–242. https://doi.org/10.1016/j.radmeas.2009.03.016

Sahu, I. D., & Lorigan, G. A. (2015). Biophysical EPR studies applied to membrane proteins. *Journal of Physical Chemistry & Biophysics*, *5*(6), doi:10.4172/2161-0398.1000188. https://doi.org/10.4172/2161-0398.1000188

Sahu, I. D., & Lorigan, G. A. (2018). Site-directed spin labeling EPR for studying membrane

proteins. *BioMed Research International*, *2018*(1). https://doi.org/10.1155/2018/3248289

Schweiger, A., & Jeschke, G. (2001). *Principles of pulse electron paramagnetic resonance*. Oxford University Press.

Serio, A., Chiarini, M., Tettamanti, E., & Paparella, A. (2010). Electronic paramagnetic resonance investigation of the activity of Origanum vulgare L. essential oil on the Listeria monocytogenes membrane. *Letters in Applied Microbiology*, *51*(2), 149–157. https://doi.org/10.1111/j.1472-765X.2010.02877.x

Sezer, M. Ö., Ece, E., Uslu, A., Ozmen, A., & Sayin, U. (2019). Determination of the irradiation effects on senna (Casia acutifolia) leaves by ESR technique and microbiological analysis. *Radiation Physics and Chemistry*, 108434. https://doi.org/10.1016/j.radphyschem.2019.108434

Sgherri, C., Porta, A., Castellano, S., Pinzino, C., Quartacci, M. F., & Calucci, L. (2014). Effects of azole treatments on the physical properties of Candida albicans plasma membrane: A spin probe EPR study. *Biochimica et Biophysica Acta - Biomembranes*, *1838*(1 PARTB), 465–473. https://doi.org/10.1016/j.bbamem.2013.10.015

Silvagni, A., Franco, L., Bagno, A., & Rastrelli, F. (2010). Thermoinduced lipid oxidation of a culinary oil: A kinetic study of the oxidation products by magnetic resonance spectroscopies. *Journal of Physical Chemistry A*, *114*(37), 10059–10065. https://doi.org/10.1021/jp104295c

Silván, J. M., van de Lagemaat, J., Olano, A., & del Castillo, M. D. (2006). Analysis and biological properties of amino acid derivates formed by Maillard reaction in foods. *Journal of Pharmaceutical and Biomedical Analysis*, *41*(5), 1543–1551. https://doi.org/10.1016/j.jpba.2006.04.004

Sin, D. W. M., Wong, Y. C., & Yao, W. Y. (2006). Analysis of g-irradiated melon, pumpkin, and sunflower seeds by electron paramagnetic resonance spectroscopy and gas chromatography-mass spectrometry. *Journal of Agricultural and Food Chemistry*, *54*(19), 7159–7166. https://doi.org/10.1021/jf061349u

Soncin, S., Panseri, S., Rusconi, M., Mariani, M., Chiesa, L. M., & Biondi, P. A. (2012).

Improved determination of 2-dodecylcyclobutanone in irradiated ground beef patties by gas-chromatography-mass-spectrometry (GC/MS) coupled with solid-phase microextraction (SPME) technique. *Food Chemistry*, *134*(1), 440–444. https://doi.org/10.1016/j.foodchem.2012.02.089

Song, J. M., Kim, B. K., Kim, W. Y., Kim, M. J., Ki, H. A., Lee, K. H., Kang, W. S., Kang, I. H., Kang, S. J., & Pal, S. (2009). Identification of γ-ray irradiated medicinal herbs using pulsed photostimulated luminescence, thermoluminescence, and electron spin resonance spectroscopy. *Analytical and Bioanalytical Chemistry*, *394*(7), 1931–1945. https://doi.org/10.1007/s00216-009-2877-7

Stachowicz, W., Burlińska, G., Michalik, J., Dziedzic-Goclawska, A., & Ostrowski, K. (1993). Applications of EPR spectroscopy to radiation treated materials in medicine, dosimetry, and agriculture. *Applied Radiation and Isotopes*, *44*(1–2), 423–427. https://doi.org/10.1016/0969-8043(93)90260-H

Stachowicz, W., Burlińska, G., Michalik, J., Dziedzic-Goclawska, A., & Ostrowski, K. (1995). The EPR detection of foods preserved with the use of ionizing radiation. *Radiation Physics and Chemistry.*, *46*(4), 771–777.

Staško, A., Polovka, M., Brezová, V., Biskupič, S., & Malík, F. (2006). Tokay wines as scavengers of free radicals (an EPR study). *Food Chemistry*, *96*(2), 185–196. https://doi.org/10.1016/j.foodchem.2005.02.022

Strzelczak, G., Vanhaelewyn, G., Stachowitz, W., Goovaerts, E., Callens, F., & Michalik, J. (2001). Multifrequency EPR study of carbonate- and sulfate-derived radicals produced by radiation in shells and corallite. *Radiation Research*, *155*(4), 619–624. http://www.ncbi.nlm.nih.gov/pubmed/11260664

Subongkot, T., & Ngawhirunpat, T. (2015). Effect of liposomal fluidity on skin permeation of sodium fluorescein entrapped in liposomes. *International Journal of Nanomedicine*, *10*, 4581–4592. https://doi.org/10.2147/IJN.S86624

Suzen, S., Gurer-Orhan, H., & Saso, L. (2017). Detection of reactive oxygen and nitrogen species by electron paramagnetic resonance (EPR) technique. *Molecules*, *22*(1), 181.

https://doi.org/10.3390/molecules22010181

Szterk, A., Stefaniuk, I., Waszkiewicz-Robak, B., & Roszko, M. (2011). Oxidative stability of lipids by means of EPR spectroscopy and chemiluminescence. *JAOCS, Journal of the American Oil Chemists' Society*, *88*(5), 611–618. https://doi.org/10.1007/s11746-010-1715-6

Taghvaei, M., Sommers, C., Ceric, O., Hussain, F., Yucel, U., & Smith, J. S. (2020). Solid-phase micro extraction of food irradiation marker 2-dodecylcyclobutanone (2-DCB) from chicken jerky treated with glycerol. *Journal of Food Science*, *85*(8), 2608–2614. https://doi.org/10.1111/1750-3841.15322

Taghvaei, M., Tonyali, B., Sommers, C., Ceric, O., Linghu, Z., Smith, J. S., & Yucel, U. (2021). Formation kinetics of radiolytic lipid products in model food–lipid systems with gamma irradiation. *Journal of the American Oil Chemists' Society*, *98*(7), 737–746. https://doi.org/10.1002/aocs.12513

Tewfik, I. (2008). A rapid direct solvent extraction method for the extraction of cyclobutanones from irradiated chicken and liquid whole egg. *International Journal of Food Science and Technology*, *43*(1), 108–113. https://doi.org/10.1111/j.1365-2621.2006.01399.x

Thomsen, M. K., Lauridsen, L., Skibsted, L. H., & Risbo, J. (2005). Two types of radicals in whole milk powder. Effect of lactose crystallization, lipid oxidation, and browning reactions. *Journal of Agricultural and Food Chemistry*, *53*(5), 1805–1811. https://doi.org/10.1021/jf0485483

Tomaiuolo, M., Chiaravalle, A. E., Mangiacotti, M., Petrella, A., Di Taranto, A., & Iammarino, M. (2019). Innovative techniques for identifying a mechanically separated meat: sample irradiation coupled to electronic spin resonance. *European Food Research and Technology*, *853*. https://doi.org/10.1007/s00217-019-03340-x

Tomaiuolo, M., Mangiacotti, M., Trotta, G., Marchesani, G., Chiappinelli, A., & Chiaravalle, A. E. (2018). Identification of X-ray irradiated walnuts by ESR spectroscopy. *Radiation Physics and Chemistry*, *150*(March), 35–39. https://doi.org/10.1016/j.radphyschem.2018.04.007

Tonyali, B., McDaniel, A., Trinetta, V., & Yucel, U. (2019). Evaluation of heating effects on the morphology and membrane structure of Escherichia coli using electron paramagnetic resonance spectroscopy. *Biophysical Chemistry*, *252*(March), 106191. https://doi.org/10.1016/j.bpc.2019.106191

Tonyali, B., Sommers, C., Ceric, O., Smith, J. S., & Yucel, U. (2020). An analysis of cellulose- and dextrose-based radicals in sweet potatoes as irradiation markers. *Journal of Food Science*. https://doi.org/10.1111/1750-3841.15359

Troup, G. J., Navarini, L., Liverani, F. S., & Drew, S. C. (2015). Stable radical content and anti-radical activity of roasted arabica coffee: From in-tact bean to coffee brew. *PLoS ONE*, *10*(4), 10–16. https://doi.org/10.1371/journal.pone.0122834

Truby, F. K., & Storey, W. H. (1959). Radiation induced free radicals in lactose. *The Journal of Chemical Physics*, *31*(3), 857–858. https://doi.org/10.1063/1.1730489

Uhl, B. C., Peterson, D. G., & Yucel, U. (2020). Nano-structured lipid particles for controlled transport of hydrophobic volatile and non-volatile molecules. *Colloids and Surfaces A: Physicochemical and Engineering Aspects*, *591*(January), 124421. https://doi.org/10.1016/j.colsurfa.2020.124421

Velasco, J., Andersen, M. L., & Skibsted, L. H. (2005). Electron spin resonance spin trapping for analysis of lipid oxidation in oils: inhibiting effect of the spin trap alpha-phenyl-N-tert-butylnitrone on lipid oxidation. *Journal of Agricultural and Food Chemistry*, *53*(5), 1328–1336. https://doi.org/10.1021/jf049051w

Velasco, J., Andersen, M. L., & Skibsted, L. H. (2021). ESR spin trapping for in situ detection of radicals involved in the early stages of lipid oxidation of dried microencapsulated oils. *Food Chemistry*, *341*(September 2020), 128227. https://doi.org/10.1016/j.foodchem.2020.128227

Weil, J. A., & Bolton, J. R. (2007). *Electron Paramagnetic Resonance*. John Wiley & Sons, Inc. https://doi.org/10.1002/0470084987

Xue, Z. D., Zhang, Q. A., & Zheng, H. R. (2021). Roles of free radical on the formation of acetaldehyde in model wine solutions under different ultrasound parameters: A key bridge-link compound for red wine coloration during ageing. *Ultrasonics Sonochemistry*, *79*,

105757. https://doi.org/10.1016/j.ultsonch.2021.105757

Yamaoki, R., Kimura, S., & Ohta, M. (2010). Analysis of electron spin resonance spectra of irradiated gingers: Organic radical components derived from carbohydrates. *Radiation Physics and Chemistry*, *79*(4), 417–423. https://doi.org/10.1016/j.radphyschem.2009.11.011

Yamaoki, R., Kimura, S., & Ohta, M. (2015). Evaluation of absorbed dose in irradiated sugar-containing plant material (peony roots) by an ESR method. *Radiation Physics and Chemistry*, *117*(0910), 41–47. https://doi.org/10.1016/j.radphyschem.2015.07.010

Yarkov, S. P., Tretyakov, S. I., & Khramov, E. N. (2000). EPR evaluation of absorbed doses in gamma-irradiated animal bone tissues. *High Energy Chemistry*, *34*(5), 295–300.

Yeretzian, C., Pascual, E. C., & Goodman, B. A. (2012). Effect of roasting conditions and grinding on free radical contents of coffee beans stored in air. *Food Chemistry*, *131*(3), 811–816. https://doi.org/10.1016/j.foodchem.2011.09.048

Yordanov, N. D., & Aleksieva, K. (2007). EPR study on gamma-irradiated fruits dehydrated via osmosis. *Radiation Physics and Chemistry*, *76*(6), 1084–1086. https://doi.org/10.1016/j.radphyschem.2006.11.006

Yordanov, N. D., Aleksieva, K., Dimitrova, A., Georgieva, L., & Tzvetkova, E. (2006). Multifrequency EPR study on freeze-dried fruits before and after X-ray irradiation. *Radiation Physics and Chemistry*, *75*(9), 1069–1074. https://doi.org/10.1016/j.radphyschem.2006.03.072

Yordanov, Nicola D., & Aleksieva, K. (2009). Preparation and applicability of fresh fruit samples for the identification of radiation treatment by EPR. *Radiation Physics and Chemistry*, *78*(3), 213–216. https://doi.org/10.1016/j.radphyschem.2008.10.003

Yordanov, Nicola D., & Georgieva, E. (2004). EPR and UV spectral study of gamma-irradiated white and burned sugar, fructose and glucose. *Spectrochimica Acta - Part A: Molecular and Biomolecular Spectroscopy*, *60*(6), 1307–1314. https://doi.org/10.1016/j.saa.2003.10.027

Yordanov, Nicola D., & Mladenova, R. (2004). EPR study of free radicals in bread. *Spectrochimica Acta - Part A: Molecular and Biomolecular Spectroscopy*, *60*(6), 1395–1400. https://doi.org/10.1016/j.saa.2003.10.039

Yordanov, Nicola D., & Pachova, Z. (2006). Gamma-irradiated dry fruits: An example of a wide variety of long-time dependent EPR spectra. *Spectrochimica Acta - Part A: Molecular and Biomolecular Spectroscopy*, *63*(4), 891–895. https://doi.org/10.1016/j.saa.2005.10.023

Yu, L., Fang, W., He, Y., Cai, W., Wei, W., & Tian, C. (2021). Secondary structure and transmembrane topology analysis of the N-terminal domain of the inner membrane protein EccE1 from M. smegmatis using site-directed spin labeling EPR. *Biochimica et Biophysica Acta - Biomembranes*, *1863*(2). https://doi.org/10.1016/j.bbamem.2020.183515

Yuan, J. F., Chen, Z. Y., Wang, D. H., Gong, M. G., & Qiu, Z. J. (2021). Microwave-induced free radicals production in red wine and model wine by electron paramagnetic resonance spin trapping. *Journal of Food Processing and Preservation*, *45*(5), 1–7. https://doi.org/10.1111/jfpp.15407

Yucel, U., Elias, R. J., & Coupland, J. N. (2012). Solute distribution and stability in emulsion-based delivery systems: An EPR study. *Journal of Colloid and Interface Science*, *377*(1), 105–113. https://doi.org/10.1016/j.jcis.2012.03.071

Yucel, U., Elias, R. J., & Coupland, J. N. (2013). Effect of liquid oil on the distribution and reactivity of a hydrophobic solute in solid lipid nanoparticles. *JAOCS, Journal of the American Oil Chemists' Society*, *90*(6), 819–824. https://doi.org/10.1007/s11746-013-2228-x

Zalibera, M., Staško, A., Šlebodová, A., Jančovičová, V., Čermáková, T., & Brezová, V. (2008). Antioxidant and radical-scavenging activities of Slovak honeys - An electron paramagnetic resonance study. *Food Chemistry*, *110*(2), 512–521. https://doi.org/10.1016/j.foodchem.2008.02.015

Zang, S., Tian, S., Jiang, J., Han, D., Yu, X., Wang, K., Li, D., Lu, D., Yu, A., & Zhang, Z. (2017). Determination of antioxidant capacity of diverse fruits by electron spin resonance (ESR) and UV–vis spectrometries. *Food Chemistry*, *221*, 1221–1225. https://doi.org/10.1016/j.foodchem.2016.11.036

Zhang, Q.-A., Shen, Y., Fan, X., Martín, J. F. G., Wang, X., & Song, Y. (2015). Free radical generation induced by ultrasound in red wine and model wine: An EPR spin-trapping study.

*Ultrasonics Sonochemistry*, *27*, 96–101. https://doi.org/10.1016/j.ultsonch.2015.05.003

Zhao, Q., Wang, M., Zhang, W., Zhao, W., & Yang, R. (2020). Impact of phosphatidylcholine and phosphatidylethanolamine on the oxidative stability of stripped peanut oil and bulk peanut oil. *Food Chemistry*, *311*(June 2019), 125962. https://doi.org/10.1016/j.foodchem.2019.125962

Zhao, Y., Wang, F., Li, W., Li, A., & Ha, Y. (2012). 2-Dodecylcyclobutanone as an irradiation dose indicator to identify and estimate original dose in irradiated ground beef. *European Food Research and Technology*, *235*(5), 901–906. https://doi.org/10.1007/s00217-012-1818-4

Zhu, J., & Sevilla, M. D. (1990). Kinetic analysis of free-radical reactions in the low-temperature autoxidation of triglycerides. *Journal of Physical Chemistry*, *94*(4), 1447–1452. https://doi.org/10.1021/j100367a046

Zianni, R., Mentana, A., Campaniello, M., Chiappinelli, A., Tomaiuolo, M., Chiaravalle, A. E., & Marchesani, G. (2021). An investigation using a validated method based on HS-SPME-GC-MS detection for the determination of 2-dodecylcyclobutanone and 2-tetradecylcyclobutanone in X-ray irradiated dairy products. *Lwt*, *153*(May 2021), 112466. https://doi.org/10.1016/j.lwt.2021.112466

Zou, P., & Mchaourab, H. S. (2010). Increased sensitivity and extended range of distance measurements in Spin-labeled membrane proteins: Q-band double electron-electron resonance and nanoscale bilayers. *Biophysical Journal*, *98*(6), L18–L20. https://doi.org/10.1016/j.bpj.2009.12.4193

# Chapter 2 - Objectives

EPR spectroscopy can offer a fast, sensitive, and non-destructive technique to detect free radicals in food and related matrices. The broad analysis range of EPR includes but is not limited to the detection and quantification of irradiation-derived radicals (e.g., cellulose-derived radicals) in irradiated foods and characterization of membrane structures (e.g., membrane mobility). The goal of this dissertation is to show the suitability of EPR spectroscopy for the characterization of chemical and structural properties of foods and related matrices in comparison to traditional techniques.

The methods for membrane structure characterization (e.g., flow cytometry or microscopic methods) are indirect methods that are challenging due to long sample preparation time and low sensitivity. EPR spectroscopy provides a direct and non-destructive technique to analyze changes in bacterial membrane mobility due to external thermal stress. I hypothesize that the exposure of *E. coli* to extreme high temperatures (42, 50, or 65 °C) would cause an increase in the bacterial membrane mobility due to melting of membrane lipids around 40-45 °C. The changes in membrane mobility would be quantified via the mobility of a 16-doxylstearic acid (16-DSA) spin probe, an EPR active molecule that can align with the membrane, using EPR spectroscopy. The results of EPR spectroscopy would be supported by the use of particle size data using dynamic light scattering (DLS) and morphology data using transmission electron microscopy (TEM). The objective is to use EPR spectroscopy to characterize the changes in a bacterial membrane under the stress of thermal treatment without disturbing the cell integrity.

The irradiation treatment on foods is needed to be monitored due to safety concerns regarding the possible formation of toxic compounds and compliance of the irradiation dose to the regulatory limits. EPR spectroscopy can detect irradiation and quantify irradiation dose by detecting irradiation-derived free radicals. In addition, it can be used to study irradiated cellulose-rich foods and its parts subjected to different sample preparation methods. I hypothesize that the signal coming from irradiation-derived cellulose radicals would be dominant in the EPR spectra of sweet potato (SP) skin due to the rich cellulose content of SP skin. In contrast, the EPR spectra of SP flesh would be a combination of signals coming from irradiation-derived cellulose radicals and irradiation-derived dextrose radicals. I, also, hypothesize that the EPR signal of irradiation-derived dextrose radicals would be pronounced in sieved ground SP

samples due to retention of big cellulose particles on sieve. For this purpose, dried SP would be prepared at two moisture contents (48.3 and 9.7 % by drying at 150 °F for 24 or 48 h) and irradiated at 0, 5, 10, 20, 30, and 50 kGy. The EPR signal characteristics (intensity and peak shape) would be evaluated for SP samples prepared with different methods (grinding, sieving, and pelletizing) and from different sample locations (skin and flesh). The objective is to show applicability of EPR spectroscopy for irradiation detection in plant-based foods.

Quantification of irradiation-derived cellulose and dextrose radicals using EPR spectra can be challenging due to broadening of native singlet peak with irradiation. The quantification of irradiation-specific cellulose satellite and dextrose split peak separately can be conducted using a peak enhancement approach. Therefore, I hypothesize that the developed peak enhancement methods would improve the resolution of the complex EPR spectra and increase the precision of quantification. The complex EPR spectra would be analyzed by calculating total areas under all peaks (TPA), areas of irradiation-specific cellulose satellite peaks (SPA), and areas of irradiation-specific dextrose split peak (GPA) using GRAMS software. The third objective is to use the irradiation-specific cellulose satellite and dextrose split peak as irradiation indicators using EPR spectroscopy and implementing a peak enhancement method.

Irradiated lipid-containing samples are traditionally characterized with gas chromatography mass spectrometry (GC-MS). The quantification of lipid-radiolysis products (e.g., 2-DCB) is performed using internal standard (IS). The precision of quantification can be improved by choosing right IS concentration. In contrary, the EPR spectroscopy can provide a sensitive technique to study irradiation-derived radicals in lipid-containing samples. Therefore, I hypothesize that EPR spectroscopy is a good alternative to study irradiation-derived radicals in lipid-rich foods compared to traditional GC-MS analysis. In addition, I hypothesize that the precision of 2-DCB quantification using GC-MS can be improved with use of IS at right concentration. For this study, chicken jerky treats (CJT) and pig ears (PE) are chosen for lipid-rich matrices as these products are commonly commercially irradiated foods. CJT and PE samples irradiated at two doses (10 and 50 kGy) would be studied with EPR spectroscopy; the irradiated CJT samples would be tested for two IS concentrations (8 and 80 ng/g CJT), while the irradiated PE samples would be analyzed for three IS concentrations (8, 80, and 800 ng/g PE) using GC-MS. The fourth objective is to use EPR spectroscopy for irradiation detection in lipid-

containing samples and to improve the precision of GC-MS analysis for radiolysis products in lipid-containing samples.

# Chapter 3 - Evaluation of heating effects on the morphology and membrane structure of *Escherichia coli* using electron paramagnetic resonance spectroscopy[1]


## Abstract

Bacterial cell characteristics, such as size, morphology, and membrane integrity, are affected by environmental conditions. Thermal treatment results in related structural changes, extent of which is determined by the microorganism's survival skills and inactivation kinetics. The objective of this study was to characterize changes in cell structure of *Escherichia coli* during heating using the combined analysis of dynamic light scattering (DLS), electron paramagnetic resonance (EPR) spectroscopy, and transmission electron microscopy (TEM) techniques. The size of E. coli cells increased from 2.3 μm to 3.0 μm with heating up to 50 °C followed by a shrinkage with further heating up to 70 °C. The morphological changes were verified using transmission electron microscopy. Related changes in membrane integrity were quantified via the mobility of 16-doxylstearic acid (16-DSA) spin probe using EPR spectroscopy. Two order parameters S1 and S2 defined on x- and y-axes, respectively, decreased with increasing temperature indicating loss of membrane integrity. The combined techniques as in this study can be used to further understand factors that play role in survival behavior of microorganisms.


## Introduction

The survival kinetics of microorganisms is determined by the effects of external stresses, such as heat and antimicrobial compounds, on cell size, morphology, and membrane structure (Broeckx et al., 2016; Glover et al., 1999). The extent of these changes is determined by inactivation mechanisms and the resistance of microorganisms to the applied stress. The heating process can

[1] Tonyali B, McDaniel A, Trinetta V, Yucel U. (2019). Evaluation of heating effects on the morphology and membrane structure of *Escherichia coli* using electron paramagnetic resonance spectroscopy. Biophysical Chemistry, (252), 106191. doi: 10.1016/j.bpc.2019.106191.

damage multiple cellular elements, such as disruption of the peptidoglycan cell wall and damage to RNA, DNA, and enzymes. Microorganisms can resist thermal stresses by altering their cellular properties (i.e. adjustment of lipid bilayer viscosity and rearrangement of the membrane layer to maintain the membrane functionality). However, cellular alterations can tolerate a maximum change, after which the cell structure irreversibly gets damaged (Serio et al., 2010). The destruction of these elements interferes with the replication and the self-maintenance mechanisms of the cell. Moreover, changes such as the disengagement of the membrane from the cell wall, formation of pores, release of cell components out of the cell, and alterations in outer and inner cell membrane structures have been previously reported (Baatout et al., 2005). The increased cell membrane permeability, observed in parallel with increased membrane fluidity, disrupts the control over the transport mechanisms and eventually leads to the loss of internal homeostasis (Cebrián et al., 2017). Indeed, this kind of cell damage is known to result in compromised metabolic cell functions as well as leaching of the cell components (Glover et al., 1999; Katsui et al., 1982). Early studies measured particle size with microscopic methods, which require analysis of large number images and tedious sample preparation steps (Trueba et al., 1982). More recent studies commonly used flow cytometry to characterize membrane structure and mobility. This technique is based on use of fluorescence probes and the measurement is taken on each cell at a single time (Clementi et al., 2014). The changes in the membrane integrity under different stresses, such as temperature (Baatout et al., 2005) and ultrasound (Li et al., 2016), were previously investigated using this technique. In flow cytometry analysis, membrane integrity is characterized using dyes to stain specific components (e.g. DNA) in bacteria cell. The dying step requires time for permeabilization and washing steps afterwards which are challenging and time-consuming. Moreover, the cell aggregations might interfere with the sensitivity of measurements (Rieseberg et al., 2001). Recently, Vargas et al. (2017) showed the usability of dynamic light scattering (DLS) measurements to study the growth (i.e., size and population) of *E.coli* and *S.aureus* in the lag phase as an alternative to the traditional methods. Electron Paramagnetic Resonance (EPR) spectroscopy is a non-destructive technique, which has been used to study membrane structures (Glover et al., 1999; Kong et al., 2018; Serio et al., 2010). EPR spectroscopy is sensitive to the presence of molecules with unpaired electrons, where the spin relaxation of electrons is determined by the mobility of the molecules. In a spin-labeling technique, a stable free radical (i.e., spin probe) is introduced to the system and serves as

a reporter molecule. The interaction between the spin probe and the target molecule, i.e. the cell membrane, is used for characterization studies. For example, a nitroxide radical with an aliphatic carbon chain aligns itself along the lipid bilayer, and the specific rotation on each axes is responsible for the shape of the complex slow-tumbling spectra (Kong et al., 2018; Kveder et al., 2004; Serio et al., 2010). The hyperfine splitting of slow-tumbling spectra is typically associated with the extent of rotational diffusivity of the spin probe on each axes (Rottem et al., 1970). Previously Glover et al. (Glover et al., 1999) used an aliphatic spin probe 5-doxyl-stearic acid (5-DSA) to characterize the membrane integrity of *Proteus mirabilis, Staphylococcus aureus,* and *Saccharomyces cerevisiae* under the action of surfactants. Similarly, other researchers used similar aliphatic spin probes to study the integrity and fluidity of human sperm plasma membranes (Kveder et al., 2004), *Listeria monocytogenes* cell membranes (Serio et al., 2010), and bovine retina membranes (Duda et al., 2017) as a function of various external stresses. Therefore, we propose that EPR techniques can be used to characterize the changes in bacterial membrane, which eventually provides information for their survival ability. The objective of this study is to evaluate the effect of heating on the cell morphology and membrane mobility of *E. coli* by the combined analytical techniques of EPR, DLS, and transmission electron microscopy (TEM).

## Materials and Methods

### Materials

*Escherichia coli* cultures (ATCC® 12435™) were obtained from American Type Culture Collection (ATCC®; Manassas, VA). The stock solutions were stored on Trypticase Soy Agar slants (TSA; Becton, Dickinson and Company, Sparks, MD) at 4 °C, and the cultures were grown in Tryptic Soy Broth (TSB; Becton, Dickinson and Company, Sparks, MD) prior to use. The spin probe, 16-doxylstearic acid (16-DSA; >95.0 % purity), was purchased from Enzo Life Sciences (NY, USA). Potassium chloride (KCl; Fisher Scientific, USA), peptone water (Bacto™ Peptone, Becton, Dickinson and Company, Sparks, MD) and phosphate-buffered saline (PBS; VWR International, LLC, Solon, OH) were analytical grade and used without any modification.

## Growth Curve

The cell count and absorbance measurements were performed following the method given in Fujikawa et al. (Fujikawa et al., 2004) with some modifications. Briefly, an isolated colony of *E. coli* was inoculated into 10 mL of TSB and incubated at 35 °C overnight. 5 µL of the overnight (ca. 18 hours) incubated cultures were transferred to 50 mL of TSB and kept at 35 °C. Every three hours, the optical density was measured using a UV-Vis spectrophotometer at 600 nm (Genesys, 10S UV-Vis, Thermo-Fisher). For *E. coli* enumeration, samples were serially diluted in 0.1% peptone water (Bacto™ Peptone, Becton, Dickinson and Company, Sparks, MD) and spread plated on TSA following the standard plate count agar method. All plates were incubated (VWR Incubator Gr Con 6, 85CF, Germany) at 35°C for 24 hours. Cell counts results were reported in logarithmic scale.

## Particle Size Analysis

The particle size of *E. coli* cells was measured using a dynamic light scattering (DLS) instrument (DelsaMax Pro, Beckman Coulter, Brea, CA) based on the method described by Saini et al. (Saini et al., 2011) and Walker et al. (Walker et al., 2005) with modifications. Briefly, *E. coli* cells were grown in TSB at 35 °C until early stationary phase (ca. 9-12 hours). The cell samples (5 mL) were centrifuged at 3800 rpm for 15 minutes (Allegra X-14R Centrifuge, Beckman Coulter) and resuspended in 5 mL of KCl solution (10 mM). The centrifugation and resuspension steps were repeated once. The twice rinsed cells were then diluted with 5 mL KCI solution to have a final concentration of $10^5$-$10^6$ cells/mL. The effect of heating from 35 to 70 °C at a rate of 1 °C/min on cell size was studied using flow cell setup with the DLS instrument. The instrument operated at 45 mW with a wavelength of 532 nm. The average of five acquisitions of hydrodynamic diameter is reported for each measurement.

## Membrane Mobility Analysis by EPR

The membrane mobility of *E. coli* cells were measured with EPR based on the method described by Glover et al. (Glover et al., 1999) with some modifications. Briefly, cell suspension in the early stationary phase (ca. 9-12 hours at 35°C) was centrifuged (3800 rpm for 15 minutes) and resuspended in glass vials containing fresh PBS (2.5 mL). Aliquots of 16-DSA solution (2.5

mM) was added to the cell suspension to have a final concentration of 400 µM. The cultures were incubated at 35 °C for 1 hour to ensure 16-DSA partition into the membrane. Incubated cultures were heated to 42, 50, or 65 °C with gentle stirring in a hermetically sealed vial using a block heater (Heating/Stirring Module, Reacti-Therm III, Pierce). When the culture temperature was reached to set temperature (ca. 1 °C/min), the cell suspensions were centrifuged at 4300 rpm for 15 minutes and the supernatant was discarded. The cell pellets (ca. 50 mg) were transferred to borosilicate capillary tubes (VWR International, ID:0.5-0.6 mm) for EPR measurements. The EPR measurements were performed at room temperature in an EPR spectrometer operating at X-band (SpinscanX, ADANI, Belarus). The samples were analyzed under the following measurement conditions: center field 335 mT, sweep width 12 mT, modulation frequency 100 kHz, modulation amplitude 600 uT, microwave power 6 mW.

## Transmission Electron Microscopy (TEM) Analysis

TEM imaging of the *E. coli* cells were conducted in the Microscopy Facility, Division of Biology, at Kansas State University. The negative staining procedure was adapted from Trinetta et al. (2008). Briefly, post fixation of cells was carried out by 1% osmium tetroxide in 0.1 M cacodylate buffered solution. Cells were treated with ethanol, and propylene oxide, respectively. Thin sections were attached on copper grids and analyzed with a CM 100 TEM (Thermo Fisher Scientific). The images were captured with a Hamamatsu C8484 digital camera using an AMT digital image capture system (Chazy, NY).

## Statistical Analysis

The results were analyzed with analysis of variance (ANOVA) for significant of difference ($\alpha < 0.05$), and post-ANOVA calculations were performed using Tukey`s multiple comparison test to evaluate differences between treatments by using Minitab software (v16, Minitab, Inc.).

# Results and Discussion

## Cell size

DLS analysis is based on the movement of the scattered particles and measures the hydrodynamic diameter (Vargas et al., 2017). The hydrodynamic diameter is not actual size; however, this technique is reliable and allows direct and real-time monitoring in the characterization of the changes. Therefore, we hypothesize that this issue did not interfere with the results. The growth curve of *E. coli* at 35 °C was created using optical density measurements at 600 nm and microbial counts in Log CFU/ml (Figure 3-1). The cells reached to stationary phase after 9 h of incubation with a 9-log population count. The cells at the early stationary phase were used for subsequent experiments as they are healthiest and most resistant to external stresses. We also monitored the size of *E. coli* cells during the different growth stages as hydrodynamic diameters using DLS technique. The *E. coli* cell size was ca. 2400 nm at the early stationary phase (Figure 3-2). This is similar to previous data reported as measured by using optical microscopy (Galaev et al., 2007; Reshes et al., 2008). The cell size effectively remained unchanged at the later stationary phase up to 24 h, however slightly but significantly ($p < 0.05$) larger size (ca. 3000 nm) was observed at the exponential growth phase. This is probably because the cell growth and cell division rates are increased, and therefore the number of large cells ready to divide is the highest in the exponential phase (Akerlund et al., 1995). In contrast, the cells were in smaller size due to slower growth rate in the stationary phase.

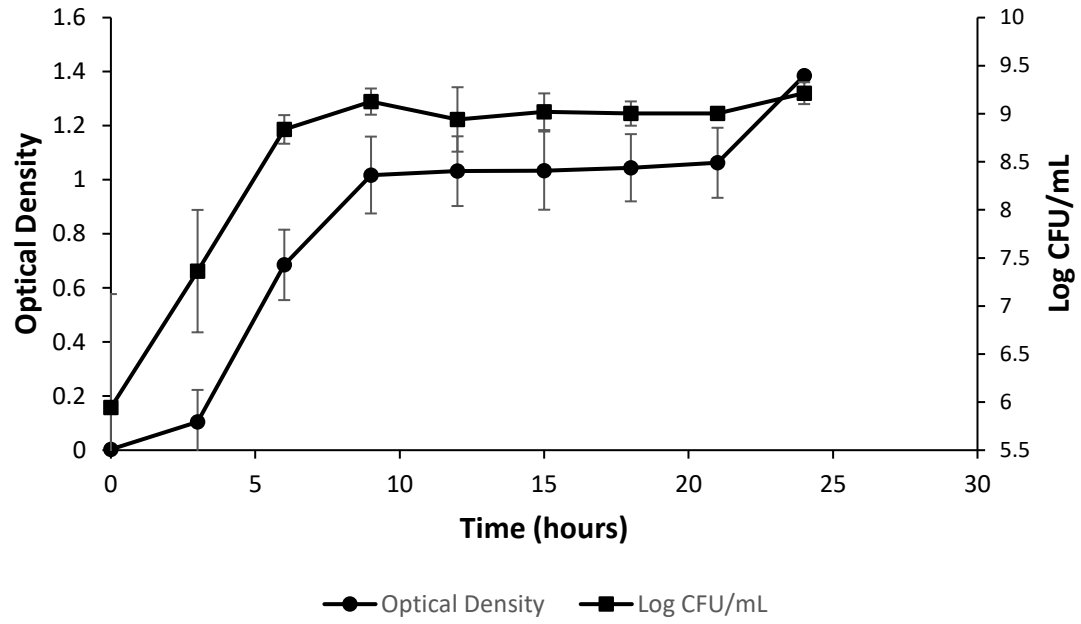


**Figure 3-1** Optical Density (O.D.) and log counts for *E. coli* cells grown at 35 °C.

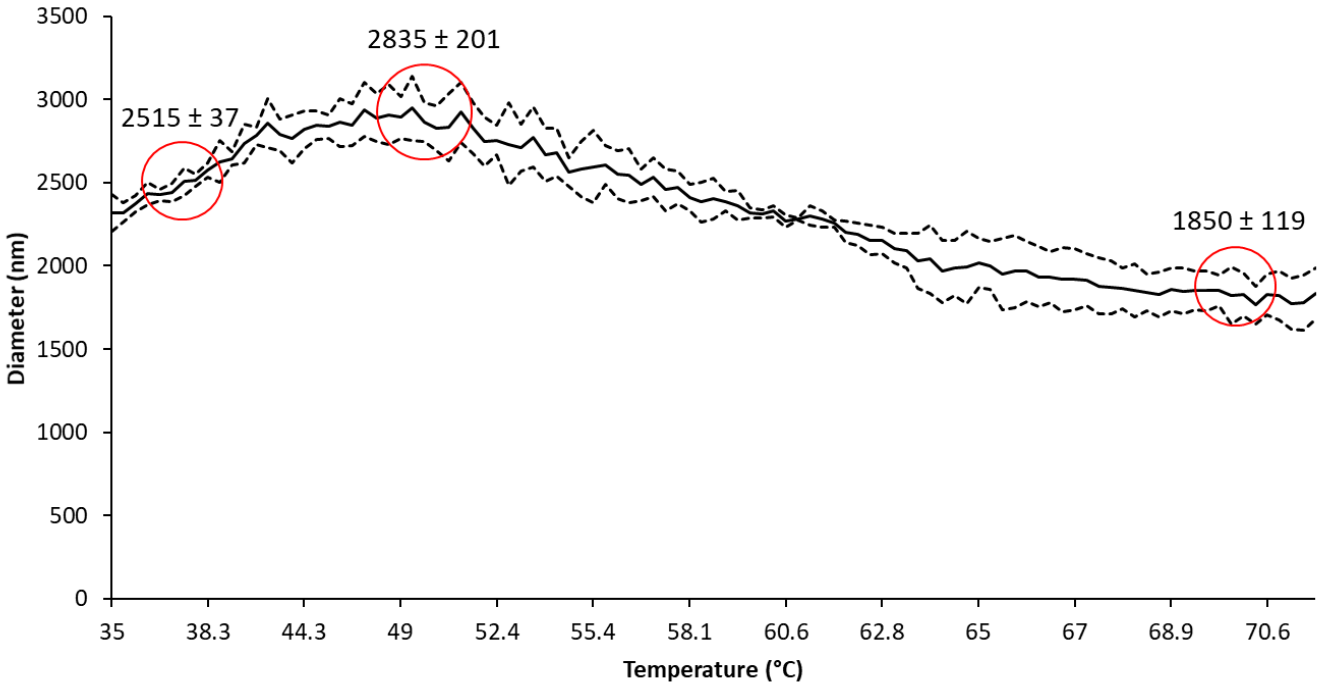


**Figure 3-2** Hydrodynamic diameter of *E. coli* cells with heat treatment (35–70 °C). The solid line represents the mean of individual particle size measurements (n=4) and the dash lines represent ± standard deviations.

In parallel to particle size measurements, the net surface charge of *E. coli* cells at their stern layer were also measured as zeta potential values, which largely remained unchanged at around -25 to -30 mV during growth. Other studies reported varying surface charge potentials (e.g., ca. between -60 and -140 mV) of *E. coli* cells during the growth cycle (Bot & Prodan, 2010; Feile et al., 1980). However, the techniques used in these studies are completely different, such as impedance spectroscopy and intracellular microelectrodes. The stern later charge measured as zeta potential is affected by the ionic strength of the solution, and in our case the measurements were conducted after dispersing cells in KCl solution (10 mM), which resulting in lower surface charge potentials and eventually masking the fine differences that might be resulting from any compositional changes during growth.

The aliquots (170 µL) of *E. coli* cell suspensions were being heated from 35 to 70 °C at a rate of 1 °C/min in the flow chamber of the DLS instrument, and the cell diameter was automatically measured at 30 sec intervals (Figure 3-2). The cell size first gradually increased up to ca. 3000 nm until around 50 °C, followed by a decrease to ca. 2000 nm with further heating to 70 °C (Figure 3-2). Similarly, Kim et al. (2012) and Gabriel and Nakano (2009) observed that inactivation of *E. coli* cells starts around 50 °C. Mackey et al. (1991) also indicated that membrane lipids melted around 40 °C and ribosomal subunits and soluble cytoplasmic proteins denatured irreversibly around 47 °C. After cell damage starts at temperatures above 50 °C, the cells lose their ability for homeostasis accompanied to disruption of membrane integrity and porosity. Therefore, continuing the heating results in reduction of the cell size likely due to leaching of cell components. The overall data for DLS measurement had high precision (standard deviations of our data were smaller than 10 % from the mean values). The standard deviation was small and less than 5 % from the mean around the optimum growth temperature of the cells (37 °C). During heating, it increased; however, it was still under 10 %. The small deviation from the mean suggests that DLS is a good alternative for particle size analysis. In the next section, we investigated the changes in the membrane integrity and mobility using the EPR spectroscopy due to heating.

## Membrane Mobility Analysis by EPR

The spin probe 16-DSA, produces an isotropic three-line spectra in solutions when it is not bound characteristic to fast tumbling spectra of nitroxide spin probes where hyperfine separations of parallel and perpendicular axes are averaged out (McConnell, 1976; Smith & Butler, 1976). The spin probe can penetrate the bacterial membrane to provide structural information as illustrated in Figure 3-3. The fast-tumbling spectra of the 16-DSA in its solution is a characteristic triplet signal for the nitroxide radical, where the rotation times on each molecular axes are averaged out (Figure 3-4A). Once it is immobilized in the phospholipid membrane, it produces an anisotropic spectrum hyperfine splitting determined by spin relaxation times of individual molecular axes as shown in Figure 3-4B.

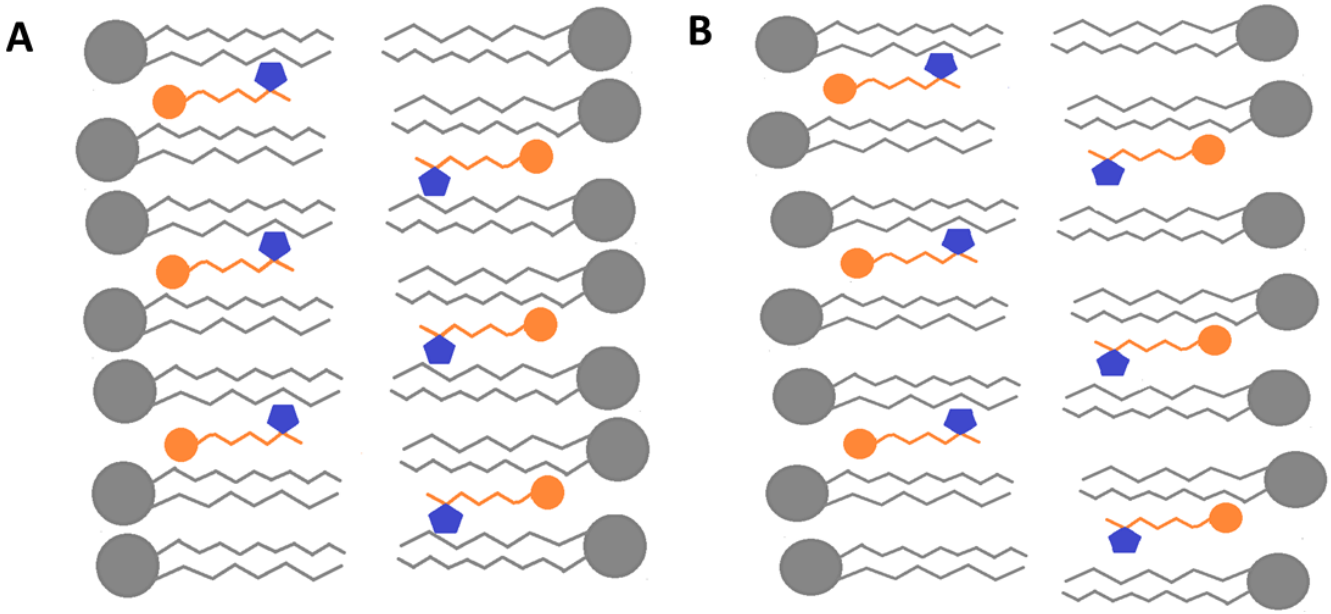


**Figure 3-3** The cartoon representation of alignment of spin probe 16-DSA (orange molecule) in the cell membrane A) at growth conditions, and B) after heating (not to the scale). The blue group on the spin probe represents the nitroxide group.

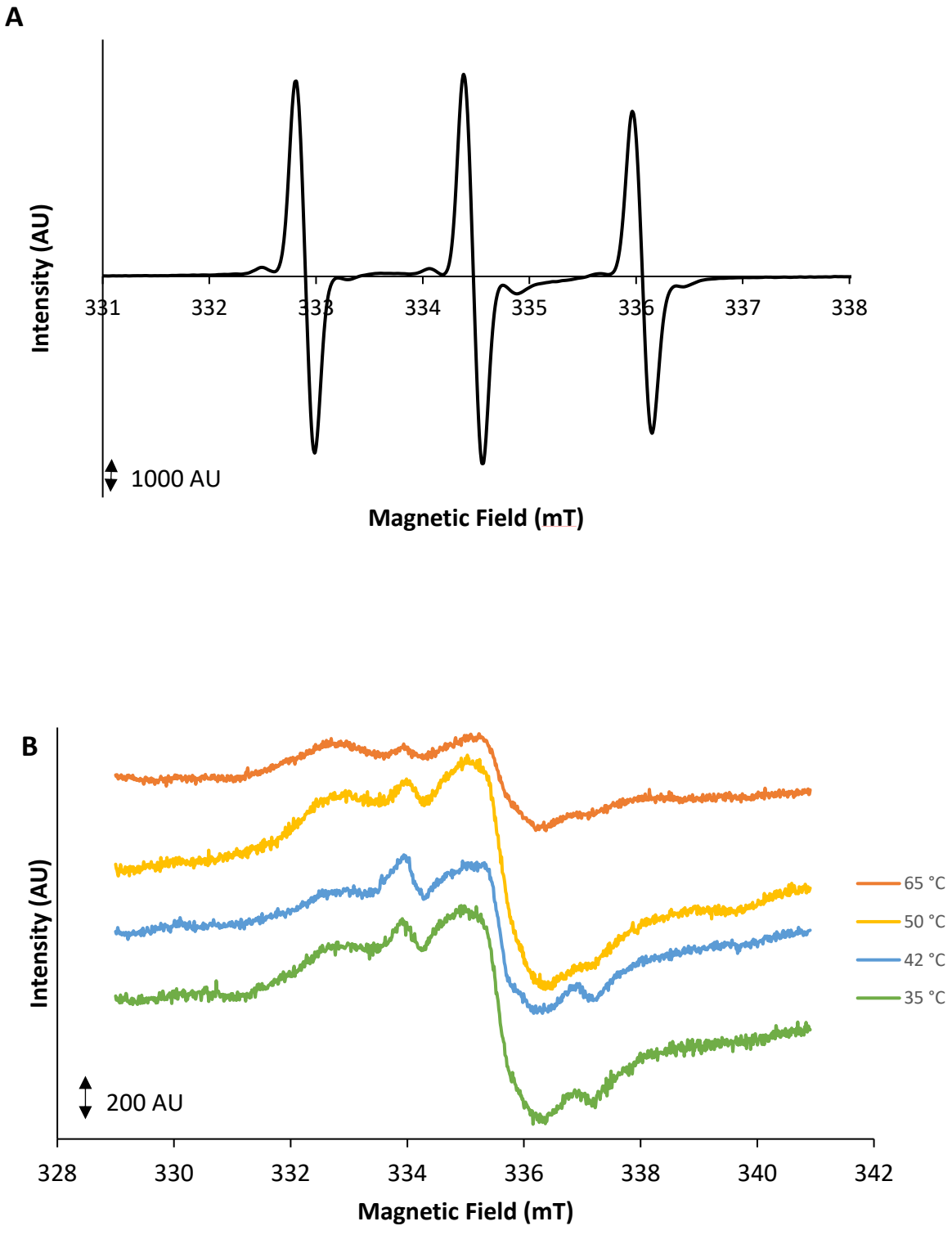


**Figure 3-4** EPR spectra of 16-DSA in A) PBS (400 uM solution) with the fast-tumbling spectra, and B) *E. coli* cells at 35, 42, 50, and 65 °C.

The interaction between the spin probe and phospholipids causes distortion in the signal, and the shape of the EPR spectra was affected by heating due to changes in the mobility of the spin probe in interaction with the membrane. The spectra of the 35 °C indicate the control sample without heating. The change in the peak shape with heating is enhanced at the high-field region, where the position of the peak located around 339 mT showed decreasing hyperfine separation, while 337 mT diffused out with increasing temperature. The faster mobility of molecules with higher rotational diffusivities in parallel and perpendicular axes resulted in decreased spectral anisotropy. These changes were quantified by the order parameters $S_1$ and $S_2$ defined from the anisotropic hyperfine peaks associated with the two perpendicular axes (Subczynski et al., 2009):

$$S_1 = (A_{zz} - A_{xx}) / (A_{zz,max} - A_{xx,min}) \quad (4)$$

$$S_2 = (A_{zz} - A_{yy}) / (A_{zz,max} - A_{yy,min}) \quad (5)$$

where $A_{xx}$ is the hyperfine coupling constant related to motion on the x-axis, $A_{yy}$ is the hyperfine coupling constant related to motion on the y-axis, $A_{zz}$ is the hyperfine coupling constant related to motion on the parallel axis, and $(A_{zz,max} - A_{xx,min})$ and $(A_{zz,max} - A_{yy,min})$ are the hyperfine coupling constants for the rigid spectra. The measurements of hyperfine coupling constants were shown in Figure 3-5. Rigid spectra values (2.73 and 2.78 mT for $S_1$ and $S_2$, respectively) are obtained under immobilized spin probe conditions in freeze-dried powders and in agreement with the literature (Freed, 1976; Glover et al., 1999; Kong et al., 2018). The order parameter is close to 0 in the fast tumbling spectra, while it is close to 1 in the slow tumbling spectra (i.e., when the spin probe is completely immobilized) (Glover et al., 1999).

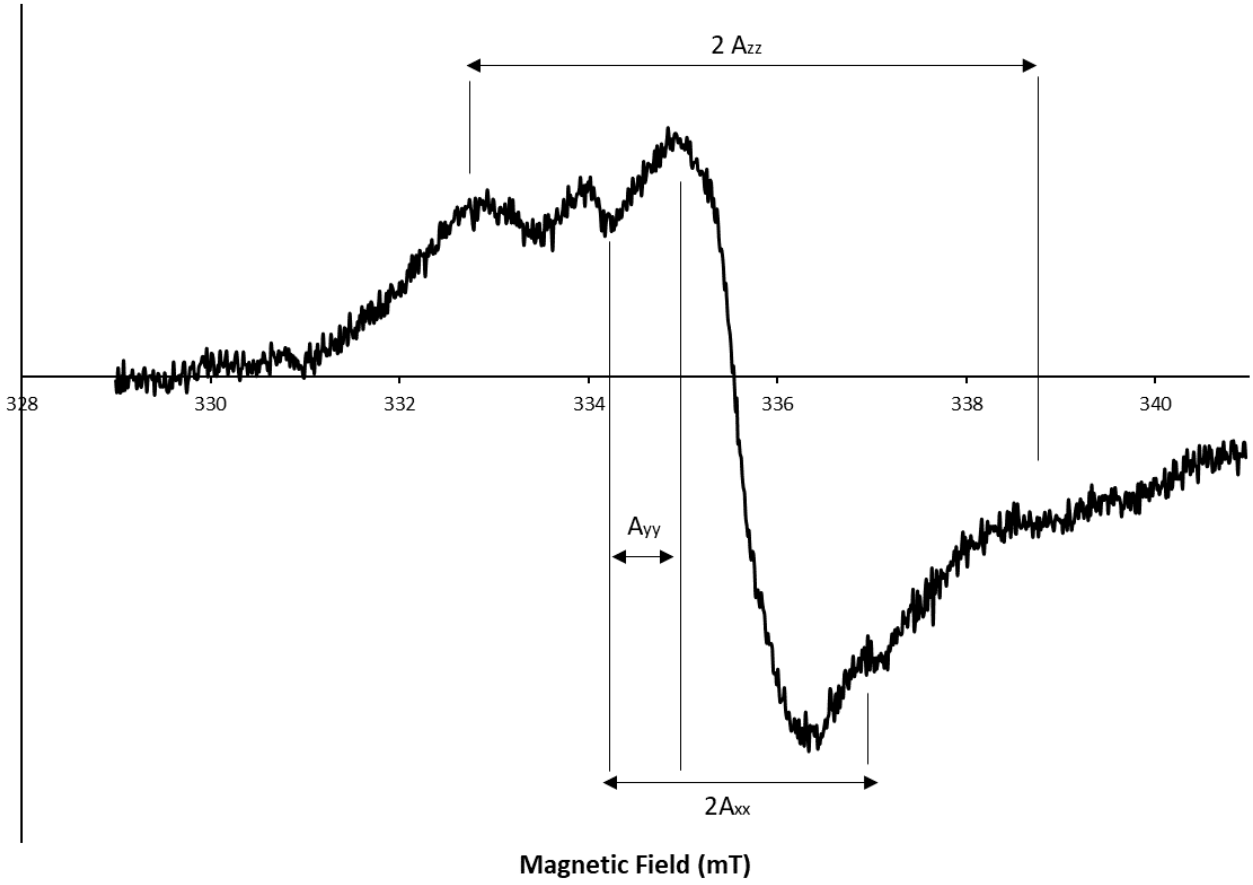


**Figure 3-5** Hyperfine coupling positions in the slow-tumbling EPR spectra.

The Gram-negative *E. coli* cells have two membranes separated by a thin cell wall. The outer membrane acts as a selective permeability barrier. The inner lipopolysaccharide layer is a selective barrier for small molecules and its rigid structure controls the passive diffusion of lipophilic compounds (Silhavy et al., 2010; Zgurskaya et al., 2015). Although the spin-probe initially partitions to both inner and outer membrane, we assume that the spin probe is likely to wash-away from outer membrane with the double-rinse. Therefore, we expect the contributions coming from the outer membrane is expected to be small as compared to inner membrane, yet there is still probability that some small amount remains and contributes to the complex EPR spectra.

The order parameters $S_1$ and $S_2$ after heating to different temperatures were shown in Figure 3-6. The lipid molecules exhibit molecular rotation (e.g. gauche-trans isomerization and lateral

diffusion) along the parallel and perpendicular axes of carbon-carbon bond alkyl chain (Nakagawa, 2003; Subczynski et al., 2009; van Meer et al., 2008). When the spin probe interacts with the cell membrane, the tail part (alkyl chain) continues rotational motion; however, the head structure (containing nitrogen moiety) is hindered by the membrane (Subczynski et al., 2009). Therefore, the long axis of the tail part produces an anisotropic motion while the head structure governs a "wobbling" movement (Sgherri et al., 2014; Subczynski et al., 2009). The motion direction of spin probe can be visualized as a cone shape. A rigid medium result in a smaller conical radius and motion amplitude to give a greater difference in hyperfine separations (Smith & Butler, 1976). This restricted motion is reflected in the EPR spectra and order parameters. The high magnitude of the order parameters at 35 °C indicate the control cells at the growth conditions where the spin probe is largely immobilized within the membrane. The motion of the spin probe molecule is largely restricted at the parallel axes aligned in the direction of bilayer structure of cell membrane, while it retains limited mobility at the x and y axes. The order parameter $S_1$ was significantly larger ($p < 0.05$) than $S_2$ probably related to the preferred alignment of the spin probe and the position nitroxide group within the membrane structure. The x-axis with the longer nitroxide dimension was freer to move between the phospholipids forming the bilayer, while the wobbling motion of the y-axis was more restricted with the peripheral fatty acid chains.

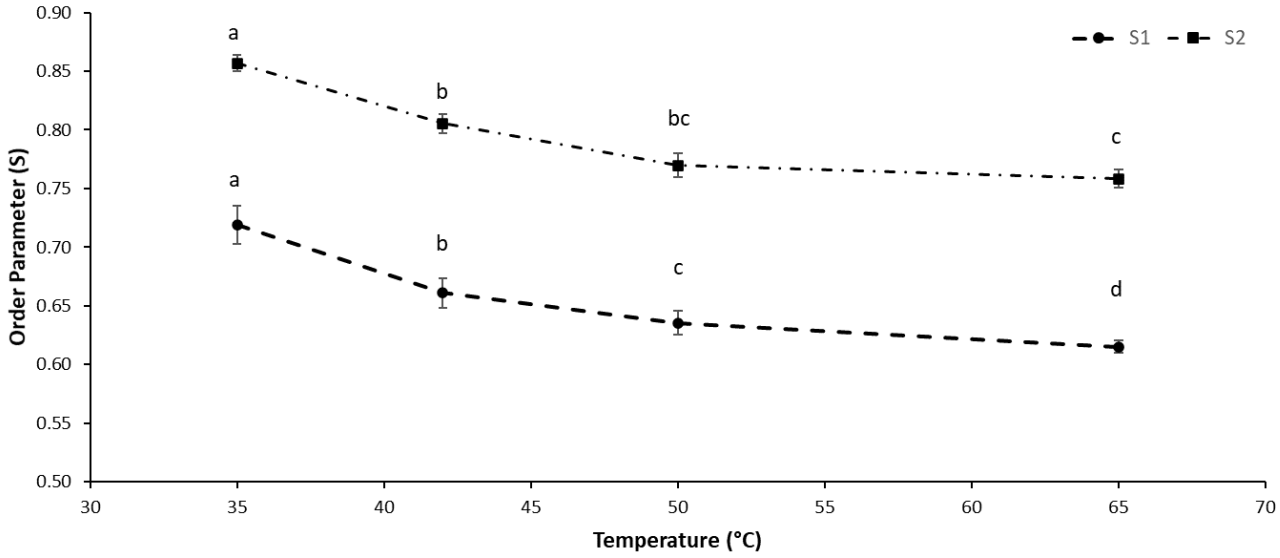


**Figure 3-6** The order parameters $S_1$ and $S_2$ calculated using eqns. 4 and 5, respectively. The different letters on the data indicate difference ($p < .05$) for the same parameters at different temperatures.

Both order parameters $S_1$ and $S_2$ decreased with increasing temperature indicating less restricted motion, and damage to membrane integrity. Similarly, Rottem et al. (1970) showed that the outermost peaks in EPR spectra of DSA spin probes approached to each other (decrease in $2A_{zz}$ values) with less restricted motion in an investigation of mycoplasma membrane and effects of growth conditions. Moreover, Hubbell & McConnell (1971) discussed the effect of temperature on the order parameter of aliphatic spin probes through phase transition of polymethylene chains of phospholipid membranes. When membranes heated above chain melting temperatures the order parameter abruptly changes indicating loss of membrane integrity. Similar observations was also reported by Mackey et al. (1991) on melting of membrane lipids and changing structure of cell components. Therefore, we hypothesize that based on the thermal resistance of microorganisms are related to the phospholipid composition of their cell membranes. The bacterial cells tolerate, survive, and finally go through adaptations under stress conditions, such as changing temperatures and the presence of essential oils or antibiotics. Other researchers studied the effect of stress conditions such as surfactant (Glover et al., 1999), essential oils (Serio et al., 2010), ultrasound (Li et al., 2016), and the combination of ultrasound and antibiotics (Rediske et al., 1999) on the cell membrane structure. Similar to our findings, these researchers related the loss of cell membrane integrity and disruption of tight packing to the phospholipid composition and structure.

The membrane integrity determines the cells ability for homeostasis, and a compromised membrane structure can result in dysfunction of the cell membrane activity and its selective permeability functionality. Baatout et al. (2005) observed increased membrane permeability in *E. coli* cells submitted to 50, 60, and 70 °C temperature treatments and stated that an increase in membrane permeability was linked to damaged membrane integrity. The loss of membrane barrier functionality and increased permeability can eventually lead to leaching of cell components outside the cell to cause shrinkage. In the next section, we investigated the changes in cell morphology as a result of heating using TEM imaging.

## Cell Morphology Analysis by TEM

The untreated (control) *E. coli* cells showed their characteristic rod shape morphology, and undamaged cell integrity with an intact membrane structure as shown in Figure 3-7A1 and 3-

7A2. The thin lines extended from the cells are the flagella. Heating the cells resulted in swelling (Figure 3-7B1 and 3-7B2) as they reached to their largest size at around 50 °C characterized by DLS measurements. The thickness of the gap between the inner membrane and cell wall decreased compared to non-heated cells due to swelling (i.e., indicated with red circles in Figure 3-7B). This enlargement compromised the cell membrane integrity as a result of two related phenomena: the increased mobility of the fatty acid chains and loss of lipoprotein structure with increasing temperature, and increased separation between molecules forming the membrane with enlargement. Similar observations were also reported by Munna et al. (2016).

Further heating (up to 65 °C) caused the cells to shrink (Figure 3-7C1 and 3-7C2). At this extreme point, the cell components leach out of the cell due to compromised cell membrane functionality. Without the internal resistance the membrane collapse observed as a much larger and irregular separation of the membrane from the cell wall (Figure 3-7C). Similarly, Russell (2003) reported that the severe damage to the inner membrane at high temperatures led to cell leakage and eventually to death. This was explained as the thermal degradation of inner membrane lipoproteins by high temperature. Baatout et al. (2005) stated the bacterial cells undergo several changes such as membrane separation from the cell wall, pore formation, and leakage of cell components to the outer environment when they are exposed to temperatures higher than they can tolerate (e.g. 25 to 42 °C for *E. coli*). The swelling and shrinking of bacterial cells characterized with DLS and TEM analyses were in agreement with changes observed indicating changes in membrane integrity, which was consistently degraded with continuing heating as quantified by EPR measurements.

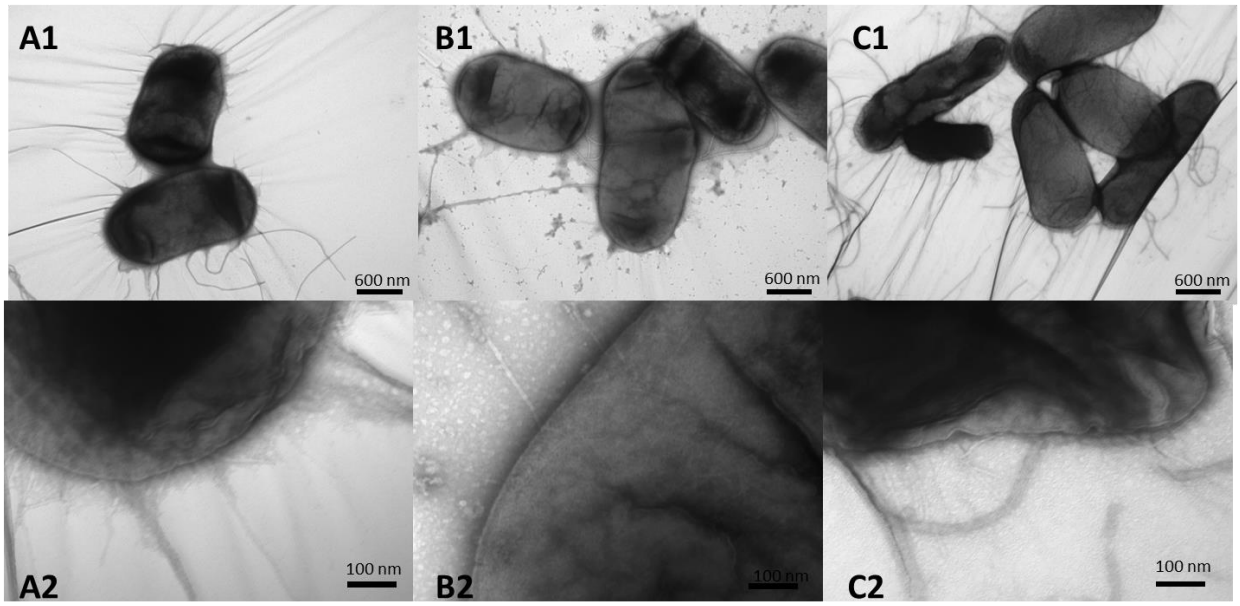


**Figure 3-7** TEM images of *E. coli* cells A) incubated at 35 °C, and heated to B) 50 °C, and C) 65 °C. The first row images are taken with x13,500 magnification; second row images are taken with x92,000 magnification.

## Conclusions

The present study showed that the EPR analysis showed the order of the (decreasing order parameter) in combination with DLS and TEM techniques, this information can be used to compare the effects of environmental stresses that determine bacterial survival behavior changes in *E. coli* membrane integrity with temperature. Our findings suggested the analysis of cell size, morphology, and membrane mobility can be used in parallel to provide a deeper understanding of structural changes related to bacterial thermal resistance. Multiple and related structural changes occur with external stresses, and their characterization is important to thoroughly understand survival skills of microorganisms. The combined approach proposed in this study can be helpful for further understanding of these changes that affect membrane integrity in combination with compositional information.

## Acknowledgement

This work is supported by the USDA National Institute of Food and Agriculture, Hatch project 1014344. The authors thank Dr. Dan Boyle for his help on TEM analysis.

# References


Akerlund, T., Nordstrom, K., & Bernander, R. (1995). Analysis of cell size and DNA content in exponentially growing and stationary-phase batch cultures of Escherichia coli. *Journal of Bacteriology*, *177*(23), 6791–6797. https://doi.org/10.1128/jb.177.23.6791-6797.1995

Baatout, S., De Boever, P., & Mergeay, M. (2005). Temperature-induced changes in bacterial physiology as determined by flow cytometry. *Annals of Microbiology*, *55*(1), 73–80.

Bot, C. T., & Prodan, C. (2010). Quantifying the membrane potential during E. coli growth stages. *Biophysical Chemistry*, *146*(2–3), 133–137. https://doi.org/10.1016/j.bpc.2009.11.005

Broeckx, G., Vandenheuvel, D., Claes, I. J. J., Lebeer, S., & Kiekens, F. (2016). Drying techniques of probiotic bacteria as an important step towards the development of novel pharmabiotics. *International Journal of Pharmaceutics*, *505*(1–2), 303–318. https://doi.org/10.1016/j.ijpharm.2016.04.002

Cebrián, G., Condón, S., & Mañas, P. (2017). Physiology of the Inactivation of Vegetative Bacteria by Thermal Treatments: Mode of Action, Influence of Environmental Factors and Inactivation Kinetics. *Foods*, *6*(12), 107. https://doi.org/10.3390/foods6120107

Chung, H. J., Bang, W., & Drake, M. A. (2006). Stress response of Escherichia coli. *Comprehensive Reviews in Food Science and Food Safety*, *5*(3), 52–64. https://doi.org/10.1111/j.1541-4337.2006.00002.x

Clementi, E. A., Marks, L. R., Roche-Håkansson, H., & Håkansson, A. P. (2014). Monitoring Changes in Membrane Polarity, Membrane Integrity, and Intracellular Ion Concentrations in Streptococcus pneumoniae Using Fluorescent Dyes. *Journal of Visualized Experiments*, *84*, 1–8. https://doi.org/10.3791/51008

Dejanović, B., Mirosavljević, K., Noethig-Laslo, V., Pečar, S., Šentjurc, M., & Walde, P. (2008). An ESR characterization of micelles and vesicles formed in aqueous decanoic acid/sodium decanoate systems using different spin labels. *Chemistry and Physics of Lipids*, *156*(1–2), 17–25. https://doi.org/10.1016/j.chemphyslip.2008.08.003

Duda, M., Kawula, K., Pawlak, A., Sarna, T., & Wisniewska-Becker, A. (2017). EPR studies on the properties of model photoreceptor membranes made of natural and synthetic lipids. *Cell Biochemistry and Biophysics*, *75*(3–4), 433–442. https://doi.org/10.1007/s12013-017-0795-

4

Feile, H., Porter, J. S., Slayman, C. L., & Kaback, H. R. (1980). Quantitative Measurements of Membrane Potential in Escherichia Coli. *Biochemistry*, *19*(15), 3585–3590. https://doi.org/10.1021/bi00556a026

Freed, J. H. (1976). Theory of slow tumbling ESR spectra for nitroxides. In L. J. Berliner (Ed.), *Spin Labeling* (pp. 53–132). Academic Press, Inc. https://doi.org/10.1016/j.neurobiolaging.2011.12.002

Fujikawa, H., Kai, A., & Morozumi, S. (2004). A new logistic model for Escherichia coli growth at constant and dynamic temperatures. *Food Microbiology*, *21*(5), 501–509. https://doi.org/10.1016/j.fm.2004.01.007

Gabriel, A. A., & Nakano, H. (2009). Inactivation of Salmonella, E. coli and Listeria monocytogenes in phosphate-buffered saline and apple juice by ultraviolet and heat treatments. *Food Control*, *20*(4), 443–446. https://doi.org/10.1016/j.foodcont.2008.08.008

Galaev, I. Y., Dainiak, M. B., Plieva, F., & Mattiasson, B. (2007). Effect of matrix elasticity on affinity binding and release of bioparticles. Elution of bound cells by temperature-induced shrinkage of the smart macroporous hydrogel. *Langmuir*, *23*(1), 35–40. https://doi.org/10.1021/la061462e

Glover, R. E., Smith, R. R., Jones, M. V., Jackson, S. K., & Rowlands, C. C. (1999). An EPR investigation of surfactant action on bacterial membranes. *FEMS Microbiology Letters*, *177*(1), 57–62. https://doi.org/10.1016/S0378-1097(99)00289-X

Halder, S., Yadav, K. K., Sarkar, R., Mukherjee, S., Saha, P., Haldar, S., Karmakar, S., & Sen, T. (2015). Alteration of Zeta potential and membrane permeability in bacteria: a study with cationic agents. *SpringerPlus*, *4*(1), 1–14. https://doi.org/10.1186/s40064-015-1476-7

Hubbell, W. L., & McConnell, H. M. (1971). Molecular motion in spin-labeled phospholipids and membranes. *Journal of the American Chemical Society*, *93*(2), 314–326.

Katsui, N., Tsuchido, T., Hiramatsu, R., Takano, M., & Shibasaki, I. (1982). Heat-Induced Blebbing and Vesiculation of the Outer Membrane of Escherichia coli. *Journal of Bacteriology*, *151*(3), 1523–1531.

Kim, S. Y., Sagong, H. G., Choi, S. H., Ryu, S., & Kang, D. H. (2012). Radio-frequency heating to inactivate Salmonella Typhimurium and Escherichia coli O157:H7 on black and red pepper spice. *International Journal of Food Microbiology*, *153*(1–2), 171–175.

https://doi.org/10.1016/j.ijfoodmicro.2011.11.004

Kong, L., Yucel, U., Yoksan, R., Elias, R. J., & Ziegler, G. R. (2018). Characterization of amylose inclusion complexes using electron paramagnetic resonance spectroscopy. *Food Hydrocolloids*, *82*, 82–88. https://doi.org/10.1016/j.foodhyd.2018.03.050

Kveder, M., Rakoš, R., Gavella, M., Lipovac, V., Pifat, G., Pečar, S., & Schara, M. (2004). EPR investigation of cell membrane fluidity upon external oxidative stimulus. *Applied Magnetic Resonance*, *27*(1–2), 77–86. https://doi.org/10.1007/BF03166303

Li, J., Ahn, J., Liu, D., Chen, S., Ye, X., & Ding, T. (2016). Evaluation of ultrasoundinduced damage to Escherichia coli and Staphylococcus aureus by flow cytometry and transmission electron microscopy. *Applied and Environmental Microbiology*, *82*(6), 1828–1837. https://doi.org/10.1128/AEM.03080-15

Mackey, B. M., Miles, C. A., Parsons, S. E., & Seymour, D. A. (1991). Thermal denaturation of whole cells and cell components of Escherichia coli examined by differential scanning calorimetry. *Journal of General Microbiology*, *137*(10), 2361–2374. https://doi.org/10.1099/00221287-137-10-2361

McConnell, H. M. (1976). Molecular Motion in Biological Membranes. In L. J. Berliner (Ed.), *Spin Labeling* (pp. 525–560). Academic Press, Inc.

Munna, M. S., Zeba, Z., & Noor, R. (2016). Influence of temperature on the growth of Pseudomonas putida. *Stamford Journal of Microbiology*, *5*(1), 9. https://doi.org/10.3329/sjm.v5i1.26912

Nakagawa, K. (2003). Diffusion coefficient and relaxation time of aliphatic spin probes in a unique triglyceride membrane. *Langmuir*, *19*(12), 5078–5082. https://doi.org/10.1021/la026813d

Rediske, A. M., Roeder, B. L., Brown, M. K., Nelson, J. L., Robison, R. L., Draper, D. O., Schaalje, G. B., Robison, R. A., & Pitt, W. G. (1999). Ultrasonic Enhancement of Antibiotic Action on Escherichia coli Biofilms: an In Vivo Model. *Antimicrobial agents and chemotherapy*, *43*(5), 1211–1214. https://doi.org/10.1128/AAC.43.5.1211

Reshes, G., Vanounou, S., Fishov, I., & Feingold, M. (2008). Cell shape dynamics in Escherichia coli. *Biophysical Journal*, *94*(1), 251–264. https://doi.org/10.1529/biophysj.107.104398

Rieseberg, M., Kasper, C., Reardon, K. F., & Scheper, T. (2001). Flow cytometry in biotechnology. *Applied Microbiology and Biotechnology*, *56*(3–4), 350–360.

https://doi.org/10.1007/s002530100673

Rottem, S., Hubbell, W. L., Hayflick, L., & McConnell, H. M. (1970). Motion of fatty acid spin labels in the plasma membrane of mycoplasma. *Biochimica et Biophysica Acta (BBA) - Biomembranes*, *219*(1), 104–113. https://doi.org/10.1016/0005-2736(70)90065-9

Russell, A. D. (2003). Lethal effects of heat on bacterial physiology and structure. *Science Progress*, *86*(Pt 1-2), 115–137. https://doi.org/10.3184/003685003783238699

Saini, G., Nasholm, N., & Wood, B. D. (2011). Implications of Growth and Starvation Conditions in Bacterial Adhesion and Transport. *Journal of Adhesion Science and Technology*, *25*(17), 2281–2297. https://doi.org/10.1163/016942411X574952

Serio, A., Chiarini, M., Tettamanti, E., & Paparella, A. (2010). Electronic paramagnetic resonance investigation of the activity of Origanum vulgare L. essential oil on the Listeria monocytogenes membrane. *Letters in Applied Microbiology*, *51*(2), 149–157. https://doi.org/10.1111/j.1472-765X.2010.02877.x

Sgherri, C., Porta, A., Castellano, S., Pinzino, C., Quartacci, M. F., & Calucci, L. (2014). Effects of azole treatments on the physical properties of Candida albicans plasma membrane: A spin probe EPR study. *Biochimica et Biophysica Acta - Biomembranes*, *1838*(1 PARTB), 465–473. https://doi.org/10.1016/j.bbamem.2013.10.015

Silhavy, T. J., Kahne, D., & Walker, S. (2010). The bacterial cell envelope. *Cold Spring Harbor Perspectives in Biology*, *2*(5), 1–16. https://doi.org/10.1101/cshperspect.a000414

Smith, I. C. P., & Butler, K. W. (1976). Oriented Lipid Systems as Model Membranes. In L. J. Berliner (Ed.), *Spin Labeling* (pp. 411–451). Academic Press, Inc. https://doi.org/10.1016/b978-0-12-092350-2.50016-3

Subczynski, W. K., Widomska, J., & Feix, J. B. (2009). Physical properties of lipid bilayers from EPR spin labeling and their influence on chemical reactions in a membrane environment. *Free Radical Biology and Medicine*, *46*(6), 707–718. https://doi.org/10.1016/j.freeradbiomed.2008.11.024

Trinetta, V., Rollini, M., Limbo, S., & Manzoni, M. (2008). Influence of temperature and sakacin A concentration on survival of Listeria innocua cultures. *Annals of Microbiology*, *58*(4), 633–639. https://doi.org/10.1007/BF03175568

Trueba, F. J., van Spronsen, E. A., Traas, J., & Woldringh, C. L. (1982). Effects of temperature on the size and shape of Escherichia coli cells. *Archives of Microbiology*, *131*(3), 235–240.

https://doi.org/10.1007/BF00405885

van Meer, G., Voelker, D. R., & Feigenson, G. W. (2008). Membrane lipids: where they are and how they behave. *Nature Reviews Molecular Cell Biology*, *9*(2), 112–124. https://doi.org/10.1038/nrm2330

Vargas, S., Millán-Chiu, B. E., Arvizu-Medrano, S. M., Loske, A. M., & Rodríguez, R. (2017). Dynamic light scattering: A fast and reliable method to analyze bacterial growth during the lag phase. *Journal of Microbiological Methods*, *137*(April), 34–39. https://doi.org/10.1016/j.mimet.2017.04.004

Walker, S. L., Hill, J. E., Redman, J. A., & Elimelech, M. (2005). Influence of growth phase on adhesion kinetics of Escherichia coli D21g. *Appl Environ Microbiol*, *71*(6), 3093–3099. https://doi.org/10.1128/AEM.71.6.3093

Zgurskaya, H. I., López, C. A., & Gnanakaran, S. (2015). Permeability Barrier of Gram-Negative Cell Envelopes and Approaches To Bypass It. *ACS Infectious Diseases*, *1*(11), 512–522. https://doi.org/10.1021/acsinfecdis.5b00097

# Chapter 4 - An Analysis of Cellulose- and Dextrose-Based Radicals in Sweet Potatoes as Irradiation Markers[2]


## Abstract

Dried sweet potatoes (SP) are often irradiated for improved safety and shelf-life. Formation of irradiation-derived radicals was analyzed using electron paramagnetic resonance (EPR) spectroscopy. These irradiation-specific radicals can be used to characterize the irradiation history of dry plant-based foods containing cellulose and sugars. The signal characteristics (intensity and peak shape) was evaluated at different sample locations (skin and flesh), as a function of sample preparation method (grinding, sieving, and pelletizing). The signal intensity was quantified based on double integration of the peaks as area under the curve (AUC) values, which increased with irradiation dose. The sieving caused ca. 50% decrease in total signal intensity as compared to non-sieved samples due to loss of cellulose-based radicals. The flesh of irradiated SP showed complex EPR spectra with multiple satellite peaks of cellulose radicals (333.5 and 338.8 mT) and split peak of dextrose radicals (337.4 mT); while skin spectra was distinctive of cellulose radicals. In this study, we demonstrated the effects of sample composition and preparation method on formation and analysis of irradiation-specific radicals based on EPR.


## Introduction

The food industry has developed many processing methods to protect foods against spoilage and pathogenic microorganisms as well as to extend shelf life. Food irradiation is an environmentally-friendly non-thermal technology that can effectively eliminate pathogenic organisms and fungi in perishable foods, such as fruits and vegetables (Zanardi et al., 2018). It is a clean technology that does not produce chemical residue, waste-water, combustion gases as compared to other methods (Slave et al., 2014). Although the irradiated products are not very common in the current human food market due to negative consumer perception, irradiated pet

[2] Tonyali B, Sommers C, Ceric O, Smith J S, Yucel U. (2020). An analysis of cellulose- and dextrose- based radicals in sweet potatoes as irradiation markers. Journal of Food Science, (85), 2745-2753. https://doi.org/10.1111/1750-3841.15359

food products is a growing market (Aleksieva & Yordanov, 2018). In the U.S.A., the Food and Drug Administration (FDA) has approved the use of irradiation in both human and animal food products to a predetermined maximum dose (FDA, 2001, 2015).

The maximum allowed irradiation dose varies based on product type, expected purpose, and anticipated shelf life. Irradiation doses used for insect disinfestation (e.g., in dried fruits) are typically less than 1 kGy, while irradiation doses used for pest control (e.g., in papayas) and spoilage microorganisms control (e.g., *E.coli* in ground beef) are between 1-10 kGy, and 4.5-7 kGy (refrigerated and frozen) (Miller, 2005; Tomaiuolo et al., 2018). The maximum irradiation dose allowed for animal foods (up to 50 kGy) is higher than human foods (up to 30 kGy, except the special cases like sterilization of foods used solely in the National Aeronautics and Space Administration (NASA) space flight programs, which might go up to 100 kGy) (FDA, 2001, 2015). Although these values indicate the maximum authorized dose, the doses generally used in industry are much lower. For example, the maximum dose allowed for oysters is 5.5 kGy, but they are commercially irradiated below 1 kGy to kill pathogens of concern and at the same time to ensure oysters remain alive (Jakabi et al., 2003). Irradiation induces the formation of irradiation-specific free radicals in the biological matrix as a function of total irradiation dose. Indeed, conventional alanine dosimeters are based on measurement of alanine radical using electron paramagnetic resonance (EPR) spectroscopy (Morsy, 2012).

EPR analysis has been approved by European Committee of Normalization (CEN) as a detection method for irradiation in samples rich in crystalline sugar (CEN, 2001), bones (CEN, 1997), and cellulose (CEN, 2000). However, the formation and stability of free radicals depends on many factors such as duration of treatment, composition of sample matrix, and post-treatment storage conditions (Jo, Sanyal, Park, & Kwon, 2016; Malec-Czechowska, Strzelczak, Dancewicz, Stachowicz, & Delincee, 2003; Yamaoki, Kimura, & Ohta, 2010; Yordanov & Aleksieva, 2007). Therefore, the detection, identification, and quantification of radicals as irradiation markers is still challenging. Different approaches to sample preparation for EPR analysis were investigated to improve EPR detection. Many researchers performed freeze drying (Jo et al., 2018), oven drying (Ahn, Sanyal, Akram, & Kwon, 2014), alcoholic extraction (Ahn et al., 2014; De Jesus, Rossi, & Lopes, 1999; Yordanov & Aleksieva, 2009), alkali hydrolysis (Ahn et al., 2014), and grinding (Ahn, Akram, & Kwon, 2012) to address this problem.

Sweet potatoes (SP) are popular dog treats that are often irradiated. SP is rich in carbohydrates and fibers, and typically have low moisture content (Miller, 2005). The low moisture nature of irradiated SP makes it a good candidate for EPR spectroscopy analysis. However, since irradiated SP is available in the market either with or without skin, it is important to understand the effect of compositional change in the formation of the irradiation-derived radicals for the same type of product. Like other fruits and vegetables, SP is a is multi-component food system with varying compositional attributes at the outer layer (e.g., skin) and inner layer (e.g., flesh). The skin predominantly contains insoluble fiber (e.g., cellulose, hemi-cellulose, and lignin etc.), whereas the flesh has high amounts of sugar (e.g. glucose, fructose, etc.) in addition to other polysaccharides (e.g., starch and dietary fiber). Accordingly, the type of irradiation-specific radicals is expected to be determined by the nature and amount of radical precursors (e.g., fibers and sugars) found in the sample.

There is a limited number of studies that compare different parts of fruits and vegetables or investigate the effect of sample preparation on EPR peak shape and signal intensity. In a recent study, Jo et al. (2016) applied an alcohol wash to show that total dietary fiber determines the overall EPR signal intensity in both irradiated orange peels and flesh. Same researchers also found that EPR signal intensity negatively correlates with the amount of water in the sample. In another study, Ahn et al. (2012) found that EPR spectra shape and signal intensity of irradiated sugars was affected by grinding time, which probably affected by the homogeneity and distribution of radicals. Grinding was mainly applied for preparation of irradiated grains prior to EPR measurements. Korkmaz and Polat (2000) found that the grinding process can result in formation of grinding-specific free radicals in irradiated wheat kernels causing a distortion in the irradiation-specific peak locations. Overall, the literature is limited to explain the formation of different types of free radicals in a complex environment of fruits and vegetables as affected by sample composition and distribution of components in combination with sample preparation method on EPR spectra (shape and signal intensity). In addition, there is a lack of understanding of the behavior of such radicals at high irradiation doses, which can be the cause of adulteration and hard to quantify. Therefore, in this study, various sample preparation methods such as grinding, sieving, and pelletizing were evaluated by comparison of the peak shapes and signal intensities of EPR spectra. The effect of non-irradiated and irradiated skin and flesh of SP on

peak shape of EPR signal was also characterized in comparison to irradiated glucose and cellulose standards.

## Materials and Methods

### Materials

SP was purchased from a local store. The cellulose and dextrose standards (analytical grade) were purchased from Thermo-Fisher Scientific (Waltham, MA, USA). Quartz EPR tubes (OD:5 mm, ID:4 mm) were obtained from Wilmad-Lab Glass (Warminster, PA, USA).

### Preparation of Dried Sweet Potatoes

Dried SP were prepared following the method described by Baldus (2009) with some modifications. In brief, the SP were washed with tap water to remove surface dirt, rinsed with distilled water, and excess water was removed with a paper towel. Then, they were cut into slices (2 cm in thickness). The SP slices were dried in a dehydrator (Tribest, Sedona SD-P9000) at 150°F for 24 h or 48 h. Moisture content analysis of SP was conducted by oven-drying (90 °C, 24 h).

The first two batches of SP samples, cellulose, and dextrose standards were irradiated together in the same irradiation chamber, at the USDA Eastern Regional Research Center at 10 and 50 kGy doses using a Cesium-137 source. The third batch of the samples was irradiated at Gateway America at the same doses. All samples (before and after irradiation) were shipped under refrigerated conditions. They were put in double-zipper storage bags, placed into a storage box containing desiccants, and kept in a freezer at -80°C until analysis. All samples were prepared in triplicate.

### Sample Preparation for EPR Analysis

The SP was freeze-dried (0.220 mbar for 48 h) as our preliminary experiments showed that residual water can distort the EPR spectra. The controlled variables for the effect of sample preparation on EPR measurement were described below and summarized in Table 4-1. Freeze-dried SP (5 g) was pulverized in a waring blender (50 mL) (model 34FL97) for 1 min in pulses (i.e., 15 sec grinding at full speed, 5 sec stopping interval a total of 3 pulses). Pulverized samples were sieved (through 212 µm mesh-screen) and pelletized as cylinders using a hydraulic pelletizer (ca. 3 mm in diameter and 7 mm in length). All samples were weighed (80 mg) and transferred into a quartz EPR tube (OD:5 mm & ID:4 mm, Wilmad-LabGlass). The sample

weight was determined by preliminary experiments to obtain a uniform cylindrical pellet, which was centered at the EPR cavity to prevent line broadening. Similar to above, freeze-dried (0.220 mbar for 48 h) SP, and cellulose and dextrose standard samples were ground, pelletized, and then weighed (80 mg) into quartz EPR tubes. In order to compare skin and flesh samples, the SP skins were removed from the flesh before freeze drying.

**Table 4-1** Different sample preparation methods.

| | **Grinding** | **Sieving** | **Pelleting** |
|---|---|---|---|
| **Powder** | x | | |
| **Sieve** | x | x | |
| **Pellet** | x | | x |
| **Sieve + Pellet** | x | x | x |

Presence of x indicates application of the treatment.

## EPR Analysis

The EPR measurements were conducted in a SpinscanX spectrometer (ADANI, Minsk, Belarus) operating at X-band with a modulation frequency of 100 kHz at room temperature. SP, SP skin, SP flesh, and dextrose and cellulose standards were scanned at the following measurement conditions: center field 334.5 mT, sweep width 11 mT, modulation frequency 100 kHz, modulation amplitude 600 uT, microwave power 1 mW, time constant 496 ms. The measurement conditions were determined with preliminary experiments (results not shown) based on previous literature (Yordanov & Aleksieva, 2009). For example, modulation amplitude was determined to be 600 uT for a smother peak shape but without excess broadening at higher time constant values.

## Statistical analysis

All experiments were performed in triplicate unless otherwise was stated. Analysis of variance (ANOVA) was applied using MINITAB software (Minitab Version16, State College, Pa., USA).

Tukey`s multiple comparison test was applied to evaluate the differences between treatments (significant when $p < 0.05$).

## Results and Discussion

### EPR Analysis of the SP and Effect of Sample Preparation

SP prepared by different sample preparation methods were analyzed for their EPR absorption spectra (Figure 4-1). The complex shape of the EPR spectra was related to the presence of different free radicals in the samples. The intensity of the sieved + pelletized sample was smaller than other samples, with line broadening and additional line splitting (e.g., around 336.5 mT). This is probably related to the nature of free radicals that were screened. The complex spectra of the un-sieved samples resembled each other and contributions from different radicals averaged out with a line distortion. To evaluate the line broadening ($A_l$), we measured the separation between the middle point of the spectra (the point that the spectra crosses x-axis) and the maximum slope of peak. $A_l$ values of sieved samples were 25% lower than $A_l$ values of pelleted samples both for or 24 and 48 h samples. In order to explain the nature of specific free radicals that form the complex spectra, dextrose and cellulose powders were irradiated at 5, 10, 20, 30, and 50 kGy to serve as standards.

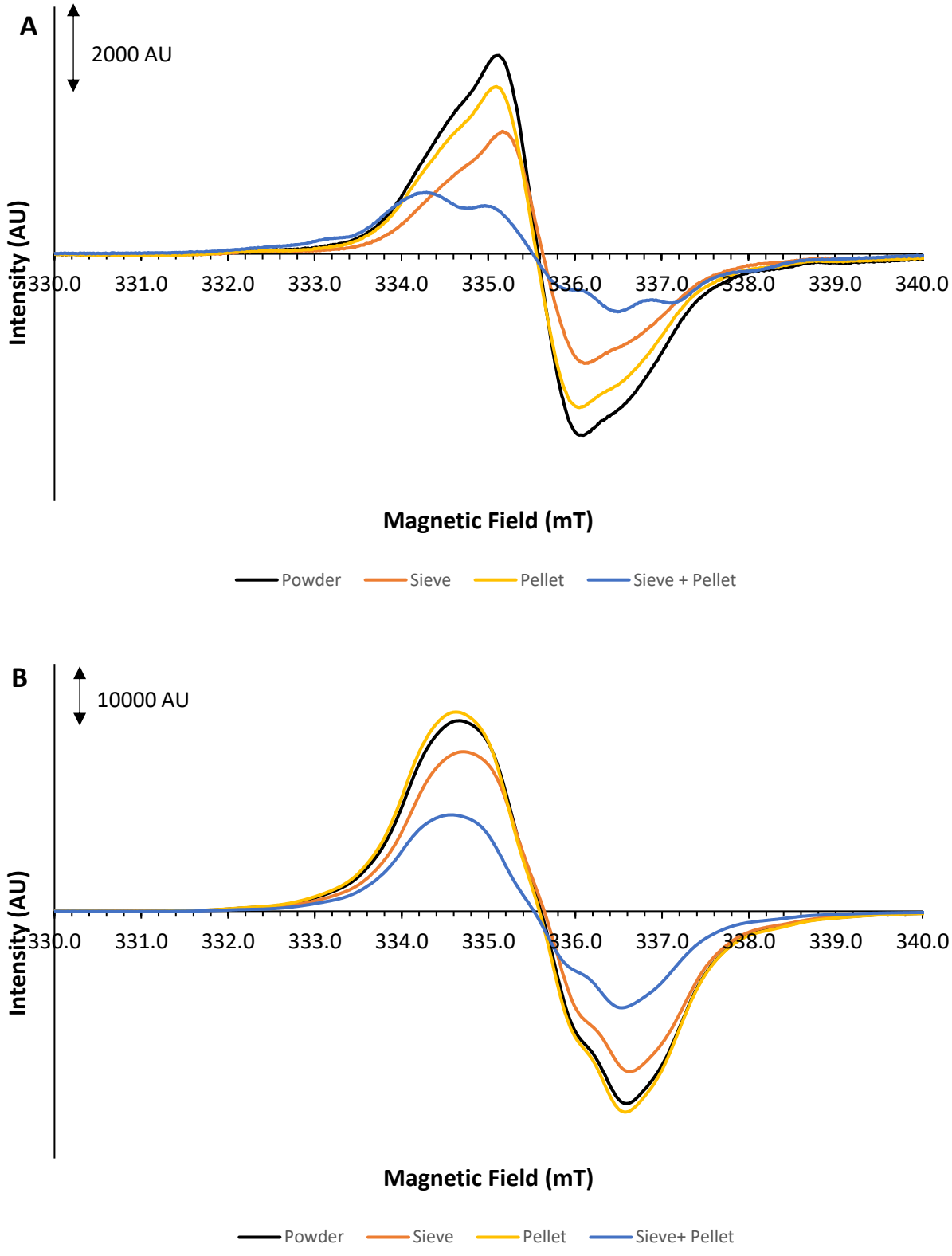


**Figure 4-1** EPR signals of grounded, sieved, pelletized, and sieved and pelletized SP prepared with (A) 24 hr and (B) 48 hr drying

The cellulose standard showed satellite peaks around 333 and 339 mT (Figure 4-2A). The g-values of these satellite peaks in high and low field were 2.02 and 1.99, respectively. The dextrose standard showed a shoulder structure around 337 mT (Figure 4-2B). This shoulder structure of a Gaussian peak is referred to as a split peak. Depending on their relative amounts, both irradiation-specific cellulose and dextrose radicals contribute to the complex EPR signal of SP. Dextrose contribution was more pronounced in the sieved samples observed as a split-peak and half-formed shoulder structure in sieved and pelleted samples and sieved samples, respectively (Figure 4-1). This is probably because the large cellulose fibers couldn't pass through the sieve, resulting in loss of cellulose-based radicals and concentrating the glucose-based radicals in the sieved samples. It is known that the length of the cellulose fibers is variable and can go up to 850 µm, larger than the mesh size (212 µm) (Reddy & Yang, 2005). When the samples were pelleted, the EPR signal noticeably decreased, regardless of their moisture content (Figure 4-1). In order to quantify the extent of this decrease, the total area under the curve (AUC) was calculated by double-integration of the EPR spectra using GRAMS/AI™ Spectroscopy Software (Thermo Scientific™, Version 9). The AUC of sieved samples were 67 and 20% lower than powder samples prepared with 24-h and 48-h drying, respectively. Similarly, when the samples were pelleted, the EPR signal noticeably increased as well (Figure 4-1). The AUC of pelleted samples were 40 and 21% higher than sieved samples prepared with 24 h and 48 h drying, respectively. The pelleting step improved sample uniformity within the EPR cavity and minimized the air volume. EPR spectroscopies that operate at X-band has a wavelength around 3 cm (Hagen, 2013). Hence, the samples extended in EPR tubes are exposed to a variety of microwave radio frequency magnetic field (e.g., change in intensity and wave distribution) (Hyde et al., 2019). The magnetic field intensity follows a cosine function with respect to sample axis (Hyde et al., 2019). The variation enhances the Gaussian effect in the spectra, which causes loss in the signal intensity (Hyde et al., 2019). Therefore, more compact samples (close to the center of cavity) are desirable in EPR measurements to maximize the magnetic field strength and have an uniform magnetic field wave distribution without losing signal (Hagen, 2013).
Overall, EPR spectra of the irradiated SP comprised of multiple peaks as compared to singlet line in the control SP (Figure 4-3 and 4-4). The main peaks of irradiated SP were broader about 0.6 and 0.4 mT than control SPs for 24 and 48 h samples, respectively. The signal characteristics of

the irradiated SP included a shoulder (ca. 336.9 mT) around the main peak and two additional satellite peaks at low- and high-field regions (333.1 and 338.8 mT, respectively). The shoulder was related to dextrose radicals while the satellite peaks separated by 3 mT from the center peak were related to cellulose radicals. Similar cellulose contribution was observed in other irradiated fruits such as goji berry fruits (Mladenova et al., 2019), oranges (Jo et al., 2018), and mushrooms (Malec-Czechowska et al., 2003), contributions from sugar-derived radicals in carob pods (Tuner & Polat, 2017), pineapple and fig (Guzik et al., 2015), and papaya, melon, and cherry (Yordanov & Aleksieva, 2007).

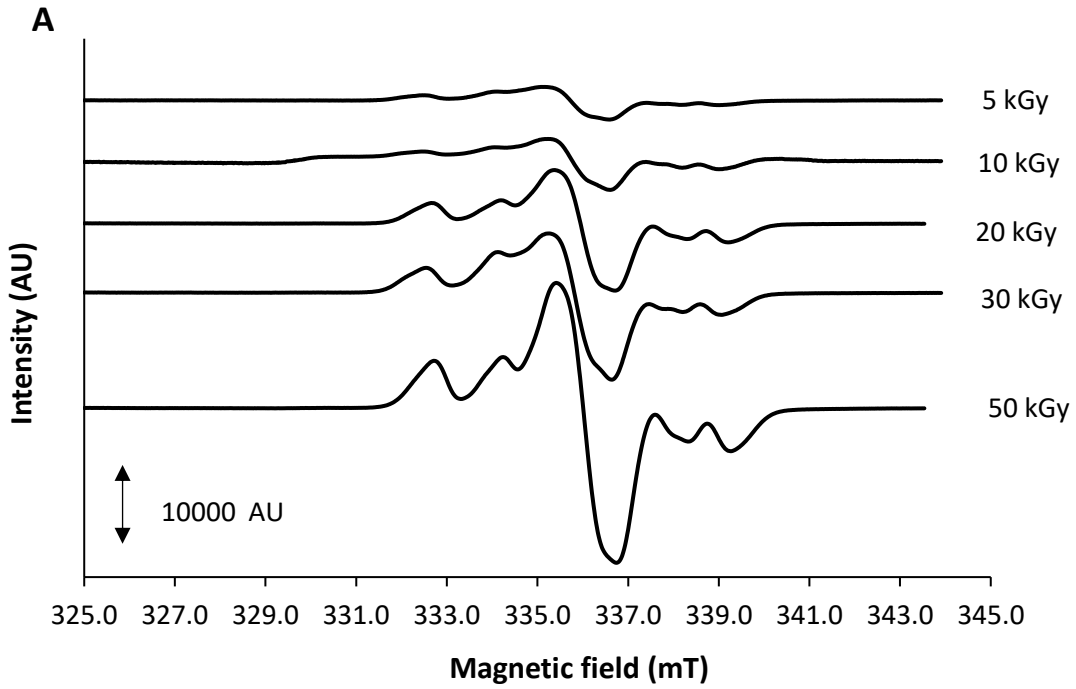

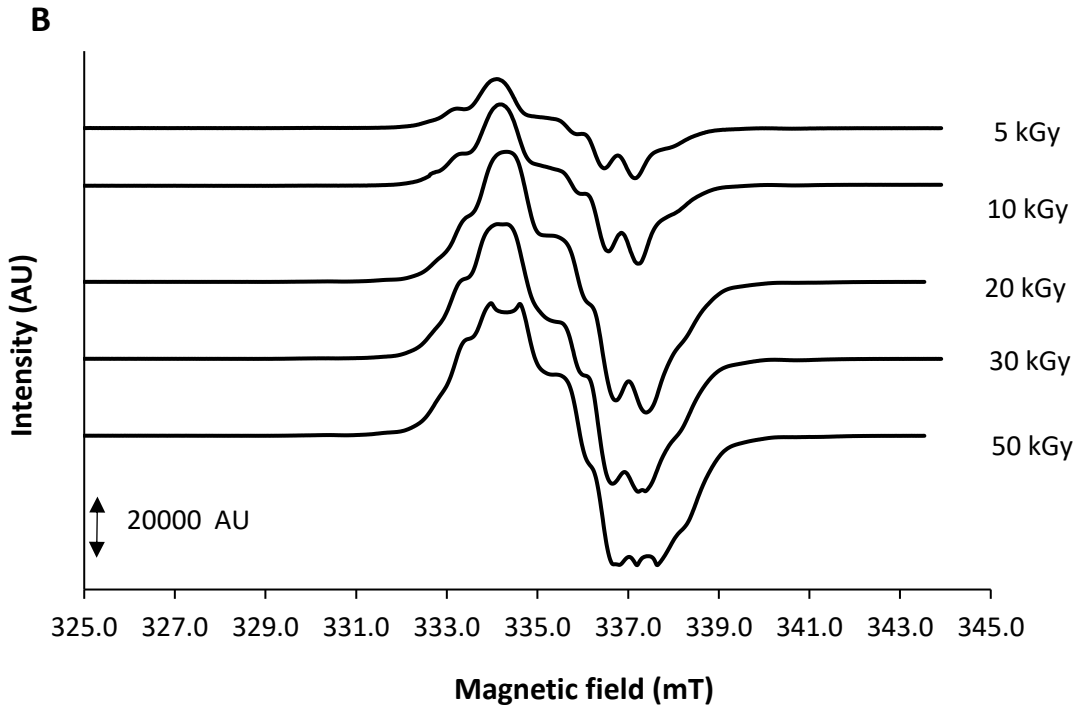


**Figure 4-2** EPR signal of freeze-dried (A) cellulose and (B) dextrose standards irradiated at different doses, from top to bottom: 0, 5, 10, 20, 30, and 50 kGy.

## Effect of Moisture Content

The EPR spectra of control samples (non-irradiated) were compared to the irradiated SP for powdered and pelleted conditions as described above. Control SP showed a singlet (g = 2.003) as shown in Figure 3A and 3B. Similarly, this singlet line is common to non-irradiated fruits (e.g., goji berry fruits (Mladenova et al., 2019), carob pods (Tuner & Polat, 2017), walnuts (Tomaiuolo et al., 2018), tomatoes (Aleksieva, Georgieva, Tzvetkova, & Yordanov, 2009), and orange peels (Jo et al., 2018), which was attributed to the presence of organic radicals (e.g., semiquinones (Aleksieva et al., 2009; Jo et al., 2018; Tomaiuolo et al., 2018; Tuner & Polat, 2017) or $Mn^{2+}$ ions (Mladenova et al., 2019)). In our study, the singlet in SP was related to ascorbic acid radicals (Furuta et al., 1998). Although the contribution of this singlet to the complex EPR spectra of irradiated samples is negligible, the extent of its effect increases with the sample moisture content during irradiation due to lower overall EPR signal, as explained next in more detail.

The moisture content of SP samples that were dried for 24 h or 48 h were 50% and 10%, respectively. Preliminary EPR data showed that moisture in SP samples can interfere with the spectra; therefore, both samples freeze-dried to a similar moisture content. The signal intensity of 48 h dried SP was higher than that of 24 h dried SP. This is because the longer drying process increases the crystalline sugar and cellulose content in the final product (Guzik et al., 2015). Therefore, higher amounts of irradiation-specific radicals (i.e., associated to the higher signal intensity in 48 h dried samples) can be stabilized in the crystalline regions of the food matrix (Ahn et al., 2014; Guzik et al., 2015). Hence, the second drying (i.e., freeze drying) only aids in preventing water interference during EPR analysis and doesn't affect the free-radical formation and stability prior to sample preparation.

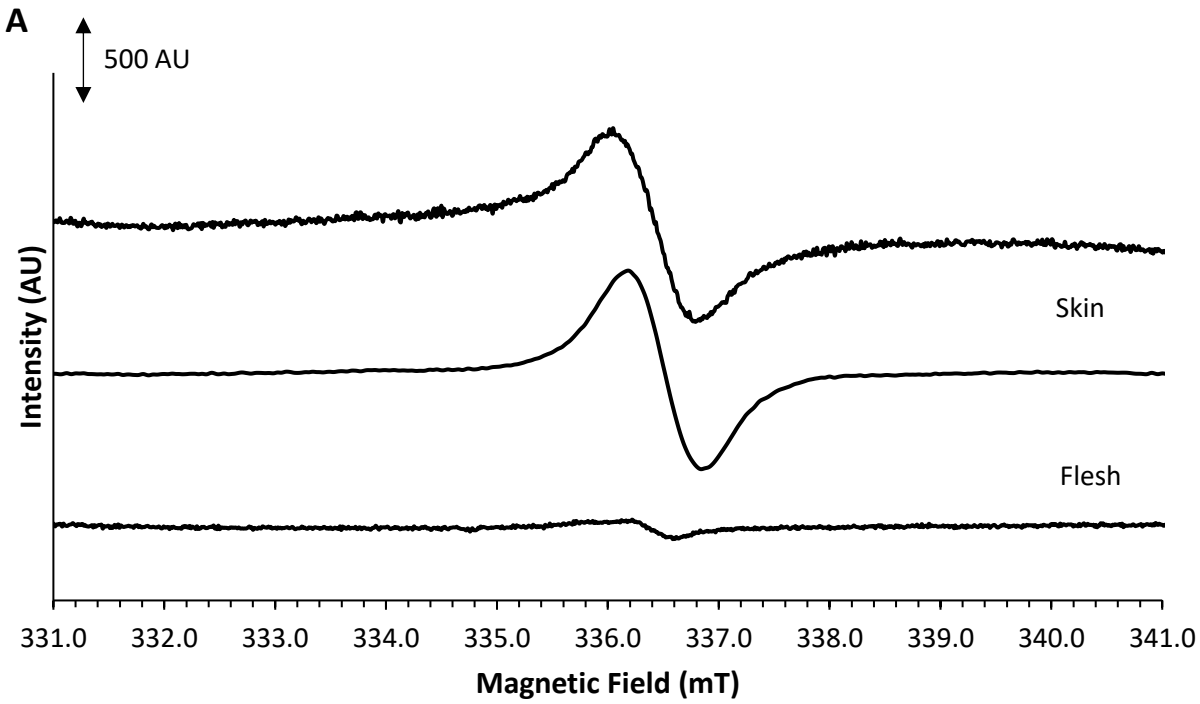

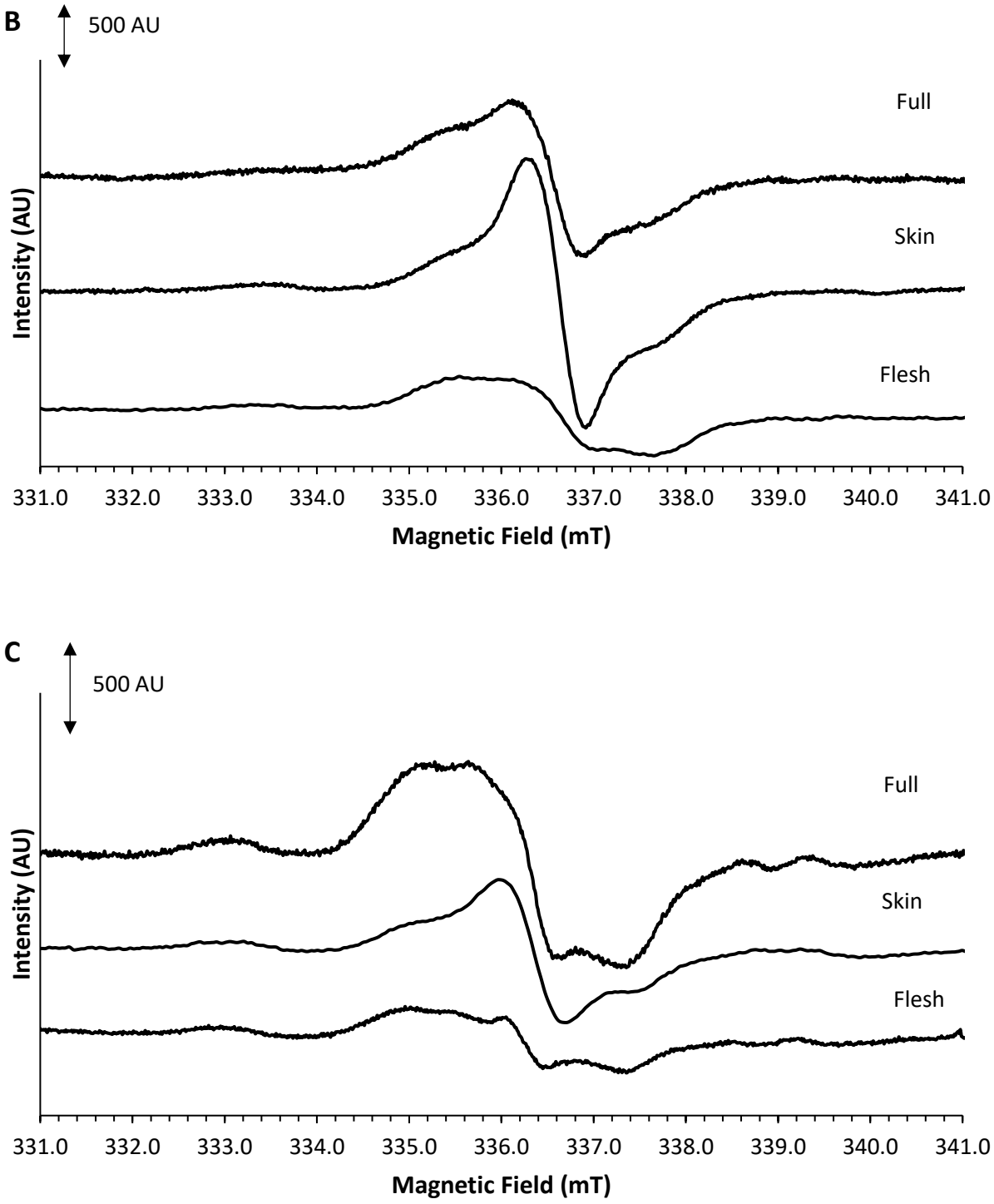


**Figure 4-3** EPR signal of SP samples with 24 hr drying treatment and irradiated at (A) 0, (B) 10, and (C) 50 kGy. The solid lines represent the spectra of sample parts from top to bottom: full, skin, and flesh

## Contributions of Skin and Flesh of SP to the Complex Spectra

We previously showed that sieving can significantly change signal shape due to loss of large cellulose fibers that entrap the cellulose-radicals. Following this observation, the flesh and skin of SP were analyzed separately due to their different concentrations of cellulose and glucose (Figure 4-3 and 4-4). The shape of EPR spectra of SP flesh resembled a combination of dextrose and cellulose radicals: the split-peak at 336.9 mT characteristics of dextrose radicals and the satellite peaks at low- and high-field (ca. 333 and 339 mT) characteristics of cellulose signal. Whereas, the cellulose radicals were more pronounced in SP skin spectra with satellite peaks at low- and high-field (ca. 333.5 and 337.87 mT). This is as expected since the cellulose concentration is higher in SP skin than the flesh (Aleksieva et al., 2009; Yordanov & Aleksieva, 2007). Similar to our findings, Jo et al. (2016) observed higher signal intensity of cellulose in orange peels (total dietary fiber content ~90%) than in orange flesh (total dietary fiber content ~70%) at the same moisture content (ca. 9.7%). Similarly, Malec-Czechowska et al. (2003) observed attributes of cellulose radicals in cellulose-rich mushroom hats but multicomponent spectra of sugar and cellulose radicals in mushroom legs. The specific attributes of irradiation-specific cellulose and dextrose radicals were not as clear in 48 h dried SP as in 24 h dried SP (Figure 4B and C), probably because excess line broadening due to high spin exchange masked the resolution of fine peak attributes, especially at high irradiation doses (i.e., 50 kGy).

In addition to peak shape, the signal intensities of skin and flesh samples were also different. The total signal intensity is a function of peak height and the extent of line broadening. Therefore, we analyzed the AUC values of EPR peaks, which considers line broadening as well as peak height, to get a more precise differentiation for the amount of free radicals. AUC values of skin samples were significantly higher ($p < 0.05$) than that of flesh samples (Table 4-2). This was probably due to the abundance of radiation-derived cellulose radicals in the skin due to high fiber content. Similarly, Jo et al., (2016) found a positive correlation between EPR signal intensity and total dietary fiber content in irradiated orange peel and flesh.

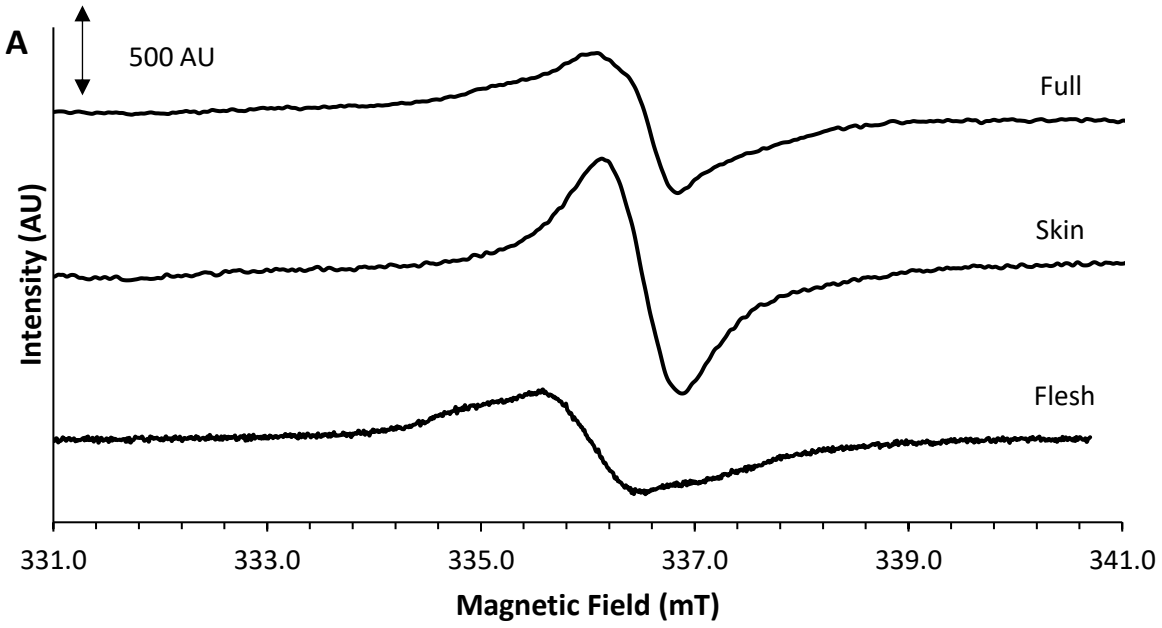
A
500 AU
Full
Skin
Flesh
Intensity (AU)
331.0
333.0
335.0
337.0
339.0
341.0
Magnetic Field (mT)

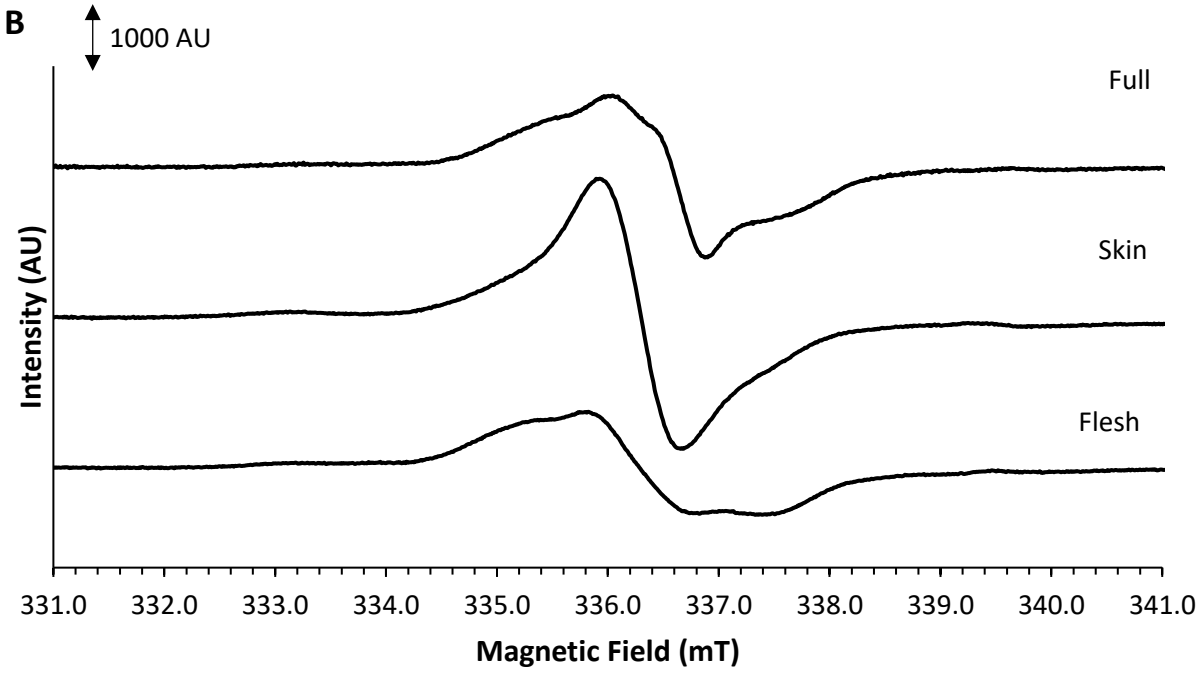
B
1000 AU
Full
Skin
Flesh
Intensity (AU)
331.0
332.0
333.0
334.0
335.0
336.0
337.0
338.0
339.0
340.0
341.0
Magnetic Field (mT)

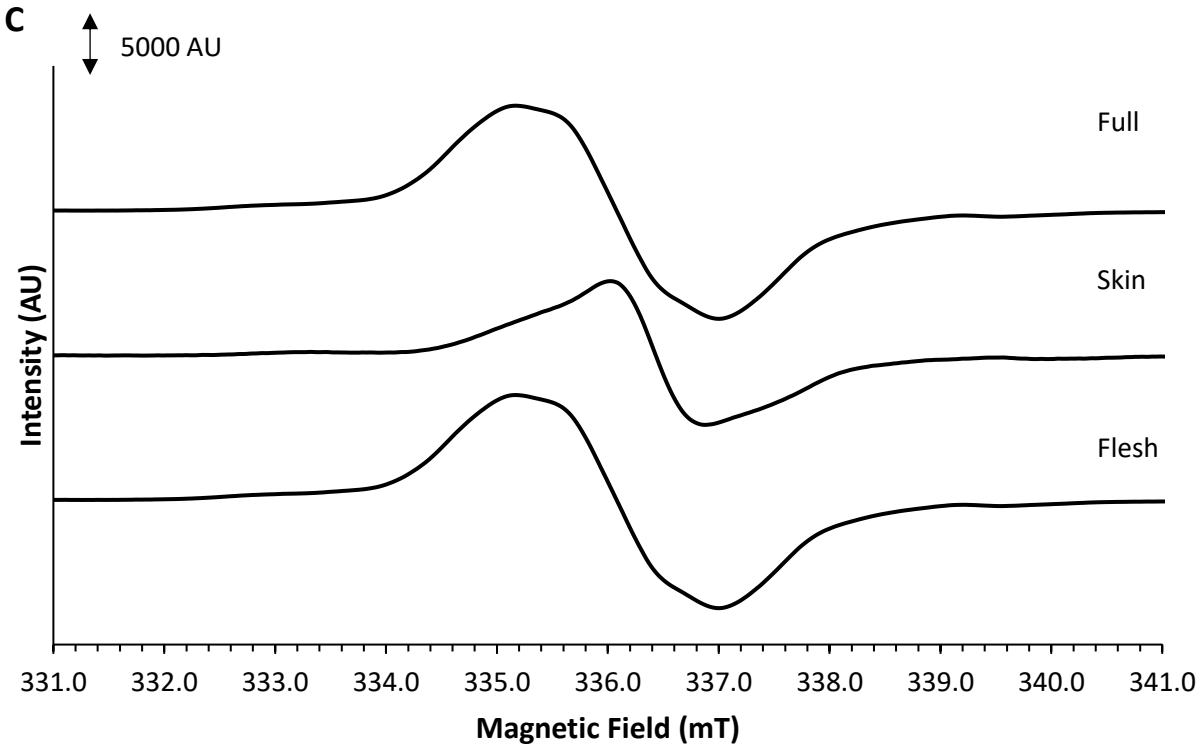


**Figure 4-4** EPR signal of SP samples with 48 hr drying treatment and irradiated at (A) 0, (B) 10, and (C) 50 kGy. The solid lines represent the spectra of sample parts from top to bottom: full, skin, and flesh

## Effect of Irradiation Dose

The next step is to confirm the detection of irradiation-derived dextrose and cellulose radicals at low- and high-irradiation doses. For this purpose, we analyzed AUC values of full spectra. The AUC of control samples were significantly ($p < 0.05$) lower than irradiated samples (Table 4-2). The higher signal intensity of the 48 h dried SP was attributed to the formation of Maillard radicals during extended drying (Rufián-Henares et al., 2013). The AUC further increased with irradiation dose, and the extent of this increase was higher for the SP samples with low moisture content (48 h dried; 182.4 AUC/dose) than high moisture samples (24 h dried; 19.3 AUC/dose). Therefore, a second confirmation from the increase of AUC of satellite peaks was applied. Furthermore, the AUC of the satellite peaks, which were observed only in irradiated SP, also significantly ($p < 0.05$) increased with irradiation dose. Previous studies used a similar approach

to quantify irradiation dose based on analysis of cellulose satellite peaks in orange peels and flesh (Jo et al., 2016, 2018) and walnuts (Tomaiuolo et al., 2018).

The AUC of skin and flesh samples were also analyzed separately at low and high irradiation doses (Table 4-2). The AUC of skin and flesh samples significantly ($p < 0.05$) increased with increasing irradiation doses both for low- and high- moisture samples. The increase in low moisture samples (48 h dried; 187.3 AUC/dose) was higher than high moisture samples (24 h dried; 8.4 AUC/dose) for flesh samples. Similarly, the increase in low moisture samples (48 h dried; 377.4 AUC/dose) was higher than high moisture samples (24 h dried; 35.7 AUC/dose) for skin samples. Moreover, the extents of increases in skin samples were higher than that of flesh samples, which is parallel to our findings in the previous part. Other researchers observed an increasing dose-response curve between signal intensity and irradiation dose in carob pods (Tuner & Polat, 2017), Foeniculi fructus (Yamaoki et al., 2009), and banana, papaya, and fig (Guzik et al., 2015).

**Table 4-2** Area under the curve (AUC) values of skin, flesh, and full SP irradiated at different doses.

| | **24 h dried SP** | | | **48 h dried SP** | | |
|---|---|---|---|---|---|---|
| **Irradiation dose (kGy)** | 0 | 10 | 50 | 0 | 10 | 50 |
| **Skin** | $312 \pm 67^{C,y}$ | $1012 \pm 58^{B,y}$ | $2211 \pm 171^{A,y}$ | $1945 \pm 555^{C,y}$ | $7901 \pm 622^{B,y}$ | $21541 \pm 3500^{A,y}$ |
| **Flesh** | $130 \pm 20^{C,z}$ | $352 \pm 31^{B,z}$ | $595 \pm 26^{A,z}$ | $880 \pm 7^{C,z}$ | $3062 \pm 24^{B,z}$ | $9840 \pm 35^{A,z}$ |
| **Full** | $1052 \pm 237^{C}$ | $1525 \pm 117^{B}$ | $2109 \pm 252^{A}$ | $1496 \pm 13^{C}$ | $3565 \pm 28^{B}$ | $10699 \pm 1063^{A}$ |

Data are presented as mean ± standard deviation (n=3). Different capitalized letters (A, B, C) in the same row indicate significant difference between irradiation doses ($p < 0.05$). Different lower-case letters (y,z) in the same column indicate significant difference between skin and flesh samples at the same irradiation dose ($p < 0.05$).

## Conclusion

In summary, the accuracy and reliability of EPR analysis was affected by sample preparation techniques and pretreatments, which modulate signal intensity and peak shape. For example,

including a sieving step in sample preparation will help to improve the uniformity of particle size distribution but can result in loss of cellulose particles, which can lead to decrease in signal intensity (e.g., decrease to half), especially in samples rich in cellulose, such as skin. The AUC analysis of full spectra showed an opportunity for an EPR dose quantification method with a further confirmation based on AUC of cellulose satellite peaks. Our findings demonstrate that irradiation-derived dextrose and cellulose radicals can be used for detection and quantification of irradiation, whereas the sample preparation method and composition is critically important for high precision and accuracy.

## Acknowledgement

This project was supported by FDA Vet-LIRN Cooperative Agreement U-18FD005842, and partially supported by the USDA National Institute of Food and Agriculture, Hatch project 1014344. Contribution no. 19-258-J from the Kansas Agricultural Experiment Station.

## References

Ahn, J. J., Akram, K., & Kwon, J. H. (2012). Electron Spin Resonance Analyses of Grinding- and Radiation-Induced Signals in Raw and Refined Sugars: A Comparative Study. *Food Analytical Methods*, *5*(5), 1196–1204. https://doi.org/10.1007/s12161-012-9364-z

Ahn, J. J., Sanyal, B., Akram, K., & Kwon, J. H. (2014). Alcoholic extraction enables EPR analysis to characterize radiation-induced cellulosic signals in spices. *Journal of Agricultural and Food Chemistry*, *62*(46), 11089–11098. https://doi.org/10.1021/jf502258r

Aleksieva, K., Georgieva, L., Tzvetkova, E., & Yordanov, N. D. (2009). EPR study on tomatoes before and after gamma-irradiation. *Radiation Physics and Chemistry*, *78*(9), 823–825. https://doi.org/10.1016/j.radphyschem.2009.05.013

Aleksieva, K. I., & Yordanov, N. D. (2018). Various approaches in EPR identification of gamma-irradiated plant foodstuffs: A review. *Food Research International*, *105*(August 2017), 1019–1028. https://doi.org/10.1016/j.foodres.2017.11.072

Baldus, D. (2009). *Animal Chew* (Patent No. US 7,537,794 B2).

De Jesus, E. F. O., Rossi, A. M., & Lopes, R. T. (1999). An ESR study on identification of gamma-irradiated kiwi, papaya and tomato using fruit pulp. *International Journal of Food*

*Science and Technology*, *34*(2), 173–178. https://doi.org/10.1046/j.1365-2621.1999.00250.x

European Committee for Standardization (CEN). (1997). *(EN1786) Foodstuffs-detection of irradiated food containing bone: analysis by electron paramagnetic resonance*. http://ec.europa.eu/food/food/biosafety/irradiation/1786-1996_en.pdf.

European Committee for Standardization (CEN). (2000). *(EN1787) Foodstuffs-detection of irradiated food containing cellulose by ESR spectroscopy.* http://ec.europa.eu/food/food/biosafety/irradiation/1787-2000_en.pdf.

European Committee for Standardization (CEN). (2001). *(EN13708) Foodstuffs-detection of irradiated food containing crystalline sugar by ESR spectroscopy*. http://ec.europa.eu/food/food/biosafety/irradiation/13708-2001_en.pdf.

FDA (The Food and Drug Administration). (2015). *Code of Federal Regulations, Title 21, part 179.26*. Irradiation in the production, processing and handling of food (2018). https://www.accessdata.fda.gov/scripts/cdrh/cfdocs/cfcfr/CFRSearch.cfm?fr=179.26 Last accessed

Furuta, S., Suda, I., Nishiba, Y., & Yamakawa, O. (1998). High tert-Butylperoxyl Radical Scavenging Activities of Sweet Potato Cultivars with Purple Flesh. In *Food Science and Technology International, Tokyo* (Vol. 4, Issue 1). https://doi.org/10.3136/fsti9596t9798.4.33

Guzik, G. P., Stachowicz, W., & Michalik, J. (2015). Identification of irradiated dried fruits using EPR spectroscopy. *NUKLEONIKA*, *60*(November 2014), 627–631. https://doi.org/10.1515/nuka-2015-0093

Hagen, W. R. (2013). EPR Spectroscopy. In R. R. Crichton & R. O. Louro (Eds.), *Practical Approaches to Biological Inorganic Chemistry* (First, pp. 53–75). Elsevier B.V. https://doi.org/10.1016/B978-0-444-56351-4.00003-8

Hyde, J. S., Sidabras, J. W., & Mett, R. R. (2019). Uniform Field Resonators for EPR Spectroscopy: A Review. *Cell Biochemistry and Biophysics*, *77*(1), 3–14. https://doi.org/10.1007/s12013-018-0845-6

Jakabi, M., Gelli, D. S., Torre, J. C. M. D., Rodas, M. A. B., Franco, B. D. G. M., Destro, M. T., & Landgraf, M. (2003). Inactivation by ionizing radiation of Salmonella Enteritidis, Salmonella Infantis, and Vibrio parahaemolyticus in oysters (Crassostrea brasiliana). *Journal of Food Protection*, *66*(6), 1025–1029. https://doi.org/10.4315/0362-028X-

66.6.1025

Jo, Y., Sanyal, B., Ameer, K., & Kwon, J. H. (2018). Characterization of DNA comet and cellulose radical signal in Valencia oranges treated with different forms of ionizing radiation. *Postharvest Biology and Technology*, *135*(January 2017), 68–76. https://doi.org/10.1016/j.postharvbio.2017.08.004

Jo, Y., Sanyal, B., Park, H. J., & Kwon, J. H. (2016). Ethanol extraction-based drying enhanced ESR radical detection in oranges irradiated to different ionizing radiations during storage. *Postharvest Biology and Technology*, *112*, 170–175. https://doi.org/10.1016/j.postharvbio.2015.10.005

Malec-Czechowska, K., Strzelczak, G., Dancewicz, A. M., Stachowicz, W., & Delincee, H. (2003). Detection of irradiation treatment in dried mushrooms by photostimulated luminescence, EPR spectroscopy and thermoluminescence measurements. *European Food Research and Technology*, *216*(2), 157–165. https://doi.org/10.1007/s00217-002-0615-x

Miller, R. B. (2005). *Electronic Irradiation of Foods: An introduction to The Technology*. https://doi.org/10.1007/0-387-28386-2

Mladenova, R. B., Aleksieva, K. I., & Nacheva, I. B. (2019). Effect of gamma irradiation on antiradical activity of goji berry fruits (Lycium barbarum) evaluated by EPR spectroscopy. *Journal of Radioanalytical and Nuclear Chemistry*, *320*(3), 569–575. https://doi.org/10.1007/s10967-019-06520-x

Morsy, M. a. (2012). Simple EPR / Alanine dosimeter for medical application. *Open Journal of Radiology*, *2012*(December), 120–125. https://doi.org/10.4236/ojrad.2012.24022

Reddy, N., & Yang, Y. (2005). Structure and properties of high quality natural cellulose fibers from cornstalks. *Polymer*, *46*(15), 5494–5500. https://doi.org/10.1016/j.polymer.2005.04.073

Rufián-Henares, J. Á., Guerra-Hernández, E., & García-Villanova, B. (2013). Effect of red sweet pepper dehydration conditions on Maillard reaction, ascorbic acid and antioxidant activity. *Journal of Food Engineering*, *118*(1), 150–156. https://doi.org/10.1016/j.jfoodeng.2013.03.034

Slave, R. M., Negut, C. D., & Grecu, V. V. (2014). ESR on some gamma-irradiated aromatic herbs. *Romanian Journal of Physics*, *59*(7–8), 826–833.

Tomaiuolo, M., Mangiacotti, M., Trotta, G., Marchesani, G., Chiappinelli, A., & Chiaravalle, A.

E. (2018). Identification of X-ray irradiated walnuts by ESR spectroscopy. *Radiation Physics and Chemistry*, *150*(March), 35–39. https://doi.org/10.1016/j.radphyschem.2018.04.007

Tuner, H., & Polat, M. (2017). ESR detection of irradiated carob pods (Ceratoniasiliqua L) and its dosimetric feature. *Radiation Physics and Chemistry*, *141*(July), 196–199. https://doi.org/10.1016/j.radphyschem.2017.07.016

Yamaoki, R., Kimura, S., & Ohta, M. (2010). Analysis of electron spin resonance spectra of irradiated gingers: Organic radical components derived from carbohydrates. *Radiation Physics and Chemistry*, *79*(4), 417–423. https://doi.org/10.1016/j.radphyschem.2009.11.011

Yamaoki, R., Tsujino, T., Kimura, S., Mino, Y., & Ohta, M. (2009). Detection of organic free radicals in irradiated Foeniculi fructus by electron spin resonance spectroscopy. *Journal of Natural Medicines*, *63*(1), 28–31. https://doi.org/10.1007/s11418-008-0284-6

Yordanov, N. D., & Aleksieva, K. (2007). EPR study on gamma-irradiated fruits dehydrated via osmosis. *Radiation Physics and Chemistry*, *76*(6), 1084–1086. https://doi.org/10.1016/j.radphyschem.2006.11.006

Yordanov, Nicola D., & Aleksieva, K. (2009). Preparation and applicability of fresh fruit samples for the identification of radiation treatment by EPR. *Radiation Physics and Chemistry*, *78*(3), 213–216. https://doi.org/10.1016/j.radphyschem.2008.10.003

Zanardi, E., Caligiani, A., & Novelli, E. (2018). New Insights to Detect Irradiated Food: an Overview. *Food Analytical Methods*, *11*(1), 224–235. https://doi.org/10.1007/s12161-017-0992-1

# Chapter 5 - A new approach for analysis of the complex electron paramagnetic resonance (EPR) spectra of irradiated sweet potatoes


## Abstract

Electron paramagnetic resonance (EPR) spectroscopy is an unambiguous technique to analyze free radicals. Dried sweet potatoes (SP), which are often irradiated and consumed as human and pet foods, can provide crystalline cellulose-rich environment to stabilize the irradiation-specific free radicals, the resolution of which can be masked by natural organic radicals in the sample. The performance of EPR analysis can be improved by implementing a peak enhancement method. In this study, SP samples were prepared at two moisture contents (48.3 and 9.7 % by drying at 150 °F for 24 or 48 h) and irradiated at 0, 5, 10, 20, 30, and 50 kGy. The slow-tumbling EPR spectra of non-irradiated SP had a singlet peak located at 334.5 mT, while irradiated SP were characterized with satellite peaks located 3 mT apart from center peak and a split peak at 335.4 mT. The complex EPR spectra were analyzed as a function of irradiation dose by calculating total areas under all peaks (TPA) and areas of irradiation-specific satellite peaks (SPA). TPA increased with irradiation dose at a rate of 573.4 AU/dose ($R^2$ = 0.98) and 14.7 AU/dose ($R^2$ = 0.65) for low- and high-moisture samples, respectively. High-field SPA was shown to be more sensitive to irradiation dose as compared to low-field SPA, however with high variability for both. The resolution of satellite peaks was further improved by peak enhancement procedure: higher linearity ($R^2$ of SPA increased from 0.98 to 0.99 for low moisture, and 0.77 to 0.94 for high-field of high moisture SP) and lower variability (coefficient of variation less than 30%). Overall, this study demonstrates that the peak enhancement procedure proposed in this study can be used to improve the EPR analysis of irradiated fruits and vegetables.


## Introduction

Irradiation has been available as a non-thermal process for food products to improve their shelf life and safety for many decades. The first commercial application of irradiation was for decontamination of spices in Germany in 1958 (Ehlermann, 2016). Currently, irradiation is used

in more than 40 countries for a variety of fresh and processed foods, such as spices, grains, salads, beef patties, fresh and dried fruits and vegetables (Aleksieva et al., 2014). In the U.S., the Food and Drug Administration (FDA) determines the maximum irradiation dose allowed specific to product type and purpose. Typically, low (<1 kGy) and medium doses (between 1-10 kGy) are used for sprout inhibition, enzyme deactivation, and pathogenic decontamination, while high doses (up to 30 kGy in seasonings and spices) are allowed for sterilization (FDA (The Food and Drug Administration), 2001, 2015; Miller, 2005). Animal foods (animal treats, chews, bagged complete diets, feed ingredients, etc.) are typically irradiated at higher doses (i.e., up to 50 kGy) than human foods (FDA (The Food and Drug Administration), 2001, 2015).

The irradiation process can form irradiation-specific chemical compounds, such as 2-alkylcyclobutanones (2-ACBs) with potential carcinogenicity and irradiation-specific free radicals (Crews et al., 2012; Klaassen et al., 2013). The irradiation treatment is considered safe within the regulation limits as these compounds do not show toxicity below the threshold. Yet, over the last decade or so, numerous cases of illness and death in dogs have been reported in the U.S. due to consumption of imported irradiated chicken jerky treats. A similar outbreak of neurological disorders and deaths in cats occurred in Australia due to consumption of irradiated dry cat food (FDA (The Food and Drug Administration), 2014). Potential reasons of these outbreaks were investigated by multiple research groups and the FDA using various toxicological and analytical techniques; however, the exact causes remain undetermined FDA, 2013; Child et al., 2009; Zhu et al., 2012). These recent events created a public safety interest for the detection and quantification of irradiation products.

A suitable method should be accurate, precise, sensitive, reliable, and suitable to the product characteristics (Akram et al., 2012; Stewart, 2001). GC-MS was used to study radiolytic lipid decomposition products (e.g., 2-ACBs and hydrocarbons) in irradiated lipid-rich products, such as fish (Kwon et al., 2007), poultry products (Morehouse et al., 1993), pork, chicken, and salmon (Obana et al., 2005), chicken jerky dog treats (Taghvaei et al., 2020). However, GC-MS analysis requires multiple sample preparation steps and are not suitable for lipid-poor samples, such as dried sweet potatoes (SP), which can be consumed as human or pet food products.

SP are typically low in moisture content and rich in cellulose and other carbohydrates (Miller, 2005). The crystalline and semi-crystalline regions in SP can serve as a suitable environment to stabilize irradiation-specific free radicals formed from crystalline sugar (European Committee

for Standardization (CEN), 2001) and cellulose (European Committee for Standardization (CEN), 2000), which can be analyzed by electron paramagnetic resonance (EPR) spectroscopy. In earlier studies, the EPR spectroscopy was used to detect irradiation in dry food material such as herbs (Bortolin et al., 2020), spices (Yamaoki et al., 2011), pistachios, hazelnuts, peanuts (D'Oca & Bartolotta, 2011), dried mushrooms (Malec-Czechowska et al., 2003), red melon and pumpkin seeds (Sin et al., 2006), orange peels (Jo et al., 2018), kiwi, papaya, and tomato (De Jesus et al., 1999). Although some of these researchers showed potential for the use of EPR for analysis of the irradiation specific radicals, quantification of the irradiation dose requires further research. The objectives of this study were to analyze irradiated SP using powder (slow tumbling) EPR spectra in comparison to glucose and cellulose standards, and to develop a peak enhancement technique for quantitative analysis of irradiation-specific cellulose satellite peaks and glucose split peak.

## Material and Methods

### Materials

Sweet potatoes were purchased from a local market. Glucose and cellulose (analytical grade) were obtained from Thermo-Fisher Scientific (Waltham, MA, USA). Quartz EPR tubes (OD:5 mm, ID:4 mm) were purchased from Wilmad-Lab Glass (Warminster, PA, USA).

### Preparation of Irradiated SP

SP were prepared following the method described by Baldus (2009) with some modifications. Sweet potatoes were gently washed and dried with a paper towel. They were cut into pieces (2 cm in thickness) and dried in a dehydrator (Tribest, Sedona SD-P9000) at 150 °F for either 24 hours (high-moisture SP) or 48 hours (low-moisture SP). Moisture content analysis was conducted by oven-drying (90 °C, 24 h), while protein and fat content analyses were performed using Kjeldahl and acid hydrolysis methods following AOAC 990.03 and 954.02, respectively. The SP samples, cellulose, and glucose standards were irradiated at the USDA Eastern Regional Research Center with 5, 10, 20, 30, and 50 kGy doses using a Cesium-137 source as explained in our previous work (Tonyali et al., 2020). The samples were shipped under refrigerated conditions. The non-irradiated and irradiated samples were placed in double-zipper storage bags, put into a storage box containing desiccants, and stored in a freezer at -80 °C until analysis.

Glucose and cellulose standards were prepared by irradiating them at the respective doses, which were stored similarly to SP samples. All samples were prepared in triplicate.

## EPR Analysis

Prior to EPR analysis, SP samples were pulverized using a waring blender (model 34FL97) for 1 minute in pulses (i.e., 15 s grinding at full speed, 5 s stop, 3 cycles in total) to yield fine particles (i.e., particle size smaller than 100 µm). Samples were freeze-dried (0.220 mbar for 72 hours) prior to pulverization to remove residual moisture and improve signal quality. The pulverized samples were compressed into cylindrical pellets (80 mg, with dimensions ca. D:3 mm, L:7 mm) using a pharmaceutical pellet maker. Similarly, irradiated cellulose and glucose powders, were freeze dried and pelleted. Pellets were inserted into a quartz tube (Wilmad-LabGlass, OD:5 mm, ID:4 mm) for subsequent EPR measurements at room temperature (~23 ± 1 °C). The EPR measurements were performed in a SpinscanX spectrometer (ADANI, Minsk, Belarus) operating at X-band microwave frequency with a 100 kHz field modulation. SP were scanned at the following measurement conditions: center field 334.5 mT, sweep width 11 mT, modulation frequency 100 kHz, modulation amplitude 600 uT, microwave power 1 mW, time constant 496 ms.

## Analysis of EPR Spectra

EPR spectra were analyzed using GRAMS/AI™ Spectroscopy Software (Thermo Scientific™, Version 9). Total areas under all the peaks (TPA) , only cellulose satellite peaks (SPA), and glucose split peak (GPA) were calculated by double integration of the respective peaks. In addition to raw spectra, non-irradiated SP spectra was subtracted from irradiated SP spectra prior to integration for TPA analysis. Non-irradiated SP spectra was not subtracted from irradiated SP spectra for SPA and GPA analysis since non-irradiated SP spectra did not have glucose split peak and cellulose satellite peaks. Besides integration method, SPA and GPA were also analyzed using by peak enhancement method. Peak enhancement is an artificial intelligence tool applied for analysis of complex spectra to improve resolution in various spectroscopy data (Li et al., 2016). One common technique to improve the resolution is the second derivative method (De Aragão & Messaddeq, 2008; Li et al., 2016). In this approach, the second-order derivative of the

complex EPR spectra was taken to enhance the resolution of cellulose and glucose peaks, and to deconvoluted them for individual analysis. Savitzky-Golay function was used to smooth the spectra. Following the second order derivative and baseline correction, the enhanced signal was simulated using a peak fitting procedure (assuming mixed Gaussian and Lorentzian line broadening). The area under the fitted peak was calculated for quantification.

## Results and Discussion

### Evaluation of spectra of Irradiated SP

Slow tumbling powder spectra of non-irradiated SP exhibited a singlet characterized with g = 2.0030 ± 0.0003, which was attributed to organic radicals present in the plant matrix (Figure 5-1) (Aleksieva et al., 2009; Jo et al., 2018). Other researchers observed a similar singlet in the range of 2.0031 to 2.0040 in non-irradiated dried fruit and vegetable samples, such as blue plum, apricot, peaches (Yordanov & Pachova, 2006), mushrooms (Malec-Czechowska et al., 2003), tomatoes (Aleksieva et al., 2009), orange peels (Jo et al., 2018), and figs (Guzik et al., 2015). A similar singlet of a lower intensity than oven-dried SP was also present in the freeze-dried SP (i.e., without heat treatment). This suggests that the singlet was related to semiquinones present in the vegetable matrix (Aleksieva et al., 2009; Jo et al., 2018).

Signal-to-noise ratio was significantly lower in high-moisture SP samples (moisture content at ca. 50%) than low-moisture SP samples (moisture content at ca. 10%) (Figure 5-1). The residual moisture in the SP decreased the signal quality in two ways: by decreasing the crystalline environment to stabilize free radicals during irradiation; and by absorbing significant electromagnetic energy at the X-band frequencies used for organic radicals due to its high dielectric constant (Weil & Bolton, 2007). Similarly, the effects of the removal of residual water via oven-drying, freeze-drying, and alcoholic wash prior to slow-tumbling EPR spectra analysis were also presented (Ahn et al., 2014; Delincée & Soika, 2002; Jo et al., 2018). Therefore, all samples were freeze-dried prior to EPR analysis to remove residual moisture and improve signal quality.

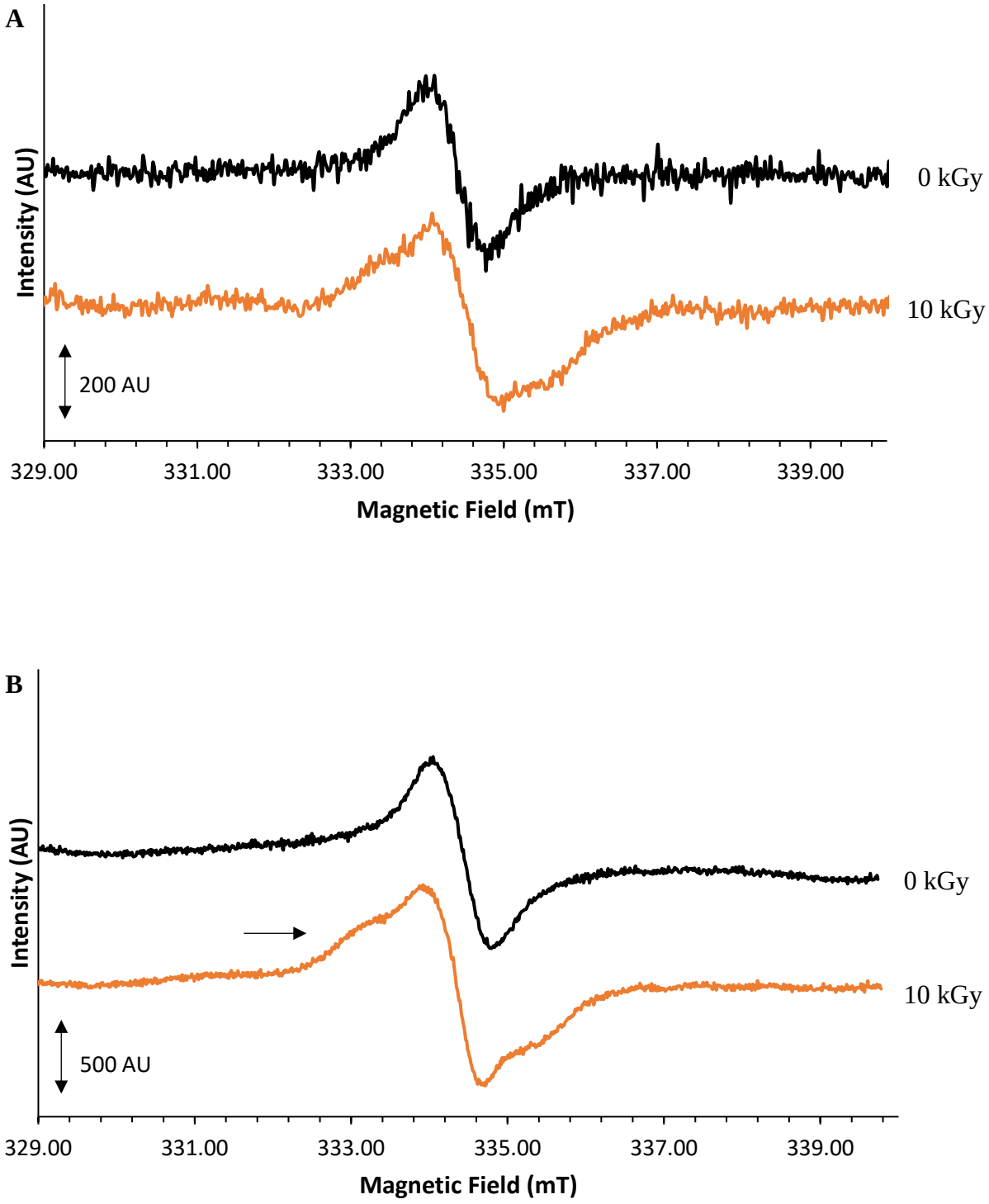


**Figure 5-1** EPR signal of 0 and 10 kGy irradiated SPT sample with 24 h dry time A) before and B) after freeze drying.

The EPR spectra of the irradiated samples were more complex than that of the non-irradiated samples (Figure 5-2). The spectra of irradiated SP had a split peak structure (dash arrow in Figure 5-2A) and two satellite peaks in high and low field (solid arrows in Figure 5-2A). The irradiation-specific cellulose and glucose radicals, also known as hydroxyalkyl radicals, are the main contributors of the complex multicomponent spectra of irradiated SP (Shahbaz et al., 2015). In order to characterize the peak, shape irradiated glucose and cellulose standards were analyzed at the respective doses (Figure 5-3). The split in the main peak around 335.4 mT (g = 1.99 ± 0.01) in spectra of SP samples was attributed to irradiation-specific glucose-radicals when the glucose standard was analyzed as shown in Figure 5-3A. Previous research indicated similar spectra for glucose radicals in dried fruits with a g-value around 2.00 (Guzik et al., 2015; Shahbaz et al., 2015; Yamaoki et al., 2010, 2011; Yordanov & Pachova, 2006). The second set of peaks separated by 3 mT from the main signal (g values 2.024 ± 0.001 and 1.985 ± 0.004) were coming from irradiation-specific cellulose radicals by comparison of Figure 5-2 and Figure 5-3B. Similarly, previous research indicated irradiation-specific cellulose peaks in irradiated fruits and vegetables with similar g-values (Jo et al., 2018; Prasuna et al., 2008; Tomaiuolo et al., 2018; Yamaoki et al., 2010).

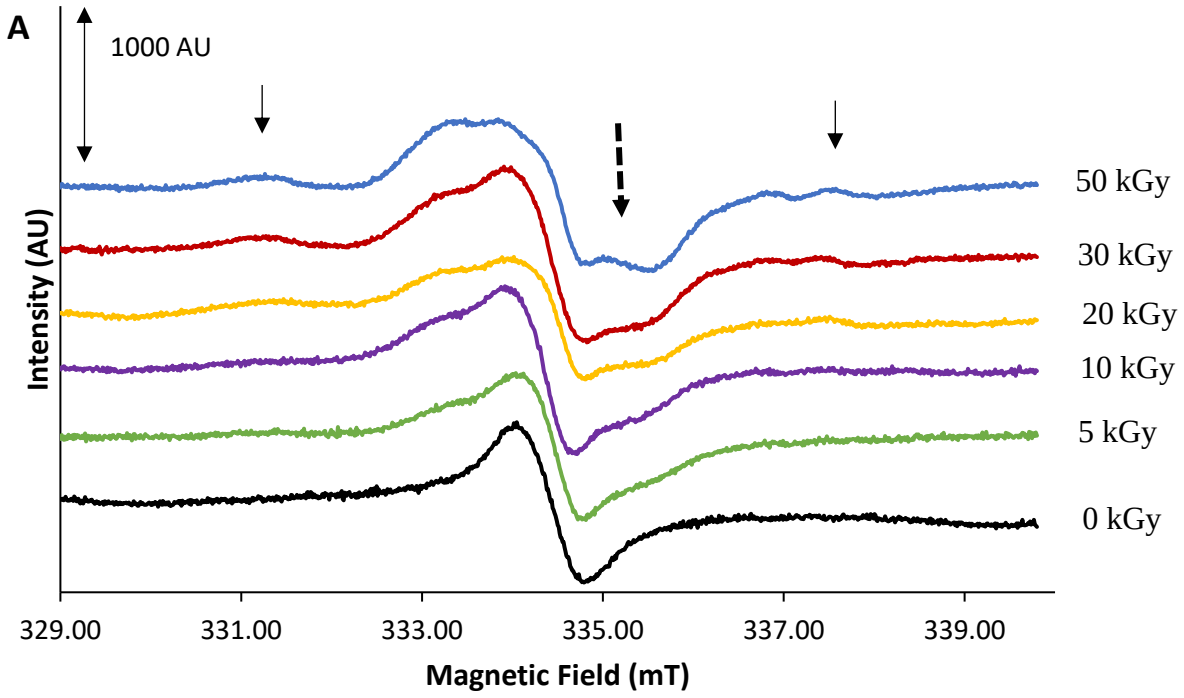

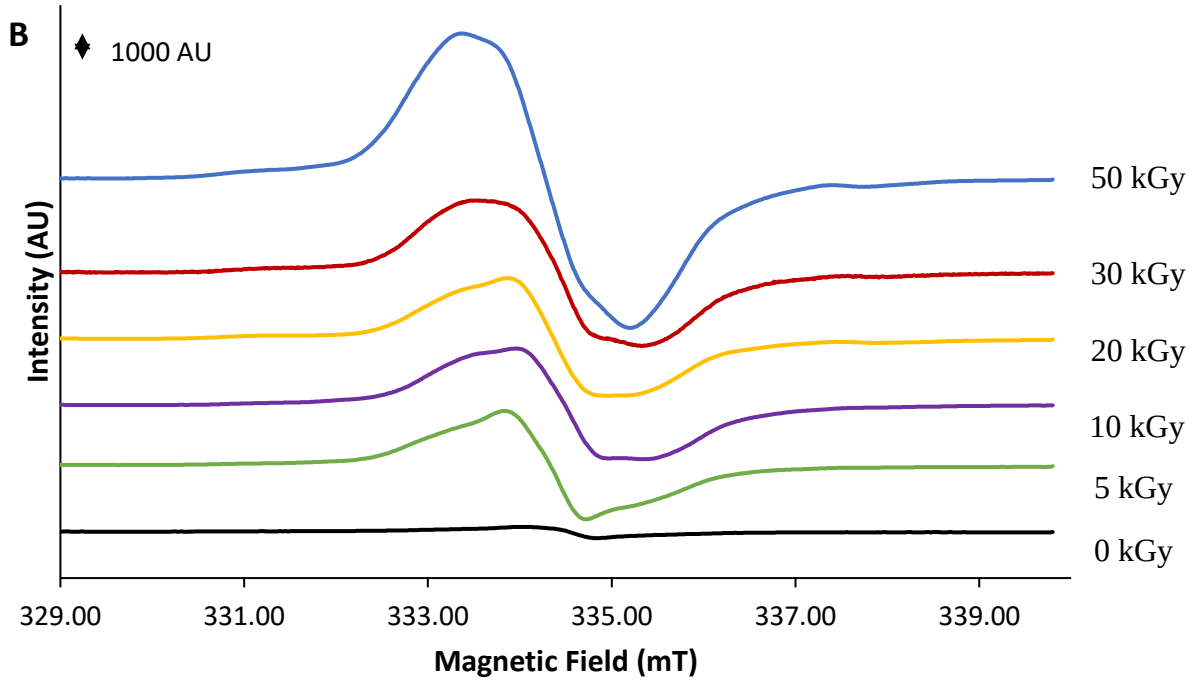


**Figure 5-2** EPR signal of SP samples irradiated at 0, 5, 10, 20, 30, and 50 kGy with A) 24 h drying B) 48 h drying treatment.

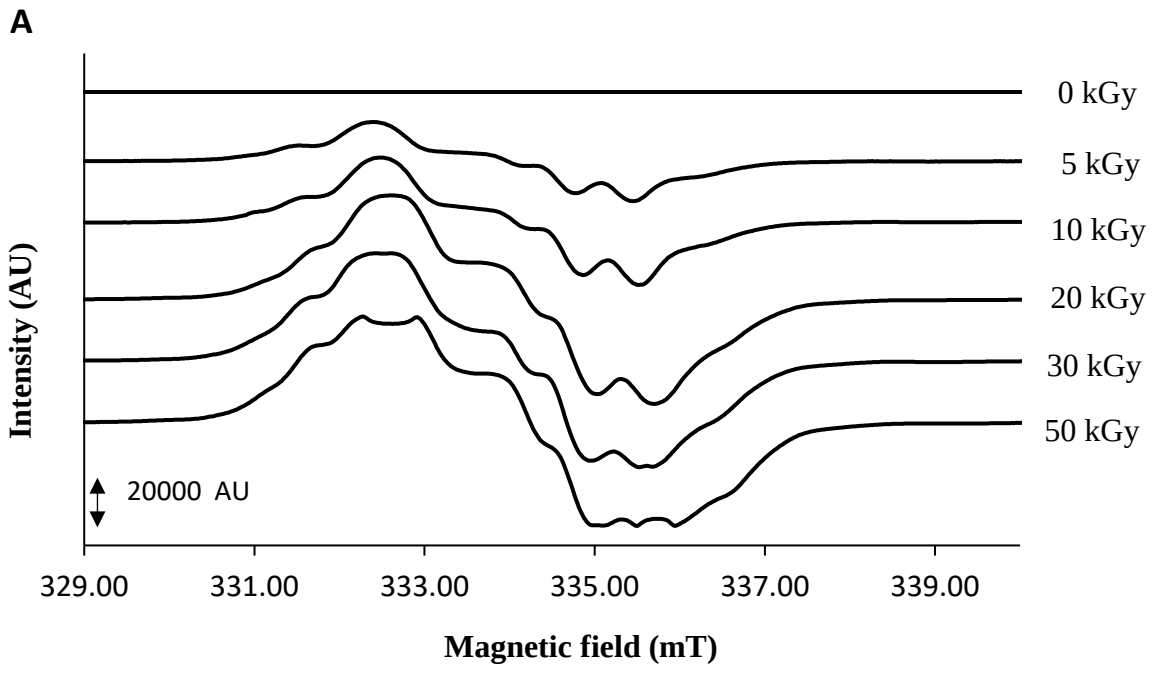

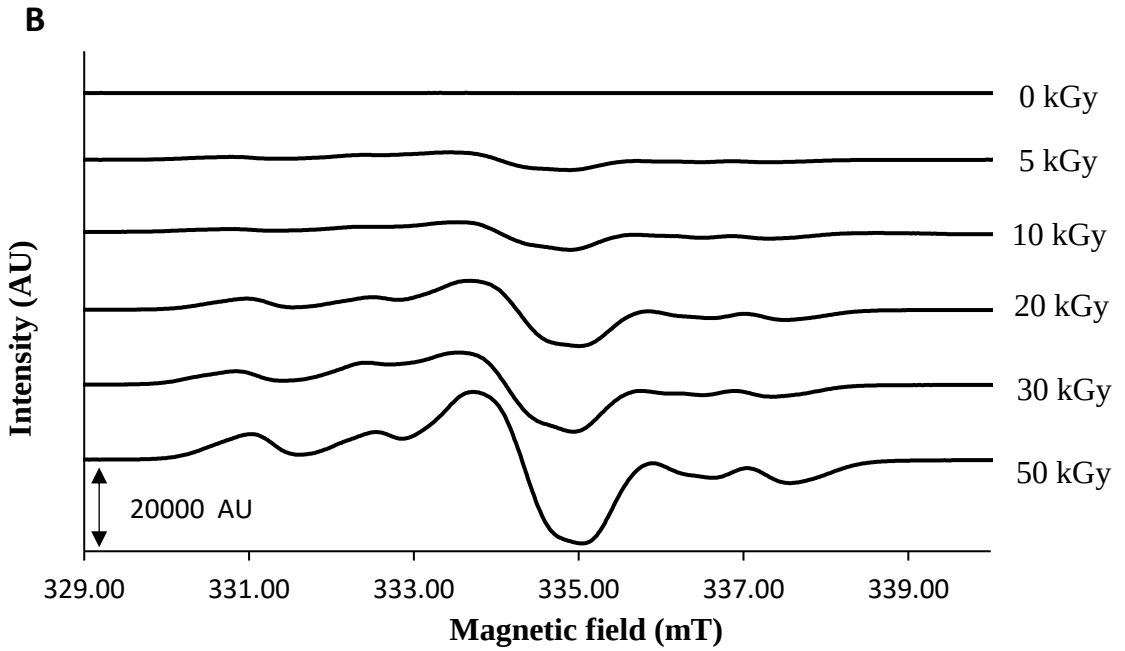


**Figure 5-3** EPR signal of A) glucose standards B) cellulose standards irradiated at 0, 5, 10, 20, 30, and 50 kGy.

## Evaluation of dose response of SP with total peak areas (TPA)

The first approach was to evaluate the dose-response of the irradiation process on the EPR signal of SP from the TPA values calculated by double-integration of the complex spectra as a function of irradiation dose (i.e., dose-TPA curve). TPA calculation included all the peaks (irradiation specific and not specific), therefore, the effect of center singlet on TPA needed to be understood and accounted for as the common contributor in both irradiated and non-irradiated samples. The TPA of the non-irradiated samples was coming from only the center singlet, which was present in both freeze-dried (no heat treatment) and oven-dried samples. The heat applied during oven drying increased the TPA from 415 A.U. in only freeze-dried SP to 1075 and 1289 A.U. in 24 h and 48 h oven-dried SP, respectively. TPA of non-irradiated low-moisture samples (1289 ± 223 A.U.) was statistically ($p > 0.05$) similar to that of high-moisture sample (1075 ± 151 A.U.).

### TPA of low and high moisture irradiated samples before subtraction

The slope of the dose-TPA curve for high moisture SP was 14.7 AU/dose (Figure 5-4A). The correlation factor of the curve was $R^2 = 0.65$, which deviated from linearity. TPA of high moisture SP sample irradiated at 5 kGy was statistically ($p < 0.05$) lower than high moisture SP sample irradiated at 50 kGy. TPA of low moisture samples increased with irradiation dose at a rate of 573.4 AU/dose (Figure 5-4B). The correlation factor of the linear curve was $R^2 = 0.98$. TPA of low moisture SP sample irradiated at 5 kGy was not statistically ($p > 0.05$) different than low moisture SP sample irradiated at 50 kGy. This was probably due to high deviation of low moisture SP sample irradiated at 50 kGy. However, when TPA of low moisture SP sample irradiated at 5 kGy was compared to that of 30 kGy, a statistical difference was found ($p < 0.05$). Overall, TPA increased with irradiation dose and was affected by moisture content. There was a significant difference ($p < 0.05$) between TPA of low moisture and high moisture SP samples, even at low irradiation dose. The low moisture SP samples irradiated at 5 kGy had significantly higher ($p = 0.0001$) TPA than that of high moisture SP samples. This might be due to crystallinity of environment (Sanyal et al., 2012). With decreasing moisture content, the amount of crystalline starch increases (Liao et al., 2019). This crystalline environment serves to stabilize higher amounts of irradiation-derived free radicals (Sanyal et al., 2012).

### TPA of low and high moisture irradiated samples after subtraction

In order to eliminate the interference from the center singlet, non-irradiated spectra (i.e., control samples) was subtracted from irradiated spectra prior to calculation of TPA. Obviously, the subtraction process decreased the TPA values, but improved the dose response, especially in low-moisture samples (Figure 5-4). TPA of low-moisture SP samples increased with irradiation dose at a rate of 572.4 AU/dose ($R^2 = 0.98$), which was similar as compared to prior to subtraction. This is related to the fact that 0 kGy sample had a TPA value of 0 AU after subtraction, while that for 50 kGy sample was not affected by subtraction ($p < 0.05$). This difference resulted in a slightly higher formation rate with irradiation dose due to the subtraction process. On the other hand, the slope of the dose-TPA curve of high-moisture SP samples was 16.9 AU/dose ($R^2 = 0.61$), which was higher as compared to prior to subtraction. Similar to low-moisture SP samples, subtraction of 0 kGy sample slightly enhanced the formation rate.

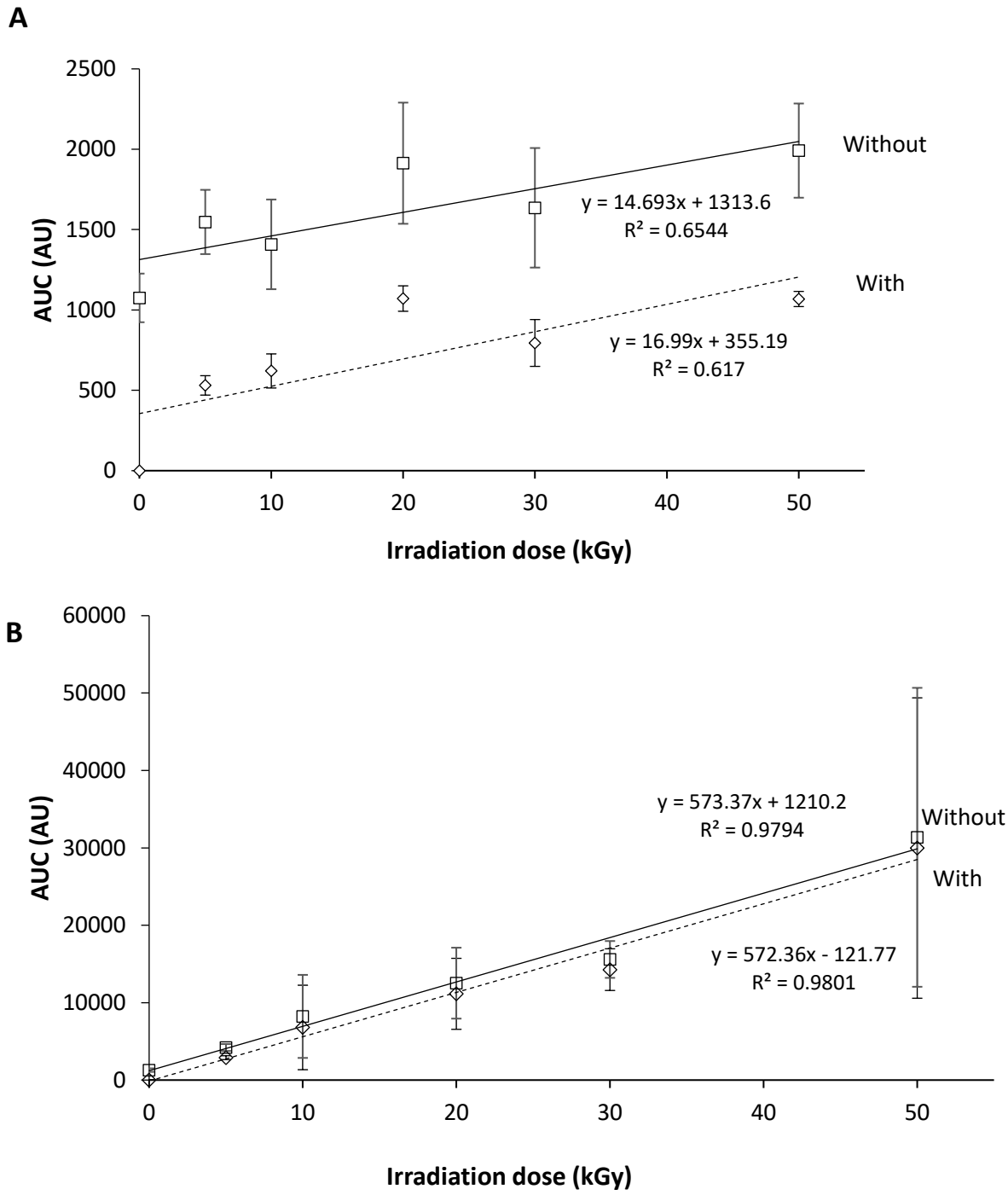


**Figure 5-4** TPA of irradiated (0, 5, 10, 20, 30, and 50 kGy) SP samples with (◊) and without (□) control subtraction with A) 24 h drying B) 48 h drying treatment. The results are expressed as means (n=3) and standard deviation. The dash and solid lines represent the trendlines of with and without control subtraction, respectively.

### Evaluation of dose response with SPA

The sensitivity of the EPR analysis can be improved by focusing on the irradiation-specific satellite peaks, which is expected to improve the dose-response behavior. For this purpose, SPA was analyzed using two approaches: integration and peak enhancement.

In integration method, SPA was calculated by double integration of the high field (centered at 331.2 mT) and low field peaks (centered at 337.4 mT) (Figure 5-5). In this approach, the control spectrum was not subtracted since the center peak was not involved in the calculations.

The sum of SPA for low-moisture SP increased with irradiation dose at a rate of 4.9 AU/dose, while sum of SPA of high-moisture SP increased at a rate of 2.1 AU/dose using integration method. Correlation coefficients of sum SPA were 0.82 and 0.99 for high-moisture and low-moisture SP, respectively. The correlation of sum of SPA with irradiation dose was in parallel with results of TPA, which supported that increasing irradiation dose increased concentration of irradiation-specific cellulose radicals. These correlation coefficients of sum SPA were higher than correlation coefficients of TPA for high-moisture ($R^2$ = 0.65) and low-moisture ($R^2$ = 0.98) SP. The improved linearity in SPA, especially for high-moisture SP, suggested that analysis of satellite peaks from cellulose radicals was a good candidate for irradiation detection studied in cellulose-rich foods.

Sensitivity is proportional with number of spins in EPR measurements. Since high spin polarization takes place in low and high fields in EPR measurements, these fields are more sensitive (Coffey et al., 2013). Therefore, the high and low field SPA peaks were analyzed separately to observe individual correlations with irradiation dose. The SPA of high field increased with irradiation dose at a rate of 1.3 AU/dose, while SPA of low field increased with irradiation dose at a rate of 0.8 AU/dose for high-moisture samples (Figure 5-5A). SPA of low field peak showed higher correlation factor with irradiation dose compared to high field satellite peak for high-moisture SP samples ($R^2$ =0.89 and 0.77, respectively). SPA of high field increased with irradiation dose at a rate of 2.6 AU/dose, while SPA of low field increased with irradiation dose at a rate of 2.3 AU/dose for low-moisture samples (Figure 5-5B). The correlation factors of SPA are similar in low-moisture SP ($R^2$ =0.96 and 0.98 for low and high field satellite peaks, respectively). Similar to our study, researchers previously observed an increase in signal intensity of satellite peaks with increasing irradiation dose (Jo et al., 2018; Tomaiuolo et al.,

2018). The higher formation rate in high field compared to low field was probably due to higher sensitivity of high field than low field (Coffey et al., 2013; Nordio, 1976).

Coefficient of variation (CV) was calculated to address variation in SPA analysis and a CV value higher than 30% is considered as high variation (Brown, 1998). CV of high field SPA of high-moisture SP samples were less than 25% at all doses, whereas CV of low field SPA of high-moisture SP samples were less than 35% at all doses. Meanwhile, CV of high field and low field SPA of low-moisture SP samples were less than 50% at all doses. Although SPA of low and high-moisture SP exhibited high correlation coefficients, they had high variations. Moreover, CV of low field SPA was higher at lower doses (33% at 5 kGy) than higher doses (23% at 50 kGy) for high-moisture SP. Therefore, we applied a peak enhancement method to study SPA in an attempt to increase resolution and minimize variability, especially in low doses. In this method, the high field satellite peak located between 330.3 and 331.9 mT and low field satellite peak located between 336.7 and 338.1 mT were subjected to second-derivative. The combination of Gaussian and Lorentzian peaks was simulated to fit high and low field satellite peaks separately.

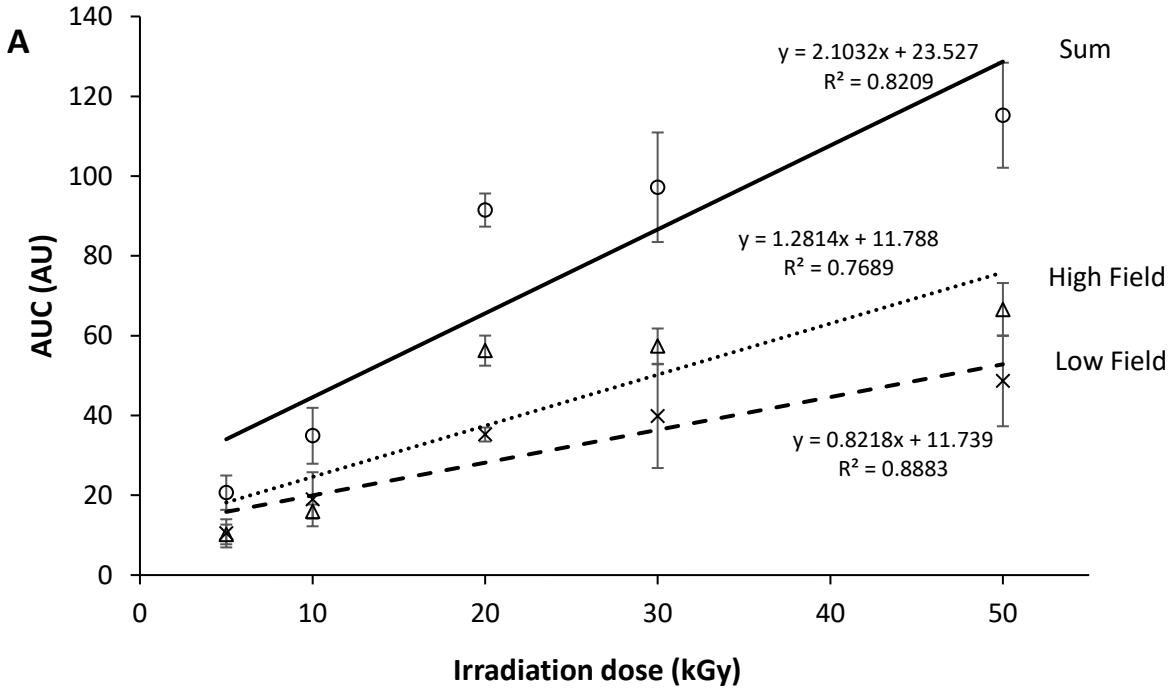

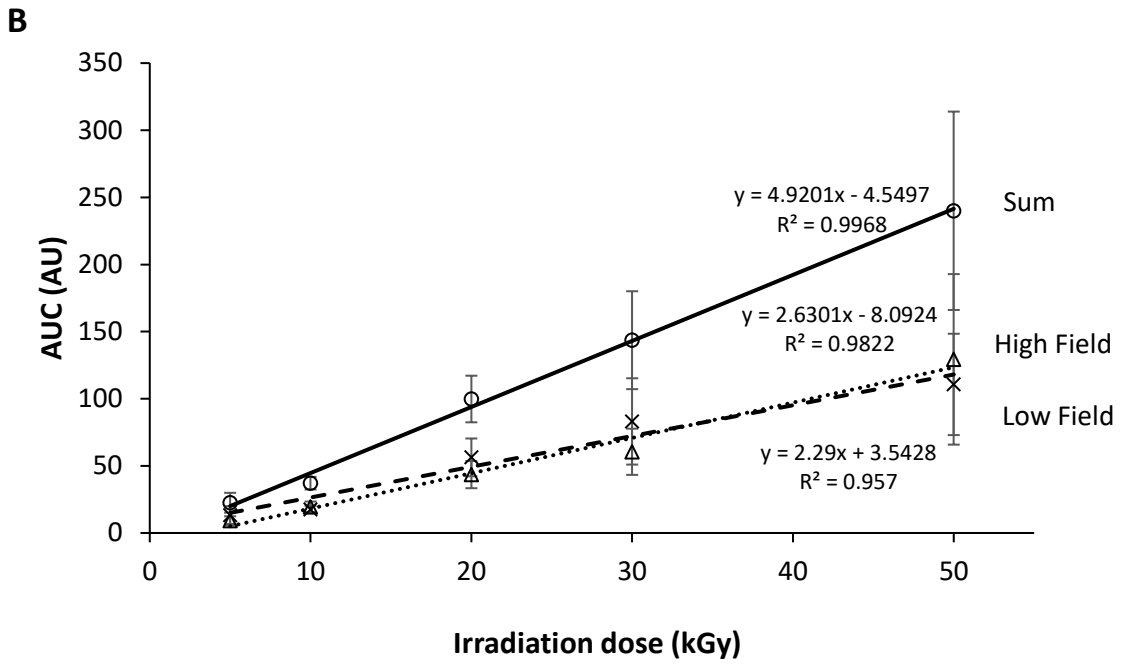


**Figure 5-5** SPA of high field (Δ), low field (x), and sum (○) of satellite peaks using integration method for SP samples irradiated at 5, 10, 20, 30, and 50 kGy with A) high-moisture B) low-moisture SP. The results are expressed as means (n=3) and standard deviation. The round dot, dash dot, and solid lines represent the trendlines of high field, low field, and sum SPA, respectively.

As expected, SPA using peak enhancement increased with irradiation dose (Figure 5-6). The sum of SPA for low-moisture SP increased with irradiation dose at a rate of 0.05 AU/dose, while sum of SPA of high-moisture SP increased at a rate of 0.008 AU/dose using the peak enhancement method. Correlation coefficients of sum SPA were 0.96 and 0.97 for high-moisture and low-moisture SP, respectively. The correlation coefficients of sum SPA were high for both samples. Moreover, the linearity improved with the use of the peak enhancement method, especially for high-moisture SP ($R^2$ = 0.82 using integration method).

The SPA of high field increased with irradiation dose at a rate of 0.0048 AU/dose, while SPA of low field increased with irradiation dose at a rate of 0.0032 AU/dose for high-moisture samples (Figure 5-6A). SPA of high field and low field peak had high and similar correlation factors ($R^2$ =0.97 and 0.94 for low and high field, respectively) for high-moisture SP samples. The SPA of high field increased with irradiation dose at a rate of 0.032 AU/dose, while SPA of low field increased with irradiation dose at a rate of 0.015 AU/dose for low-moisture samples (Figure 5-

6B). Meanwhile, SPA of high field peak had higher correlation factor ($R^2$ =0.99) than that of low field ($R^2$ =0.91) for low-moisture SP. The higher formation rates for high-field peaks were also observed for SPA using integration method, which was attributed to higher sensitivity of high field than low field. The SPA of low field peak using peak enhancement showed higher correlation ($R^2$ = 0.97) than SPA of low field peak using integration method for ($R^2$ =0.89) for high-moisture SP. Similarly, SPA of high field peak using peak enhancement had higher correlation ($R^2$ = 0.94) than SPA of high field peak using integration method for ($R^2$ =0.77) for high-moisture SP. The improved linearity and higher formation rates in SPA, especially in high-moisture samples, would serve better for quantification of irradiation doses in SP samples. In addition to linearity, CV decreased to less than 25% for high-moisture samples at all doses. CV of high field SPA of high-moisture SP samples were less than 22% at all doses and CV of low field SPA of high-moisture SP samples were less than 25% at all doses. Similarly, CV of high field SPA was less than 13% and CV of low field SPA was less than 20% of low-moisture SP samples at all doses. Overall, CV of SPA using the peak enhancement method was lower than that of integration method for both low and high moisture SP samples.

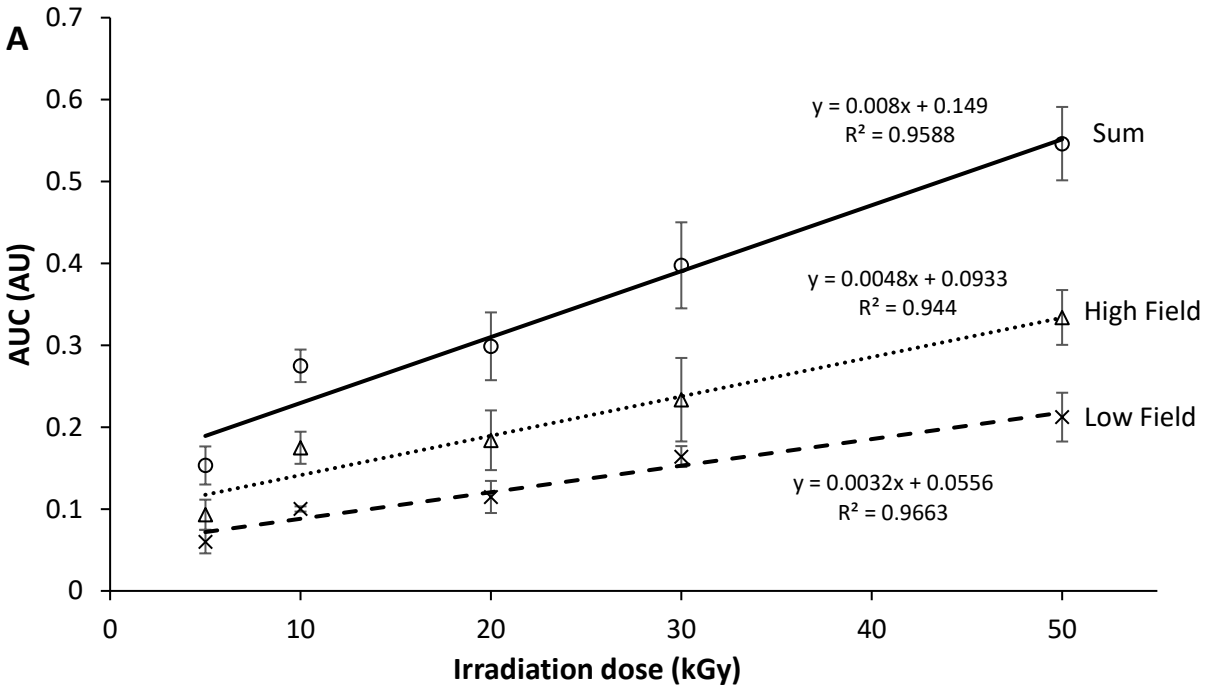

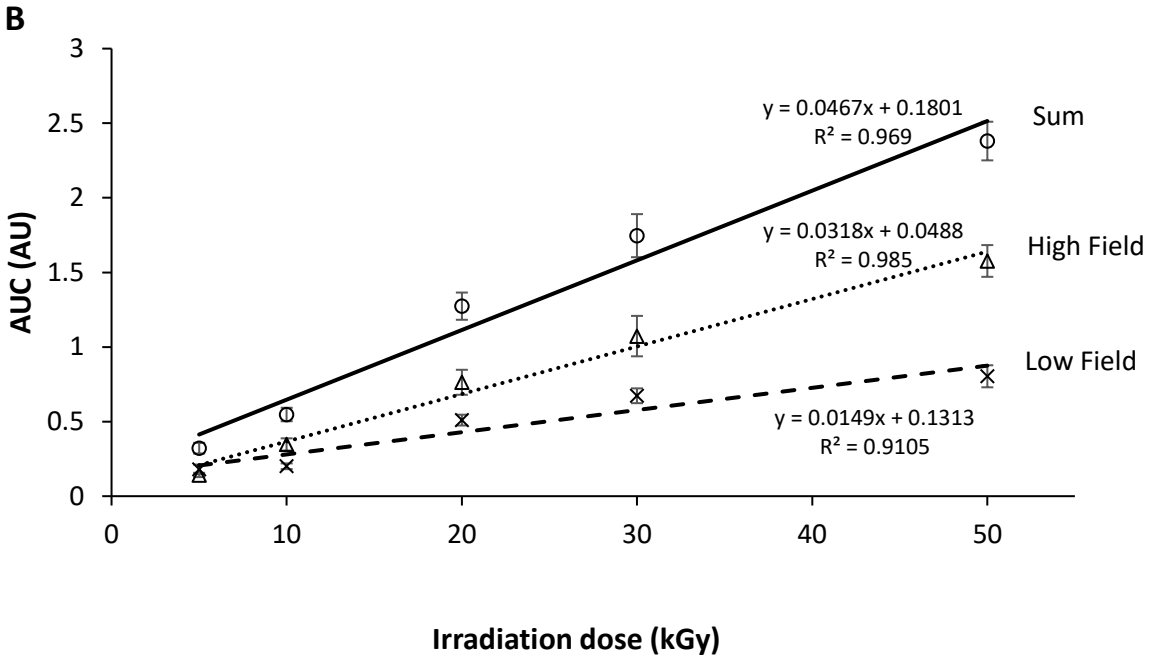


**Figure 5-6** SPA of high field (Δ), low field (x), and sum (○) of satellite peaks using peak enhancement method for SP samples irradiated at 5, 10, 20, 30, and 50 kGy with A) high-moisture B) low-moisture. The results are expressed as means (n=3) and standard deviation. The round dot, dash dot, and solid lines represent the trendlines of high field, low field, and sum SPA, respectively.

## Evaluation of dose response with GPA

Besides cellulose satellite peaks, irradiation-specific glucose split peak was analyzed to study its dose response using integration and peak enhancement methods. Only the split peak located at low field (335.4 ± 0.1 mT) was investigated since the high field peak was not resolved during EPR scans due to instrument limitations.

In integration method, GPA was calculated by double integration of the peak located between 335 and 336 mT (Figure 5-7A). GPA of low-moisture SP increased with irradiation dose at a rate of 32.1 AU/dose, while GPA of high-moisture SP increased at a rate of 1.33 AU/dose. GPA increased with increasing irradiation dose for both samples, as expected. Correlation coefficients of GPA were 0.92 and 0.96 for high-moisture and low-moisture SP, respectively. Although GPA had high linearity for both samples, overall CV of GPA were high (35%), especially at low

irradiation doses of high-moisture SP samples, such as 5 and 10 kGy. A similar result was reported for SPA of high-moisture samples using integration method.

The peak enhancement method was applied to GPA to decrease variation and improve peak resolution. Similar to integration method, GPA increased with irradiation dose for high and low-moisture SP samples (Figure 5-7B). GPA of high-moisture samples had a correlation factor of $R^2$ = 0.92, while GPA of low-moisture samples had a correlation factor of $R^2$ =0.97. These correlation coefficients were similar to the correlation coefficients of GPA using integration method. However, CV decreased to less than 20% for high-moisture and low-moisture samples at all doses. Thus, GPA using peak enhancement method had lower variation than that of integration method. The linear dose-response graphs and high correlation coefficients indicated that split peak of glucose radical can serve as an irradiation marker for irradiation detection and quantification in glucose-rich foods.

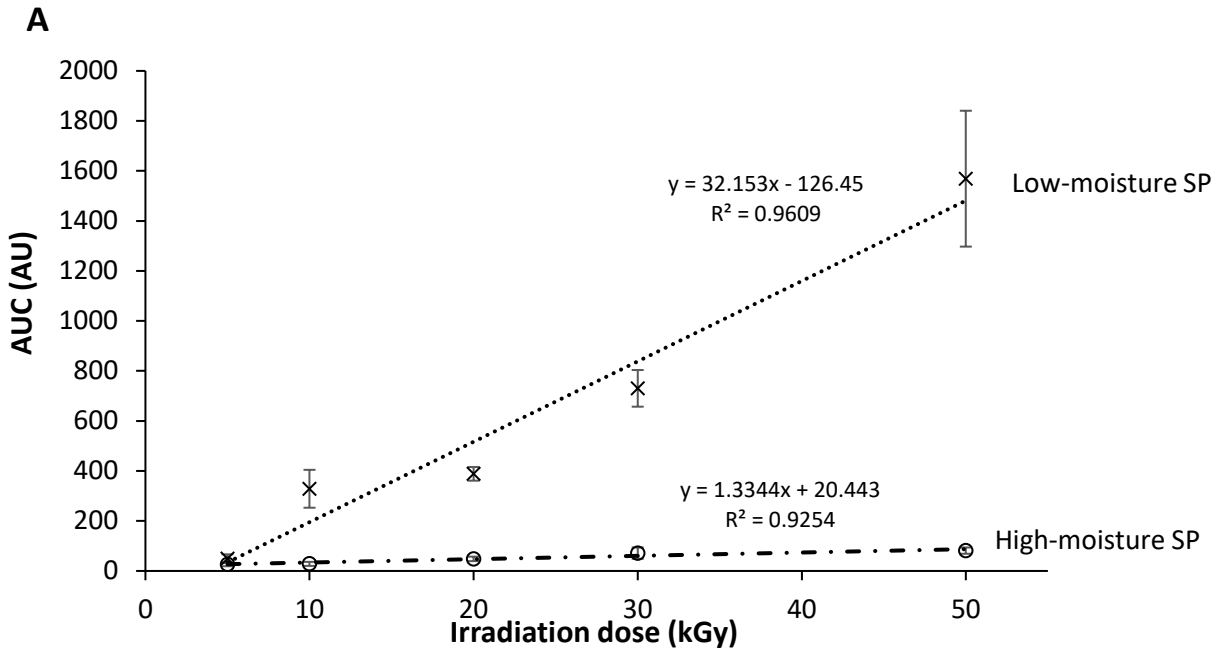

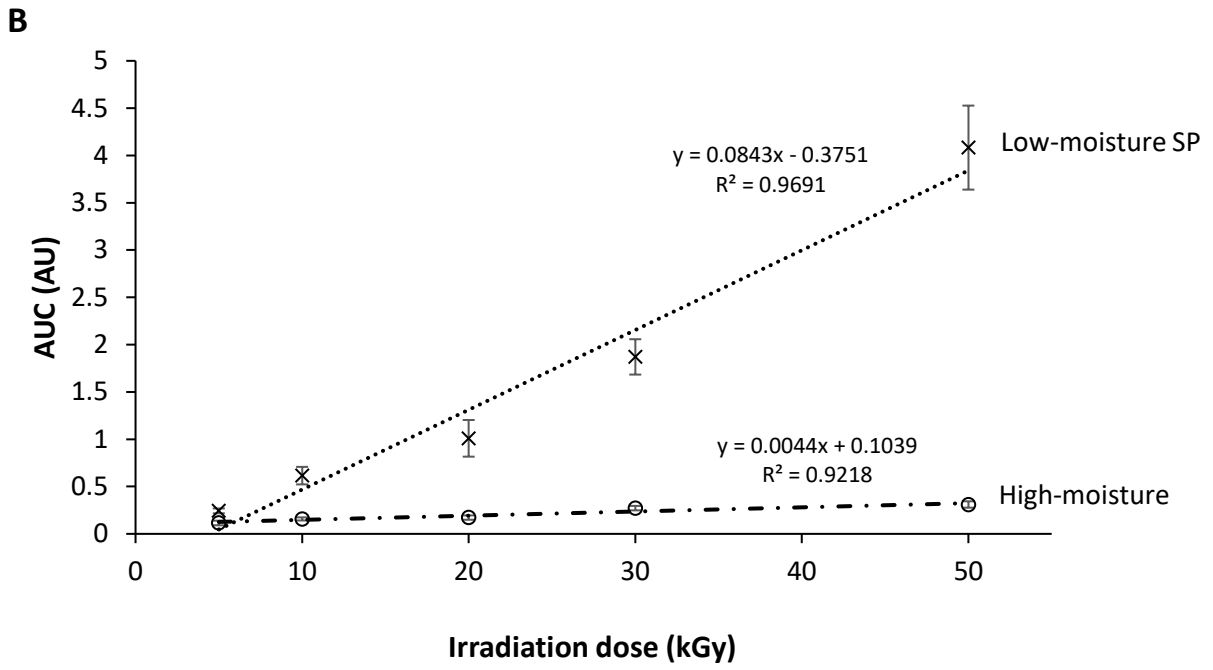


**Figure 5-7** GPA of high-moisture (○) and low-moisture (x) SP samples irradiated at 5, 10, 20, 30, and 50 kGy using A) integration B) peak enhancement method. The results are expressed as means (n=3) and standard deviation. The dash dot and round dot lines represent the trendlines for high-moisture and low-moisture SP, respectively.

As to our knowledge, our study is the first study to use an external data analysis method for peak enhancement. However, in a recent study, researchers applied deconvolution to investigate the number and characteristics of the lines constituting the EPR spectrum of irradiated glucose (Belahmar et al., 2020). They studied the principal Gaussian contributions that constitute the spectrum of glucose as a function of absorbed dose and storage time (Belahmar et al., 2020). Although they used a data analysis method to study EPR spectra, they did not attempt to enhance signal resolution as in our study. The results of our study suggested that spectra shape can be used to differentiate non-irradiated and irradiated SP samples based on characteristics of irradiation-derived radicals. However, the EPR spectra of irradiated plant origin foods are complex, therefore, it is challenging to accurately analyze the dose response of a material especially at high-moisture levels. Peak enhancement analysis provided increased correlation factor of dose-response graphs with lower variability. Overall, by using the technique proposed in this study irradiation-specific cellulose satellite peaks and glucose split peak in an EPR spectra

can be analyzed, detected, and potentially quantified in both low- and high-moisture plant-based foods rich in sugar and cellulose, such as dried sweet potatoes.

## Acknowledgement

This project was supported by FDA Vet-LIRN Cooperative Agreement U-18FD005842, and partially supported by the USDA National Institute of Food and Agriculture, Hatch project 1014344. Contribution no. 19-258-J from the Kansas Agricultural Experiment Station.

## References

Ahn, J. J., Sanyal, B., Akram, K., & Kwon, J. H. (2014). Alcoholic extraction enables EPR analysis to characterize radiation-induced cellulosic signals in spices. *Journal of Agricultural and Food Chemistry*, *62*(46), 11089–11098. https://doi.org/10.1021/jf502258r

Akram, K., Ahn, J.-J., & Kwon, J.-H. (2012). Analytical Methods for the Identification of Irradiated Foods. In E. Belotserkovsky & Z. Ostaltsov (Eds.), *Ionizing Radiation* (Issue October, pp. 1–36).

Aleksieva, K., Georgieva, L., Tzvetkova, E., & Yordanov, N. D. (2009). EPR study on tomatoes before and after gamma-irradiation. *Radiation Physics and Chemistry*, *78*(9), 823–825. https://doi.org/10.1016/j.radphyschem.2009.05.013

Aleksieva, K. I., Dimov, K. G., & Yordanov, N. D. (2014). Identification of gamma-irradiated fruit juices by EPR spectroscopy. *Radiation Physics and Chemistry*, *103*, 27–30. https://doi.org/10.1016/j.radphyschem.2014.05.008

AOAC International Official methods of analysis, 18th Ed., (2005a)., Rockville, MD, USA. Methods # 954.02 and 990.03

Baldus, D. (2009). *( 12 ) United States Patent ( 45 ) Date of Patent : May 26, 2009 FR*.

Belahmar, A., Mikou, M., & Saidou, A. M. (2020). Deconvolution of the EPR spectrum measured on irradiated glucose and analysis of the dosimetric properties of the main lines composing this spectrum. *Radiation Physics and Chemistry*, *166*(October 2019), 108519. https://doi.org/10.1016/j.radphyschem.2019.108519

Bortolin, E., Cardamone, C., Chiaravalle, A. E., Deiana, G., Di Schiavi, M. T., D'Oca, M. C., Marchesani, G., Quattrini, M. C., Sangiorgi, E., Tomaiuolo, M., & Boniglia, C. (2020).

Irradiation detection of herbal ingredients used in plant food supplements by Electron Spin Resonance on samples pre-treated with alcoholic extraction. *Radiation Physics and Chemistry*, *176*(August 2019), 108946. https://doi.org/10.1016/j.radphyschem.2020.108946

Brown, C. E. (1998). Coefficient of Variation. In *Applied Multivariate Statistics in Geohydrology and Related Sciences* (pp. 155–157). Springer Berlin Heidelberg. https://doi.org/10.1007/978-3-642-80328-4_13

Child, G., Foster, D. J., Fougere, B. J., Milan, J. M., & Rozmanec, M. (2009). Ataxia and paralysis in cats in Australia associated with exposure to an imported gamma-irradiated commercial dry pet food. *Australian Veterinary Journal*, *87*(9), 349–351. https://doi.org/10.1111/j.1751-0813.2009.00475.x

Coffey, A. M., Truong, M. L., & Chekmenev, E. Y. (2013). Low-field MRI can be more sensitive than high-field MRI. *Journal of Magnetic Resonance*, *237*(1), 169–174. https://doi.org/10.1016/j.jmr.2013.10.013

Crews, C., Driffield, M., & Thomas, C. (2012). Analysis of 2-alkylcyclobutanones for detection of food irradiation: Current status, needs and prospects. *Journal of Food Composition and Analysis*, *26*(1–2), 1–11. https://doi.org/10.1016/j.jfca.2011.11.006

D'Oca, M. C., & Bartolotta, A. (2011). Evaluation of the original dose in irradiated dried fruit by EPR spectroscopy. *Radiation Measurements*, *46*(9), 813–815. https://doi.org/10.1016/j.radmeas.2011.03.027

De Aragão, B. J. G., & Messaddeq, Y. (2008). Peak separation by derivative spectroscopy applied to FTIR analysis of hydrolized silica. *Journal of the Brazilian Chemical Society*, *19*(8), 1582–1594. https://doi.org/10.1590/s0103-50532008000800019

De Jesus, E. F. O., Rossi, A. M., & Lopes, R. T. (1999). An ESR study on identification of gamma-irradiated kiwi, papaya and tomato using fruit pulp. *International Journal of Food Science and Technology*, *34*(2), 173–178. https://doi.org/10.1046/j.1365-2621.1999.00250.x

Delincée, H., & Soika, C. (2002). Improvement of the ESR detection of irradiated food containing cellulose employing a simple extraction method. *Radiation Physics and Chemistry*, *63*(3–6), 437–441. https://doi.org/10.1016/S0969-806X(01)00533-3

Ehlermann, D. A. E. (2016). The early history of food irradiation. *Radiation Physics and Chemistry*, *129*, 10–12. https://doi.org/10.1016/j.radphyschem.2016.07.024

European Committee for Standardization (CEN). (2000). *(EN1787) Foodstuffs-detection of*

*irradiated food containing cellulose by ESR spectroscopy.* http://ec.europa.eu/food/food/biosafety/irradiation/1787-2000_en.pdf.

European Committee for Standardization (CEN). (2001). *(EN13708) Foodstuffs-detection of irradiated food containing crystalline sugar by ESR spectroscopy*. http://ec.europa.eu/food/food/biosafety/irradiation/13708-2001_en.pdf.

FDA (The Food and Drug Administration). (2014). *FDA Progress Report on Ongoing Investigation into Jerky Pet Treats*. http://www.fda.gov/AnimalVeterinary/SafetyHealth/ProductSafetyInformation/ucm371465.htm

FDA (The Food and Drug Administration). (2015). *Code of Federal Regulations, Title 21*. *Volume 3*, CITE: 21CFR179.26

FDA (The Food and Drug Administration). (2013). *Investigation Rationale and Results*. https://www.fda.gov/AnimalVeterinary/SafetyHealth/ProductSafetyInformation/ucm360951.htm

Gadgil, P., Hachmeister, K. A., Smith, J. S., & Kropf, D. H. (2002). 2-Alkylcyclobutanones as irradiation dose indicators in irradiated ground beef patties. *Journal of Agricultural and Food Chemistry*, *50*(20), 5746–5750. https://doi.org/10.1021/jf020323+

Guzik, G. P., Stachowicz, W., & Michalik, J. (2015). Identification of irradiated dried fruits using EPR spectroscopy. *NUKLEONIKA*, *60*(November 2014), 627–631. https://doi.org/10.1515/nuka-2015-0093

Hijaz, F. M., & Smith, J. S. (2010). Levels of 2-Dodecylcyclobutanone in Ground Beef Patties Irradiated by Low-Energy X-Ray and Gamma Rays. *Journal of Food Science*, *75*(9), 156–160. https://doi.org/10.1111/j.1750-3841.2010.01869.x

Jo, Y., Sanyal, B., Ameer, K., & Kwon, J. H. (2018). Characterization of DNA comet and cellulose radical signal in Valencia oranges treated with different forms of ionizing radiation. *Postharvest Biology and Technology*, *135*(January 2017), 68–76. https://doi.org/10.1016/j.postharvbio.2017.08.004

Klaassen, C., Casarett, L. J., & Doull, J. (2013). *Casarett & Doull's Toxicology: The Basic Science of Poisons, Eighth Edition*. McGraw-Hill Education. https://books.google.com/books?id=qLhU3GO81ssC

Kwon, J. H., Kausar, T., Noh, J., Kim, D. H., Byun, M. W., Kim, K. S., & Kim, K. S. (2007).

The identification of irradiated seasoned filefish (Thamnaconus modestus) by different analytical methods. *Radiation Physics and Chemistry*, *76*(11–12), 1833–1836. https://doi.org/10.1016/j.radphyschem.2007.03.011

Li, Y., Pan, C., Xue, Y., Meng, X., & Ding, Y. (2016). A novel signal enhancement method for overlapped peaks with noise immunity. *Spectroscopy Letters*, *49*(4), 285–293. https://doi.org/10.1080/00387010.2016.1144614

Liao, L., Liu, H., Gan, Z., & Wu, W. (2019). Structural properties of sweet potato starch and its vermicelli quality as affected by heat-moisture treatment. *International Journal of Food Properties*, *22*(1), 1122–1133. https://doi.org/10.1080/10942912.2019.1626418

Malec-Czechowska, K., Strzelczak, G., Dancewicz, A. M., Stachowicz, W., & Delincee, H. (2003). Detection of irradiation treatment in dried mushrooms by photostimulated luminescence, EPR spectroscopy and thermoluminescence measurements. *European Food Research and Technology*, *216*(2), 157–165. https://doi.org/10.1007/s00217-002-0615-x

Miller, R. B. (2005). *Electronic Irradiation of Foods: An introduction to The Technology*. https://doi.org/10.1007/0-387-28386-2

Morehouse, K. M., Kiesel, M., & Ku, Y. (1993). Identification of Meat Treated with Ionizing Radiation by Capillary Gas Chromatographic Determination of Radiolytically Produced Hydrocarbons. *Journal of Agricultural and Food Chemistry*, *41*(5), 758–763. https://doi.org/10.1021/jf00029a015

Nordio, P. L. (1976). General Magnetic Resonance Theory. In L. J. Berliner (Ed.), *Spin Labeling Theory and Applications* (pp. 5–52). Academic Press.

Obana, H., Furuta, M., & Tanaka, Y. (2005). Analysis of 2-Alkylcyclobutanones with Accelerated Solvent Extraction To Detect Irradiated Meat and Fish. *Journal of Agricultural and Food Chemistry*, *53*(17), 6603–6608. https://doi.org/10.1021/jf0506636

Prasuna, C. P. L., Chakradhar, R. P. S., Rao, J. L., & Gopal, N. O. (2008). EPR as an analytical tool in assessing the mineral nutrients and irradiated food products-vegetables. *Spectrochimica Acta - Part A: Molecular and Biomolecular Spectroscopy*, *71*(3), 809–813. https://doi.org/10.1016/j.saa.2008.02.003

Sanyal, B., Chatterjee, S., Variyar, P. S., & Sharma, A. (2012). Application of EPR Spectroscopy to Identify Irradiated Indian Medicinal Plant Products. *Journal of Food Science*, *77*(6), 710–718. https://doi.org/10.1111/j.1750-3841.2012.02697.x

Shahbaz, H. M., Kyung, H. K., Kim, H. Y., & Kwon, J. H. (2015). Analysis of electron spin resonance spectra for the identification of complex ESR signals using irradiated standard marker materials. *Journal of Radioanalytical and Nuclear Chemistry*, *306*(1), 93–97. https://doi.org/10.1007/s10967-015-4075-8

Sin, D. W. M., Wong, Y. C., & Yao, W. Y. (2006). Analysis of g-irradiated melon, pumpkin, and sunflower seeds by electron paramagnetic resonance spectroscopy and gas chromatography-mass spectrometry. *Journal of Agricultural and Food Chemistry*, *54*(19), 7159–7166. https://doi.org/10.1021/jf061349u

Soncin, S., Panseri, S., Rusconi, M., Mariani, M., Chiesa, L. M., & Biondi, P. A. (2012). Improved determination of 2-dodecylcyclobutanone in irradiated ground beef patties by gas-chromatography-mass-spectrometry (GC/MS) coupled with solid-phase microextraction (SPME) technique. *Food Chemistry*, *134*(1), 440–444. https://doi.org/10.1016/j.foodchem.2012.02.089

Stewart, E. M. (2001). Detection Methods for Irradiated Foods. In R. A. Molins (Ed.), *Food Irradiation: Principles and Applications* (pp. 347–372). Wiley-Interscience.

Taghvaei, M., Sommers, C., Ceric, O., Hussain, F., Yucel, U., & Smith, J. S. (2020). Solid-phase micro extraction of food irradiation marker 2-dodecylcyclobutanone (2-DCB) from chicken jerky treated with glycerol. *Journal of Food Science*, *85*(8), 2608–2614. https://doi.org/10.1111/1750-3841.15322

Tomaiuolo, M., Mangiacotti, M., Trotta, G., Marchesani, G., Chiappinelli, A., & Chiaravalle, A. E. (2018). Identification of X-ray irradiated walnuts by ESR spectroscopy. *Radiation Physics and Chemistry*, *150*(March), 35–39. https://doi.org/10.1016/j.radphyschem.2018.04.007

Tonyali, B., Sommers, C., Ceric, O., Smith, J. S., & Yucel, U. (2020). An analysis of cellulose- and dextrose-based radicals in sweet potatoes as irradiation markers. *Journal of Food Science*. https://doi.org/10.1111/1750-3841.15359

Weil, J. A., & Bolton, J. R. (2007). *Electron Paramagnetic Resonance*. John Wiley & Sons, Inc. https://doi.org/10.1002/0470084987

Yamaoki, R., Kimura, S., & Ohta, M. (2010). Analysis of electron spin resonance spectra of irradiated gingers: Organic radical components derived from carbohydrates. *Radiation Physics and Chemistry*, *79*(4), 417–423. https://doi.org/10.1016/j.radphyschem.2009.11.011

Yamaoki, R., Kimura, S., & Ohta, M. (2011). Electron spin resonance characterization of radical components in irradiated black pepper skin and core. *Radiation Physics and Chemistry*, *80*(11), 1282–1288. https://doi.org/10.1016/j.radphyschem.2011.06.009

Yordanov, N. D., & Pachova, Z. (2006). Gamma-irradiated dry fruits: An example of a wide variety of long-time dependent EPR spectra. *Spectrochimica Acta - Part A: Molecular and Biomolecular Spectroscopy*, *63*(4), 891–895. https://doi.org/10.1016/j.saa.2005.10.023

Zhu, J. ting, Feng, M., Yan, J. min, Liu, C. quan, Ha, Y. ming, Gao, M. xu, Yang, P., Wang, Z. dong, Wang, D. ning, Li, S. rong, & Gu, G. qiang. (2012). Toxicological Evaluation of Chicken-Breast Meat with High-Dose Irradiation. *Journal of Integrative Agriculture*, *11*(12), 2088–2096. https://doi.org/10.1016/S2095-3119(12)60467-5

# Chapter 6 - Interaction of 2-dodecylcyclobutanone (2-DCB) and internal standard in irradiated chicken jerky treats and pig ears in solid-phase microextraction (SPME) coupled gas chromatography-mass spectrometry (GC-MS) analysis


## Abstract

Chicken jerky treats (CJT) and pig ears (PE) are irradiated foods that were commercially analyzed with gas chromatography (GC-MS). These lipid-containing products produce irradiation-specific 2-dodecylcyclobutanone (2-DCB), a radiolysis product of palmitic acid during irradiation. Electron paramagnetic resonance (EPR) spectroscopy and solid-phase microextraction (SPME)-coupled gas chromatography were used to estimate the irradiation history of these products. In addition, the factors such as IS concentration, matrix properties, and analyte concentrations that are important for the sensitivity of GC-MS analysis were investigated. Spiked and irradiated samples were studied at two irradiation levels (10 and 50 kGy) and different internal standard (IS) concentrations (8 and 80 ng/g sample for CJT; 8, 80, and 800 ng/g sample for PE) to evaluate the interaction of IS and 2-DCB as a function of their concentrations and matrix properties to improve the precision and accuracy of the SPME-coupled GC-MS analysis. IS and 2-DCB were quantified by calculating the area under IS peak (ISA) and the area under 2-DCB peak (DCA), respectively. EPR spectra of non-irradiated PE and CJT exhibited a singlet line. After irradiation, irradiated PE had a signal centered at g = 1.996 ± 0.003 due to isotropic $CO_2^-$ radical, while the signal intensity of singlet line in CJT increased. Although the irradiation-specific peak in PE and the increased signal intensity of the central peak in CJT can be used for irradiation detection, they could not be resolved to quantify irradiation doses. GC-MS analysis showed that ISA of CJT irradiated at 50 kGy was significantly higher ($p<0.01$) than that of 10 kGy at IS concentration of 8 ng/g CJT. There was

no significant difference in ISA at a high IS concentration (80 ng/g CJT). ISA was significantly higher ($p<0.01$) at a higher irradiation dose for IS concentrations of 8 and 80 ng/g PE. ISA remained unchanged at a high IS concentration (800 ng/g PE). No significant difference in ISA was observed with irradiation dose at any IS concentrations for PE and CJT. The extent of increase in DCA was significantly affected by IS concentration in irradiated CJT and PE samples, while this effect was not observed for spiked samples. This suggests a possible matrix effect, where the release of 2-DCB is affected by IS concentration in irradiated samples.

## Introduction

Irradiation is a non-thermal process used for human and animal food products for different purposes such as extending shelf life and preventing the growth of pathogenic and spoilage microorganisms (Zianni et al., 2021). The irradiation process is considered safe within doses determined by regulatory agencies, e.g., the Food and Drug Administration (FDA) and European Commission (EC). However, there have been some reports of serious illness in dogs associated with the consumption of irradiated animal treats such as chicken jerky treats (FDA, 2014). Although no link between irradiated animal treats and pet illness was found, there is a still need for investigating the irradiation history of pet food products. Chicken jerky treats (CJT) and pig ears (PE) are popular dog treats that contain lipids, specifically palmitic acid. Under irradiation, palmitic acid forms 2-dodecylcyclobutanone (2- DCB), which is a unique radiolysis product and is not detected in non-irradiated foods that are processed with other treatments (e.g., heating, pasteurization, and freezing) (Campaniello et al., 2019; Driffield et al., 2014). Previously, researchers have studied 2-DCB in irradiated food products, such as beef patties, chicken, and salmon (Obana et al., 2005), minced chicken, turkey, duck, beef, pork (Campaniello et al., 2019), and dry-cured ham (Blanch et al., 2009). Obana et al. (2005) mentioned that no 2-DCB was detected in non-irradiated samples, while 2-DCB was detected in irradiated beef patties, chicken, and salmon samples even at low doses as 0.7 kGy. Similarly, 2-DCB was identified in minced chicken, turkey, duck, beef, pork after irradiation at 0.5 kGy, while no 2-DCB was observed before irradiation (Campaniello et al., 2019).

The European Commission approved the use of 2-DCB for detection of irradiation above 0.5 kGy in the European Standard (EN1785) method (2003). This method requires Soxhlet extraction and gas chromatography-mass spectrometry detection (GC-MS). However, soxhlet

extraction requires a long extraction time and the use of organic solvents (Crews et al., 2012). Meanwhile, solid-phase microextraction (SPME) can be a suitable alternative to the time-consuming extraction procedure since it is a rapid and solvent-free technique (Campaniello et al., 2019). In addition, it can extract and concentrate organic compounds even at low concentrations from food matrices (Blanch et al., 2009).

The efficiency of SPME can be affected by various parameters such as fiber type, incubation temperature, incubation time, and food matrix (Caja et al., 2008). By incorporating internal standard (IS), SPME can be used quantitatively. IS addresses variability in sample preparation and instrumental conditions. Hence, the use of IS can improve the accuracy and precision of quantitative analysis (Ouyang & Pawliszyn, 2006). However, selecting a proper IS is challenging since it needs to have characteristics similar to the analyte (e.g., molecular weight, polarity, and boiling point) (Zenkevich et al., 2007). Some researchers used isotopically labeled standards, which are compounds in which some atoms are replaced by their stable isotopes. However, they are usually expensive and unavailable for many analytes (Kenessov et al., 2016; Orazbayeva et al., 2017; Stokvis et al., 2005). Although IS needs to behave similar to the analyte, a competition between the analyte and IS could result in poor selectivity as well as low efficiency for extraction (Zenkevich et al., 2007). Previously, Moosavi and Ghassabian (2018) discussed how IS and the analyte of interest might affect each other's signals. They suggested that IS concentration should be low enough to avoid analyte signal suppression by IS and high enough to prevent IS signal suppression by the analyte. Oliver-Pozo et al. (2015) conducted SPME-coupled GC analysis to study volatile compounds from virgin olive oil and mentioned that analytes in the headspace might interact and compete during the fiber adsorption process.

Besides 2-DCB, irradiation, also, causes the formation of irradiation-specific free radicals in food systems. Electron paramagnetic resonance (EPR) spectroscopy is based on the interaction of free radicals with an external magnetic field. It is a sensitive and fast technique and can be used for the detection of irradiation-specific free radicals. Earlier our group showed that EPR characterization of irradiation is suitable for lipid-poor dry food materials, such as sweet potatoes (Tonyali et al., 2020).

Therefore, the aim of this study is to evaluate the IS (2,4-di(tert-pentyl)cyclohexanone) and 2-DCB interaction for irradiation history of high-lipid-containing (PE) and low-lipid-containing

(CJT) pet foods using GC-MS analysis. In addition, it is aimed to study the irradiation-specific free radicals for irradiation history of the CJT and PE samples using EPR spectroscopy.

## Materials and Methods

### Materials

The analytical standards of 2-DCB as analyte and 2,4-di(tert-pentyl)cyclohexanone and 2-cyclohexylcyclohexanone as internal standards were purchased from Sigma-Aldrich (St. Louis, MO). The polydimethylsiloxane/divinylbenzene (PDMS/DVB 65µm, 23 Ga), the polydimethylsiloxane (PDMS with coating diameters of 7 and 100 µm, 23 Ga), and carboxen/ polydimethylsiloxane (CAR/PDMS 75µm, 23 Ga) SPME fibers were purchased from Supelco (Bellefonte, PA). Optima grade methanol and ethanol, analytical grade methanol, hexane, chloroform, boron trifluoride, and KCl were obtained from Fisher Scientific (Waltham, MA). Raw chicken tenderloins (Tyson Foods, Springdale, AR) were purchased from a local market. Pig ears were obtained from the Animal Science and Industry Department of Kansas State University.

### Preparation and Irradiation of CJT and PE

CJT and PE were prepared following the protocol described in Taghvaei et al. (2020). Briefly, CJT were prepared by drying raw chicken tenderloins in a food dehydrator (Sedona SD-P9000, Korea) at 155 °F for 48 hours. The PEs were cleaned from hair using a razor and washed to remove the blood and hair. They were dried in a dehydrator at 155 °F for 48 h. Both the PE and CJT samples were irradiated at Gateway America (Gulfport, MS) using a Cobalt-60 source. The target irradiation doses (10 and 50 kGy) were verified using an alanine dosimeter. The CJT and PE samples (before and after irradiation) were shipped under refrigerated conditions. They were stored in a freezer (–80 °C) until further analysis.

### CJT and PE fatty acid methyl esters (FAME) analysis

The extraction of chicken fat for FAME analysis was conducted following the method described in Taghvaei et al. (2020). Briefly, the chicken was homogenized with hexane (T18BS1, IKA, Germany). After filtering the slurry with Whatman #40, hexane was removed using a rotary evaporator at 45 °C (RE121, Buchi, Switzerland). The fatty acid methyl esters were obtained

using the boron trifluoride method (Ackman, 1998). After removing hexane, 100 mg of oil was mixed with 3 mL of methanol solution of boron trifluoride (14%) and kept at 100 °C for 40 minutes. The methyl esters were extracted from the mixture using hexane. Later, 1 mL of extract was analyzed in GC-MS system (HP5972 and HP 5890, Agilent Technologies) equipped with an HP-23 FAME column (30 m × 0.25 mm × 0.25 µm, Agilent Technologies). The column was kept at 60 °C for 4 minutes, then heated to 195 °C at 20 °C/min, and held at 195 °C for 5 minutes. The injector temperature was 250 °C. The fragment ions between 30 to 400 m/z were scanned with the MS. The FAME were identified by comparing their mass spectrum with that of the National Institute of Standards and Technology (NIST 14) database.

The extraction of fat from pig ears was conducted following the method described in Bligh and Dyer (1959) with some modifications. In brief, pig ears (1.6 g) were mixed with 4 mL of chloroform, 4 mL of methanol, and 2 mL of water. The mixture was centrifuged at 2,000 rpm for 10 minutes (Allegra X-14R Centrifuge, Beckman Coulter). After centrifugation, the lower layer was removed, 2 mL of chloroform was added onto residue and centrifuged again. The lower layer from the second centrifuge was combined with the lower layer from the first centrifuge. The mixture was mixed with 0.5 mL of KCI solution (1 M) and 0.5 mL of water. Later, 2 mL from the mixture was dried using a rotary evaporator. The extracts were analyzed at the Kansas Lipidomics Research Center, Kansas State University. For FAME analysis, 2 mL of extract was mixed with 1 mL of methanolic HCl (3 M) and heated at 78 °C for 30 minutes. Later, 2 mL of hexane was added, the mixture was vortexed for 30 seconds, and centrifuged for 7 minutes. After removal of the upper phase, 2 mL of hexane was added to the aqueous phase and the mixture was centrifuged again. The upper phase from the second centrifuge was combined with the upper phase from the first centrifuge. The organic phase was dried under a flush of nitrogen gas and re-dissolved in 100 µL of hexane. One µL from the mixture was injected into a GC Agilent 6890N system coupled with a flame ionization detector. Helium was used as the carrier gas at a flow rate of 1.5 mL/min. The GC column was DB-23 capillary column (60 m × 0.25 mm × 0.25 µm, Agilent Technologies). The column was kept at 150 °C for 1 minute, then heated to 175 °C at 25 °C/min, increased to 230 °C at 4 °C/min, and held at 230 °C for 8 minutes. The FAME were identified by comparison of retention times of the compounds in the sample with the retention times of Supelco 37 component fatty acid methyl ester mix standards (CRM47885, certified reference material, Sigma-Aldrich).

## Analysis of irradiation-derived radicals using EPR spectroscopy

### Sample preparation for EPR spectroscopy

CJT and PE were ground in a Waring blender (50 mL) (model 34FL97) for 1 min in pulses. Ground samples were pelletized as cylinders using a hydraulic pelletizer (ca. 7 mm in length and 3 mm in diameter). All samples were weighed (80 mg) and transferred into a quartz EPR tube (OD:5 mm & ID:4 mm, Wilmad-LabGlass).

### EPR analysis

The EPR measurements were conducted in a SpinscanX spectrometer (ADANI, Minsk, Belarus) operating at X-band with a modulation frequency of 100 kHz. Samples were scanned at the following measurement conditions: center field 334.5 mT, sweep width 11 mT, modulation frequency 100 kHz, modulation amplitude 600 uT, and microwave power 1mW.

## SPME-coupled GC-MS analysis

### Sample preparation and SPME

A stock solution of 2-DCB (1000 ppm) was prepared by dissolving an appropriate amount of pure standard into ethanol. A stock solution of 2,4-di(tert-pentyl)cyclohexanone (10000 ppm) was prepared using methanol. Working standard solutions (1 ppm) was prepared daily by subsequent dilution of stock solutions with water. The working standard solutions were used to spike non-irradiated CJT and PE samples.

Both irradiated and non-irradiated CJT and PE were ground in a Waring blender (50 mL) (model 34FL97, McConnellsburg, PA) for 1 min in pulses. Ground irradiated CJT and PE were diluted with water at a 1:5 ratio (g sample: mL water) and homogenized at 30000 rpm for 1 minute (Fisher Scientific, Omni International Stainless Steel Saw Tooth Probe, TH115, 10 mm (D) x 115 mm (L)). Homogenized CJT was spiked with IS to a final concentration of 8 or 80 ng IS /g CJT and homogenized non-irradiated CJT was also spiked with 2-DCB (41 and 84 ng/g CJT equivalent to 2-DCB in 10 and 50 kGy samples). Homogenized PE was spiked with IS to a final concentration of 8, 80, or 800 ng/g PE and homogenized non-irradiated PE was also spiked with 2-DCB (100 and 310 ng/g PE equivalent to 2-DCB in 10 and 50 kGy samples). Samples were homogenized for another 1 min. An aliquot of the mixture (3 mL) was transferred to a siliconized headspace vial (75.5 x 22.5 mm, SUPELCO). After adding a small magnetic stirrer,

the vials were immediately sealed with a crimp cap (20 mm, PTFE/Silicone Septa, SUPELCO). Sealed vials were thermally equilibrated at 80 °C (Pierce Heating/Stirring Module, Rockford, IL) with magnetic stirring slowly for 30 minutes without splashing. The SPME fiber (PDMS/DVB) was exposed to the headspace of the vial at the same temperature for 15 minutes.

### GC-MS analysis

Analysis of 2-DCB was performed using a GC-MS chromatography system (HP5973 and HP 6890, Agilent Technologies, Santa Clara, CA) equipped with an HP-5MS (60 m × 0.25 mm × 0.25 µm, Agilent Technologies, Santa Clara, CA) column. The target compounds were desorbed from the fiber at 250 °C for 1 min at splitless mode. The GC-MS conditions were adapted from Taghvaei et al. (2020) with modifications. Helium was used as a carrier gas at a flow rate of 1 mL/min. The GC column was heated from 50 °C to 300 °C at 10 °C/min and kept at 300 °C for 3 mins. The MS conditions were as follows: the source and the quad line temperatures were maintained at 230 °C and 150 °C, respectively. The following ions were selected: m/z 84, m/z 98, and m/z 112 for 2-DCB, and m/z 139, m/z 153, and m/z 168 for IS. Data acquisition and quantification from the MS was performed using an HP-ChemStation system. The analytes were identified by comparing their mass spectrum with that of the National Institute of Standards and Technology (NIST 14) database and verified by comparing their mass spectrum with that of analytical (external) standards. IS and 2-DCB were quantified by calculating the area under the IS peak (ISA) and the area under the 2-DCB peak (DCA).

### Statistics

All experiments were performed in triplicate unless otherwise stated. Analysis of variance (ANOVA) was applied using a general linear model (GLM) in MINITAB software (Minitab Version16, State College, Pa., USA). Tukey`s multiple comparison test was applied to evaluate the differences between treatments (significant when $p < 0.05$).

## Results and Discussion

### Analysis of irradiation-derived radicals using EPR spectroscopy

Non-irradiated (control) PE and CJT samples exhibited a singlet line around $g = 2.0047 \pm 0.003$ in EPR spectra. Other researchers attributed the peak around $g = 2.005$ to inorganic radicals

coming from meat samples containing bone structure (Negut & Cutrubinis, 2017). After irradiation, PE sampled gave a signal centered at g = 1.996 ± 0.003 in addition to the singlet line. The signal located at g = 1.996 was probably due to isotropic $CO_2^-$ radical (Negron-Mendoza et al., 2015). However, the $CO_2^-$ radical peak could not be resolved to quantify irradiation doses. This was probably because the broadening of the singlet line after irradiation partially hindered it.

The EPR spectra of the irradiated CJT sample had the same singlet line as before irradiation but with higher signal intensity. Although the increased signal intensity of the singlet line in CJT and the irradiation-specific peak in PE can be used for irradiation detection, they could not be resolved to quantify irradiation doses. These results suggest that EPR spectroscopy can indicate irradiation detection in lipid-rich samples such as CJT and PE, but it is limited for dose quantification of these samples.

## SPME fiber and internal standard selection

The affinity for 2-DCB of three different stationary phases with different coating diameters (PDMS with coating diameters of 7 and 100 µm, CAR/PDMS with coating diameter of 75 µm, and PDMS/DVB with coating diameter of 65 µm) was tested. PDMS/DVB with a coating diameter of 65 µm showed the highest affinity and had a higher slope in 2-DCB concentration vs the 2-DCB peak area graph. Previous research found that higher slope yields better differentiation between samples irradiated at different doses (Taghvaei et al., 2020). Therefore, PDMS/DVB was used in this study.

A preliminary study was conducted to compare efficiencies (e.g., how well they mimic 2-DCB) of two IS: 2,4-di(tert-pentyl)cyclohexanone and 2-cyclohexylcyclohexanone. The efficiencies of the two IS were evaluated by comparing the ratio of DCA to ISA. The dose-response graphs of the two IS were prepared at a concentration of 80 ng/g CJT and 2-DCB concentrations of 5, 10, 25, 50, 75, 200, and 400 ng/g CJT. The dose-response graph increased linearly for both IS; however, the slope of the curve with 2,4-di(tert-pentyl)cyclohexanone (0.0219) was an order of magnitude higher than 2-cyclohexylcyclohexanone (0.0034). The higher slope yields easier differentiation for samples of different irradiation doses. Therefore, 2,4-di(tert-pentyl)cyclohexanone was selected as the internal standard in the study. CJT samples were tested at two 2-DCB concentrations (63 and 175 ng/g CJT equivalent to 2-DCB in 10 and 50 kGy samples) and two IS concentrations (8 and 80 ng/g CJT). Meanwhile, PE samples were analyzed

at two 2-DCB concentrations (158 and 363 ng/g PE equivalent to 2-DCB in 10 and 50 kGy samples) and three IS concentrations (8, 80, and 800 ng/g PE).

## ISA and DCA in CJT

The ISA of CJT irradiated at 50 kGy was significantly higher ($p<0.01$) than that of 10 kGy at IS concentration of 8 ng/g CJT (Figure 6-1A). The significant increase in ISA with increasing 2-DCB concentration suggests an interaction and competition phenomena between IS and 2-DCB. Oliver-Pozo et al. (2015) mentioned that the SPME efficiency was highly affected by the competition and interaction between volatile analytes during fiber adsorption. Moreover, this competition becomes significant when one analyte with high concentration and high affinity replaces another analyte with less concentration and less affinity on the fiber (Oliver-Pozo et al., 2015). A similar observation was mentioned in a study with volatile compounds from aqueous solutions (Gionfriddo et al., 2015). These researchers stated that the analytes with stronger affinity for the fiber displaced other analytes with less affinity. DCA of CJT irradiated at 50 kGy was significantly higher ($p<0.05$) than that of 10 kGy at IS concentration of 8 ng/g CJT (Figure 6-1B). An increase in 2-DCB amount with increasing irradiation dose was previously reported for ground beef between 0.5 and 7 kGy (Zhao et al., 2012), ground beef between 1 and 4.5 kGy (Gadgil et al., 2005), ground beef between 0.5 and 8 kGy (Soncin et al., 2012), chicken, turkey, duck, beef, and pork between 0.05 and 3 kGy (Campaniello et al., 2019), cheese and milk between 0.5 and 5 kGy (Zianni et al., 2021).

When IS concentration increased to 80 ng/g CJT, no significant difference ($p >0.05$) was observed between ISA (668,000 A.U.) at irradiation doses 10 and 50 kGy. This observation supported that the interaction between IS and 2-DCB was significant at low IS concentration. DCA of CJT irradiated at 50 kGy (100,175 A.U.) was significantly higher ($p<0.05$) than DCA of CJT irradiated at 10 kGy (37,409 A.U.) at IS concentration of 80 ng/g CJT. DCA increased with irradiation dose at both IS concentrations: it increased 300 % at IS concentration of 8 ng/g CJT and increased 160 % at IS concentration of 80 ng/g CJT. The reduction in the extent of increase in DCA with respect to IS concentration suggests a certain interaction between analytes; 2-DCB and IS. This observation is further supported by the coefficient of variation (CV) which was calculated to address variability. CV of ISA (8 ng/g CJT) was 13% at 10 kGy and 21% for 50 kGy. When IS concentration was increased to 80 ng/g CJT, the CV of ISA decreased to 3% at

10 kGy and 1% at 50 kGy. The lower variation in ISA at high IS concentration than at low IS concentration showed that the competition is more pronounced at lower IS concentration. The competition between analytes can be reflected results in high variation and deviation in linearity (Oliver-Pozo et al., 2015). A similar result was obtained for virgin olive oil samples where a deviation in the linearity of the calibration curve for volatile samples from virgin olive oil was observed due to the competition between the analyte and IS (Fortini et al., 2017).

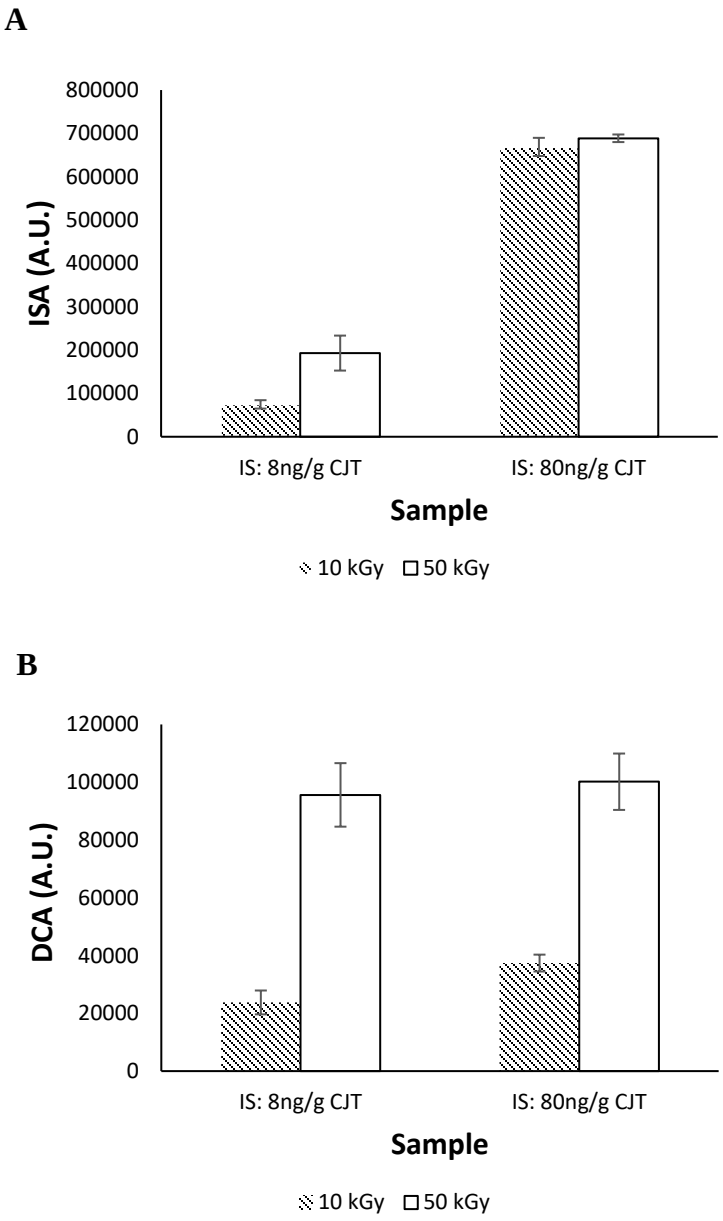


**Figure 6-1** ISA and DCA from irradiated (10 and 50 kGy) CJT samples with IS concentrations (8 and 80 ng/g CJT) for A) ISA and B) DCA. The results are means of three measurements and bars indicate standard deviation.

The effect of matrix and its components on the release of 2-DCB and interaction between IS and 2-DCB are tested in the next step. The matrix effect is defined as the effect of other compounds in the sample (except the target compound) on the assay (e.g., extraction efficiency) (Taylor, 2005). For this analysis, non-irradiated samples were spiked with 2-DCB externally at equivalent doses of 10 and 50 kGy (63 and 175 ng/g CJT, respectively) and IS at concentrations of 8 and 80 ng/g CJT. There was no significant difference ($p > 0.05$) between ISA of CJT samples spiked at 10 and 50 kGy at IS concentration of 8 ng/g CJT (Figure 6-2A). Similarly, no difference was observed at IS concentration of 80 ng/g CJT. In addition, spiked CJT samples had increasing DCA with increasing 2-DCB spiking levels, as expected (Figure 6-2B). However, DCA did not significantly increase ($p>0.05$) with increasing IS concentrations, which was not unlike irradiated samples. The release of analytes takes place in three partition steps during SPME: extraction from fat to aqueous solution, volatilization to headspace, and adsorption to the fiber in an irradiated sample system (Soncin et al., 2012; Taghvaei et al., 2020). In irradiated samples, 2-DCB is embedded in the lipid tissue of the food matrix and is extracted from the fat matrix to an aqueous environment. Subsequently, it is released to headspace prior to adsorption by the SPME fiber (Soncin et al., 2012). Meanwhile, 2-DCB is not bound to lipid tissue in spiked non-irradiated samples and it has a physical interaction with the matrix. Therefore, in spiked non-irradiated samples, 2-DCB goes through two-step partitioning steps: equilibrium in headspace and adsorption to the fiber. These results suggested a possible matrix effect, where the release of 2-DCB was affected by its location in the sample medium. Furthermore, the matrix components such as salts, proteins, and polysaccharides might affect the solid-liquid equilibrium and suppress or enhance the 2-DCB extraction (Zianni et al., 2021). Hence, proteins in the CJT matrix could affect the release of 2-DCB from the matrix in irradiated samples.

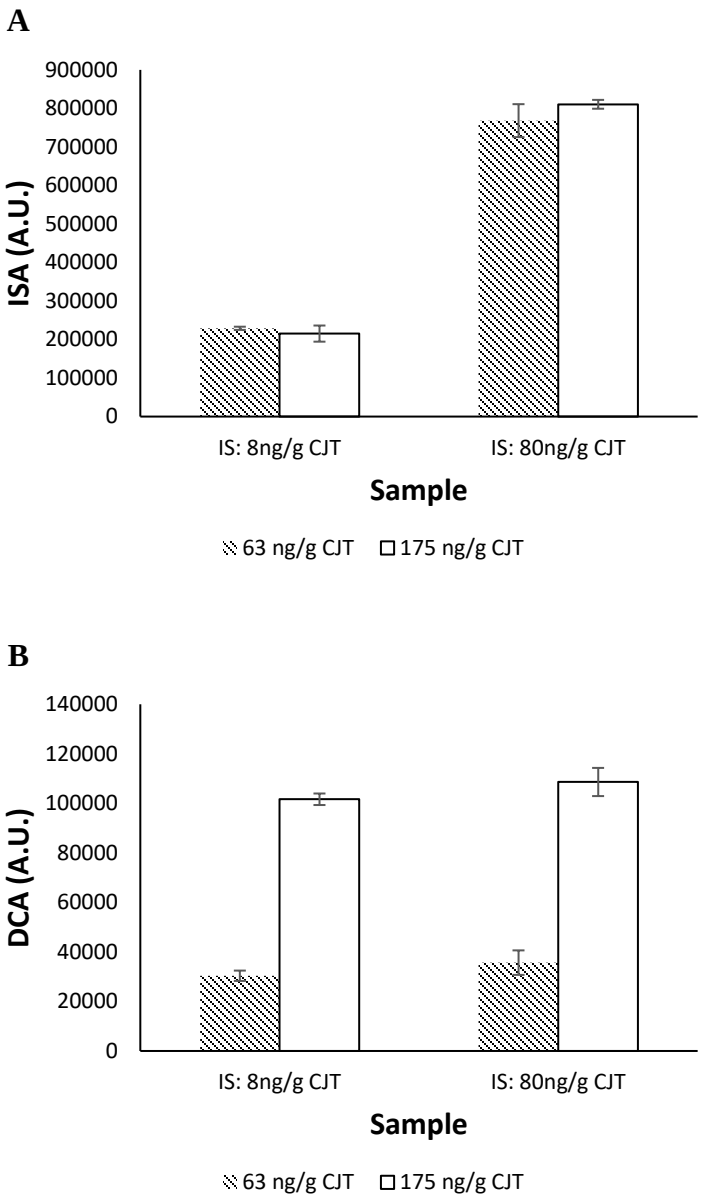


**Figure 6-2** ISA and DCA from non-irradiated CJT samples with IS concentrations (8 and 80 ng/g CJT) and 2-DCB concentrations (63 and 175 ng/g CJT) for A) ISA and B) DCA. The results are means of three measurements and bars indicate standard deviation.

## ISA and DCA in PE

The interaction between IS and 2-DCB was studied in the complex matrix of PE to test the competition phenomenon in other matrices. ISA significantly increased ($p < 0.05$) with increasing irradiation dose from 10 to 50 kGy at IS concentration of 8 ng/g PE (Figure 6-3A).

This observation is similar to the findings of irradiated CJT samples. Hence, it supports the hypothesis that there is an interaction between IS and 2-DCB at low IS concentration regardless of the food matrix. DCA of PE irradiated at 50 kGy was significantly higher ($p<0.05$) than that of 10 kGy at IS concentration of 8 ng/g PE (Figure 6-3B). The increase in DCA with increasing irradiation dose was parallel to the results of irradiated CJT.

Similar to the CJT study, PE samples were analyzed at IS concentration of 80 ng/g PE. A significant increase ($p < 0.05$) in ISA with irradiation dose was observed at IS concentration of 80 ng/g PE. This result was different than the results of irradiated CJT, where there was no significant difference in ISA at a high concentration of IS (80 ng/g CJT). Therefore, the interaction of IS and 2-DCB is significant at a high concentration of IS (80 ng/g PE) as well as low concentration (8 ng/g PE) in PE samples. This might be due to the difference in compositions of food matrices of CJT and PE. For instance, pig ears contain collagen due to the cartilage tissue, whereas chicken breasts used to prepare CJT in this study are composed of muscles. Another difference between CJT and PE matrices is the fat content, PE has a fat content of 16.1 %, while CJT has a fat content of 2.6 %. Moreover, they differ in palmitic acid content. According to the fatty acid analysis (Table 6-1), palmitic acid contributes to 22.8 % of total fatty acid in PE, while it contributes to 31 % of total fatty acid in CJT. Therefore, PE is richer in palmitic acid than CJT by total tissue weight. Since 2-DCB is derived from palmitic acid through cyclisation and the formation of a cyclobutanone ring, higher palmitic acid content leads to a higher 2-DCB concentration from irradiation. Thus, PE has more 2-DCB compounds than CJT at the same irradiation dose, which could affect the interaction between IS and 2-DCB. As expected, a significant increase ($p<0.05$) in DCA with increasing irradiation dose was found for the PE samples with IS of 80 ng/g PE.

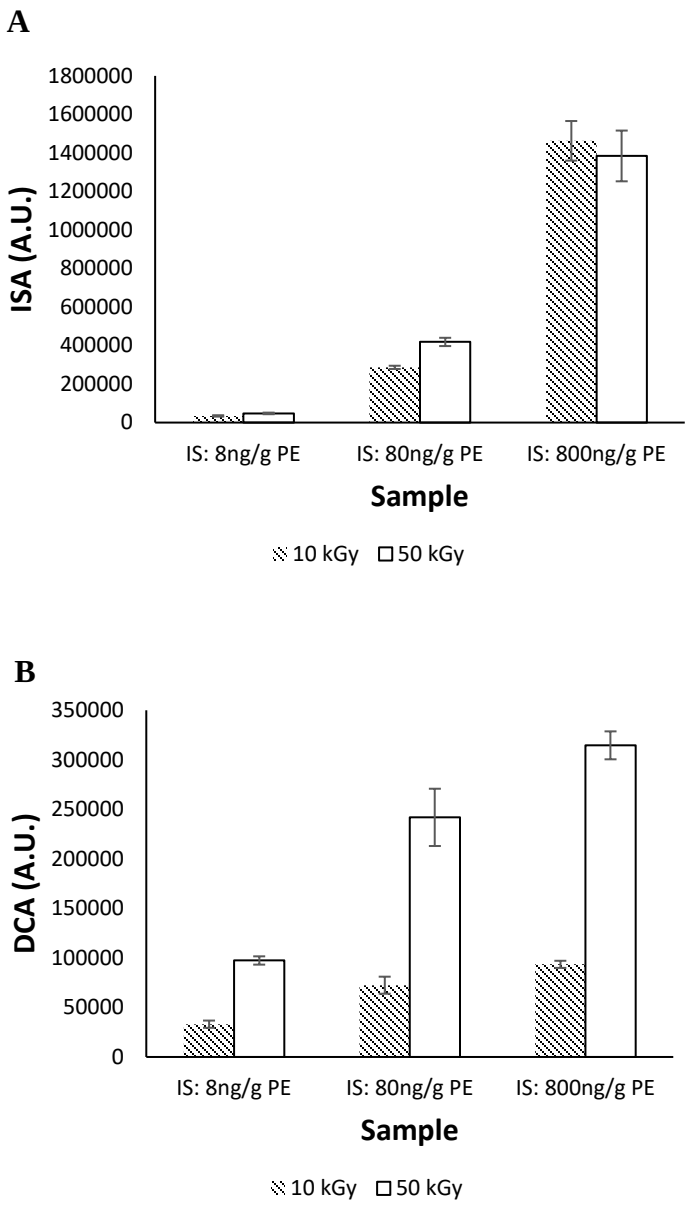


**Figure 6-3** ISA and DCA from irradiated (10 and 50 kGy) PE samples with IS concentrations (8, 80, and 800 ng/g PE) for A) ISA and B) DCA. The results are means of three measurements and bars indicate standard deviation.

**Table 6-1** The fatty acid compositions of chicken jerky treats and pig ears.

| Fatty acids (% of total fatty acids) | Chicken Jerky Treats | Pig Ears |
|---|---|---|
| **C14:0 Myristic acid** | 1.20 ± 0.08 | 1.68 ± 0.04 |
| **C16:0 Palmitic acid** | 30.81 ± 0.79 | 22.82 ± 0.30 |
| **C16:1 Palmitoleic acid** | 9.96 ± 0.46 | 5.70 ± 0.06 |
| **C18:0 Stearic acid** | 9.22 ± 1.48 | 6.78 ± 0.10 |
| **C18:1 Oleic acid** | 33.11 ± 1.51 | 44.62 ± 0.24 |
| **C18:2 Linoleic acid** | 15.04 ± 0.44 | 8.42 ± 0.11 |
| **C18:3 Linolenic acid** | 0.67 ± 0.01 | 0.37 ± 0.02 |

Data are presented as mean ± standard deviation (n=3).

In the next step, IS concentration was adjusted to a higher IS concentration for PE samples, 800 ng/g PE. There was no significant difference ($p > 0.05$) between IS AUC (1,380,000 A.U.) of PE samples irradiated at 10 and 50 kGy (Figure 6-3A). This result indicates that food matrix components (e.g., fat content) affect the interaction between IS and 2-DCB and the partition equilibrium (Rocha et al., 2001). Therefore, a higher concentration of IS was needed to study PE samples (800 ng/g PE) compared to CJT samples (80 ng/g CJT) in this study. A significant increase ($p<0.05$) in DCA was found with increasing irradiation dose. However, the extent of increase in DCA with increasing irradiation dose decreased with increasing IS concentration. This finding is similar to the results of irradiated CJT samples. A similar observation from both matrices (i.e., CJT and PE) supports the hypothesis that the interaction of IS with 2-DCB at low concentrations might be related to the extraction of 2-DCB from the matrix. Yet, it appears that the concentration might become significant depending on the matrix composition.

The CV of ISA (8 ng/g PE) was 10.4 % at 10 kGy and 8.7 % for 50 kGy. When IS concentration was increased to 80 ng/g PE, the CV of ISA decreased to 2.9 % at 10 kGy and 5.1% at 50 kGy. Further increase of IS concentration to 800 ng/g PE decreased CV to below 10% for both doses. The lower variation in ISA at IS concentration of 800 ng/g PE than others endorses the significance of the competition phenomena between analytes at low IS concentrations.

The possible suppressing effect of matrix on the release of 2-DCB from the lipid fractions of tissue was studied using spiked non-irradiated PE samples. For this analysis, non-irradiated samples were spiked with 2-DCB externally at equivalent doses of 10 and 50 kGy (158 and 363 ng/g PE, respectively) and IS at concentrations of 8, 80, and 800 ng/g PE. There was no significant difference ($p > 0.05$) between ISA of PE samples spiked at 10 and 50 kGy at IS concentration of 8 ng/g PE (Figure 6-4A). Similarly, no difference was observed at IS concentrations of 80 and 800 ng/g PE. The outcomes of irradiated and spiked samples of PE and CJT were parallel. It suggests that IS and 2-DCB behaved similarly in two different lipid-containing food matrices. DCA of spiked PE samples increased with increasing 2-DCB concentration (Figure 6-4B). IS concentration did not have a significant effect ($p>0.05$) on DCA. This is probably related to the matrix-free release of 2-DCB from the solution to the headspace.

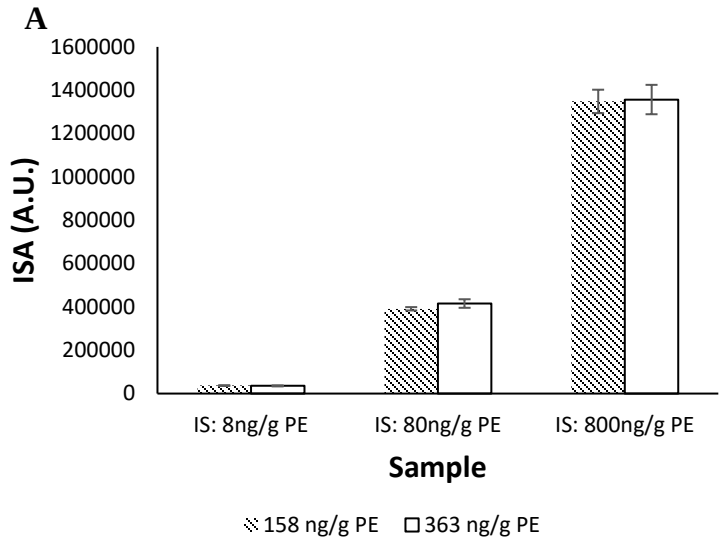


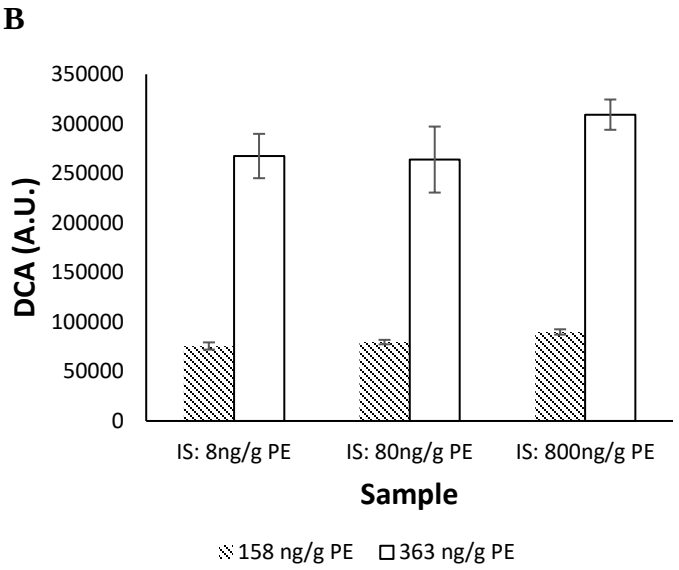


**Figure 6-4** ISA and DCA from non-irradiated PE samples with IS concentrations (8, 80, and 800 ng/g PE) and 2-DCB concentrations (158 and 363 ng/g PE) for A) ISA and B) DCA. The results are means of three measurements and bars indicate standard deviation.

## ISA and DCA comparison between CJT and PE samples

DCA of CJT and PE samples were compared to study the effect of fat content on 2-DCB formation. DCA of PE irradiated at 10 kGy was significantly higher ($p < 0.05$) than that of CJT at IS concentration of 8 ng/g sample. A significant difference was observed between DCA of PE

and CJT irradiated at 50 kGy at IS concentration of 8 ng/g sample. Similar results were reported for IS concentration of 80 ng/g sample. This result could be due to the higher palmitic content of PE than CJT. PE has 3.7 % palmitic acid of total tissue weight, while CJT only has 0.8 % palmitic acid. Therefore, more 2-DCB was probably produced under irradiation in PE samples compared to CJT samples. Previously, Campaniello et al. (2019) observed poultry samples (turkey and chicken) had less 2-DCB amounts than beef and pork samples at irradiation doses of 0.5, 1, and 3 kGy. The authors mentioned that it was due to less amount of lipid fractions in poultry samples than beef and pork samples. Similarly, high-fat samples such as minced beef had higher 2-DCB concentrations than low-fat samples such as beef thigh for irradiation doses 0.7-7 kGy (Obana et al., 2005).

## Conclusion

The quantitative use of SPME can be challenging due to variables such as IS concentration, matrix properties, and analyte concentrations. The competition phenomena between analytes can compromise the sensitivity of the method. In addition, the matrix effect could interfere with the dose-response graph, which can decrease the precision and accuracy of 2-DCB quantification. In our study, IS concentration of 80 ng/g CJT and 800 ng/g PE prevented the analyte competition issues and addressed the matrix effect in the samples. Therefore, selecting the appropriate IS concentration can aid to solve some of these problems. The results of this study can aid in future research that uses SPME to understand the interactions of volatile compounds. In addition, it can also be used to improve the quantification of irradiation doses, which could be utilized by regulation agencies to detect and regulate the irradiation doses used in the industry for lipid-containing samples.

## Acknowledgment

This project was funded by FDA Vet-LIRN Cooperative Agreement U-18FD005842 and partially supported by the USDA National Institute of Food and Agriculture, Hatch project 1014344.

# References


Ackman, R. G. (1998). Remarks on official methods employing boron trifluoride in the preparation of methyl esters of the fatty acids of fish oils. *Journal of the American Oil Chemists' Society*, *75*(4), 541–545. https://doi.org/10.1007/s11746-998-0263-9

Blanch, G. P., Caja, M. del M., Flores, G., & Castillo, M. L. R. del. (2009). Identification of 2-dodecylcyclobutanone and linear-alkanes as irradiation markers in sliced dry-cured ham. *Food Chemistry*, *113*(2), 616–620. https://doi.org/10.1016/j.foodchem.2008.07.046

Bligh, E. G., & Dyer, W. J. (1959). A Rapid method of total lipid extraction and purification. *Canadian Journal of Biochemistry and Physiology*, *37*(8).

Caja, M. M., Ruiz del Castillo, M. L., & Blanch, G. P. (2008). Solid phase microextraction as a methodology in the detection of irradiation markers in ground beef. *Food Chemistry*, *110*(2), 531–537. https://doi.org/10.1016/j.foodchem.2008.02.024

Campaniello, M., Marchesani, G., Zianni, R., Tarallo, M., Mangiacotti, M., & Chiaravalle, A. E. (2019). Validation of an alternative method for the identification of 2-dodecylcyclebutanone (2-DCB) of irradiated meats by solid-phase microextraction (SPME) gas chromatography–mass spectrometry (GC-MS). *International Journal of Food Science and Technology*, 1–9. https://doi.org/10.1111/ijfs.14353

Crews, C., Driffield, M., & Thomas, C. (2012). Analysis of 2-alkylcyclobutanones for detection of food irradiation: Current status, needs and prospects. *Journal of Food Composition and Analysis*, *26*(1–2), 1–11. https://doi.org/10.1016/j.jfca.2011.11.006

Driffield, M., Speck, D., Lloyd, A. S., Parmar, M., Crews, C., Castle, L., & Thomas, C. (2014). Methods of analysis for 2-dodecylcyclobutanone and studies to support its role as a unique marker of food irradiation. *Food Chemistry*, *146*, 308–313. https://doi.org/10.1016/j.foodchem.2013.09.046

European Committee for Standardization (CEN). (2003). *(EN1785) Detection of irradiated food containing fat: gas chromatographic/mass spectrometric analysis of 2-alkylcyclobutanones.* https://ec.europa.eu/food/system/files/2016-10/biosafety-irradiation-legislation-1785-2003_en.pdf

FDA (The Food and Drug Administration). (2014). *FDA Progress Report on Ongoing Investigation into Jerky Pet Treats*. http://www.fda.gov/AnimalVeterinary/SafetyHealth/ProductSafetyInformation/ucm371465.

htm

Fortini, M., Migliorini, M., Cherubini, C., Cecchi, L., & Calamai, L. (2017). Multiple internal standard normalization for improving HS-SPME-GC-MS quantitation in virgin olive oil volatile organic compounds (VOO-VOCs) profile. *Talanta*, *165*(September 2016), 641–652. https://doi.org/10.1016/j.talanta.2016.12.082

Gadgil, P., Smith, J. S., Hachmeister, K. A., & Kropf, D. H. (2005). Evaluation of 2-dodecylcyclobutanone as an irradiation dose indicator in fresh irradiated ground beef. *Journal of Agricultural and Food Chemistry*, *53*(6), 1890–1893. https://doi.org/10.1021/jf048641r

Gionfriddo, E., Souza-Silva, É. A., & Pawliszyn, J. (2015). Headspace versus Direct Immersion Solid Phase Microextraction in Complex Matrixes: Investigation of Analyte Behavior in Multicomponent Mixtures. *Analytical Chemistry*, *87*(16), 8448–8456. https://doi.org/10.1021/acs.analchem.5b01850

Kenessov, B., Koziel, J. A., Bakaikina, N. V., & Orazbayeva, D. (2016). Perspectives and challenges of on-site quantification of organic pollutants in soils using solid-phase microextraction. *TrAC - Trends in Analytical Chemistry*, *85*, 111–122. https://doi.org/10.1016/j.trac.2016.04.007

Moosavi, S. M., & Ghassabian, S. (2018). Linearity of Calibration Curves for Analytical Methods: A Review of Criteria for Assessment of Method Reliability. In *Calibration and Validation of Analytical Methods - A Sampling of Current Approaches* (Issue Cell Interaction-Regulation of Immune Responses, Disease Development and Management Strategies, pp. 1–15). InTech. https://doi.org/10.5772/intechopen.72932

Negron-Mendoza, A., Uribe, R. M., Ramos-Bernal, S., Camargo-Raya, C., Gomez-Vidales, V., & Kobayashi, K. (2015). Calcium carbonate as a possible dosimeter for high irradiation doses. *Applied Radiation and Isotopes*, *100*, 55–59. https://doi.org/10.1016/j.apradiso.2014.11.024

Negut, C. D., & Cutrubinis, M. (2017). ESR Standard Methods for Detection of Irradiated Food. In *Electron Spin Resonance in Food Science*. Elsevier Inc. https://doi.org/10.1016/B978-0-12-805428-4.00001-5

Obana, H., Furuta, M., & Tanaka, Y. (2005). Analysis of 2-alkylcyclobutanones with accelerated solvent extraction to detect irradiated meat and fish. *Journal of Agricultural and Food*

*Chemistry*, *53*(17), 6603–6608. https://doi.org/10.1021/jf0506636

Oliver-Pozo, C., Aparicio-Ruiz, R., Romero, I., & García-González, D. L. (2015). Analysis of Volatile Markers for Virgin Olive Oil Aroma Defects by SPME-GC/FID: Possible Sources of Incorrect Data. *Journal of Agricultural and Food Chemistry*, *63*(48), 10477–10483. https://doi.org/10.1021/acs.jafc.5b03986

Orazbayeva, D., Kenessov, B., Koziel, J. A., Nassyrova, D., & Lyabukhova, N. V. (2017). Quantification of BTEX in Soil by Headspace SPME–GC–MS Using Combined Standard Addition and Internal Standard Calibration. *Chromatographia*, *80*(8), 1249–1256. https://doi.org/10.1007/s10337-017-3340-0

Ouyang, G., & Pawliszyn, J. (2006). Recent developments in SPME for on-site analysis and monitoring. *TrAC - Trends in Analytical Chemistry*, *25*(7), 692–703. https://doi.org/10.1016/j.trac.2006.05.005

Rocha, S., Ramalheira, V., Barros, A., Delgadillo, I., & Coimbra, M. A. (2001). Headspace solid phase microextraction (SPME) analysis of flavor compounds in wines. Effect of the matrix volatile composition in the relative response factors in a wine model. *Journal of Agricultural and Food Chemistry*, *49*(11), 5142–5151. https://doi.org/10.1021/jf010566m

Soncin, S., Panseri, S., Rusconi, M., Mariani, M., Chiesa, L. M., & Biondi, P. A. (2012). Improved determination of 2-dodecylcyclobutanone in irradiated ground beef patties by gas-chromatography-mass-spectrometry (GC/MS) coupled with solid-phase microextraction (SPME) technique. *Food Chemistry*, *134*(1), 440–444. https://doi.org/10.1016/j.foodchem.2012.02.089

Stokvis, E., Rosing, H., & Beijnen, J. H. (2005). Stable isotopically labeled internal standards in quantitative bioanalysis using liquid chromatography/mass spectrometry: Necessity or not? *Rapid Communications in Mass Spectrometry*, *19*(3), 401–407. https://doi.org/10.1002/rcm.1790

Taghvaei, M., Sommers, C., Ceric, O., Hussain, F., Yucel, U., & Smith, J. S. (2020). Solid-phase micro extraction of food irradiation marker 2-dodecylcyclobutanone (2-DCB) from chicken jerky treated with glycerol. *Journal of Food Science*, *85*(8), 2608–2614. https://doi.org/10.1111/1750-3841.15322

Taylor, P. J. (2005). Matrix effects: The Achilles heel of quantitative high-performance liquid chromatography-electrospray-tandem mass spectrometry. *Clinical Biochemistry*, *38*(4),

328–334. https://doi.org/10.1016/j.clinbiochem.2004.11.007

Tonyali, B., Sommers, C., Ceric, O., Smith, J. S., & Yucel, U. (2020). An analysis of cellulose- and dextrose-based radicals in sweet potatoes as irradiation markers. *Journal of Food Science*. https://doi.org/10.1111/1750-3841.15359

Zenkevich, I. G., Makarov, E. D., & Makarova, I. Y. (2007). Quantitative chromatographic analysis under changes in the composition of samples in the course of sample preparation: A modification of the double internal standard method. *Journal of Analytical Chemistry*, *62*(8), 748–755. https://doi.org/10.1134/S1061934807080102

Zhao, Y., Wang, F., Li, W., Li, A., & Ha, Y. (2012). 2-Dodecylcyclobutanone as an irradiation dose indicator to identify and estimate original dose in irradiated ground beef. *European Food Research and Technology*, *235*(5), 901–906. https://doi.org/10.1007/s00217-012-1818-4

Zianni, R., Mentana, A., Campaniello, M., Chiappinelli, A., Tomaiuolo, M., Chiaravalle, A. E., & Marchesani, G. (2021). An investigation using a validated method based on HS-SPME-GC-MS detection for the determination of 2-dodecylcyclobutanone and 2-tetradecylcyclobutanone in X-ray irradiated dairy products. *Lwt*, *153*(May 2021), 112466. https://doi.org/10.1016/j.lwt.2021.112466

# Chapter 7 - Conclusion

There is a broad need to study the applicability of EPR spectroscopy for the chemical and physical characterization of food and food-related systems. There has been an interest in using EPR spectroscopy for many research areas including but not limited to irradiation-derived radicals and biological membranes. It can offer fast, sensitive, and non-destructive measurements compared to the traditional methods.

The study of changes in biological membranes under different external stresses can be benefited by the use of EPR spectroscopy. Bacterial membranes can respond to increasing thermal stress by increasing membrane mobility. In our study, *E.coli* increased the membrane mobility with increasing thermal stress up to a maximum threshold, after which the membrane integrity was lost. I showed that EPR spectroscopy in combination with DLS and TEM techniques can be used to study the changes in membrane mobility. This information and the EPR method used in the present work can be used thoroughly to understand thermal inactivation kinetics on microorganisms. In addition, this technique can further be developed to investigate the other inactivation mechanisms (e.g., surfactants).

Irradiation-derived radicals have been used as irradiation dose indicators for fruits and vegetables. This presents an opportunity for EPR spectroscopy for the characterization of the irradiation history of fruits and vegetables. The irradiation-derived radicals from SP can be analyzed using EPR spectroscopy as a function of irradiation dose. Sample preparation such as sieving can change the composition of the sample by holding the big molecules, i.e., cellulose. The retention of cellulose particles on the sieve caused the loss of the signal from irradiation-derived cellulose signals in EPR spectra. The EPR spectra changed with the composition of the sample at different parts of SP. Both irradiation-derived radicals, cellulose and dextrose, were identified in the EPR spectra of SP flesh. The irradiation-derived cellulose signals were more pronounced in the spectra of SP skin due to the cellulose-rich content of the skin. The results of this study proposed that EPR spectroscopy can serve as a suitable technique to analyze the irradiation-derived radicals in both low- and high-moisture plant-based foods rich in sugar and cellulose, such as dried sweet potatoes.

The suitability of EPR spectroscopy to study the irradiation history of lipid-containing products (irradiation-derived radicals) was studied and compared to SPME-coupled GC-MS

analysis (lipid-radiolysis product, 2-DCB). The results from this study showed that EPR analysis can indicate the irradiation process in lipid-containing products, however, it was limited for dose identification. Meanwhile, the irradiated lipid-containing samples were detected and differentiated for irradiation dose using GC-MS. The precision of this method was further enhanced by choosing the appropriate IS concentration to eliminate the matrix effect and analyte interaction.

The analysis of irradiation-derived cellulose satellite peaks and glucose split peak can be challenging because the broadening of the native peak with irradiation partially hinders them. The quantification of these radicals can be improved with a peak enhancement approach, which enhances the resolution of EPR spectra. The high-resolution spectra advance the precision of free radical concentration determination. The higher precision yields easier differentiation for samples of different irradiation doses. This approach can benefit the regulatory agencies and the industry to monitor the irradiation dose by using the irradiation-derived cellulose satellite peaks and glucose split peak as irradiation indicators for plant-based samples.

The EPR spectroscopy methods are not commonly used for food and food-related matrices. Since it is not a well-known technique, there are certain research gaps regarding the suitability of the EPR spectroscopy method that can be improved by performing more research. The methods used in the present work can serve as a base for regulatory agencies to establish guidelines and for future researchers to help fill the gap in the literature for use of EPR. In future studies, the EPR spectroscopy method can be extended for other matrices such as mixed vegetable-meat matrices and lipid-rich dairy products for irradiation studies. The EPR technique for membrane mobility can be further used to better understand the response of microorganisms to different external stresses. Also, the potential of EPR spectroscopy to investigate the radicals generated from the Maillard reaction and complex starch-protein-lipid structures can be pursued. Therefore, the use of EPR can greatly aid in answering research questions that more traditional methods have not been able to answer yet.

# Appendix A - Sample preparation techniques

Sweet potatoes (SP) were subjected to different sample preparation techniques (i.e., grinding, sieving, and pelletizing) prior to EPR analysis (Chapter 4). In addition to those techniques, other approaches such as oven-drying, freeze-drying, and solvent extraction were also conducted.

The removal of residual water prior to slow-tumbling EPR spectra analysis were studied using oven-drying or freeze-drying. The irradiated SP was dried in an oven at 150°F for 24 h. After 24 h, SP were ground, weighed (80 mg), and transferred into a quartz EPR tube (OD:5 mm & ID:4 mm, Wilmad-LabGlass). Meanwhile, another set of irradiated SP was dried using a freeze-dryer (0.220 mbar for 72 hours). Freeze-dried SP were ground, weighed (80 mg), and transferred into a quartz EPR tube (OD:5 mm & ID:4 mm, Wilmad-LabGlass). Both samples were analyzed using a SpinscanX EPR spectrometer (ADANI, Minsk, Belarus) operating at X-band with a modulation frequency of 100 kHz at room temperature. Samples were scanned at the following measurement conditions: center field 334.5 mT, sweep width 11 mT, modulation frequency 100 kHz, modulation amplitude 600 uT, and microwave power 1 mW.

Solvent extraction approach was performed for fast-tumbling analysis as an alternative to slow-tumbling analysis. Ground SP (1.5 g) was mixed with 10 mL of ethanol solution of POBN (500 µM) and mixed using a tumbler for 10 minutes. Subsequently, the supernatant was transferred to a capillary EPR tube (VWR International, ID:0.5-0.6 mm) for EPR measurements. The EPR measurements were performed at room temperature in an EPR spectrometer operating at X-band (SpinscanX, ADANI, Belarus). The samples were analyzed under the following measurement conditions: center field 334 mT, sweep width 20 mT, modulation frequency 100 kHz, modulation amplitude 400 uT, microwave power 3 mW.

The EPR signals of SP before and after freeze-drying were given in Figure A-1. The signal-to-noise ratio of the EPR spectra increased after freeze-drying. The residual moisture in the SP decreased the signal quality in two ways: by decreasing the crystalline environment to stabilize free radicals during irradiation; and by absorbing significant electromagnetic energy at the X-band frequencies used for organic radicals due to its high dielectric constant (Weil & Bolton, 2007). Moreover, the irradiation-derived signal (shoulder around 333.1 mT) was resolved after freeze drying.

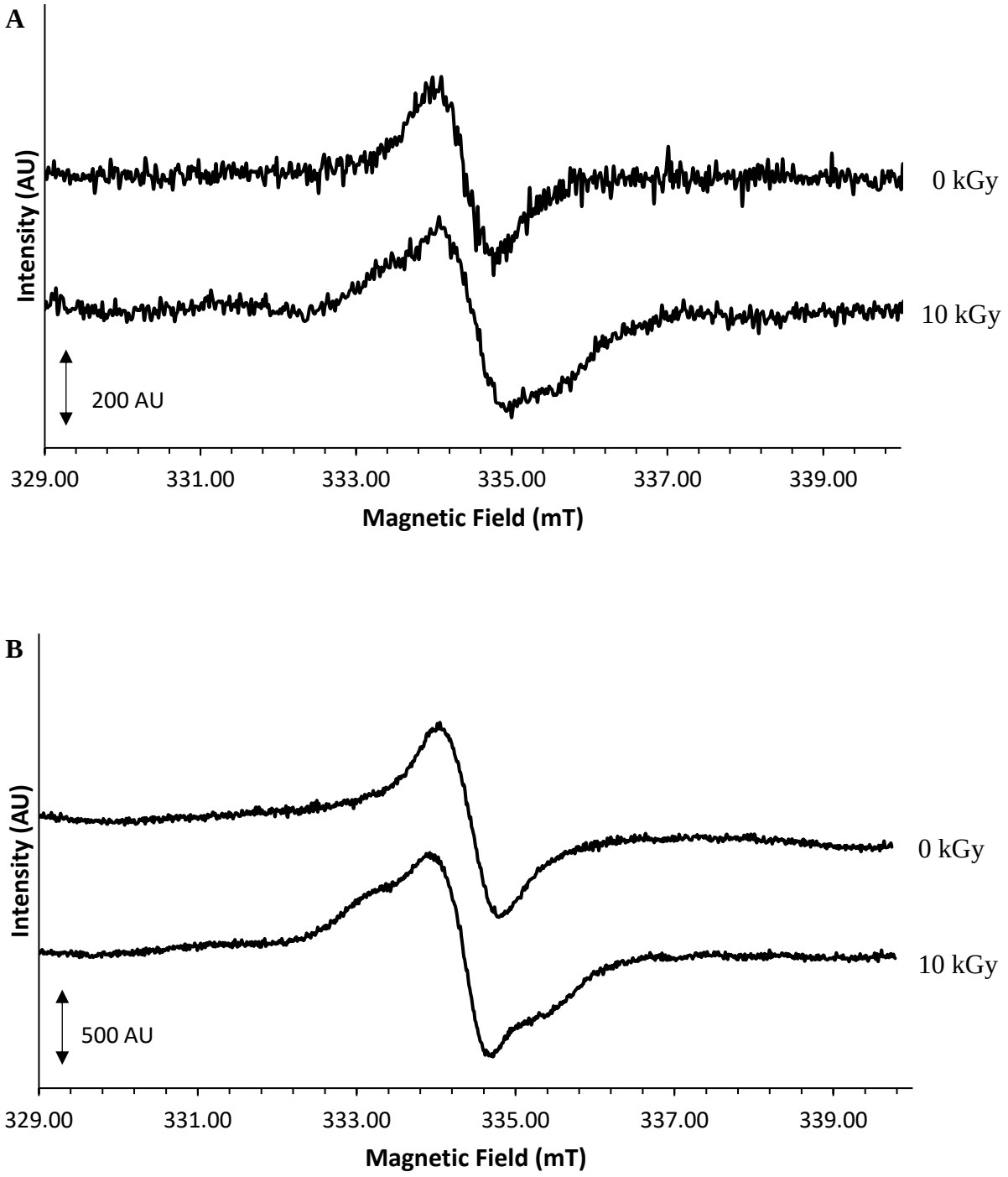


**Figure A-1** EPR signal of 0 and 10 kGy irradiated SP sample with 24 h drying A) before and B) after freeze drying.

EPR signals of SP with oven drying were given in Figure A-2. The signal intensity of SP increased with increasing irradiation dose. However, the signal intensities of oven-dried SP were lower than the signal intensities of freeze-dried SP, probably due to heat treatment. Therefore, freeze-drying was chosen to prepare the samples for subsequent analysis.

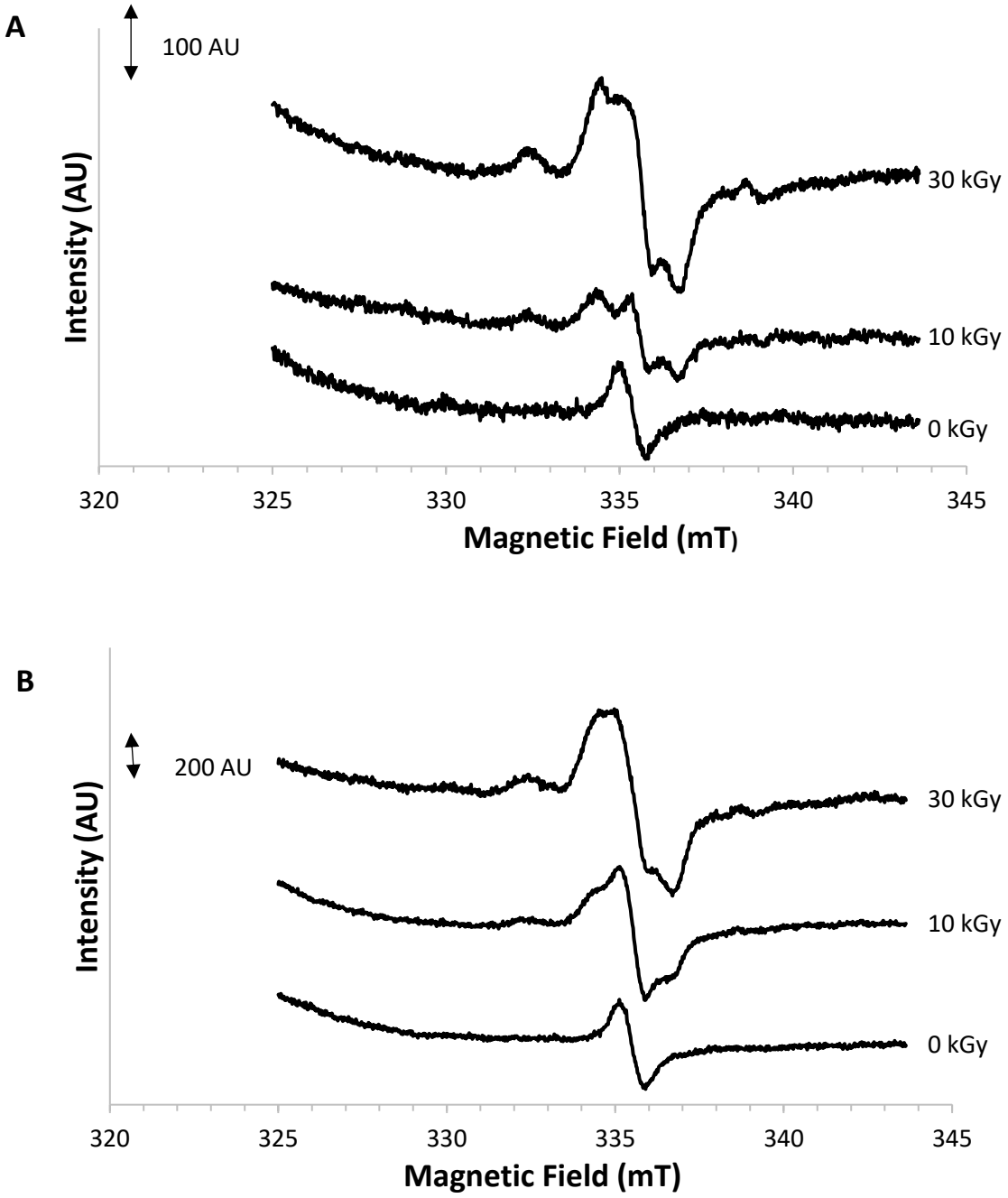


**Figure A-2**: EPR signal of SP samples irradiated at 0, 5, and 30 kGy after further oven-dried at 150 °F for 24 hours for samples pre-dried for A) 24 h B) 48 h.

EPR signals of SP prepared with solvent extraction were given in Figure A-3. The characteristic signals of irradiation-derived cellulose radicals and dextrose radicals were not observed in the spectra of solvent-extracted SP. The irradiation-specific radicals might not be extracted from SP matrix and not captured with the POBN spin trap.

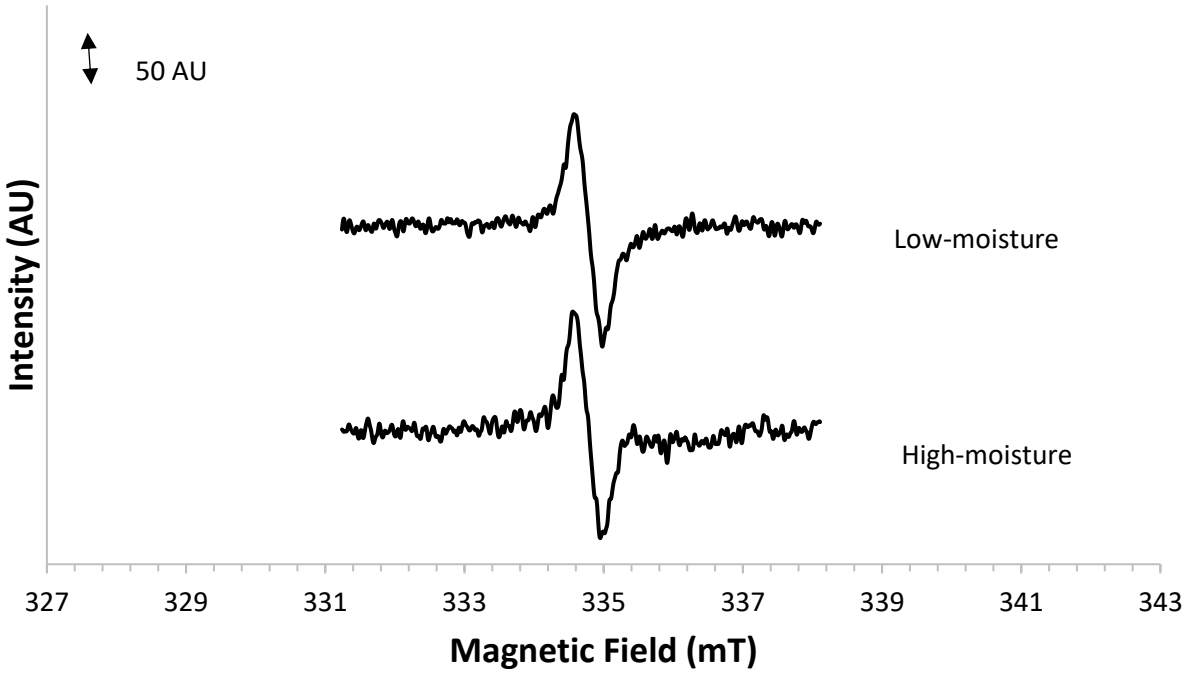


**Figure A-3:** EPR signal of solvent extracted SP samples irradiated at 5 kGy.

# Appendix B - Standard curves using non-irradiated CJT

Control (non-irradiated) CJT samples were spiked with 2-DCB and IS to obtain a calibration curve. This calibration curve could be used for quantification of 2-DCB concentration in irradiated samples or unknown samples in future studies. The ground non-irradiated CJT samples were mixed with water using a ratio of 1:5 (CJT:water). In brief, bulk mixture was homogenized using the homogenizer for 1 min and spiked with IS to final concentration of 80 ng IS /g CJT and 2-DCB to final concentration of 30, 60, 80, 100, 120, and 140 ng 2-DCB /g CJT using working solutions (1 ppm IS and 1 ppm 2-DCB working solutions). After homogenizing the spiked samples for another minute, aliquots from the mixture (3 mL) were transferred to a vial. The samples in the vials were homogenized for 1 min, capped, and centrifuged (100xg, Allegra X-14R Centrifuge, Beckman Coulter) for 10 mins. The vials were incubated at 80 °C for 30 minutes and 15 mins with the SPME fiber (PDMS/DVB).

IS had low variation (9.2%) among spiked control CJT samples (Figure B-1). 2-DCB areas increased with 595 A.U./2-DCB concentration with increasing spiking levels and had a correlation coefficient of 0.99 (Figure B-1).

2-DCB/IS increased with 2-DCB concentration with 0.0021 A.U./2-DCB concentration and a correlation coefficient greater than 0.99 (Figure B-2). Moreover, 2-DCB/IS had a variation less than 8% at all 2-DCB concentrations. This external calibration curve can be used to calculate 2-DCB concentration in commercially irradiated samples by comparing 2-DCB/IS (A.U) values.

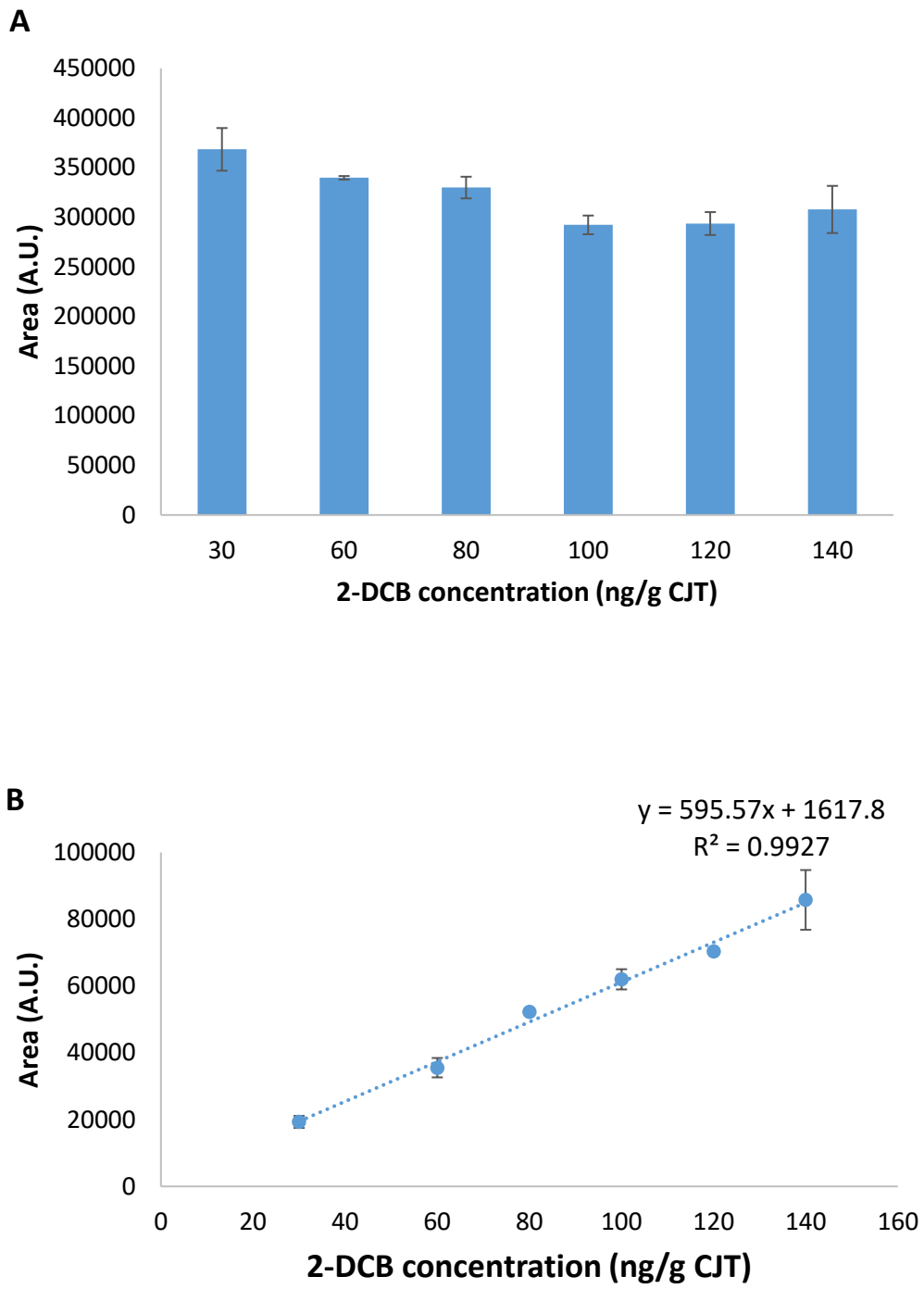


**Figure B-2:** ISA and DCA from non-irradiated CJT samples with IS concentration (80 ng/g CJT) and 2-DCB concentrations (30, 60, 80, 100, 120, and 140 ng 2-DCB /g CJT) for A) ISA and B) DCA. The values are mean values of two vials and the error bars represent standard deviation.

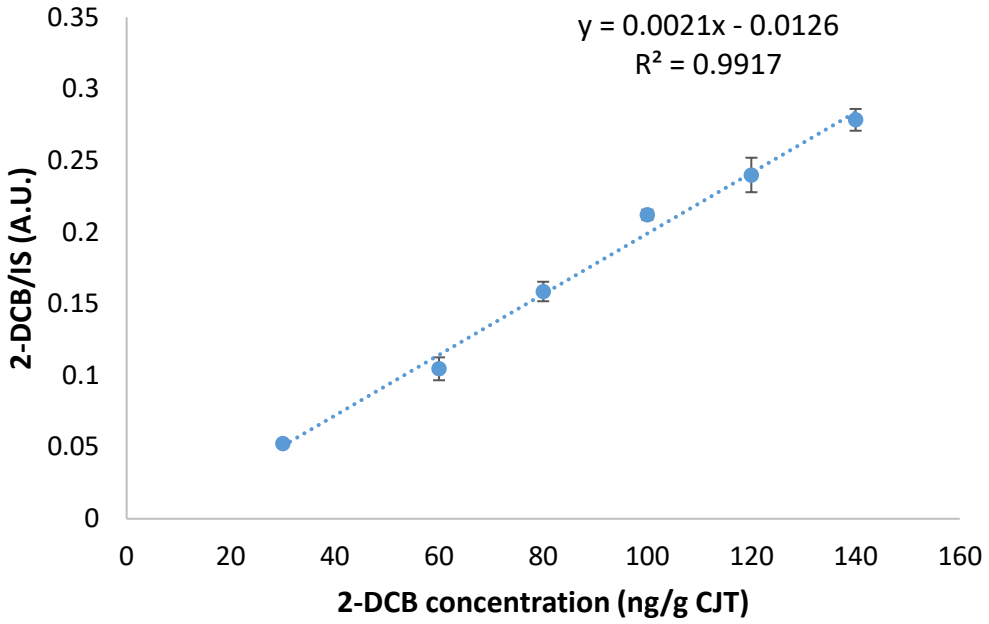


**Figure B-3:** Ratio of areas of 2-DCB and IS from spiked CJT at different 2-DCB spiking levels. The values are mean values of two vials and the error bars represent standard deviation.

# Appendix C - GC-MS chromatograms

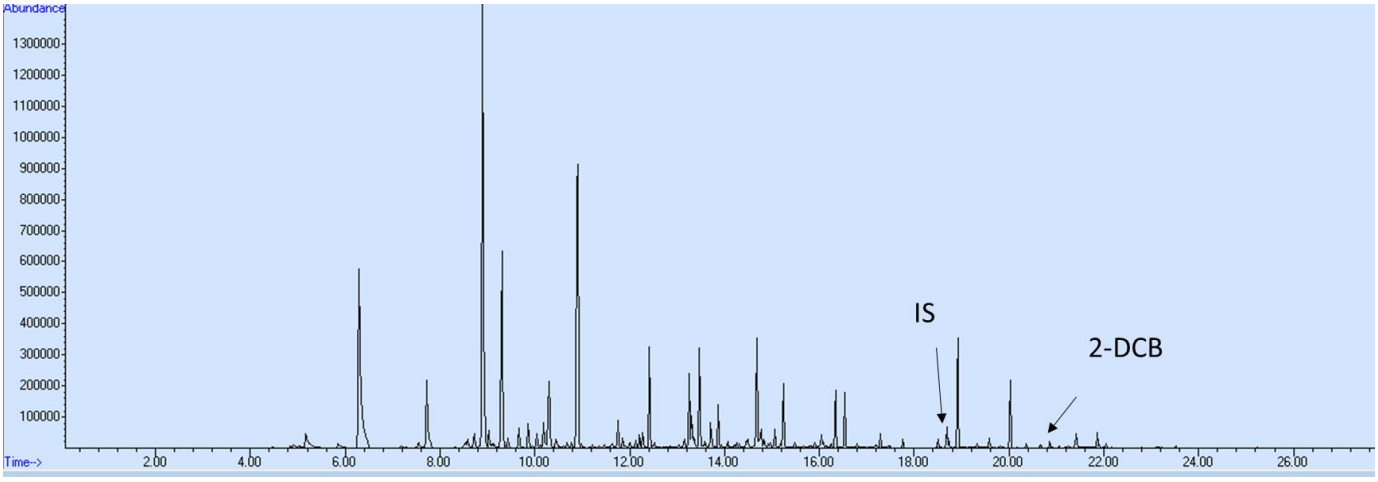


**Figure C-1:** A chromatogram of irradiated CJT.

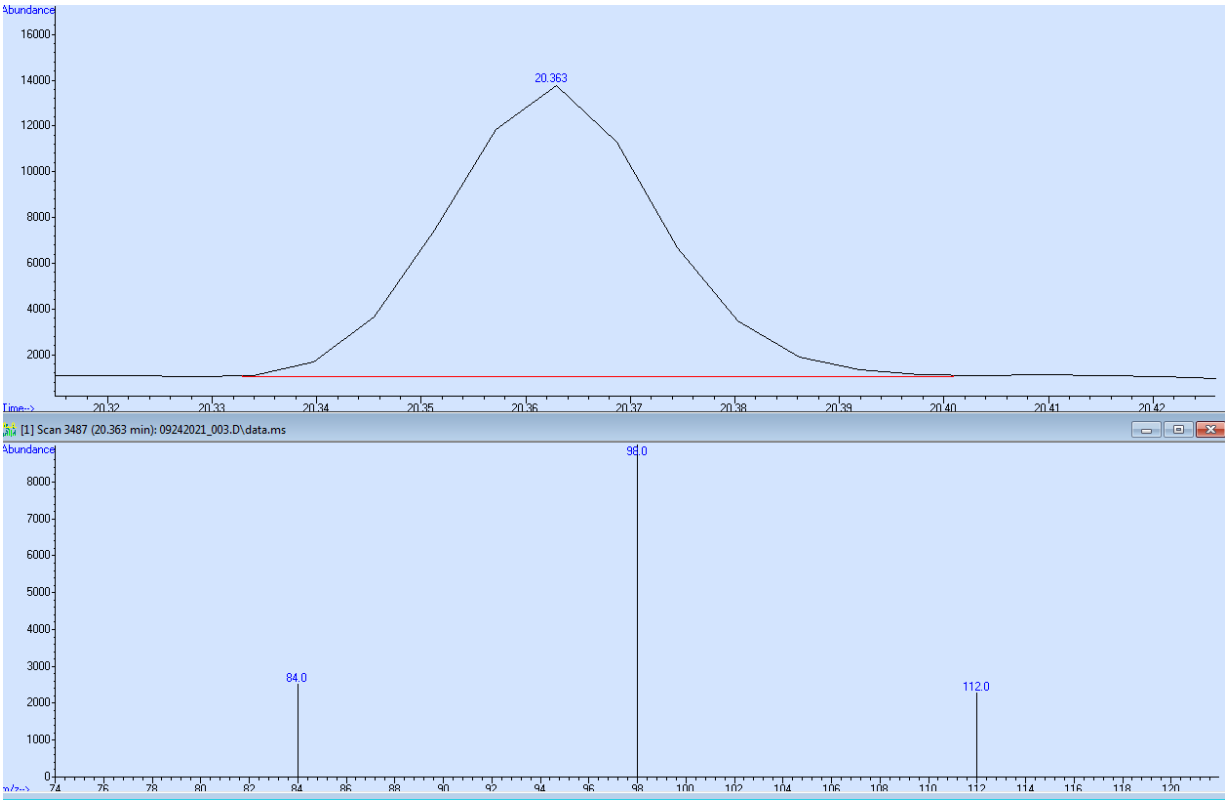


**Figure C-2:** The peak of 2-DCB with monitored ions m/z of 84, 98, and 112.

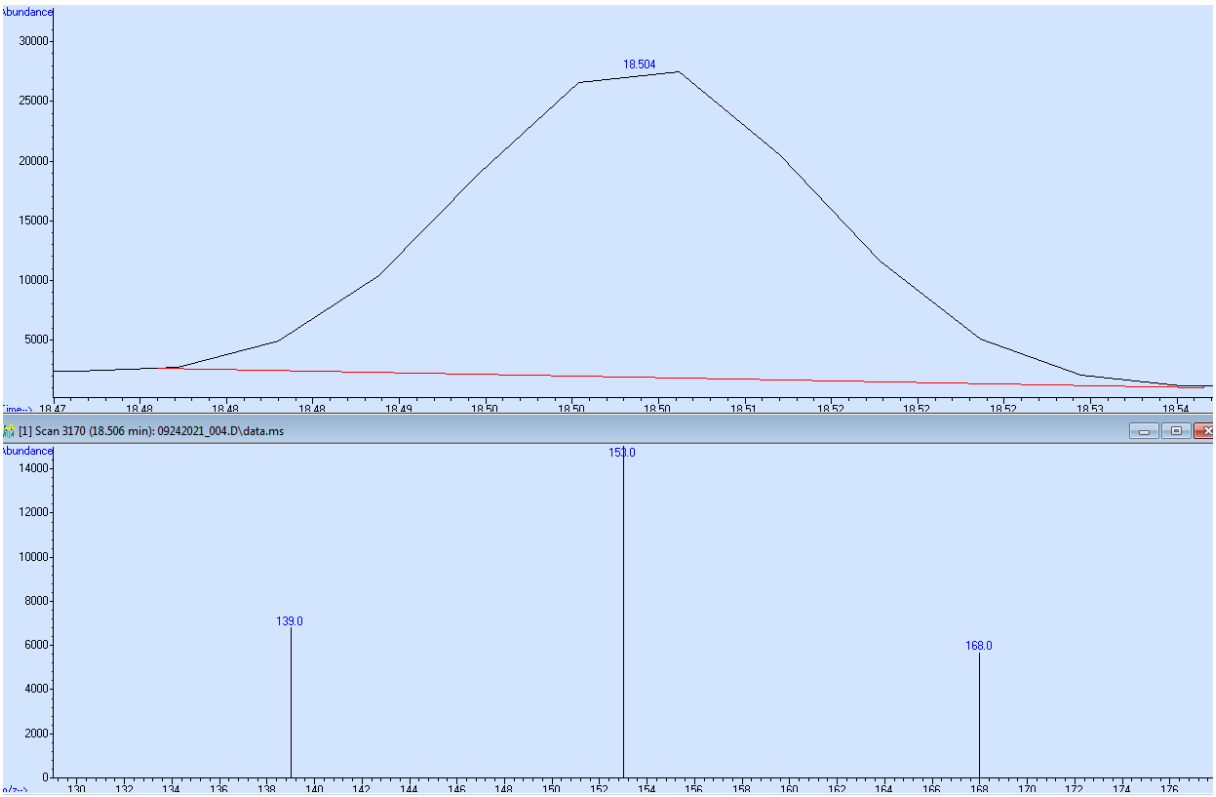


**Figure C-3:** The peak of IS with monitored ions m/z of 139, 153, and 168.

# Appendix D - Blind Method Tests

The irradiation study of CJT was funded by FDA Vet-LIRN Cooperative Agreement U-18FD005842. As a part of this project, analysis of 2-DCB in CJT samples were subjected to blind method test (BMT).

Briefly, 10 g of unknown sample was mixed with 39,200 uL of water and homogenized for 1 minute. 800 uL of IS (1 ppm working solution) was added to the mixture and the mixture was homogenized for 1 minute. Later, 8 g of the mixture was transferred to the beakers (5 beakers, 8 g each). The first beaker was mixed with 249.6 uL of 2-DCB working solution (1 ppm solution) and 1350.4 uL of water and homogenized for 1 minute. Aliquots of the homogenate (3 g) was transferred to the vials (2 vials, 3 g each). The final spiked 2-DCB concentration in these vials was 156 ng 2-DCB/g CJT. The second beaker was mixed with 166.4 uL of 2-DCB working solution (1 ppm solution) and 1433.6 uL of water and homogenized for 1 minute. Aliquots of the homogenate (3 g) was transferred to the vials (2 vials, 3 g each). The final spiked 2-DCB concentration in these vials was 104 ng 2-DCB/g CJT. The third beaker was mixed with 83.2 uL of 2-DCB working solution (1 ppm solution) and 1516.8 uL of water and homogenized for 1 minute. Aliquots of the homogenate (3 g) was transferred to the vials (2 vials, 3 g each).

The final spiked 2-DCB concentration in these vials was 52 ng 2-DCB/g CJT. The fourth beaker was mixed with 1600 uL of water and homogenized for 1 minute. Aliquots of the homogenate (3 g) was transferred to the vials (2 vials, 3 g each). These vials were not spiked with 2-DCB.

Lastly, the fifth beaker was mixed with 1600 uL of water and homogenized for 1 minute. Later, this mixture was mixed with the negative control mixture (1:1, w/w). The new mix was homogenized for 1 minute. Aliquots of the homogenate (3 g) was transferred to the vials (2 vials, 3 g each). These vials were diluted with negative control samples (1:1 dilution). A magnetic bar was added to each vial and the vials were immediately capped. The vials were incubated at 80°C with magnetic stirring for 30 minutes and another 15 minutes with fiber.

The results of the samples were evaluated using following steps:

#1: To establish the method linearity ($R^2$) for each sample

The linearity of the graph obtained using non-diluted and three spikes at 52, 104, and 156 ng 2-DCB/g CJT vs 2-DCB/IS was evaluated.

Acceptance criteria for $R^2$

Excellent: >0.990

Good: 0.0975-0.990

Satisfactory: 0.950-0.975

Below expectations: <0.950

#2: To determine 2-DCB concentration and its error in each sample

The 2-DCB concentration (referred to as unknown) in the sample was calculated obtained using non-diluted and three spikes at 52, 104, and 156 ng 2-DCB/g CJT vs 2-DCB/IS following the standard addition method. Once the unknown (concentration) and unknown error are calculated, relative standard deviation (RSD, %) will be calculated using the formula below:

RSD (%) = ((unknown error)/(unknown))*100

Acceptable Error ranges:

Very good: < 25 %

Satisfactory: 25 % <… < 30 %

Below expectations: > 30%

#3: To evaluate the matrix effect of the method by establishing linearity ($R^2$)

The linearity of the graph obtained using diluted, non-diluted, and three spikes at 52, 104, and 156 ng 2-DCB/g CJT vs 2-DCB/IS was evaluated.

During this study, five unknown samples (sample A, B, C, D, and E) were analyzed. The areas of 2-DCB/IS from first sample A were given results in Figure D-1. As expected, 2-DCB/IS increased with increasing 2-DCB spiking levels. In addition, diluted sample had lower 2-DCB/IS value than no-spiked sample.

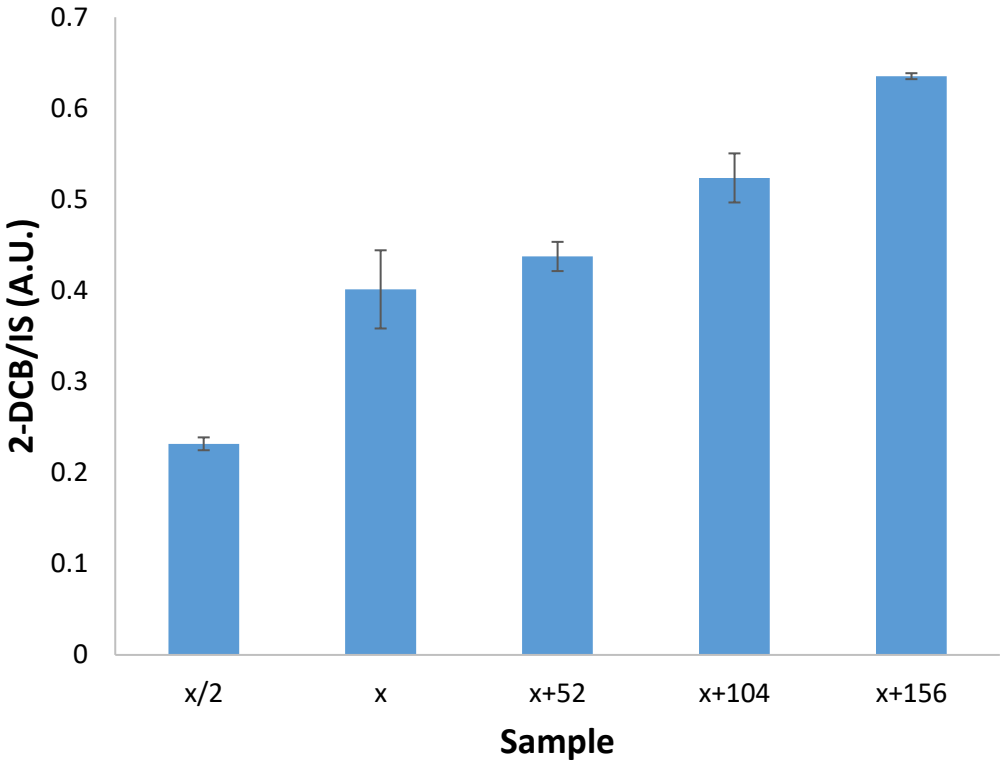


**Figure D-1:** Ratio of areas of 2-DCB and IS from sample A prepared spiking with 156 ng 2-DCB/g CJT, 104 ng 2-DCB/g CJT, 52 ng 2-DCB/g CJT, no-spiking, and diluting with the control sample. The values are mean values of two vials and the error bars represent standard deviation.

The method linearity for this sample was 0.955 (Figure D-2). According to acceptance criteria (criteria#1), this value is in the range of "satisfactory". The 2-DCB concentration in the unknown sample was calculated following the standard addition method. Briefly, the intercept of the trendline equation ($y = 0.0015x + 0.3811$) was divided to the slope of the trendline equation from Figure D-2. The 2-DCB concentration in sample A was 251 ng/g CJT. The relative standard deviation (RSD %) was 20 %, which was in the range of "very good" according to acceptable criteria (criteria#2).

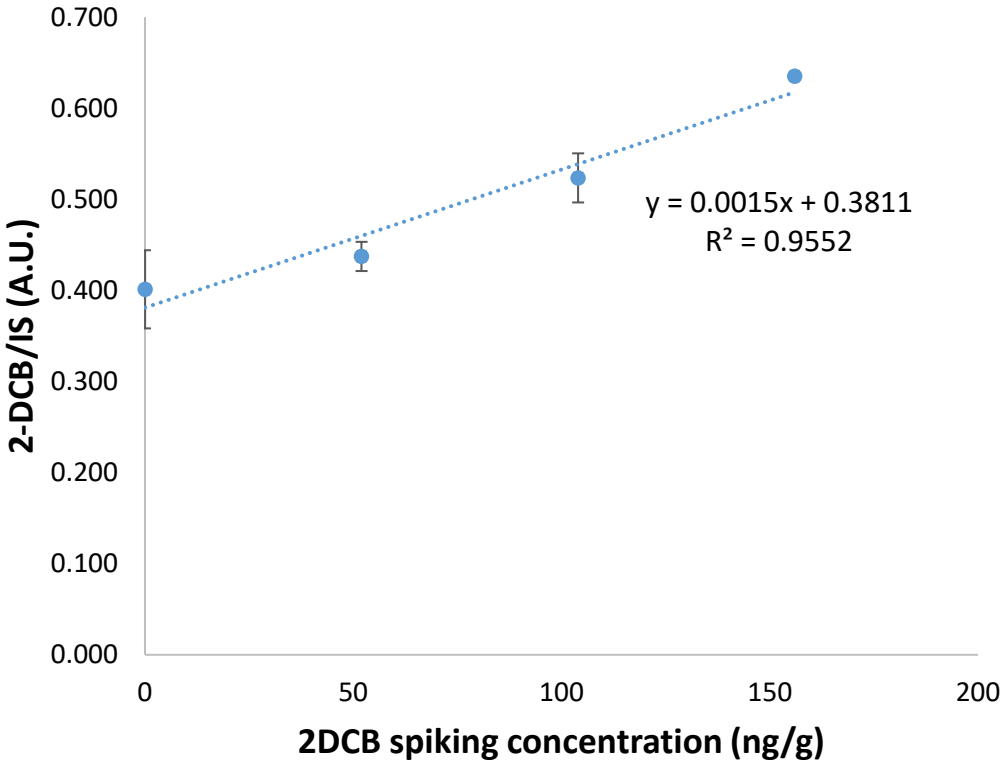


**Figure D-2:** Ratio of areas of 2-DCB and IS from sample A prepared spiking with 156 ng 2-DCB/g CJT, 104 ng 2-DCB/g CJT, 52 ng 2-DCB/g CJT, and no-spiking at different 2-DCB spiking levels. The values are mean values of two vials and the error bars represent standard deviation.

The matrix effect of the method was evaluated using the linearity of the graph obtained using diluted, non-diluted, and three spikes at different calculated 2-DCB concentrations (Figure D-3).The linearity was 0.979.

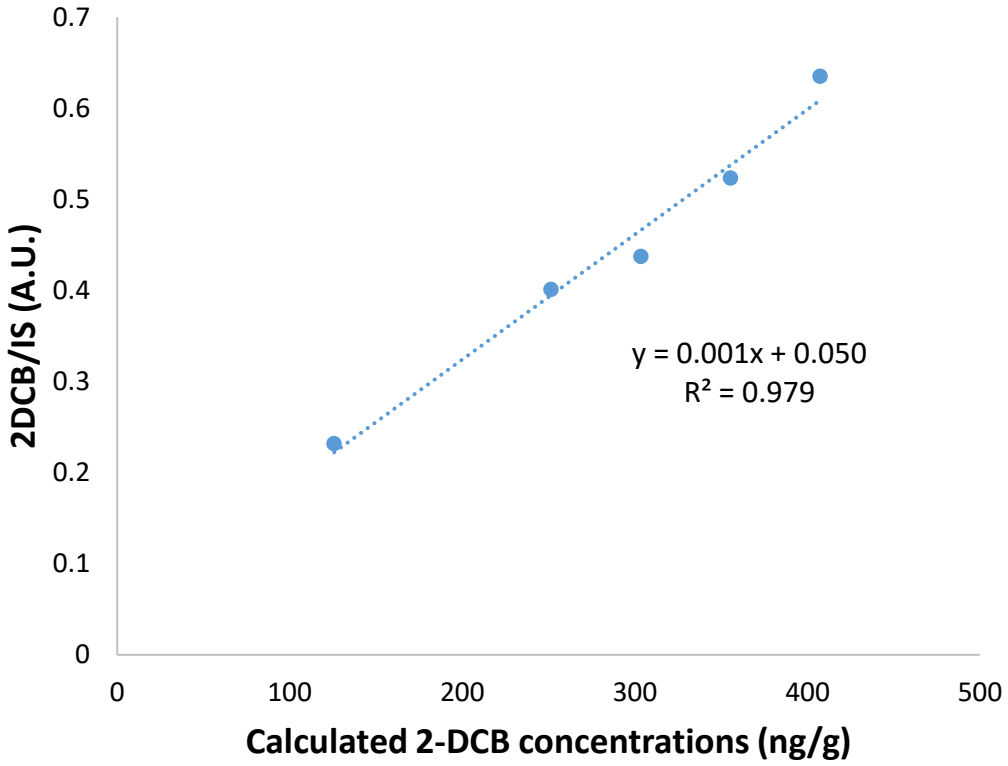


**Figure D-3:** Ratio of areas of 2-DCB and IS from sample A prepared spiking with 156 ng 2-DCB/g CJT, 104 ng 2-DCB/g CJT, 52 ng 2-DCB/g CJT, no-spiking, and diluting with the control sample at different calculated 2-DCB concentrations. The values are mean values of two vials and the error bars represent standard deviation.

The areas of 2-DCB/IS from sample B were given in Figure D-4. As expected, 2-DCB/IS increased with increasing 2-DCB spiking levels. In addition, diluted sample had lower 2-DCB/IS value than no-spiked sample.

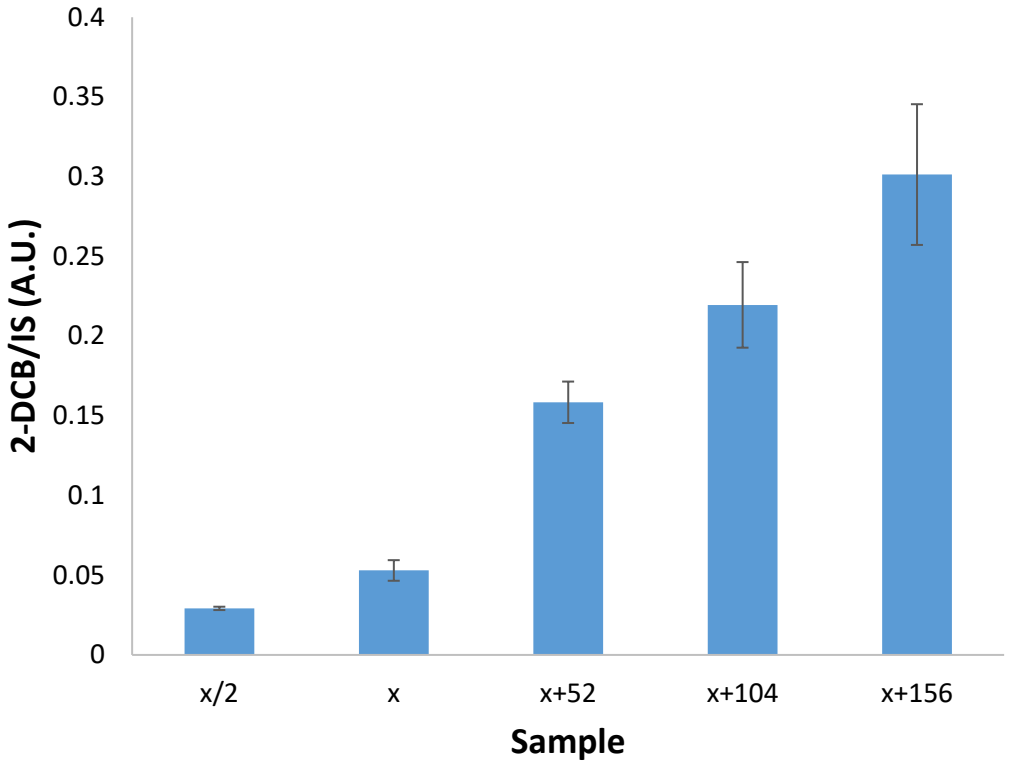


**Figure D-4:** Ratio of areas of 2-DCB and IS from sample B prepared spiking with 156 ng 2-DCB/g CJT, 104 ng 2-DCB/g CJT, 52 ng 2-DCB/g CJT, no-spiking, and diluting with the control sample. The values are mean values of two vials and the error bars represent standard deviation.

The method linearity for sample B was 0.989 (Figure D-5). According to acceptance criteria (criteria#1), this value is in the range of "good". The 2-DCB concentration in the unknown sample (sample B) was calculated following the standard addition method. Briefly, the intercept of the trendline equation (y = 0.002x + 0.062) was divided to the slope of the trendline equation from Figure D-5. The 2-DCB concentration in sample B was 40 ng/g CJT. The relative standard deviation (RSD %) was 24 %, which was in the range of "very good" according to acceptable criteria (criteria#2).

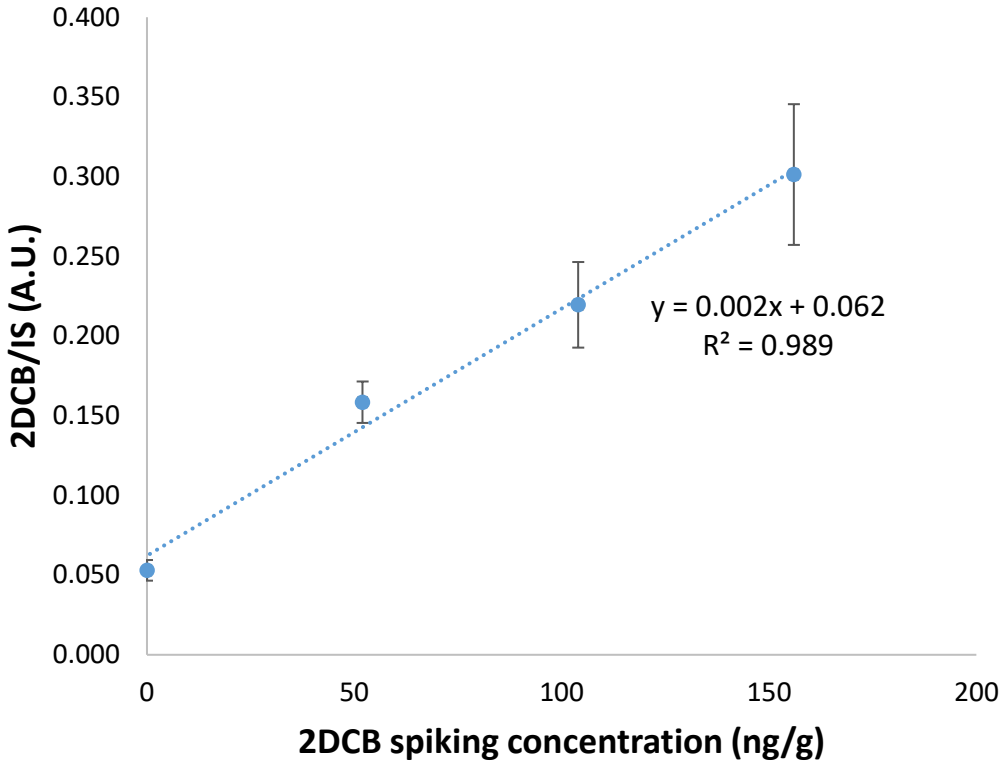


**Figure D-5:** Ratio of areas of 2-DCB and IS from sample B prepared spiking with 156 ng 2-DCB/g CJT, 104 ng 2-DCB/g CJT, 52 ng 2-DCB/g CJT, and no-spiking at different 2-DCB spiking levels. The values are mean values of two vials and the error bars represent standard deviation.

The matrix effect of the method for sample B was evaluated using the linearity of the graph obtained using diluted, non-diluted, and three spikes at different calculated 2-DCB concentrations (Figure D-6). The linearity was 0.993.

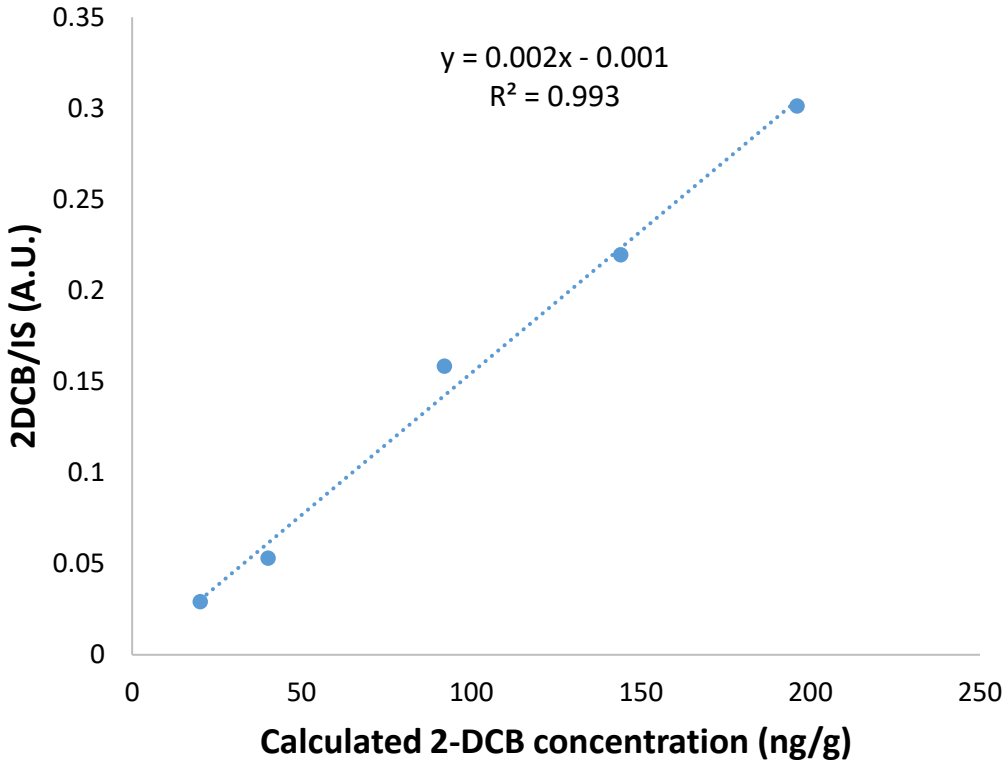


**Figure D-6:** Ratio of areas of 2-DCB and IS from sample B prepared spiking with 156 ng 2-DCB/g CJT, 104 ng 2-DCB/g CJT, 52 ng 2-DCB/g CJT, no-spiking, and diluting with the control sample at different calculated 2-DCB concentrations. The values are mean values of two vials and the error bars represent standard deviation.

The areas of 2-DCB/IS from sample C were given in Figure D-7. As expected, 2-DCB/IS increased with increasing 2-DCB spiking levels. In addition, diluted sample had lower 2-DCB/IS value than no-spiked sample.

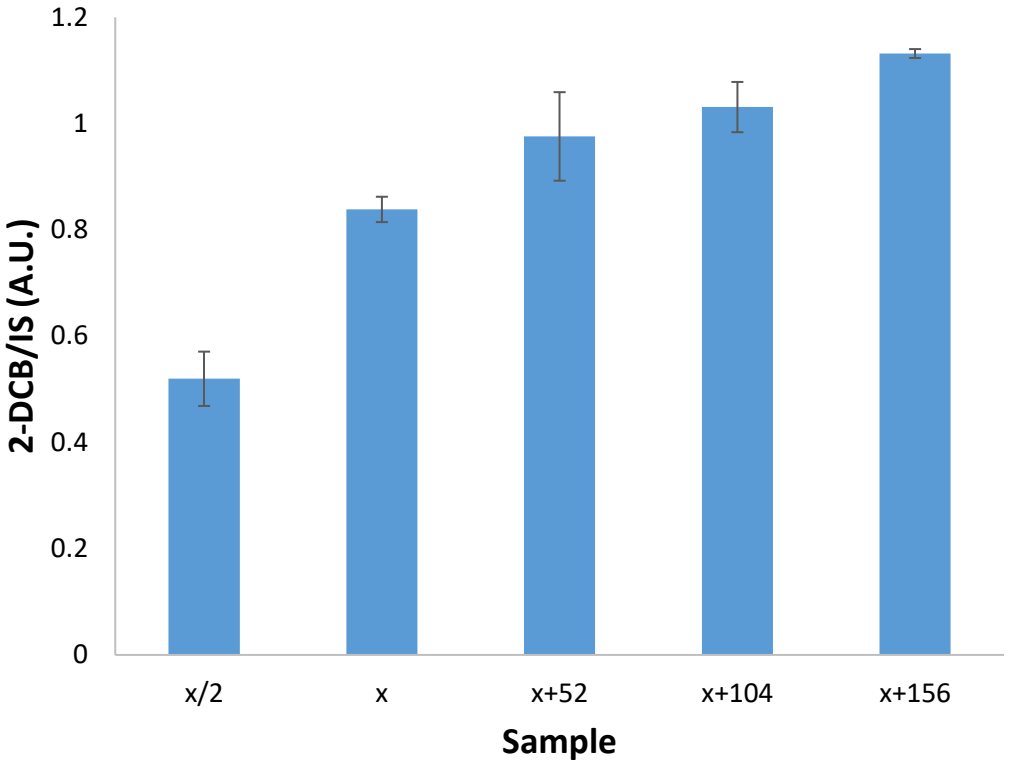


**Figure D-7:** Ratio of areas of 2-DCB and IS from sample C prepared spiking with 156 ng 2-DCB/g CJT, 104 ng 2-DCB/g CJT, 52 ng 2-DCB/g CJT, no-spiking, and diluting with the control sample. The values are mean values of two vials and the error bars represent standard deviation.

The method linearity for sample C was 0.974 (Figure D-8). According to acceptance criteria (criteria#1), this value is in the range of "satisfactory". The 2-DCB concentration in the unknown sample (sample C) was calculated following the standard addition method. Briefly, the intercept of the trendline equation (y = 0.002x + 0.854) was divided to the slope of the trendline equation from Figure D-8. The 2-DCB concentration in sample C was 474 ng/g CJT. The relative standard deviation (RSD %) was 13 %, which was in the range of "very good" according to acceptable criteria (criteria#2).

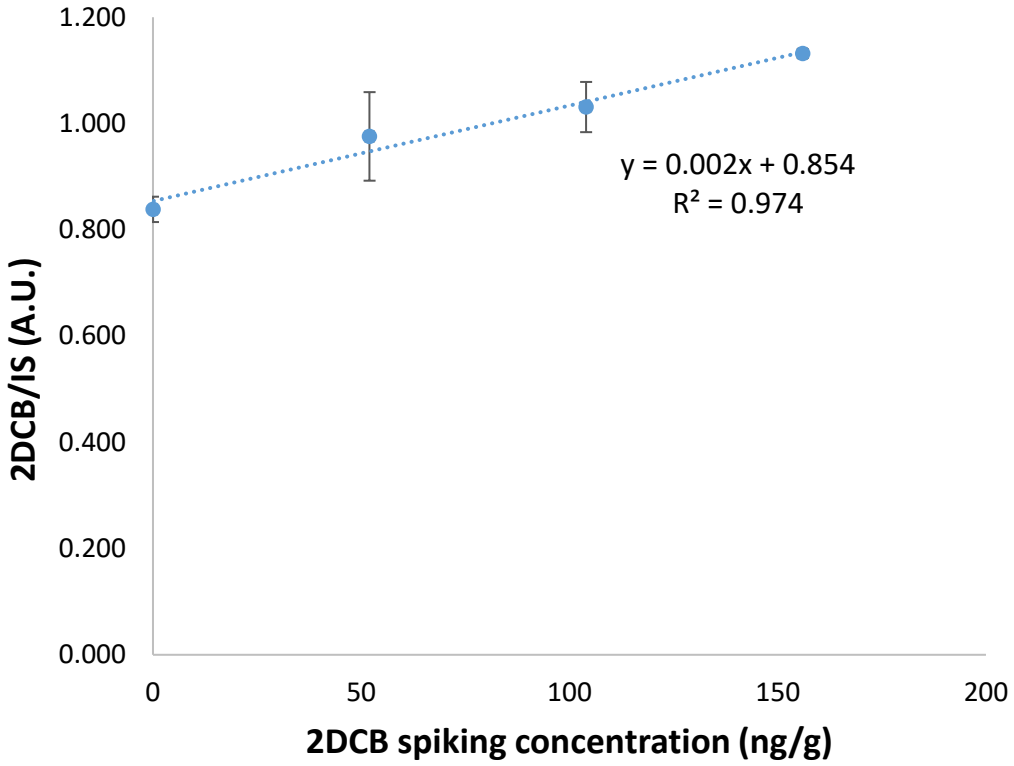


**Figure D-8:** Ratio of areas of 2-DCB and IS from sample C prepared spiking with 156 ng 2-DCB/g, 104 ng 2-DCB/g, 52 ng 2-DCB/g, and no-spiking at different 2-DCB spiking levels. The values are mean values of two vials and the error bars represent standard deviation.

The matrix effect of the method for sample C was evaluated using the linearity of the graph obtained using diluted, non-diluted, and three spikes at different calculated 2-DCB concentrations (Figure D-9).The linearity was 0.990.

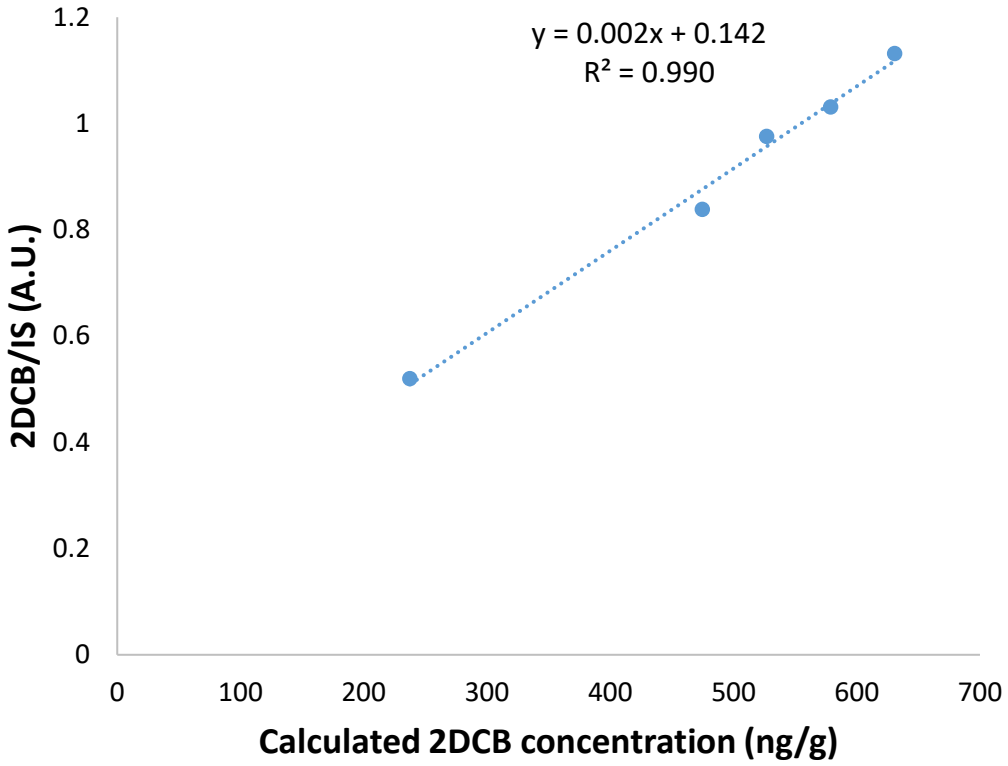


**Figure D-9:** Ratio of areas of 2-DCB and IS from sample C prepared spiking with 156 ng 2-DCB/g CJT, 104 ng 2-DCB/g CJT, 52 ng 2-DCB/g CJT, no-spiking, and diluting with the control sample at different calculated 2-DCB concentrations. The values are mean values of two vials and the error bars represent standard deviation.

The areas of 2-DCB/IS from sample D were given in Figure D-10. As expected, 2-DCB/IS increased with increasing 2-DCB spiking levels. In addition, diluted sample had lower 2-DCB/IS value than no-spiked sample.

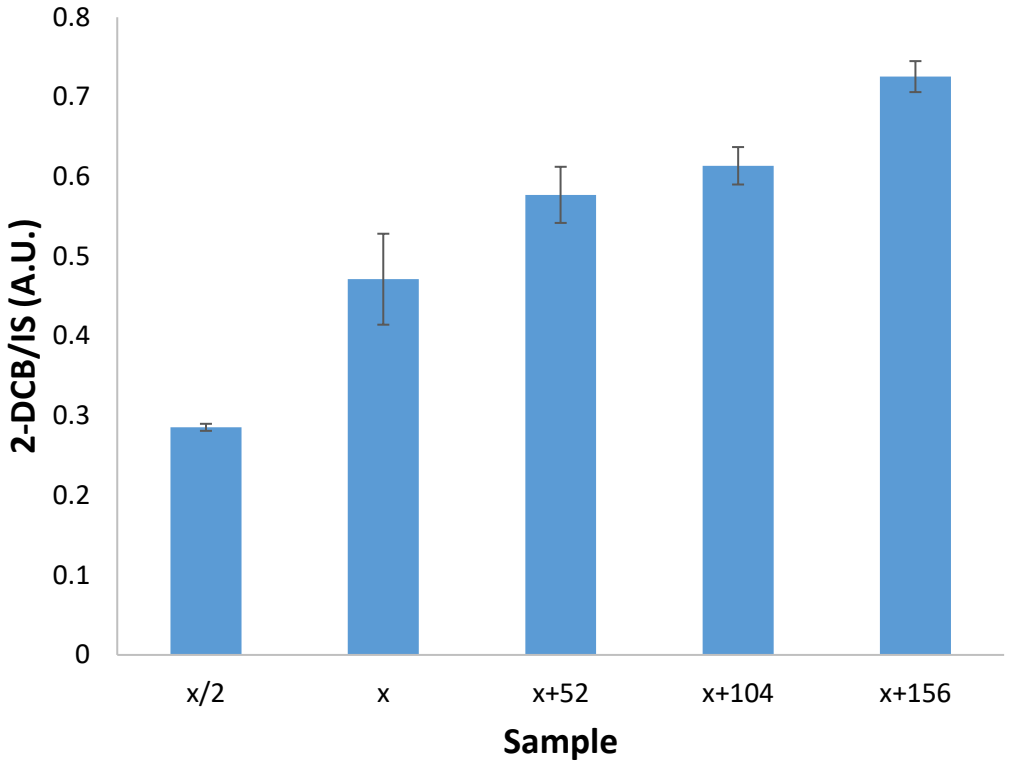


**Figure D-10:** Ratio of areas of 2-DCB and IS from sample D prepared spiking with 156 ng 2-DCB/g CJT, 104 ng 2-DCB/g CJT, 52 ng 2-DCB/g CJT, no-spiking, and diluting with the control sample. The values are mean values of two vials and the error bars represent standard deviation.

The method linearity for sample D was 0.968 (Figure D-11). According to acceptance criteria (criteria#1), this value is in the range of "satisfactory". The 2-DCB concentration in the unknown sample (sample D) was calculated following the standard addition method. Briefly, the intercept of the trendline equation (y = 0.002x + 0.477) was divided to the slope of the trendline equation from Figure D-11. The 2-DCB concentration in sample D was 310 ng/g CJT. The relative standard deviation (RSD %) was 16 %, which was in the range of "very good" according to acceptable criteria (criteria#2).

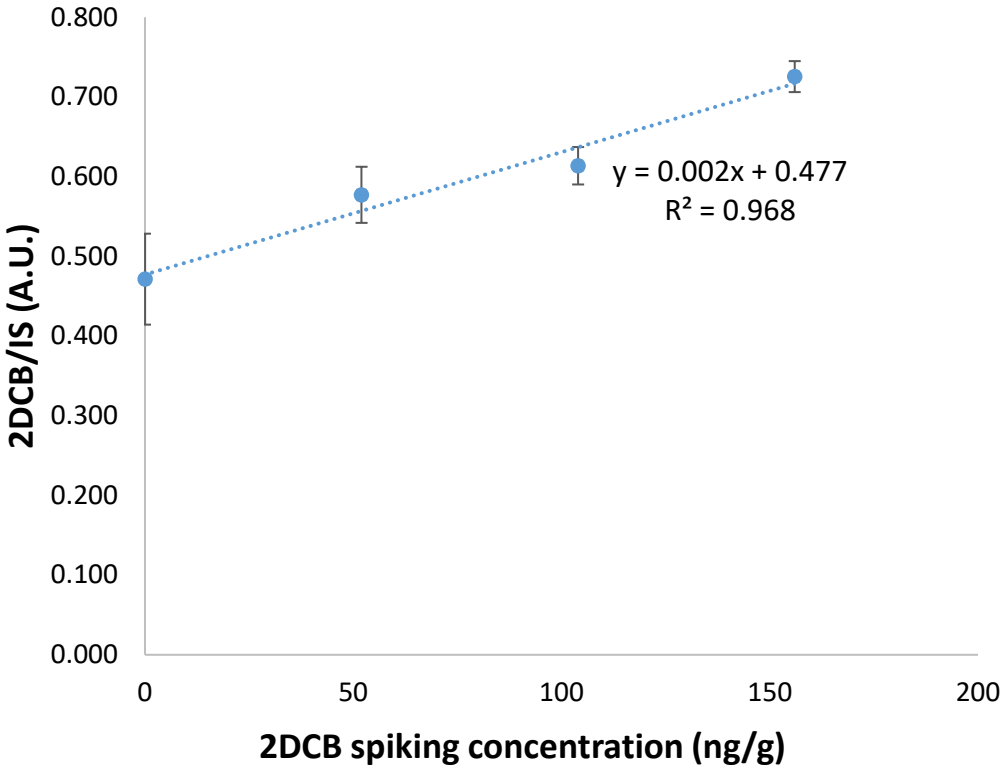


**Figure D-11:** Ratio of areas of 2-DCB and IS from sample D prepared spiking with 156 ng 2-DCB/g, 104 ng 2-DCB/g, 52 ng 2-DCB/g, and no-spiking at different 2-DCB spiking levels. The values are mean values of two vials and the error bars represent standard deviation.

The matrix effect of the method for sample D was evaluated using the linearity of the graph obtained using diluted, non-diluted, and three spikes at different calculated 2-DCB concentrations (Figure D-12).The linearity was 0.987.

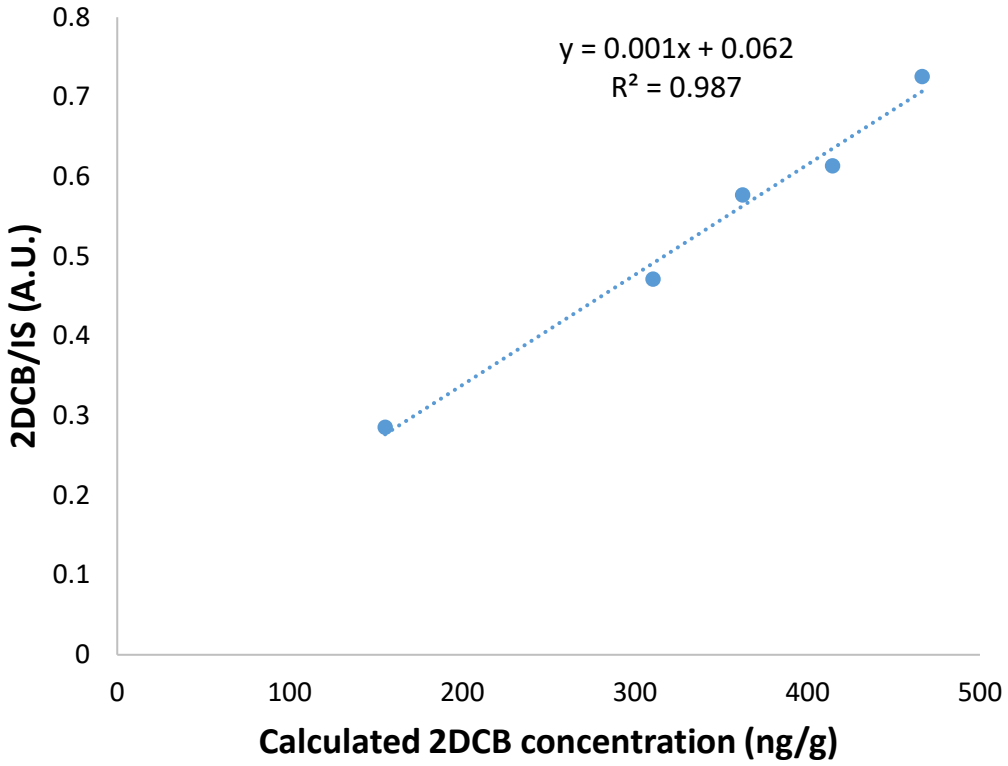


**Figure D-12:** Ratio of areas of 2-DCB and IS from sample D prepared spiking with 156 ng 2-DCB/g CJT, 104 ng 2-DCB/g CJT, 52 ng 2-DCB/g CJT, no-spiking, and diluting with the control sample at different calculated 2-DCB concentrations. The values are mean values of two vials and the error bars represent standard deviation.

The areas of 2-DCB/IS from sample E were given in Figure D-13. As expected, 2-DCB/IS increased with increasing 2-DCB spiking levels. In addition, diluted sample had lower 2-DCB/IS value than no-spiked sample.

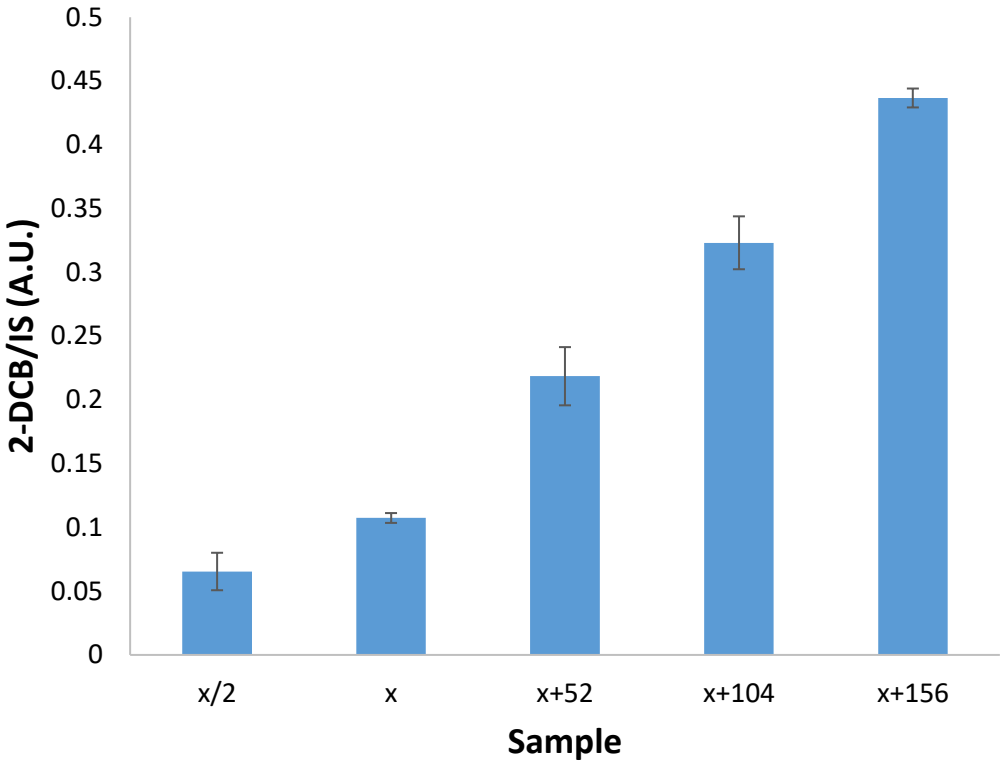


**Figure D-13:** Ratio of areas of 2-DCB and IS from sample E prepared spiking with 156 ng 2-DCB/g CJT, 104 ng 2-DCB/g CJT, 52 ng 2-DCB/g CJT, no-spiking, and diluting with the control sample. The values are mean values of two vials and the error bars represent standard deviation.

The method linearity for sample E was 1 (Figure D-14). According to acceptance criteria (criteria#1), this value is in the range of "excellent". The 2-DCB concentration in the unknown sample (sample E) was calculated following the standard addition method. Briefly, the intercept of the trendline equation (y = 0.002x + 0.108) was divided to the slope of the trendline equation from Figure D-14. The 2-DCB concentration in sample E was 51 ng/g CJT. The relative standard deviation (RSD %) was 3 %, which was in the range of "very good" according to acceptable criteria (criteria#2).

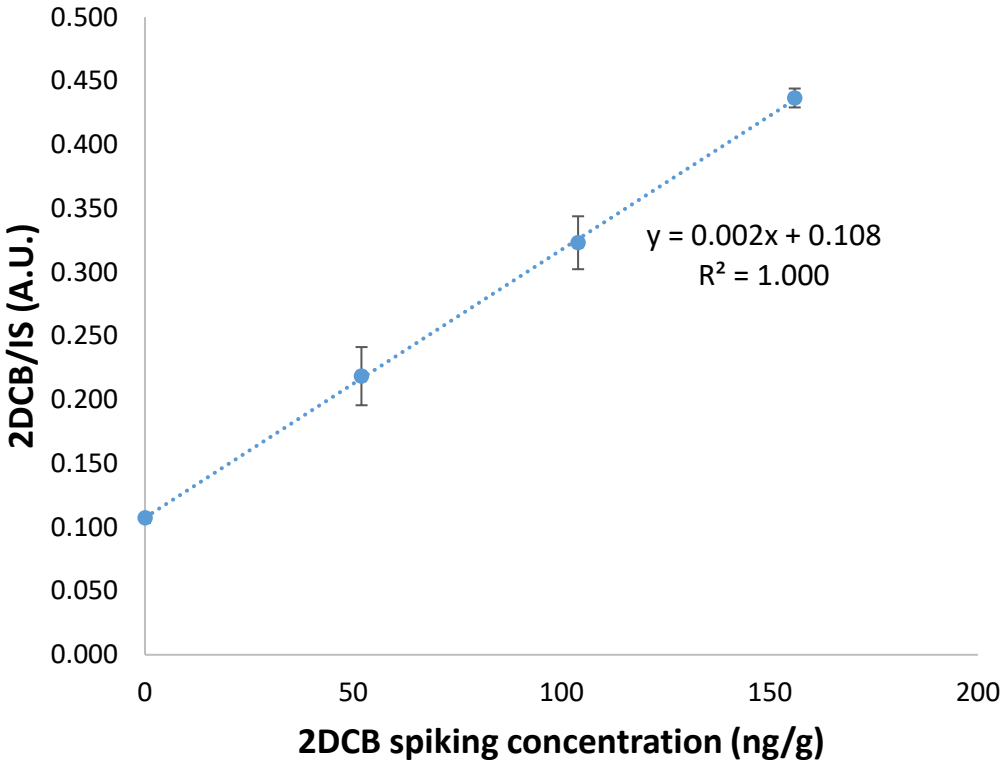


**Figure D-14:** Ratio of areas of 2-DCB and IS from sample E prepared spiking with 156 ng 2-DCB/g, 104 ng 2-DCB/g, 52 ng 2-DCB/g, and no-spiking at different 2-DCB spiking levels. The values are mean values of two vials and the error bars represent standard deviation.

The matrix effect of the method for sample E was evaluated using the linearity of the graph obtained using diluted, non-diluted, and three spikes at different calculated 2-DCB concentrations (Figure D-15).The linearity was 0.999.

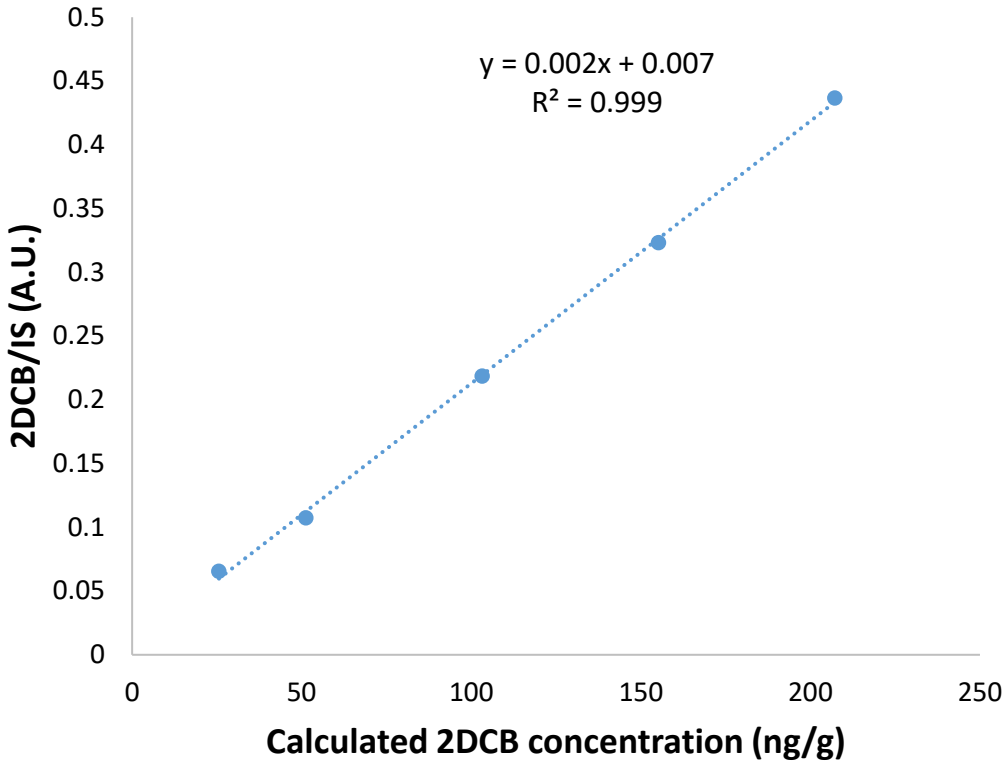


**Figure D-15:** Ratio of areas of 2-DCB and IS from sample E prepared spiking with 156 ng 2-DCB/g CJT, 104 ng 2-DCB/g CJT, 52 ng 2-DCB/g CJT, no-spiking, and diluting with the control sample at different calculated 2-DCB concentrations. The values are mean values of two vials and the error bars represent standard deviation.

# Appendix E - Dynamic Headspace Analysis

CJT samples were studied using static headspace analysis (SHS) in Chapter 6. They were also analyzed using dynamic headspace analysis (DHS). A schematic representation of DHS system was given in Figure E-1.

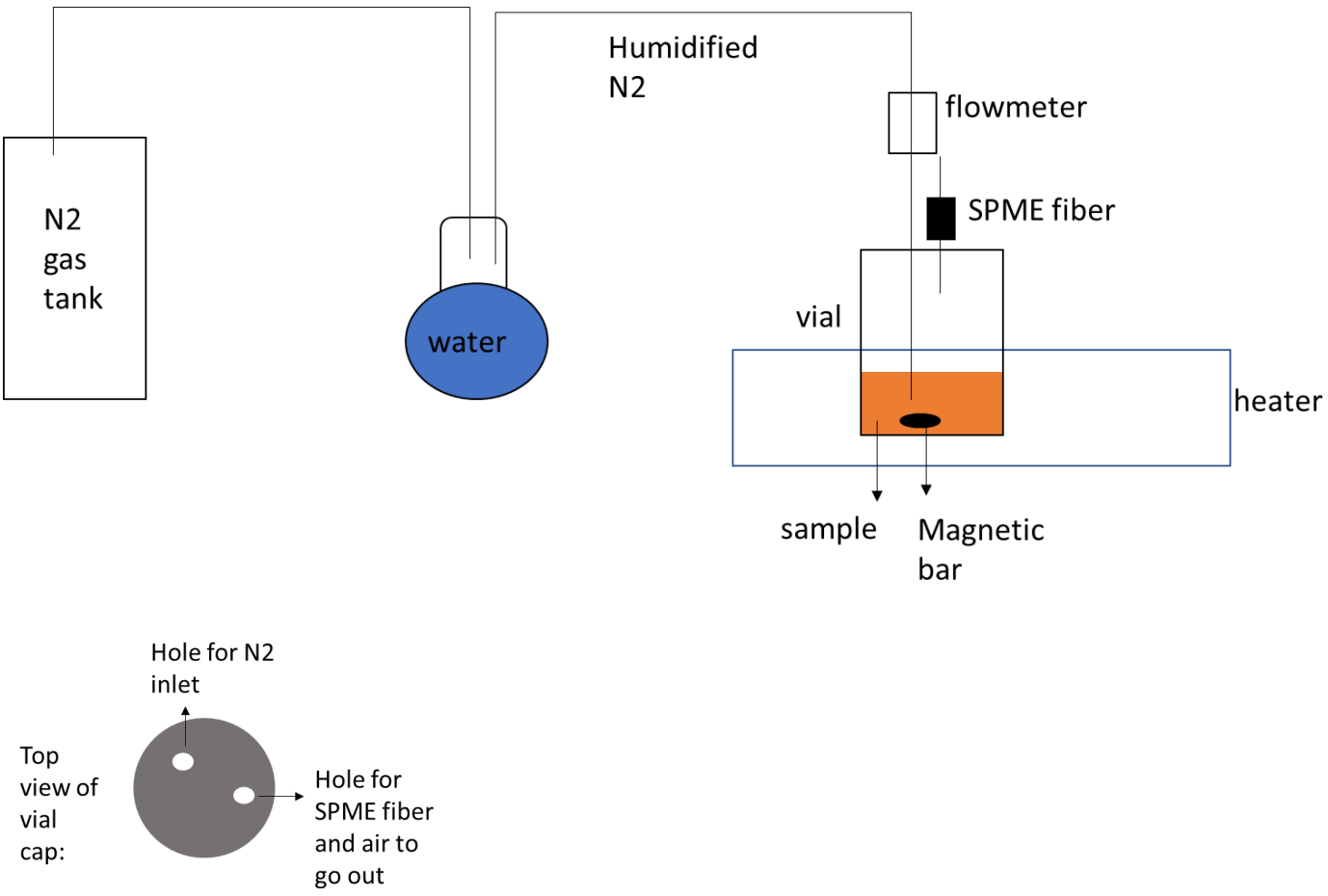


**Figure E-1:** A schematic representation of DHS system.

**Sample preparation**

Both irradiated (5 and 50 kGy) and non-irradiated CJT were ground in a Waring blender (50 mL) (model 34FL97, McConnellsburg, PA) for 1 min in pulses. Ground CJT were homogenized with water at a 1:5 ratio (g sample: mL water) at 30000 rpm for 1 minute (Fisher Scientific, Omni International Stainless Steel Saw Tooth Probe, TH115, 10 mm (D) x 115 mm (L)). Homogenized CJT was spiked with IS to a final concentration of 80 ng IS /g CJT and homogenized non-irradiated CJT was also spiked with 2-DCB (20 and 140 ng 2-DCB/g CJT). Samples were homogenized for another 1 min. An aliquot of the mixture (3 mL) was transferred to a siliconized headspace vial (75.5 x 22.5 mm, SUPELCO). After adding a small magnetic stirrer, the vials were immediately sealed with a crimp cap (20 mm, black VITON Septa, SUPELCO). Sealed vials were thermally equilibrated at 40 °C (Pierce Heating/Stirring Module, Rockford, IL) with magnetic stirring slowly for 50 minutes. Later, an SPME fiber (PDMS/DVB) was exposed to the headspace of the vial for 30 minutes at the same temperature under constant flush of nitrogen gas (25 mL/min).

**GC-MS analysis**

Analysis of 2-DCB using a GC-MS chromatography was performed following the procedure described in Chapter 6.

**Results**

The ratio of areas of 2-DCB to IS from non-irradiated samples spiked with 2-DCB (140 ng/g CJT) with DHS analysis were compared to that of SHS analysis (Figure E-2). The ratio of areas of 2-DCB to IS from DHS analysis did not show an improvement compared to the SHS analysis.

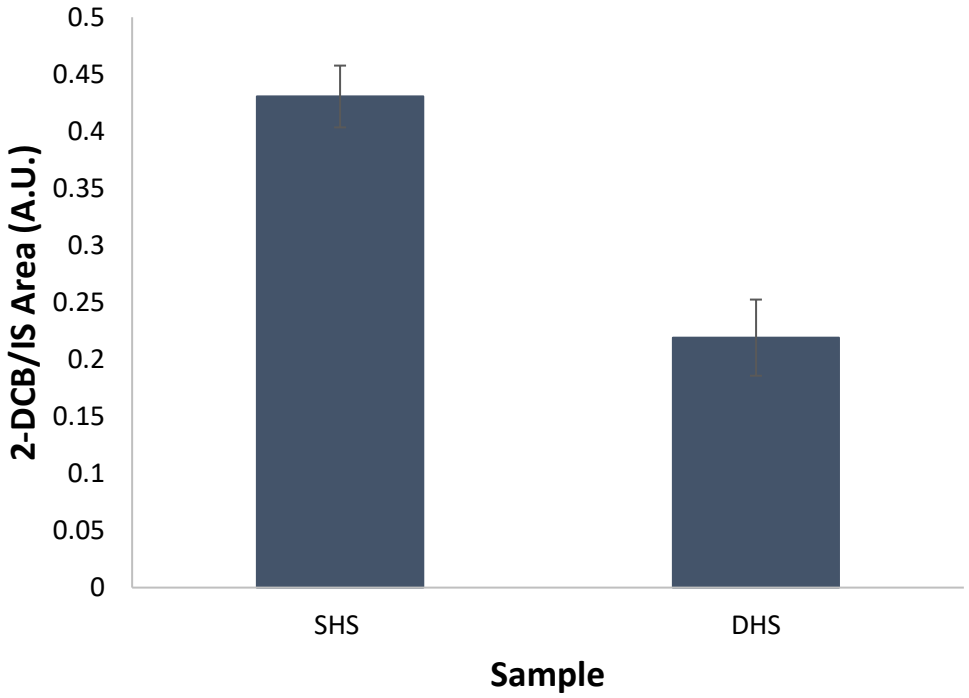


**Figure E-2:** Ratio of areas of 2-DCB to IS from non-irradiated samples spiked with 2-DCB (140 ng/g CJT) with SHS and DHS analysis. The results are means of two measurements and bars indicate standard deviation.